Shubhobrata Rudra · Ranjit Kumar Barai
Madhubanti Maitra

Block Backstepping Design of Nonlinear State Feedback Control Law for Underactuated Mechanical Systems

EXTRAS ONLINE

Springer

Block Backstepping Design of Nonlinear State Feedback Control Law for Underactuated Mechanical Systems

Shubhobrata Rudra · Ranjit Kumar Barai
Madhubanti Maitra

Block Backstepping Design of Nonlinear State Feedback Control Law for Underactuated Mechanical Systems

Springer

Shubhobrata Rudra
Department of Electrical Engineering
Techno India Salt Lake
Kolkata, West Bengal
India

Madhubanti Maitra
Department of Electrical Engineering
Jadavpur University
Kolkata, West Bengal
India

Ranjit Kumar Barai
Department of Electrical Engineering
Jadavpur University
Kolkata, West Bengal
India

ISBN 978-981-10-1955-5 ISBN 978-981-10-1956-2 (eBook)
DOI 10.1007/978-981-10-1956-2

Library of Congress Control Number: 2016947781

Printed on acid-free paper

This Springer imprint is published by Springer Nature
The registered company is Springer Science+Business Media Singapore Pte Ltd.

I dedicate this book to Sudeshna, my friend, who helped me a lot and encouraged me to believe that I too can be an author of a reference book.

Shubhobrata Rudra

Preface

The purpose of this book is to provide a detailed presentation of a novel block backstepping based control law that can address the control problems of a large class of underactuated mechanical systems in a generalized manner. Study of control problems of the underactuated systems and thereafter devising appropriate control actuations for those are presently being pursued with utmost vigor by the control research groups. The reason behind this is the appeal of the dynamic nature of the systems along with the challenges they pose. Such systems belong to a class that has a wide spectrum in reality not even restricting their domains related to Robotics, Aerospace, Industrial Processes, Marine systems etc. Consequently, a lot of theoretical propositions as well as practical application oriented approaches have been reported in the literature during the last few decades. Undoubtedly, those research contributions have enriched the literature of control engineering to a great extent, but quite often they fail to compromise between the theory and practice. Theoretical approaches can ensure global asymptotic stability during analysis, while their complicated mathematical formulations restrict their implementations on the practical systems in real-time. On the other hand, application-oriented approaches are absolutely system specific, and eventually they fail to answer the control problems of the other systems of similar nature. Therefore, design of a generalized control law based on block backstepping has been presented in this book in a structured manner.

The theory and further employment of Block backstepping based control law has been developed in a versatile manner, so that the control action generated, thereby, can ensure global asymptotic stability for most of the underactuated mechanical systems and at the same time can guarantee a desired performance during real-time implementations.

Indeed complicated state model of underactuated mechanical system restricts the straightforward applications of naïve integrator backstepping method. Therefore, the authors of this book have endeavored to establish an algebraic transformation

that could be used to reconfigure the original system model into a reduced order block-strict-feedback form. To be more precise, through this generic matrix-algebraic transformation, a higher order nonlinear underactuated system can be transfigured as a system having two cascaded blocks; the reduced order system modelled and depicted in strict feedback form followed by a dynamic block that actually represents the unobservable internal dynamics of the transformed system. Thereafter, integrator backstepping has been explored to devise a control law for the reduced order system as well as to assess and ensure the stability of internal dynamics of the entire system. Further, applications of the so devised control law on ten different systems (having completely different system dynamics) have been demonstrated in the simulation and real-time environment to corroborate the theoretical findings.

We reiterate that this book is intended to be used as a reference book by the graduate students and incumbent researchers in the areas of nonlinear control systems, mechanical systems, mechatronics, and robotics.

The book originates from the doctoral thesis prepared by the first author at the Jadavpur University of India and supervised by the second and third authors. Chapter 2 has been incorporated to provide with the prerequisite knowledge of nonlinear control theory that might be helpful to the new yet potential researchers in this domain. Thereafter, Chap. 3 has systematically presented the derivation of Block backstepping control law. At the onset, stepwise formulation of the control law has been described for the 2-DOF underactuated mechanical systems. After that, a generalized version of the control law has been presented to address the control problems of n-DOF underactuated mechanical systems. Chapter 4 has been devoted to demonstrate the applications of the control law on seven different underactuated systems, namely, inertia wheel pendulum, TORA, Furuta pendulum, acrobot, pendubot, inverted pendulum, and single dimensional Granty crane. For the first five systems, mentioned above, performances of the control law have been evaluated in the Matlab® Simulation environment. Moreover, the block backstepping control law has been employed for the inverted pendulum and overhead crane in real-time environment in a benchmark laboratory environment. For both the cases, it has been observed that the experimental outcomes have nearly corroborated with the theoretical findings. In Chap. 5, applications of the control law on higher-order systems have been portrayed, and have been substantiated with detailed simulation results. The authors hope that this reference book would be able to impart subtle yet sufficient knowledge about mathematical and implementation-oriented nuances towards control of under actuated nonlinear systems. The experiences gained by the authors while pursuing the work, are being conveyed to the research community of the future through this book.

Authors are very much grateful to Prof. Subir Kumar Saha (Mechanical Engineering Department, IIT Delhi, India) for his valuable suggestions, especially regarding presentation of the contents. Professor Subhasis Bhaumik (IIEST, Shibpur, India) has also put forward some important modifications that have enriched the contents of this book.

The first author would also like to express his deepest gratitude to Mr. Bedadipta Bain for his continuous support in all endeavors. At last, very special thanks go to Ms. Sumita Goswami for her continuous support during the final compilation of this book.

Kolkata, India Shubhobrata Rudra
Kolkata, India Ranjit Kumar Barai
Kolkata, India Madhubanti Maitra

Contents

About the Authors

Dr. Shubhobrata Rudra received his Bachelor's degree in Electrical Engineering in 2007 from West Bengal University of Technology, India, and Master of Electrical Engineering in 2010 and Ph.D. in Electrical Engineering 2015 from Jadavpur University, India. He has secured the University gold medal for standing first in the order of merit at the Master of Engineering examination. He pursued his doctoral research with Inspire Fellowship, awarded by the Department of Science and Technology (Government of India). He has published a few research articles in reputed international journals and presented several papers in different international conferences. His fields of interest include nonlinear control engineering, underactuated mechanical systems and motion control systems.

Dr. Ranjit Kumar Barai graduated in Bachelor of Electrical Engineering in 1993 and Master of Electrical Engineering in 1995 from Jadavpur University, India, and Ph.D. in Artificial Systems Science in 2007 from Chiba University, Japan. He has more than 20 years of working experience in industry, research, and teaching at graduate and postgraduate levels. He has supervised several masters and Ph.D. theses in the areas of mechatronics, robotics, and control systems. His research interests include mechatronics, robotics, control systems, machine learning and soft-computing, modelling and system identification, and real-time systems.

Prof. Madhubanti Maitra graduated in Bachelor of Electrical Engineering in 1989, Master of Electrical Engineering in 1991 and Ph.D. in Electrical Engineering in 2005 from Jadavpur University, India. She has more than 25 years of working experience in research and teaching at graduate and postgraduate levels. She has supervised several masters and Ph.D. theses in the areas of mobile communication, robotics, and control systems. Her research interests include mobile communication, robotics, control systems, machine learning and soft computing, modelling and system identification, and real-time systems.

Acronyms

DOF	Degree of Freedom
GAS	Global Asymptotic Stability
IDA	Inter connection and Damping Assignments
IWP	Inertia Wheel Pendulum
PBC	Passivity Based Control
RP	Rotating Pendulum
SMC	Sliding Mode Control
TORA	Translational Oscillator and Rotating Actuator
UMS	Underactuated Mechanical System
USV	Underactuated Surface Vessels
VTOL	Vertical Take off and Landing Aircraft

Chapter 1
Introduction

Abstract It was early 1970s, when researchers have observed that a large number of modern mechanical systems were using fewer control inputs (actuating inputs) than the number of output variables. Further inspections have revealed that those systems were exhibiting some of the common dynamical properties, and thereby could be categorized as a different subclass of the mechanical systems. Since those systems use fewer numbers of actuating inputs, they have been classified as the Underactuated mechanical systems (UMSs). A few examples of such systems are as follows different robotic systems, spacecrafts, underwater vehicles, surface vessel, helicopter, space robots, underactuated manipulators, etc. It has also been observed that this class of systems generates interesting control problems to which the naive design approaches of orthodox control theory could not be applicable. Inspired by their increasing demand in diverse industrial applications, control of the UMSs started to gain its popularity as one of the most active research fields among the control systems community.

1.1 Underactuated Mechanical System

As stated earlier, Underactuated mechanical systems (UMSs) are a special class of mechanical systems that have fewer actuating inputs (control inputs) than configuration variables (outputs from the system).

A cart-pole system, which is a typical example of the two degrees of freedom UMS, is shown in Fig. 1.1. In the cart-pole system, the actuating force is applied on the cart in a horizontal direction, and it regulates the motion of the cart. A free-moving pendulum is pivoted to the cart, whose motion is indirectly controlled by the back and forth movement of cart. The two outputs from the cart-pole system are defined as follows: horizontal deflection of the cart from the center of the rail (denoted by x), and angular displacement of the pendulum bob from its inverted position (denoted by θ). Both these outputs from the system are controlled by

Electronic supplementary material The online version of this article (doi:10.1007/978-981-10-1956-2_1) contains supplementary material, which is available to authorized users.

S. Rudra et al., *Block Backstepping Design of Nonlinear State Feedback Control Law for Underactuated Mechanical Systems*, DOI 10.1007/978-981-10-1956-2_1

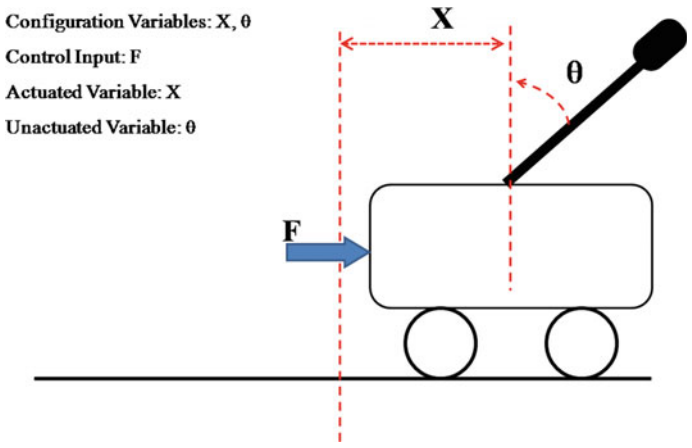

Fig. 1.1 A cart-pole system: a typical example of 2-DOF underactuated system

application of a horizontal force along the direction of the cart motion. Thus, a cart-pole system uses only one actuating input (F) to control the motion of both the configuration variables (x and θ), and therefore, justifies such categorization.

Underactuated systems possess some unique constructional features, which make them more apt for practical applications. From this perspective, there exist at least two distinct advantages in the design of controllers for underactuated systems. First, underactuated systems require less numbers of control inputs than that of the fully actuated MIMO systems, as an ordinary MIMO system is generally equipped with more actuators to generate the necessary control actions. Accordingly, those additional devices increase the cost and weight of such systems [14]. Thus, finding a way to control an underactuated version of the system would eliminate some of the actuating devices, and would either improve the overall performance or would reduce the cost of operation or would be able to achieve both the goals. Second, the underactuation provides a backup control strategy for an ordinary MIMO system as in case of actuator failure of a fully actuated MIMO system, availability of an underactuated controller may save the system from catastrophic consequences. One can think of hard real-time systems like aircraft or spacecraft, where actuator failures can be cataclysmic to the vehicle or its mission.

It is apparent that to synthesize the control objectives for such kind of systems, first the state models of these are to be derived, which are complicated enough and hence those often make the controller design tasks more difficult than that of the ordinary MIMO systems. Obtaining such a state model for devising appropriate control algorithms, a proper understanding about the reason of underactuation comes out to be an essential prerequisite.

Root causes that could make a system an underactuated one are

(i) Inherent dynamics of the system as one can find in spacecraft, helicopter, underwater vehicle, wheeled mobile robot (this type of underactuation often termed as natural underactuation).

(ii) Deliberate design of the system for some practical purposes. Examples of such systems are satellites with two thrusters, flexible-link robot (this type of underactuation often termed as intentional underactuation).
(iii) Accidental failure of an actuator in a MIMO system. In this case, the system automatically starts behaving like an underactuated system for the same output configuration.
(iv) Thoughtful use of low-order complex underactuated system. This is often done to gain the physical insights of the higher order mechanical systems' control aspects, e.g., the cart-pole system, the beam-and-ball system, the Acrobot, and the Pendubot.

Underactuation itself poses severe challenges on controller design. This is true for regulator kind of problem as well as for tracking kind of problem. Moreover, lack of controllability of UMS makes the controller design task even more complicated. These compel the researchers to have some indepth knowledge about the controllers and associated controls algorithms devised so far.

1.2 Brief State-of-the-Art on the UMSs Control

Over the last two decades, different algorithms have been proposed to address the stabilization problem of the underactuated systems. Joint research endeavors from academia and industry have led to the propositions of several advanced control algorithms. Nonetheless, among those numerous control strategies only a few could stand out as strong contenders. The followings are such a few relevant control techniques employed for the UMSs.

1.2.1 Linear Control Approaches

Linear control theory offers a very simple and easily implementable control design approach for real-world systems. In the early days of research, several linear control design techniques were proposed to address the control problem of underactuated systems. Although linear techniques are able to provide plausible solution for a particular application, even then the complicated nonlinear dynamics of such systems severely limits the generalized applications of the control laws. As a result, several redesign of the same algorithm became necessary to address the control problem of the similar types of systems.

In addition, linear approximation of the UMSs, often results in uncontrollable systems, which are not amenable to orthodox linear control algorithms for stabilization and tracking purposes. Furthermore, approximate linearization (Jacobean linearization) of a complicated nonlinear system only provides accurate linear approximation of the original system at a closed proximity of the equilibrium

points. Therefore, in case of the trajectory-tracking problem, where the desired equilibrium point is continuously moving along the reference trajectory, several linear models of the system must be obtained in order to acquire a true physical insight of the actual nonlinear system. However, the intricate mathematical manipulations make the design task extremely tedious and time consuming. Moreover, linear approximate model for the original nonlinear system often reduces the speed of response. All these shortcomings of linear control approaches have greatly motivated the design of several nonlinear control algorithms for UMSs.

1.2.2 Nonlinear Control: Present Day Approaches

To overcome the shortcomings of linear design techniques, several nonlinear control algorithms have been evolved in the last few decades. Feedback linearization is a well-known nonlinear design tool, which is widely used to address the control problem of the UMSs. Feedback Linearization is mainly a lie-algebra-based control design algorithm that transforms a nonlinear system into a linear system by a state diffeomorphism and a feedback transformation. Conversely, the complicated state model of an under actuated mechanical system restricts the direct application of feedback linearization on its control problem. Consequently, a special form of feedback linearization, namely partial feedback linearization is being used to address the control problem for such class of systems. The main advantage of this method is that it decouples the actuated and unactuated dynamics of the original underactuated systems. Therefore, from a given n-dimensional Lagrangian model of a system, it produces two decoupled state model of order n_1 and n_2. This decoupling property of partial feedback linearization simplifies the control design tasks for underactuated system. Another salient advantage of the partial feedback linearization is that it is applicable for all types of the underactuated systems irrespective of their system dynamics. The two main genres of partial feedback linearization are collocated feedback linearization and non-collocated feedback linearization. Collocated linearization refers to a feedback law, which linearizes the nonlinear equations of the underactuated systems' associated with the actuated degrees of freedom. On the other hand, non-collocated linearization refers to a special class of partial feedback linearization method that linearizes the system with respect to the passive degrees of freedom. Nonetheless, the new control appears in the both actuated and unactuated parts of the original system, and this highly complicates the controller design exercise for the decoupled system. Furthermore, like the ordinary feedback linearization approach, partial feedback linearization also suffers from the problem of lack of robustness.

Since uncertainty is a common yet intractable issue for the control of the underactuated systems, sliding mode approach-based robust controller design could be treated as a reasonable solution for the control problem of such class of systems. The behavior of the sliding mode depends only on the switching surface. Thus, sliding mode controller becomes insensitive to the parameter variations and external

disturbances. The basic idea of sliding mode design is to alter the dynamics of the system by applying a discontinuous feedback control input that forces the system to "slide" along a predefined state surface, and the system produces a desired behavior by restricting its state to this surface.

A large numbers of underactuated systems fail to satisfy the Brockett's condition of smooth feedback stabilization. Hence, those systems cannot be stabilized using smooth control input. Therefore, the non-smooth control input generated by the sliding mode control could be opted for as a natural choice to stabilize the underactuated system. Accordingly, sliding mode control finds its wide range of application on several underactuated systems like underactuated satellite, surface vessel, helicopter, TORA, ball and beam, biped robot, etc.

However, the discontinuous nature of sliding mode control often suffers with the problem of chattering, which in turn reduces the longevity of the actuators due to wear and tear of the mechanical parts. Another drawback of the sliding mode is that most of the time sliding mode controller assumes a very high value of disturbance bound. Consequently, most of the time sliding mode controller yields overconservative design approach. In order to solve the drawback of the conventional sliding mode several modifications have already been proposed. Proposed modifications, though have theoretical appeals, are too complicated for real-time applications.

Another popular nonlinear control algorithm, the Passivity-based control approach is also commonly used to address the stabilization problems of the underactuated system. The said method exploits the concept of passivity to design a stabilizing control law for complicated nonlinear systems. More precisely, the control objective is to passivize the system with a storage function, which has a minimum at the desired equilibrium point. Simply stated, this passivity-based approach is just a modified version of the orthodox energy-based control approach. This method is particularly well suited for simple mechanical systems, where the system can be stabilized by shaping the potential energy of the system. Nonetheless, the main shortcoming of the passivity-based method is that they can only be applied to address the control problems of nonlinear systems with relative degree one. A modification of the conventional passivity-based design has been proposed in the work of Ortega et al. to extend the application of passivity-based control approach for more complicated nonlinear systems. They have proposed a method of damping assignment in the passivity design to extend its application in the control problem of the higher order systems. However, similar to the complicated sliding mode design technique, this method also results in a very complex control law, which is inapt for real-time applications.

Another energy-based method, commonly known as backstepping, evolved in the early 1990s, has become an effective design tool to address the control problem of the nonlinear systems. Backstepping is a Lyapunov method-based versatile control design approach that ensures the convergence of the regulated variables to zero for nonlinear systems. The main advantage of the backstepping is that this is the only nonlinear design tool, which allows the designers to treat the control problem of an nth order system as a control problem of n numbers of first order

interconnected system. In the last two decades, backstepping has gained immense popularity as a nonlinear control design algorithm.

Backstepping is a nonlinear control design method that provides an alternative to feedback linearization. The main idea of the backstepping method is to partition the entire system into n numbers of cascaded subsystems. As a result, the states of the first subsystem acted as the control variables for the next subsystem. In backstepping approach, at first, the ideal input that can stimulate the desired output from the first subsystem is computed. Since the subsystems are connected in cascade, input to the first subsystem automatically comes from the output of the second subsystem. Ideal input to the second subsystem is computed in a similar manner to that of first subsystem. The desired inputs for all the subsystems are calculated in a sequential manner until the last subsystem is arrived. As a case in point, the desired input for the last subsystem gives the expression for the actual control input, and accordingly, the designers can implement a state feedback law for the entire nonlinear system. This recursive approach of the backstepping often serves as an advantageous feature during the design of control law for complicated nonlinear dynamic systems. Since control of UMSs is considered as a challenging design problem, backstepping-based design technique could be thought of as one the most suitable option to address the regulation problem for such class of systems.

However, the ordinary integral backstepping relies on the fact that the system under consideration is in strict feedback form. Generally, single-input single-output (SISO) nonlinear systems satisfy this condition under some simplifying assumptions. Nonetheless, in case of multivariable control problem, quite often the system structure is not available in the strict feedback or semi-strict feedback (i.e., lower triangular) form. Consequently, it is not possible to apply the integral backstepping technique in the usual manner to devise a control law for MIMO systems. Now as a case in point, the state model of an underactuated system typically resembles the structure of MIMO system, and it never possesses the strict feedback form. As a result, direct application of the ordinary integral backstepping algorithm on the stabilization problem for underactuated system is not possible. Subsequently, several research endeavors have been made in the last few years to extend the applications of backstepping control algorithm on the field of underactuated control systems. Nevertheless, most of these proposed control algorithms are either too complicated for real-time applications or they are subjected to several simplifying assumptions that make the proposed algorithm inapt for real-time applications.

1.2.3 Block Backstepping Approach

Recently, several research endeavors have been directed towards arriving at a more generalized backstepping algorithm that can efficiently address the stabilization problems of complex nonlinear systems. Block backstepping technique has emerged as one of the most efficient backstepping-based algorithm, which can address the control problem of different nonlinear multiple-input multiple-output

(MIMO) systems. At the initial stage of block backstepping design, the state model of the system is transformed into a cascade combination of two reduced order nonlinear systems. The transformation is defined in such a manner that it yields the first subsystem in strict feedback form, whereas the second subsystem represents the internal dynamics of the original system. Since the first subsystem possesses the strict feedback form, it allows the direct application of conventional integrator backstepping without any further modification. However, mere stabilization of the first subsystem does not imply the stability of the entire nonlinear systems. The stability of the overall system hinges on the stability of the internal dynamics. Therefore, proper stability analysis of the internal dynamics is required to ensure the global stability of the nonlinear system. A distinct advantage of the block backstepping control algorithm is that it possesses all the salient features of backstepping control algorithm. Conversely, it can address the control problem for a large class of nonlinear systems, where the complicated dynamics of the system restricts the straightforward application of the ordinary backstepping. Hence, block backstepping-based design technique could be regarded as the most appropriate alternative to a conventional backstepping-based feedback law for UMSs.

1.3 Motivations of Designing an Advanced Control Law

It is clear from the above discussions that tracking and stabilization kind of control problems of any UMS have gained their relevance over the last few years. The researchers identified the problems yet to be explored further. As mentioned, two important control problems for such systems, which have been focused on afresh, are stabilization problem and trajectory-tracking problem. Eventually, the stabilization problem appeared to be more challenging because most of the UMSs fall under the category of nonholonomic mechanical systems. Hence, this class of systems could not be stabilized by a smooth time-invariant state feedback law. However, simple the system is (namely, old-aged cart-pole system). Whereas, in contrast, with the control tools already in hand, in case of the trajectory-tracking problem, naïve approaches of the nonlinear control theory could be used in designing a suitable controller. As a result, several research initiatives have been developed in the last few decades to address the stabilization control problem of such systems in a generalized manner. Hence, it was established in the past that the very backstepping-based design approach might yield a solution for the convenient control of the complicated nonlinear systems. Therefore, the obvious conclusion that could be drawn is that backstepping could be treated as an alternative way of devising a generalized control law for the UMSs.

Nonetheless, all those previously proposed control algorithms are either too theoretical in nature, or they are intended to address the control problems of a particular underactuated mechanical system. Consequently, application-oriented approaches can only serve a particular control objective, but they often fail to address the control problem of similar type of systems in a generalized manner.

Main problem of the theoretical contributions is that they often produce a complicated control law that is not apt for real-life applications. In addition, those theoretical contributions often rely on many simplifying assumptions, which severely restrict their applications on practical systems. Moreover, in most of the cases, those propositions only ensure local stability of the control system around the desired equilibrium point. Keeping in view all the shortcomings of all those previously proposed approaches, a research endeavor has been undertaken during the doctoral study of the first author. Prime objective of the research endeavor was to devise an enhanced version of backstepping-based control algorithm, which can effectively address the stabilization control problems for a large class of UMSs.

Indeed, modeling error of the complicated real-time system often results in degradation of the controller performance. A control algorithm, which seems to be efficacious in the theoretical framework, may fail to provide a satisfactory performance during practical applications. This type of deterioration in the controller performance may produce catastrophic effects to the system or its mission. Therefore, proper measures should be taken to reduce the harmful effects of the modeling error. One can vet for controllers employing robust control laws, those may render the system insensitive to modeling error and parameter variations. Nevertheless, robust controllers often yield an overconservative design that is too complicated for real-time implementations. Hence, formulation of the control algorithm should be compact enough in a sense that it can provide a plausible solution for the control problems of the practical systems in real-time. Keeping this in view, need for a generic and flexible control law for the above-mentioned systems has been realized and that has led to the formulation of a novel block backstepping-based stabilization control algorithm. Further, in this work, it has thoroughly been established that such a generic control solution would be able to address the control problem of broad class of UMSs without any significant modifications. The main outcomes of the research endeavor are described below

- **Development of a modified Block backstepping controller**

This book presents a comprehensive description of designing a novel control law for a large class of UMSs in a generalized manner. However, as mentioned before, complicated state model of an UMS prevents the direct application of conventional integrator backstepping approach. Hence, an algebraic state transformation technique has been proposed to convert the state model of such systems into a strict feedback form. Basically, the proposed state transformation decomposes the state model of an n-DOF UMS into two parts, while the first part is represented by a reduced order strict feedback state model, the other part is used to represent the "internal dynamics" of the transformed system. Backstepping algorithm has been utilized to derive the complete expression of the control law for the entire nonlinear system. In addition, integral action has been incorporated in the proposed control law to reduce the adverse effects of modeling error on the controller performance. Since stability of the entire block backstepping controller depends on the stability of the zero dynamics of the transformed system, stability of the zero dynamics has

thoroughly been analyzed to ensure the global asymptotic stability of the overall system at its desired equilibrium point. Simplicity and generalized nature are the two distinctive features of this proposed control law, which make it more effective than its predecessor backstepping-based control algorithms. Use of simple algebraic manipulations makes the proposed block backstepping algorithm quite amenable to the real-time applications. Another important feature of this control algorithm is that it could be used to address the control problems of different categories of UMSs without any significant modifications.

- **Applications of the proposed control law on 2-DOF underactuated mechanical systems**

Needless to say, most of the UMSs naturally fall under the category of two degrees of freedom system. Therefore, in this book applications of the proposed method on several 2-DOF UMSs are described. During the aforesaid research program, applications of the proposed control algorithm have been studied on the following 2-DOF UMSs:

- Acrobot
- Pendubot
- Translational Oscillator and Rotating Actuator (TORA)
- Rotating Pendulum
- Inertia Wheel Pendulum (IWP)

Since all these above-mentioned UMSs belong to different categories of mechanical systems (e.g. holonomic, nonholonomic, "actuated shape variable," "unactuated shape variable," flat underactuated system, etc.), they have been selected to verify the effectiveness of the proposed control algorithm for various stabilization problems. In addition, effectiveness of the proposed control algorithm has also been corroborated to form the results of different real-time experiments. At first, the proposed control algorithm has been implemented on the real-time test bed of the inverted pendulum system to stabilize it. Thereafter, it has been employed to control the motion of a single dimension overhead crane and to reduce the oscillation of the payload during its motion. Moreover, the control law has been proved to be quite effectual in case of trajectory tracking of the holonomic systems (such as inverted pendulum, overhead crane).

- **Applications of the proposed control law on higher order underactuated mechanical systems**

In order to justify the generalized nature of the algorithm devised in this work, block backstepping control law has further been employed extensively on different higher order UMSs to study the efficacy and applicability of the same. Similar to the case of 2-DOF systems, three different UMSs have been selected for the purpose. Applications of the proposed control algorithm have been studied on the following higher order UMSs:

- Underactuated Surface Vessel (USV)
- Vertical Takeoff and Landing Aircraft (VTOL)
- 3-DOF Redundant Manipulator

Successful applications of the proposed control law on the above-mentioned systems have substantiated the generalized nature of the block backstepping control approach. Simulation results have established the theoretical claim that the proposed control algorithm requires little modifications and is versatile enough to ensure global asymptotic stability of generic UMSs.

1.4 Outline of the Book

The outline of this book is as follows:

This chapter provides an introduction and describes the main contributions of the book.

Chapter 2 provides the prerequisite knowledge of nonlinear control theory that might be helpful to the new potential researchers in this domain.

Chapter 3 is devoted for devising control algorithm for 2-DOF underactuated systems, and subsequently the proposition is extended to address the control problem of a generic *n*-DOF UMS.

Chapter 4 is devoted to demonstrate the applications of the control law on seven different UMSs, namely, inertia wheel pendulum, TORA, Furuta pendulum, acrobot, pendubot, inverted pendulum, and single dimensional Granty crane. For the first five systems, mentioned above, performances of the control law are studied in the Matlab® Simulation environment. Moreover, the performances of the block backstepping control law are also studied in real-time environment, where its application on inverted pendulum and overhead crane are considered.

Stabilization control problem of higher order UMSs are discussed in Chap. 5. Three higher order UMSs like USV, VTOL, and 3-DOF redundant manipulator are used to study the applications of the control law on the higher order systems.

Finally, Chap. 6 concludes the work described in this book. It also accentuates some open rather unexplored area of research within the field of UMSs control.

All being well, the authors expect that this book will play the role of a complete reference and give the readers subtle yet sufficient knowledge that helps them to design control laws for the other complicated UMSs.

Chapter 2
Theoretical Preliminaries

Abstract Over the last two decades, different algorithms have been proposed to address the stabilization problem of the underactuated systems. Joint research endeavors from academia and industry have led to the propositions of several advanced control algorithms. Nonetheless, among those numerous control strategies only a few could stand out as strong contenders. In this chapter, a few relevant control algorithms are being discussed to provide the prerequisite knowledge to the readers. All being well, after going through this chapter reader will not face any kind of difficulties in comprehending the contents of subsequent chapters.

2.1 Feedback Linearization

Feedback linearization is a control system design methodology especially applicable for nonlinear systems. The key idea of this approach is to algebraically transform a nonlinear system dynamics into an equivalent linear system, such that linear control technologies can be applied on the transformed system. The feedback linearization methodology is entirely different from the Jacobian linearization technique. Indeed, it can be viewed as a methodology to transform a complex nonlinear dynamics into *an equivalent simpler linear model.* The technique has two subsections one is input-state feedback linearization and the other is Input–Output Feedback Linearization [8].

2.1.1 Input-State Feedback Linearization

A generic single input nonlinear system is described by the following equation:

$$\dot{x} = f(x) + g(x)u \tag{2.1}$$

Electronic supplementary material The online version of this article (doi:10.1007/978-981-10-1956-2_2) contains supplementary material, which is available to authorized users.

S. Rudra et al., *Block Backstepping Design of Nonlinear State Feedback Control Law for Underactuated Mechanical Systems*, DOI 10.1007/978-981-10-1956-2_2

where $x \in \mathbb{R}^n, f(x): \mathbb{R}^n \rightarrow \mathbb{R}^n, g(x) \in \mathbb{R}^{n\times 1}$, u is a single dimensional control input.

Basically the input-state linearization is a two-step control design methodology. At the onset it employs a state transformation to convert the system into a linear one. Thereafter, a linear control technique is being used to design a linear control law to obtain the desired performance from the system. For the sake of better comprehensibility, following second-order nonlinear system is considered to explain the design procedure of input-state feedback linearization

$$\begin{aligned} \dot{x}_1 &= -x_1 - x_1^3 + x_2 \\ \dot{x}_2 &= x_1 - x_2 + bu \end{aligned} \tag{2.2}$$

In the above state model, b is nonzero system parameters. A careful observation of the above equations reveals that the equilibrium point of the system is located at (0, 0). Linearization of the above state model using Jacobian linearization yields the following linear state model of the system:

$$\begin{bmatrix} \dot{x}_1 \\ \dot{x}_2 \end{bmatrix} = \begin{bmatrix} -1 & 1 \\ 1 & -1 \end{bmatrix} \begin{bmatrix} x_1 \\ x_2 \end{bmatrix} + \begin{bmatrix} 0 \\ b \end{bmatrix} u \tag{2.3}$$

Linear control law can be exploited to design a control law that would give a satisfactory performance around the equilibrium point. However, performance of the system gets worse as soon as the system states start deviating from the equilibrium point. This is not at all a surprising outcome, a careful observation on the first equation reveals that the dynamics of x_1 state deviates a lot from the linearized one when $|x_1| \geq 1$. Consequently, it is very easy to understand that linear control laws fail to generate a satisfactory performance when operating point is located away from the equilibrium.

In this context, feedback linearization can give us a plausible solution. Basically the input-state linearization is a two-step control design methodology. At the onset it finds a state transform $z = z(x)$ and an input transform $u = u(x, v)$, which transform the original nonlinear system into an equivalent linear system. Thereafter, in the second step it uses some linear control design techniques to design v.

However, before start discussion on feedback linearization, let us have a close look on the system of (2.2). Minute observation reveals that the nonlinear terms not only appear in the dynamics of x_2, but it also appears in the dynamics of x_1, which further complicates the design procedure. Now if all the nonlinear terms appear in the second equation, then it would become an easier task for the designer to cancel all the nonlinearities using state feedback in a single step. However, in this case, at first a state transformation is required to convert the system model in such a way that all nonlinear terms would only appear with input u, then only one can easily utilize a state feedback to cancel all the nonlinear terms. In order to accomplish the task, following state transformation can be defined as shown in Eq. (2.4) below

$$\begin{aligned} z_1 &= x_1 \\ z_2 &= -x_1^3 + x_2 \end{aligned} \tag{2.4}$$

Above state transformation yields

$$\begin{aligned}\dot{z}_1 &= -z_1 + z_2 \\ \dot{z}_2 &= 2z_1^3 - 3z_1^2 z_2 + z_1 - z_2 + bu\end{aligned} \tag{2.5}$$

Now the following state feedback control law can be employed to make the system a linear one:

$$u = \frac{1}{b}\left(-2z_1^3 + 3z_1^2 z_2 + v\right) \tag{2.6}$$

That yields

$$\begin{aligned}\dot{z}_1 &= -z_1 + z_2 \\ \dot{z}_2 &= z_1 - z_2 + v\end{aligned} \tag{2.7}$$

Now the system would behave like a linear system in z_1, z_2 coordinate, and numerous linear control laws are there which can give us a satisfactory response from this system. Poles of the system (2.7) are located at −2, 0. The above system behaves like a badly damped linear system; now further inspection on the linear model of Eq. (2.7) reveals that the system is fully state controllable at origin. Therefore, one can design a state feedback control law to place the pole of the linear systems at desired location. Hence, if we want that the closed system will behave like a linear system with damping ratio $\zeta = 0.7$, and natural frequency $\omega_n = 5$ rad/s, then the pole must be placed at (−3.5 + 3.75j and −3.5 − 3.75j). Now, this can be easily achieved by designing a state feedback law with gain matrix $k = [\,19.999 \quad 5\,]$. Readers are encouraged to verify this design by their own. Hence, the feedback law will take the form

$$v = -[\,19.999 \quad 5\,]\begin{bmatrix} z_1 \\ z_2 \end{bmatrix} \tag{2.8}$$

Which yields the following stable dynamics:

$$\begin{bmatrix} \dot{z}_1 \\ \dot{z}_2 \end{bmatrix} = \begin{bmatrix} -1 & 1 \\ -18.999 & -6 \end{bmatrix}\begin{bmatrix} z_1 \\ z_2 \end{bmatrix} \tag{2.9}$$

Therefore, the control input u will take the form

$$u = \frac{1}{b}\left(-19.999z_1 - 6z_2 - 2z_1^3 + 3z_1^2 z_2\right) \tag{2.10}$$

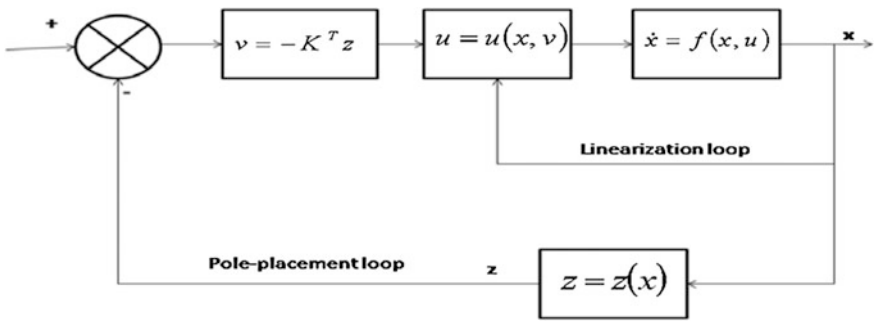

Fig. 2.1 Schematic diagram of the control law

In x_1 and x_2 coordinate, input u will take the following form:

$$u = \frac{1}{b}\left(-19.999x_1 - 6x_2 + 4x_1^3 - 3x_1^5 + 3x_1^2x_2\right) \tag{2.11}$$

A pictorial representation of the control law is given in Fig. 2.1.

Important Observations

- The input-state linearization process consisting of state transformation and input transformation, with state feedback used in both. So this is a linearization by feedback and that is why this methodology is termed as feedback linearization. It is fundamentally different from a Jacobian linearization which linearized a nonlinear system around a small region of the state plane.
- In order to implement the control law, the new state components (z_1, z_2) must be available. If they are not physically meaningful or cannot be measured directly, the original state x must be measured, and used to compute them from (2.4). In the next section, concept of output feedback linearization will be discussed in Sect. 2.1.2.

2.1.2 Output Feedback Linearization

In the preceding discussions, it has been assumed that all the states are readily available for measurement, and they can be utilized to design a state feedback according to the designer's disposal. However, most of the times practical systems fail to satisfy this requirement of state feedback linearization. Most of the cases, only output from the systems become available to the designers. In such a situation, design of input-state feedback linearization is not possible [8]. However, output from the system can be utilized to design a feedback law for the system. More precisely, output signal can be used to design a feedback law to cancel out the

nonlinear terms of systems equations. Consider the following nonlinear system as shown below in Eqs. (2.12.a, 2.12.b):

$$\dot{x} = f(x) + g(x)u \tag{2.12.a}$$

$$y = h(x) \tag{2.12.b}$$

Prime objective of the tracking control algorithm is to make the output $y(t)$, to track a desired trajectory $y_d(t)$, while keeping all the states bounded. It is assumed that the time derivatives of the reference signal (up to a sufficiently high order) are known and bounded. In order to elaborate the concept with a design problem, tracking control for the nonlinear system of Eq. (2.13) is considered.

$$\begin{aligned} \dot{x}_1 &= \cos x_2 + (x_2 + 1)x_3 \\ \dot{x}_2 &= x_1^3 + x_3 \\ \dot{x}_3 &= x_1^2 + u \\ y &= x_1 \end{aligned} \tag{2.13}$$

As stated above, prime objective of the controller design is to find out a control law that will ensure guaranteed tracking of the reference signal $y_d(t)$. However, the main challenge of this tracking control is that the input to the system has got no direct relationship with the output y. Nonetheless, successive differentiation of output with respect to time may yield an explicit relationship between output and input. Thereafter it is always possible to manipulate the input u that will ensure the guaranteed tracking of the output signal. Hence, the output signal is differentiated twice with respect to time to establish an explicit relation between input and output,

$$\ddot{y} = (x_2 + 1)u + f_1(\vec{x}) \tag{2.14}$$

where $f_1(\vec{x})$ is a function of state vector defined by

$$f_1(\vec{x}) = (x_1^3 + x_3)(x_3 - \sin x_2) + (x_2 + 1)x_1^2 \tag{2.15}$$

Clearly, Eq. (2.14) depicts an explicit relationship between output y and input u. Now a feedback control law can be used to cancel out all the nonlinearities present in the Eq. (2.14) as shown in Eq. (2.16) below

$$u = \frac{1}{x_2 + 1}(v - f_1(\vec{x})) \tag{2.16}$$

where v is an equivalent input to be designed according to the design requirement. Application of the above-mentioned control input u yields a simple double integrator relationship between equivalent input v with the output y as shown in Eq. (2.17)

$$\ddot{y} = v \tag{2.17}$$

At this stage, it is very easy to deploy standard linear control algorithm to get a desired tracking performance from the system. Tracking error e can be defined as $e = y - y_d$, now it is easy to relate the tracking error e and new control input v as shown in the following Eq. (2.18)

$$v = y_d - k_1 e - k_2 \dot{e} \tag{2.18}$$

with k_1 and k_2 are two positive design constants, which yield the following equation for closed loop error dynamics as shown in Eq. (2.19) below:

$$\ddot{e} + k_2 \dot{e} + k_1 e = 0 \tag{2.19}$$

which represents an exponential stable error dynamics. Therefore, perfect tracking can be achieved in almost all cases except the singular point that is located at $x_2 = -1$. Otherwise, this control algorithm ensures perfect tracking of a smooth reference signal. Since in this case output signal is being used to convert the system in linear form, this type of linearization is known as *input–output linearization*.

For an *n*th order nonlinear system at the time of *Input–Output Linearization,* if *r* differentiation is required to establish an explicit relationship between *input u* and *output y*, then the system can be termed as a system with **relative degree *r*** [1]. Therefore, it is easy to conclude that the system of Eq. (2.13) has a relative degree equal to two. At the time of *Input–Output Linearization* algorithm one only considers a part of closed-loop system. Frequently a part of the system dynamics is rendered *unobservable* at the time of *Input–Output Linearization.* In general, this part of the dynamics of the system is termed as the **Internal Dynamics** of the original system. Indeed, it cannot be seen from the external relationship, between equivalent input and output relationship of the system. For the tracking control of the system shown in Eq. (2.13), the internal dynamics is represented by the following equation,

$$\dot{x}_3 = x_1^2 + \frac{1}{x_2 + 1}(\ddot{y}_d - k_1 e - k_2 \dot{e} + f_1(\vec{x})) \tag{2.20}$$

In case of *Input–output linearization* it is possible to design tracking control algorithm, only when internal dynamics of the system is stable.

Zero Dynamics: The *Zero Dynamics* is defined to be the internal dynamics of the system when the system output is kept at zero by the input [1, 3]. In case of a linear system the poles of the zero dynamics are exactly the zeros of the original system. The zero dynamics is an intrinsic property of the nonlinear system, while stability of the same ensures the stability of the internal dynamics of the nonlinear system in local sense.

2.1.3 Partial Feedback Linearization

It is a special type of feedback linearization method that is being considered as one of the most useful control technique for underactuated mechanical systems [UMS] [5–7]. This method provides a natural global change of coordinates that transforms the system into a strict feedback form, and thereafter the conventional control method can be easily applied to the transformed system [9]. However, in case of the UMS neither input feedback linearization nor input–output linearization can provide a satisfactory result. Let us consider the Lagrangian model of UMS as shown in Eq. (2.21)

$$\begin{aligned} m_{11}(\boldsymbol{q})\ddot{\boldsymbol{q}}_{\boldsymbol{1}} + m_{12}(\boldsymbol{q})\ddot{\boldsymbol{q}}_2 + \boldsymbol{h}_1(\boldsymbol{q},\boldsymbol{p}) &= 0 \\ m_{21}(\boldsymbol{q})\ddot{\boldsymbol{q}}_1 + m_{22}(\boldsymbol{q})\ddot{\boldsymbol{q}}_2 + \boldsymbol{h}_2(\boldsymbol{q},\boldsymbol{p}) &= B(\boldsymbol{q})\tau \end{aligned} \tag{2.21}$$

where, $\boldsymbol{q}_1 \in \mathbb{R}^{n_1}$, $\boldsymbol{q}_2 \in \mathbb{R}^{n_2}$ and $\boldsymbol{q} = col(\boldsymbol{q}_1, \boldsymbol{q}_2) \in \mathbb{R}^n$ is the configuration vector of nth degree of freedom underactuated mechanical system. In the above representation, $\boldsymbol{q_1}$ represents passive joint configuration variables, and $\boldsymbol{q_2}$ represents active joint configuration variables. The dimension of the overall configuration manifold is $n_1 + n_2 = n$. The time derivative of the configuration vector $\boldsymbol{q}$ is expressed as $\boldsymbol{p} = \text{col}(\boldsymbol{p}_1, \boldsymbol{p}_2) \in \mathbb{R}^n$, and $\tau \in \mathbb{R}^{n_2}$ is the control input. In the above representation, $\boldsymbol{h}_1(\boldsymbol{q},\boldsymbol{p})$: $\mathbb{R}^{2n} \rightarrow \mathbb{R}^{n_1}$ and $\boldsymbol{h}_2(\boldsymbol{q},\boldsymbol{p})$: $\mathbb{R}^{2n} \rightarrow \mathbb{R}^{n_2}$ contain the coriolis, centrifugal, and gravity terms. Whereas, $m_{ij}(\boldsymbol{q})$ $q = 1, 2$, represents the components of the $n \times n$ inertia matrix, which is symmetric and positive definite for all $\boldsymbol{q}$. $B(\boldsymbol{q}) \in \mathbb{R}^{n_2 \times n_2}$ represents a full rank matrix. Due to Spong, there exists an invertible change of the control input $\boldsymbol{\tau}$ as shown in Eq. (3.19)

$$\tau = B^{-1}(\boldsymbol{q})\left(\left(\boldsymbol{h}_2(\boldsymbol{q},\boldsymbol{p}) - m_{21}(\boldsymbol{q})m_{11}^{-1}(\boldsymbol{q})\boldsymbol{h}_1(\boldsymbol{q},\boldsymbol{p})\right) + \left(m_{22}(\boldsymbol{q}) - m_{21}(\boldsymbol{q})m_{11}^{-1}(\boldsymbol{q})m_{12}(\boldsymbol{q})\right)\boldsymbol{u}\right) \tag{2.22}$$

that transforms the Lagrangian model of Eq. (2.23) into

$$\begin{aligned} \dot{\boldsymbol{q}}_1 &= \boldsymbol{p}_1 \\ \dot{\boldsymbol{q}}_2 &= \boldsymbol{p}_2 \\ \dot{\boldsymbol{p}}_1 &= \boldsymbol{f}(\boldsymbol{q},\boldsymbol{p}) + g(\boldsymbol{q})\boldsymbol{u} \\ \dot{\boldsymbol{p}}_2 &= \boldsymbol{u} \end{aligned} \tag{2.23}$$

where, $f(\boldsymbol{q},\boldsymbol{p})$: $\mathbb{R}^{2n} \rightarrow \mathbb{R}^{n_1}$, $g(\boldsymbol{q}) \in \mathbb{R}^{n_1 \times n_2}$ are given by

$$\begin{aligned} \boldsymbol{f}(\boldsymbol{q},\boldsymbol{p}) &= -m_{11}^{-1}(\boldsymbol{q})\boldsymbol{h}_1(\boldsymbol{q},p) \\ g(\boldsymbol{q}) &= -m_{11}^{-1}(\boldsymbol{q})m_{12}(\boldsymbol{q}) \end{aligned} \tag{2.24}$$

The state vector can be expressed as $\boldsymbol{X} = [\boldsymbol{q}_1 \quad \boldsymbol{p}_1 \quad \boldsymbol{q}_2 \quad \boldsymbol{p}_2] \in \mathbb{R}^{2n}$. Now it is easy to understand that control law of Eq. (2.22) can only ensure partial linearization of the system. State model of Eq. (2.23) is partially linearized. The $\boldsymbol{q_1}$ and $\boldsymbol{p_1}$ subsystem represents a nonlinear subsystem as shown in Eq. (2.25), whereas Eq. (2.26) represents linear subsystem

$$\begin{aligned} \dot{\boldsymbol{q}}_1 &= \boldsymbol{p}_1 \\ \dot{\boldsymbol{p}}_1 &= \boldsymbol{f}(\boldsymbol{q},\boldsymbol{p}) + g(\boldsymbol{q})\boldsymbol{u} \end{aligned} \tag{2.25}$$

and

$$\begin{aligned} \dot{\boldsymbol{q}}_2 &= \boldsymbol{p}_2 \\ \dot{\boldsymbol{p}}_2 &= \boldsymbol{u} \end{aligned} \tag{2.26}$$

Therefore, it is defined as partial feedback linearization. There are two PFL techniques that have been mentioned in the literature of control engineering; one is termed as collocated feedback linearization, and other one is referred as non-collocated feedback linearization.

(a) **Collocated feedback linearization**
Collocated linearization refers to a feedback law, which linearizes the nonlinear equations of the UMS associated with the actuated degrees of freedom [5–7]. This method globally transforms all the UMSs model in the form of two parallel connected fully actuated system, where the new control input appears in the dynamics of both subsystems. Collocated linearization has been extensively applied to the control of the different underactuated system like Acrobot, the three-link pendulum, rotational pendulum, etc. [9].

(b) **Non-Collocated feedback linearization**
Non-collocated linearization refers to a special class of partial feedback linearization method that linearizes the system with respect to the passive degrees of freedom. Nonetheless, the non-collocated feedback linearization is not a global transformation technique like collocated feedback linearization. It is only applicable for "Strongly Inertially Coupled" underactuated mechanical system. "Strongly Inertially coupled" system is a special class of UMSs, where the number of unactuated configuration variables is less than or equal to the number of actuated configuration variables (Spong M.W.). The major advantage of the collocated and the non-collocated linearization is that they produce a structural simplification of the control problems of any UMSs. Consequently, they are always utilized as an initial simplifying step for reduction and control of the UMSs.

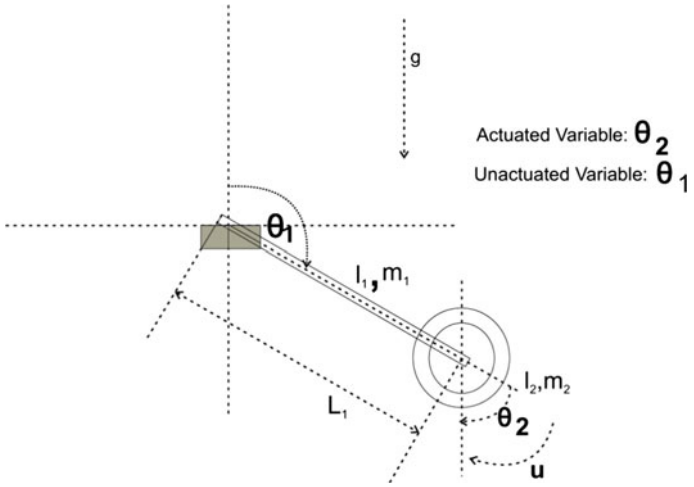

Fig. 2.2 Schematic diagram of inertia wheel pendulum

In order to explain the collocated PFL and non-collocated PFL, let us consider the Lagrangian model of inertia wheel pendulum, which is expressed in Eq. (2.27) below

$$\begin{aligned} m_{11}(q)\ddot{q}_1 + m_{12}(q)\ddot{q}_2 + h_1(q,p) &= 0 \\ m_{21}(q)\ddot{q}_1 + m_{22}(q)\ddot{q}_2 + h_2(q,p) &= \tau \end{aligned} \tag{2.27}$$

Schematic diagram of the system is shown in Fig. 2.2.

Indeed, collocated linearization is a kind of input-state feedback linearization for UMS. Now from the above Eq. (2.27), one can write

$$\ddot{q}_1 = -m_{11}^{-1}(q)(m_{12}(q)\ddot{q}_2 + h_1(q,p)) \tag{2.28}$$

Now, second actuated dynamics equation of (2.27) can be rewritten after replacing the value of q_1 by the above equation

$$\left(m_{22}(q) - m_{21}(q)m_{11}^{-1}(q)m_{12}(q)\right)\ddot{q}_2 + \left(h_2(q,p) - m_{11}^{-1}(q)h_1(q,p)\right) = \tau \tag{2.29}$$

The above equation can be linearized by applying the following control input of Eq. (2.30)

$$\tau = \left(m_{22}(q) - m_{21}(q)m_{11}^{-1}(q)m_{12}(q)\right)\left(u + \left(h_2(q,p) - m_{11}^{-1}(q)h_1(q,p)\right)\right) \tag{2.30}$$

In the above Eq. (2.30) u is actually a new control input that has to be defined according to the requirement of control designer. Therefore, equation of (2.27) takes the following form:

$$\begin{aligned} m_{11}(q)\ddot{q}_1 + h_1(q,p) &= -m_{12}(q)u \\ \ddot{q}_2 &= u \end{aligned} \tag{2.31}$$

Eventually, the above Eq. (2.31) can be rewritten in a simplified form as shown below:

$$\begin{aligned} \dot{q}_1 &= p_1 \\ \dot{p}_1 &= f(q,p) + g(q)u \\ \dot{q}_2 &= p_2 \\ \dot{p}_2 &= u \end{aligned} \tag{2.32}$$

where

$$\begin{aligned} f(q,p) &= -m_{11}^{-1}(q)h_1(q,p) \\ g(q) &= -m_{11}^{-1}(q)m_{12}(q) \end{aligned} \tag{2.33}$$

Indeed, it is one of the most common forms of feedback linearization. Please note that the collocated linearization actually linearizes the actuated degree of freedom, and decouples it from the unactuated degrees of freedom. However, non-collocated linearization is kind of input output feedback linearization. Now, if one wants to linearize the unactuated configuration variable that is q_1, an obvious choice of control input is

$$v = m_{11}^{-1}(h_1 - m_{12}u) \tag{2.34}$$

That yields

$$\begin{aligned} \ddot{q}_1 &= v \\ \ddot{q}_2 &= -m_{11}^{-1}(q)(m_{12}(q)v - h_1(q,p)) \end{aligned} \tag{2.35}$$

Consequently, the state model for the IWP can be expressed as

$$\begin{aligned} \dot{q}_1 &= p_1 \\ \dot{p}_1 &= v \\ \dot{q}_2 &= p_2 \\ \dot{p}_2 &= \frac{v-f}{g} \end{aligned} \tag{2.36}$$

Therefore, it is clear from the above-stated model that non-collocated linearization yields decoupling of unactuated degrees of freedom. However, the non-collocated linearization is not widely used to treat the control problems of UMSs, while the collocated linearization is very popular to reshape the Lagrangian

model of UMSs in a partially feedback linearized form. However, feedback linearization is not enough to address the control problem of nonlinear systems. In the next section, authors will describe a few shortcomings of feedback linearization, and then they will describe a successor of feedback linearization, namely backstepping.

2.2 Control Lyapunov Function

Before describing the concept of backstepping, authors would like to discuss a few relevant topics that would give the readers a prerequisite knowledge, which will help them to comprehend the concepts of backstepping design. Best of the authors' knowledge, Lyapunov stability criterion is one the most famous and reliable stability analysis technique that has been used to analyze the stability of any autonomous dynamical systems. However, the naïve approach of Lyapunov stability analysis does not lead to any constructive approach that could be utilized to devise a control law for complicated nonlinear systems. Therefore, a new Lyapunov function approach has been conceived to assist the design procedure for nonlinear nonautonomous control systems. Let us consider a nonautonomous time invariant nonlinear system as shown in Eq. (2.37)

$$\dot{x} = f(x,u); f(0,0) = 0 \tag{2.37}$$

It is easy to understand from that the equilibrium point of the nonlinear system mentioned in Eq. (2.37) is located at $\boldsymbol{X} = 0$. Nonetheless, if someone wants to devise a state feedback control law $u = \alpha(x)$ such that the origin of the system becomes a global asymptotic stable system, then a modified Lyapunov function approach may yield a conducive solution. It is not a difficult task to construct a positive definite, radially unbounded, continuous and smooth scalar function $V(\boldsymbol{X})$ as a Lyapunov function candidate. Moreover, an additional requirement can be placed on its time derivative along $f(x, \alpha(x))$ as shown in Eq. (2.38) below

$$\frac{\mathrm{d}V}{\mathrm{d}t} = \frac{\partial V}{\partial x} f(x, \alpha(x)) < 0; \quad x \neq 0 \tag{2.38}$$

Now, a state feedback control law may be designed to achieve the aforesaid condition of Eq. (2.38). Careful observation reveals that in this context the Lyapunov function $V(\boldsymbol{X})$ is not used to analyze stability of the system, rather it is used to find out a conducive control law that yields the condition of Eq. (2.38). *Since here Lyapunov function is used to design a control law for the nonautonomous systems, it is known as Controlled Lyapunov Function (clf)* [2].

Let us consider the scalar system of the Eq. (2.39) below

$$\dot{x} = -\sin x - x^3 + u \tag{2.39}$$

Input-State feedback stabilization control law will yield a control law that cancel out all the nonlinear entries of the above equation

$$u = \sin x + x^3 - kx \tag{2.40}$$

Application of the control input of Eq. (2.40) makes the system's origin a global asymptotically stable equilibrium. However, such inveterate approach of feedback linearization always raises a few questions, which are very important and need to be answered before practical implementation. First, what is the essence of canceling out the term x^3, while it can assist the stabilization process of the overall system? Second, what is the price a designer has to pay for introducing the x^3 term in feedback equation? Third, what are the alternative approaches that could be utilized to address the above-mentioned control problem?

Indeed, one can design $u = \alpha(x, u) = -kx + \sin x$ and may select a simple clf like $V(\boldsymbol{X}) = \frac{1}{2}x^2$ that will yield

$$\dot{V} = \frac{\partial V}{\partial x} f(x, u) = x\left(-x^3 - kx\right) = -x^4 - kx^2 \tag{2.41}$$

which is negative definite. The same negative definiteness can also be achieved with the control law of Eq. (2.40), which will yield the following time derivative for the same clf

$$\dot{V} = \frac{\partial V}{\partial x} f(x, u) = x(-kx) = -kx^2 \tag{2.42}$$

However, let us first consider the control law $u = \alpha(x, u) = -kx + \sin x$ and corresponding time derivative of the clf as shown in Eq. (2.41). A careful observation will reveal that the control signal increases linearly with x. Furthermore, the time derivative of Lyapunov Function (as shown in 2.41) decreases at a faster rate due to the presence of $-x^4$. *Actually, the term $-x^3$ of the original system assists the stabilization process, and thereby it is termed as the beneficial nonlinearities or useful nonlinearities.* Conversely, application of the control law of Eq. (2.40) yields a different time derivative of the clf that is shown in Eq. (2.42). Needless to say that here the amplitude of control signal is quite high due to the presence of $+x^3$ term in Eq. (2.40). Moreover, in this case the rate of decay of the time derivative of the clf is very poor (as shown in Eq. 2.42). In addition, it should be noted that the presence of term $+x^3$ in the feedback path makes the control law more sensitive with respect to slight change of systems parameter.

2.3 Integrator Backstepping

In order to find out an alternative control approach to overcome the shortcomings of feedback linearization, designers have conceived the concept of backstepping control law [3]. Indeed, the simplicity for first-order design can easily be extended to find out the control law for higher order nonlinear systems. In a recursive manner, one can easily construct the clf for n dimensional systems. For the sake of understandability, the authors have augmented the system of (2.39) by a simple integrator. Second-order state model of the resultant system is shown below in Eqs. (2.43.a, 2.43.b)

$$\dot{x} = -\sin x - x^3 + z \tag{2.43.a}$$

$$\dot{z} = u \tag{2.43.b}$$

Now, if the intended control objective is to ensure the regulation of $x(t)$, that is $x(t) \to 0$, as $t \to \infty$, for all $x(0)$ and $z(0)$. The state variable $z(t)$ must remain bounded during the stabilization process. Indeed, it is clear from Eqs. (2.43.a, 2.43.b) that the equilibrium of the system is located at (0, 0). Simply stated the design objective is to find out a feedback control input u for the system such that this equilibrium becomes a GAS one. The system is shown in the block diagram form in Fig. 2.3.

To construct a clf for system of Eqs. (2.43.a, 2.43.b), one can first construct a clf for its subsystem shown in the dashed box (dynamics of x). Instead of u, if z is being considered as the control input to the system of Eq. (2.43.a), then the system of Eqs. (2.43.a, 2.43.b) would become identical to that of the first-order system of Eq. (2.39). Therefore, one can easily construct a clf that is just a quadratic function of state variable x. That is $V_x = 0.5x^2$

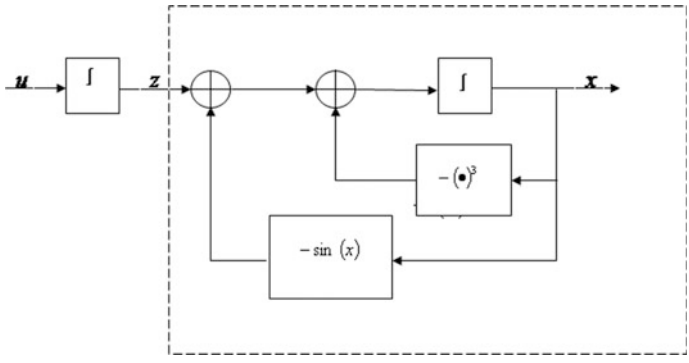

Fig. 2.3 Schematic diagram of Eqs. (2.43.a, 2.43.b)

According to the previous discussion of our last section, one can devise a feedback law $-c_1x + \sin x$ to ensure the proper regulation of the state variable x. If Eq. (2.43.a) is only considered then z appears as an input to the system as shown below

$$z = -c_1x + \sin x \tag{2.44}$$

However, one should not forget that z is not the actual control input; rather it is just an ordinary state variable. Simply stated it is not possible for the designers to shape the signal z according to their own requirements. One can only define the ideal value of the z as shown below in Eq. (2.45)

$$z_{\text{des}} = -c_1x + \sin x \cong \alpha_s(x) \tag{2.45}$$

Indeed, z is not the actual control input to the system; it only plays the role of a *virtual input* to the system of Eq. (2.43.a). The desired value of virtual control is defined as the stabilization function for the system of Eq. (2.43.a) [4]. Error can be defined as the difference between the virtual control and stabilization function as shown below

$$e = z - z_{\text{des}} = z - \alpha_s(x) = z + c_1x - \sin x \tag{2.46}$$

Now, one can rewrite the system Eqs. (2.43.a, 2.43.b) in (x, e) coordinate that will make the controller design task quite easy as illustrated in Fig. 2.4.

$$\dot{x} = -\sin x - x^3 + (z + c_1x - \sin x) - c_1x + \sin x = -c_1x - x^3 + e \tag{2.47.a}$$

$$\dot{e} = \dot{z} - \dot{\alpha}_s(x) = \dot{z} + (c_1 - \cos x)\dot{x} = u + (c_1 - \cos x)\left(-c_1x - x^3 + e\right) \tag{2.47.b}$$

The *stabilizing function* $\alpha_s(x)$ can be added up and accordingly subtracted from the $\dot{x}_1$ equation as shown in Fig. 2.4.

Then the signal $\alpha_s(x)$ is being used as a feedback control inside the dashed box and "backstep" $-\alpha_s(x)$ through the integrator as shown in Fig. 2.5.

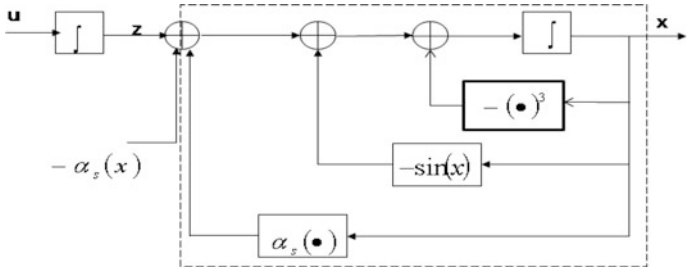

Fig. 2.4 Addition and subtraction of same stabilizing function in $\dot{x}$ equation

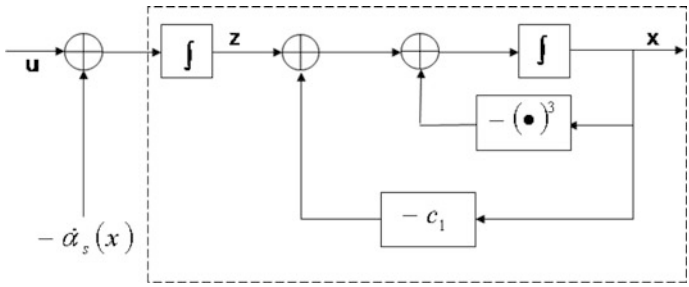

Fig. 2.5 Backstepping signal $\dot{\alpha}_s(x)$

One of the key features of backstepping is that it does not require any differentiator to realize the time derivative of $\dot{\alpha}_s(x)$ [3, 4]. Since it is a known function, it is always possible to compute its derivative analytically as shown in Eq. (2.48) below

$$\dot{\alpha}_s(x) = \frac{\partial \alpha_s}{\partial x}\dot{x} = -(c_1 - \cos x)\left(-c_1 x - x^3 + e\right) \tag{2.48}$$

A clf for the overall nonlinear system [as shown in Eqs. (2.43.a, 2.43.b)] must be constructed to design the control input for the system of Eqs. (2.43.a, 2.43.b). One obvious way of constructing the clf for the entire system is to augment a quadratic term of error variable e with it as shown in Eq. (2.49) below

$$V_a(x,z) = V(x) + \frac{1}{2}e^2 = \frac{1}{2}x^2 + \frac{1}{2}(z + c_1 x - \sin x)^2 \tag{2.49}$$

Differentiation of V_a with respect to time yields

$$\begin{aligned}\dot{V}_a(x,e,u) &= x(-c_1 x - x^3 + e) + e\left(u + (c_1 - \cos x)\left(-c_1 x - x^3 + e\right)\right) \\ &= -c_1 x^2 - x^4 + e\left(x + u + (c_1 - \cos x)\left(-c_1 x - x^3 + e\right)\right)\end{aligned} \tag{2.50}$$

Assuming that $\dot{V}_a$ be an analytic function, the design goal is to construct a control input in such a way that it could ensure the negative definiteness of $\dot{V}_a$. In order to achieve the control objective, a feedback control law can be designed to cancel out the cross-term xe, and the undesirable nonlinear terms. This is possible because u is multiplied by e due to chosen form of augmented Lyapunov function V_a. This is another salient feature of the backstepping. Hence, control input u can be chosen to make $\dot{V}_a$ negative definite in x and e. One obvious design choice is to make the bracketed term of the last Eq. (2.50) equal to $-c_2 e$, where $c_2 > 0$

$$\begin{aligned}u &= -c_2 e - x - (c_1 - \cos x)\left(-c_1 x - x^3 + e\right) \\ &= -c_2(z + c_1 x - \sin x) - x - (c_1 - \sin x)\left(z - \sin x - x^3\right)\end{aligned} \tag{2.51}$$

With this control input the derivative of the clf becomes

$$\dot{V}_a = -c_1 x^2 - x^4 - c_2 e^2 \tag{2.52}$$

Now the above definition of $\dot{V}_a$ proves that in (x, e) coordinate system the equilibrium point $(0, 0)$ is globally asymptotically stable. Now, $e = 0$ implies that $z = z_{\text{des}}$ that is virtual control becomes equal to stabilizing function, and it will ensure asymptotic stabilization of x. A careful observation of Eq. (2.45) reveals that $x = 0$ implies $z = 0$. Hence, the equilibrium point of the original system in (x, z) coordinate system $(0, 0)$ is also globally asymptotically stable. The resulting closed loop system in (x, e) coordinate is

$$\begin{bmatrix} \dot{x} \\ \dot{e} \end{bmatrix} = \begin{bmatrix} -c_1 - x^2 & 1 \\ -1 & -c_2 \end{bmatrix} \begin{bmatrix} x \\ e \end{bmatrix} \tag{2.53}$$

In the above equation, we are representing a nonlinear system in linear-like form. An important structural property of this system is that it is nonlinear "system matrix." This is another noteworthy feature of backstepping, it only cancels out undesirable nonlinear entries, whereas it does not to pay any extra effort to eliminate helpful nonlinearities from the system equation. However, another flexibility of the design is explained in the following example and consider the following system (2.54)

$$\begin{aligned} \dot{x} &= x^2 + xz \\ \dot{z} &= u \end{aligned} \tag{2.54}$$

Careful observation reveals that the system is uncontrollable at origin. Needless to say that feedback linearization fails to answer the control problems of the uncontrollable systems. However, backstepping can yield a fruitful solution to the above-mentioned problem. Now, if the equation of $\dot{x}$ is considered, then it turns out to be $f(x) = x^2$ and $g(x) = x$. Hence, clf can be constructed as $V(x) = \frac{1}{2}x^2$. Therefore, stabilizing function α_s can be designed to ensure the stabilization

$$\alpha_s(x) = -c_1 x^2 - x \tag{2.55}$$

Indeed, like the previous example here also z is playing the role of virtual control. Similar to the previous case error function can be defined as shown below

$$e = z - \alpha_s = z + c_1 x^2 + x \tag{2.56}$$

Similar to the previous case the system state model is again to be constructed in (x, e) coordinate

$$\begin{aligned}\dot{x} &= -c_1x^3 + ex \\ \dot{e} &= u + (1 + 2c_1x)\left(x^2 + xz\right)\end{aligned} \tag{2.57}$$

Now, the derivative of the augmented Lyapunov function $V_a = \frac{1}{2}x^2 + \frac{1}{2}e^2$ is shown below

$$\dot{V}_a = -c_1x^4 + e\left(u + (1 + 2c_1x)\left(x^2 + xz\right) + x^2\right) \tag{2.58}$$

The control law which makes the derivative of V_a negative definite is given by

$$u = -c_2e - (1 + 2c_1x)\left(x^2 + xz\right) - x^2 \tag{2.59}$$

The resulting system in the (x, z) coordinate is

$$\dot{x} = x^2 + xz \tag{2.60}$$

$$\dot{z} = -c_2z - c_2x - (c_1c_2 + 2)x^2 - zx - 2c_1x^2z - 2c_1x^3 \tag{2.61}$$

And its equilibrium (0, 0) is global asymptotic stable (Fig. 2.6).

It is clear from the Fig. 2.6 that an unstable and uncontrollable system can be stabilized using integrator backstepping. However, only one shortcoming of the backstepping control is that it requires the system to be in strict feedback system. However, if the system is not in strict feedback form, block backstepping can yield a plausible solution to such control problem [4]. Concept of block backstepping will be presented in the next section.

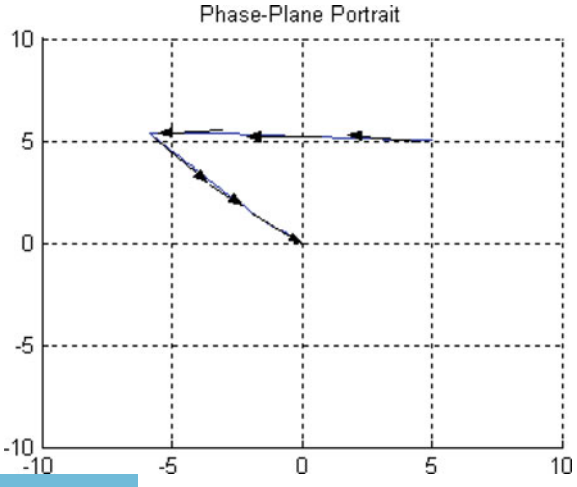

Fig. 2.6 Stabilization of an unstable system with integrator backstepping control design

2.4 Block Backstepping Design

Before proceeding to the actual concept of block backstepping, let us consider the state model of inertia wheel pendulum as shown in Fig. 2.2. As discussed above, collocated feedback linearization yields the following state model as shown in Eq. (2.62):

$$\begin{aligned} \dot{q}_1 &= p_1 \\ \dot{p}_1 &= C \sin q_1 - Du \\ \dot{q}_2 &= p_2 \\ \dot{p}_2 &= u \end{aligned} \tag{2.62}$$

where C and D are just two design constants (detailed description of C and D as well as the derivation of the state model are available in Appendix A.1). It is very easy to understand that the above-stated model is not in strict feedback form, and thereby restricts the application of conventional integrator backstepping. Therefore, one obvious choice left for the designers is to convert the state model into a form that is suitable for application of backstepping algorithm. Therefore, one can rely on algebraic state transformation as shown below

$$z_1 = q_2 - k(q_1 + p_1 + Dp_2) \tag{2.63}$$

Now the time derivative of z_1 yields

$$\dot{z}_1 = p_2 - k(p_1 + C \sin q_1) \tag{2.64}$$

However, the stabilizing function for Eq. (2.63) can be defined according to the following Eq. (2.65):

$$\alpha = -c_1 z_1 + k(p_1 + C \sin q_1) \tag{2.65}$$

Now, second error variable z_2 can be defined as shown in Eq. (2.66) below

$$z_2 = p_2 - \alpha_1 \tag{2.66}$$

Above definition of the z_2 yields

$$\dot{z}_1 = z_2 - c_1 z_1 \tag{2.67}$$

Differentiation of z_2 with respect to time

$$\dot{z}_2 = u - c_1(-c_1 z_1 + z_2) + k(2C \sin q_1 - Du) \tag{2.68}$$

Now, desired dynamics of z_2 is

$$\dot{z}_2 = -z_1 - c_2 z_2 \tag{2.69}$$

Therefore, one can select the following control input to ensure the desired dynamics for z_2 as shown below

$$u = \frac{1}{1 - kD}\left(-c_1^2 z_1 - c_1 z_2 - 2kC \sin q_1\right) \tag{2.70}$$

The control law u transforms the system into a block-strict feedback system

$$\begin{aligned} \dot{z}_1 &= -c_1 z_1 + z_2 \\ \dot{z}_2 &= -z_1 - c_2 z_2 \end{aligned} \tag{2.71}$$

However, it is not possible to reduce the order of the actual system. Therefore, it is easy to understand that the two states of the system comprise internal dynamics that has become unobservable from input output relationship of the system, where u is being considered as the input to the system and z is considered to be the output from the system. Therefore, two states of the original system can be chosen to represent the internal dynamics of the transformed system. Nevertheless, in order to derive the zeroing input for the system, let us start the derivation considering z_1 as the output from the system. Now the first-order time derivative of z_1 is shown below

$$\dot{z}_1 = p_2 - k(p_1 + C \sin q_1) \tag{2.72}$$

Subsequent differentiation of z_1 with respect to time yields

$$\ddot{z}_1 = u(1 + kD) - k(C \sin q_1 + C \cos q_1 p_1) \tag{2.73}$$

Hence, $\ddot{z}_1 = 0$ yields

$$u = \frac{k}{(1 + kD)}(C \sin q_1 + C \cos q_1 p_1) \tag{2.74}$$

That is zeroing input to the system, so when zeroing input to the system is applied to the system then the zero dynamics of the transformation can be expressed as shown below

$$\begin{aligned} \dot{q}_1 &= p_1 \\ \dot{p}_1 &= C \sin q_1 - \frac{kD}{(1 + kD)}(C \sin q_1 + C \cos q_1 p_1) \end{aligned} \tag{2.75}$$

Now, k should be selected in a judicial manner to ensure the stability of the entire nonlinear system. However, detailed discussions of block backstepping is beyond the scope of this book; for a comprehensive treatment on the said topic, readers may refer the book *Nonlinear and Adaptive Control Design* by Krstic et al.

2.5 Notes

Last few decades, the literature of nonlinear control engineering has been enriched by the potential contributions from applied mathematics and practicing engineers. However, it is impossible to discuss about all the potential design approaches of nonlinear control engineering in a single volume, as well as it is beyond the scope of this presentation. However, for detailed in-depth discussions on the said topic researchers may go through the references.

References

1. Isidori A (1991) Nonlinear control systems. Springer, Berlin
2. Khalil HK (1996) Nonlinear systems. Prentice Hall, USA
3. Kokotovic PV, Arcak M (2001) Constructive nonlinear control: a historical perspective. Automatica 37(5):637–662
4. Krstic M, Kanellakopoulos I, Kokotovic PV (1995) Nonlinear and adaptive control design. Wiley Interscience, New York
5. Liu Y, Yu H (2013) A survey of underactuated mechanical systems. IET Control Theory Appl 7 (7):921–935
6. Olfati-Saber R (2001) Nonlinear control of underactuated mechanical systems with application to robotics and aerospace vehicles. Ph.D. thesis, Department of Electrical Engineering and Computer, Massachusetts Institute of Technology
7. Van der Schaft J (1999) L2-gain and passivity in nonlinear control. Springer, New York
8. Slotine JJE, Li W (1991) Applied nonlinear control. Prentice Hall International, Upper Saddle River
9. Spong MW (1998) Underactuated mechanical systems. In: Control problems in robotics and automation, vol 230. Springer, Berlin, pp 135–150

Chapter 3
Block Backstepping Control of the Underactuated Mechanical Systems

Abstract Underactuated mechanical system [UMS] is a particular class of a multi output mechanical system that has more degrees of freedom than that of control inputs. According to Spong "*Underactuated mechanical systems have fewer control inputs than degrees of freedom and arise in applications, such as space and undersea robots, mobile robots, flexible robots, walking, brachiating, and gymnastic robots*" (Spong in Control problems in robotics and automation. Springer, Berlin, pp 135–150, 1998, [5]). Nonetheless, the complicated state model of this class of systems often makes the controller design tasks more difficult than that of the ordinary MIMO systems (Yu and Liu in IET Control Theory Appl 7:921–935, 2013, [6]). Comprehensive research on existing literature reveals that all the proposed approaches are either too complicated for practical implementation and only capable of ensuring guaranteed performance during theoretical analysis, or they are just apt for a particular application that reduces their scope of applicability on other control problems of similar nature (Rudra et al.). All these shortcomings of the previously proposed approaches had strongly motivated the authors to conceive an alternate control approach for achieving a tradeoff between theory and practice. However, while the authors were looking for a suitable control law that could be utilized to serve the said purpose, they observed different features of backstepping could help them to reach their objective. After that they toiled for a period of eighteen months, around the clock, and eventually they have devised a block backstepping control law, which is generalized enough to address the control problem of most of the UMS. Indeed, the proposed control law has initially been formulated to address only the stabilization problem of the UMS; even so, during further research it has been revealed that it can also be used to solve the tracking control problem for the same. This chapter presents a comprehensive description of

This chapter is based on :

"Nonlinear state feedback controller design for underactuated mechanical system: A modified block backstepping approach" by Shubhobrata Rudra, Ranjit Kumar Barai, and Madhubanti Maitra, which appeared in ISA Transactions, vol 53, issue 2, pp 317-326, March 2014, Copyright © 2013 ISA. Published by Elsevier Ltd. Permission obtained from Elsevier.

Electronic supplementary material The online version of this article (doi:10.1007/978-981-10-1956-2_3) contains supplementary material, which is available to authorized users.

S. Rudra et al., *Block Backstepping Design of Nonlinear State Feedback Control Law for Underactuated Mechanical Systems*, DOI 10.1007/978-981-10-1956-2_3

the control law together with some illustrations so as to make this book an easy-reading one. For the ease of understanding, at first, the proposed algorithm is described for 2-DOF UMS, and thereafter generalized version of the proposed control algorithm is presented to address the control problem of n-DOF UMSs.

3.1 Formulation of Generalized Block Backstepping Control Law for Underactuated Systems with Two Degrees of Freedom (2-DOF)

This section is structured as follows. At first, a precise description of the control problem with its proper analytical description is presented in Sect. 3.1.1. Thereafter, Sect. 3.1.2 describes the formulation of the proposed control algorithm for 2-DOF UMS in a systematic manner. After that, the stability aspects of the zero dynamics of the same is thoroughly analyzed in Sect. 3.1.3.

3.1.1 Problem Formulation

The state model of a 2-DOF underactuated system can be expressed as shown in the following Eq. (3.1):

$$\begin{aligned} \dot{q}_1 &= p_1 \\ \dot{q}_2 &= p_2 \\ \dot{p}_1 &= f_1(\boldsymbol{q},\boldsymbol{p}) + g_1(\boldsymbol{q})u \\ \dot{p}_2 &= f_2(\boldsymbol{q},\boldsymbol{p}) + g_2(\boldsymbol{q})u \end{aligned} \tag{3.1}$$

In the above equation, elements of column vector $\boldsymbol{q} = \mathrm{col}(q_1, q_2) \in \mathbb{R}^2$ represent the output variables of a generic 2-DOF UMS. Basically, the $\boldsymbol{q}$ vector represents the configuration vector of 2-DOF UMS. In addition, the time derivative of the configuration vector $\boldsymbol{q}$, is expressed as $\boldsymbol{p} = \mathrm{col}(p_1, p_2) \in \mathbb{R}^2$. Without any loss of generality, $\boldsymbol{p}$ vector can be termed as the velocity vector of the system. Additionally, $u \in \mathbb{R}$ denotes the control input to the system. In above definitions, "col" denotes the column vector. Actually, $f_1(\boldsymbol{q},\boldsymbol{p})$ and $f_2(\boldsymbol{q},\boldsymbol{p})$ are the nonlinear functions of $\boldsymbol{q}$ and $\boldsymbol{p}$ defined as $f_1(\boldsymbol{q},\boldsymbol{p}) : \mathbb{R}^4 \to \mathbb{R}$ and $f_2(\boldsymbol{q},\boldsymbol{p}) : \mathbb{R}^4 \to \mathbb{R}$. In addition $g_1(\boldsymbol{q})$ and $g_2(\boldsymbol{q})$ are the functions of the output variables (q_1, q_2) defined as $g_1(\boldsymbol{q}) : \mathbb{R}^2 \to \mathbb{R}$ and $g_2(\boldsymbol{q}) : \mathbb{R}^2 \to \mathbb{R}$. Also $f_1(\boldsymbol{q}, \boldsymbol{p})$, $f_2(\boldsymbol{q}, \boldsymbol{p})$, $g_1(\boldsymbol{q})$ and $g_2(\boldsymbol{q})$ are all C^1 functions. It implies all the four above-mentioned functions are differentiable, and they have continuous time derivatives. In addition, $f_1(\mathbf{0},\mathbf{0}) = 0$ and $f_2(\mathbf{0},\mathbf{0}) = 0$. Moreover, the state vector X can be expressed as $\boldsymbol{X} = [\,q_1 \quad q_2 \quad p_1 \quad p_2\,]^{\mathrm{T}} \in \mathbb{R}^4$.

The prime objective of the proposed control law is to devise a nonlinear state feedback control law, employing block backstepping technique such that it would ensure the asymptotic stability of the entire nonlinear system. In other words, if the

state error $\boldsymbol{E}$ is defined as $\boldsymbol{E} = \boldsymbol{X}(t) - \boldsymbol{X}_0$, where $\boldsymbol{X}(t)$ denotes the system states at time t and X_0 denotes the desired equilibrium point in the state space. Now, the goal of the control law u is to ensure that $|\boldsymbol{E}| \to 0$ as $t \to \infty$.

3.1.2 Derivation of the Control Algorithm for 2-DOF Underactuated Mechanical Systems

This subsection describes systematic development of the proposed control algorithm for 2-DOF mechanical systems. However, as discussed earlier in Sect. 2.2, application of conventional backstepping requires the system state model to be in the strict feedback form [1]. On the other hand, a minute observation on Eq. (3.1) reveals that the state model of the underactuated system is not in strict feedback form. Therefore, at the onset of the design, the state model of the system has been transformed into a block-strict feedback form. Interested readers may find the detailed mathematical formulation of block-strict feedback form in Chap. 2, Sect. 2.3.

Indeed, it is clear from the above discussion that direct application of conventional backstepping on the state model of the underactuated system is not possible. Hence, one left with an obvious choice of transforming the same into a convenient one. The pioneering work on converting the state model of the underactuated system in a convenient form was carried out by Olfati Saber [3]. Since it involves a few complex mathematical manipulations, it becomes too complicated for practical applications. So to get rid off from the shortcomings of Olfati's method, an effective transform has been proposed based on simple algebraic manipulations. At the onset of the design, state model of the system of Eq. (3.1) has been transformed into a reduced order model by means of an algebraic state transformation. Actually, the mentioned transform converts the system into a block-strict feedback form. Subsequently, in the next stage of design, expression of the control input u has been found out to stabilize the reduced order system at its origin. The derivation of the control algorithm is shown in the following steps of 1–4 as given below:

Step 1: At the onset, a new control variable $z_1 \in \mathbb{R}$ has been defined in terms of the original states. Quite often, the variable z_1 is also termed as first error variable.

$$z_1 = q_2 - k(q_1 + g_2 p_1 - g_1 p_2) \tag{3.2}$$

where k is a design constant. Now, the dynamics of z_1 is expressed in Eq. (3.3) as shown below:

$$\begin{aligned} \dot{z}_1 &= p_2 - k(p_1 + g_2 \dot{p}_1 + \dot{g}_2 p_1 - g_1 \dot{p}_2 - \dot{g}_1 p_2) \\ &= p_2 - k(p_1 + g_2(f_1 + g_1 u) + p_1 \mathbf{dg_2} \cdot \dot{\boldsymbol{q}} - g_1(f_2 + g_2 u) - p_2 \mathbf{dg_1} \cdot \dot{\boldsymbol{q}}) \\ &= p_2 - k(p_1 + g_2 f_1 + p_1 \mathbf{dg_2} \cdot \boldsymbol{p} - g_1 f_2 - p_2 \mathbf{dg_1} \cdot \boldsymbol{p}) \end{aligned} \tag{3.3}$$

In the above equation, $\mathbf{dg} = \begin{bmatrix} \frac{\partial g}{\partial q_1} & \frac{\partial g}{\partial q_2} \end{bmatrix}$. Henceforth, for ease of representation $f_1(\boldsymbol{q},\boldsymbol{p}), f_2(\boldsymbol{q},\boldsymbol{p}), g_1(\boldsymbol{q}), g_2(\boldsymbol{q})$ will be represented by f_1, f_2, g_1, g_2 respectively.

Step 2: In this step, a suitable stabilizing function should be defined to realize the desired value of the virtual input for the first subsystem. In this case a stabilizing function has been selected in a judicious manner to convert the original state model of the system into a strict feedback form. Therefore, a suitable stabilizing function has been selected to serve the said purpose, which is shown below in Eq. (3.4)

$$\alpha_1 = -c_1 z_1 + k(p_1 + g_2 f_1 + p_1 \mathbf{dg_2} \cdot \boldsymbol{p} - g_1 f_2 - p_2 \mathbf{dg_1} \cdot \boldsymbol{p}) \tag{3.4}$$

From the basic concepts of control system, it is very easy to understand that incorporation of integral action improves the steady state performance of the systems. Following the same philosophy, an integral action has also been incorporated with the state feedback law. As a matter of fact, expression of the stabilizing function [as described in Eq. (3.4)] has been modified as expressed in the following Eq. (3.5):

$$\alpha_1 = -c_1 z_1 - \lambda \chi_1 + k(p_1 + g_2 f_1 + p_1 \mathbf{dg_2} \cdot \boldsymbol{p} - g_1 f_2 - p_2 \mathbf{dg_1} \cdot \boldsymbol{p}) \tag{3.5}$$

where $\chi_1 = \int_0^t z_1 \mathrm{d}t$ and λ is a design constant.
With the above definition of stabilizing function, now the time derivative of z_1 could be expressed as shown in following Eq. (3.6):

$$\dot{z}_1 = p_2 - \alpha_1 - c_1 z_1 - \lambda \chi_1 \tag{3.6}$$

Step 3: In accordance with Eq. (3.6), the second error variable $(z_2 \in \mathbb{R})$ has been defined as the difference between stabilizing function and the virtual control in such a manner that the two variables z_1 and z_2 could be used to represent a reduced state model of the system in strict feedback form. The term reduced order will be explained in detail at Sect. 3.2.3. In this case, it has been defined according to Eq. (3.7):

$$z_2 = p_2 - \alpha_1 \tag{3.7}$$

Consequently, from Eqs. (3.6) and (3.7) one can represent the time derivative of z_1 as shown below in Eq. (3.8):

$$\dot{z}_1 = z_2 - c_1 z_1 - \lambda \chi_1 \tag{3.8}$$

Differentiation of second control variable z_2 with respect to time has resulted in:

$$
\begin{aligned}
\dot{z}_2 &= \dot{p}_2 - \dot{\alpha}_1 \\
&= f_2 + g_2 u + c_1 \dot{z}_1 + \lambda z_1 \\
&\quad - k\left[\left\{\dot{p}_1 + \dot{g}_2 f_1 + g_2 \dot{f}_1 + \dot{p}_1 \mathbf{dg_2} \cdot \boldsymbol{p} + p_1 \mathbf{dg_2} \cdot \dot{\boldsymbol{p}} + p_1\left(\frac{\partial^2 g_2}{\partial q_1^2} p_1^2 + 2\frac{\partial^2 g_2}{\partial q_1 \partial q_2} p_1 p_2 + \frac{\partial^2 g_2}{\partial q_2^2} p_2^2\right)\right\}\right. \\
&\quad \left. -\left\{\dot{g}_1 f_2 + g_1 \dot{f}_2 + \dot{p}_2 \mathbf{dg_1} \cdot \boldsymbol{p} + p_2 \mathbf{dg_1} \cdot \dot{\boldsymbol{p}} + p_2\left(\frac{\partial^2 g_1}{\partial q_1^2} p_1^2 + 2\frac{\partial^2 g_1}{\partial q_1 \partial q_2} p_1 p_2 + \frac{\partial^2 g_1}{\partial q_2^2} p_2^2\right)\right\}\right] \\
&= (f_2 + g_2 u) + c_1(z_2 - c_1 z_1 - \lambda \chi_1) + \lambda z_1 \\
&\quad - k[\{f_1 + g_1 u + f_1 \mathbf{dg_2} \cdot \boldsymbol{p} + g_2 \mathbf{df}_1 . \dot{\boldsymbol{X}} + (f_1 + g_1 u)\mathbf{dg_2} \cdot \boldsymbol{p} \\
&\quad + p_1\left(\frac{\partial g_2}{\partial q_1}(f_1 + g_1 u) + \frac{\partial g_2}{\partial q_2}(f_2 + g_2 u)\right) + p_1\left(\frac{\partial^2 g_2}{\partial q_1^2} p_1^2 + 2\frac{\partial^2 g_2}{\partial q_1 \partial q_2} p_1 p_2 + \frac{\partial^2 g_2}{\partial q_2^2} p_2^2\right)\Big\} \\
&\quad - \{f_2 \mathbf{dg_1} \cdot \boldsymbol{p} + g_1 \mathbf{df_2} \cdot \dot{\boldsymbol{X}} + (f_2 + g_2 u)\mathbf{dg_1} \cdot \boldsymbol{p} \\
&\quad + p_2\left(\frac{\partial g_1}{\partial q_1}(f_1 + g_1 u) \; + \; \frac{\partial g_1}{\partial q_2}(f_2 + g_2 u)\right) + p_2\left(\frac{\partial^2 g_1}{\partial q_1^2} p_1^2 + 2\frac{\partial^2 g_1}{\partial q_1 \partial q_2} p_1 p_2 + \frac{\partial^2 g_1}{\partial q_2^2} p_2^2\right)\Big\}\Big]
\end{aligned}
$$

$$
\begin{aligned}
&= (f_2 + g_2 u) + c_1(z_2 - c_1 z_1 - \lambda \chi_1) + \lambda z_1 - k[\{f_1 + g_1 u + f_1 \mathbf{dg_2} \cdot \boldsymbol{p} + (f_1 + g_1 u)\mathbf{dg_2} \cdot \boldsymbol{p} \\
&\quad + g_2\left(\frac{\partial f_1}{\partial q_1} p_1 + \frac{\partial f_1}{\partial p_1}(f_1 + g_1 u) + \frac{\partial f_1}{\partial q_2} p_2 + \frac{\partial f_1}{\partial p_2}(f_2 + g_2 u)\right) \\
&\quad + p_1\left(\frac{\partial g_2}{\partial q_1}(f_1 + g_1 u) + \frac{\partial g_2}{\partial q_2}(f_2 + g_2 u)\right) + p_1\left(\frac{\partial^2 g_2}{\partial q_1^2} p_1^2 + 2\frac{\partial^2 g_2}{\partial q_1 \partial q_2} p_1 p_2 + \frac{\partial^2 g_2}{\partial q_2^2} p_2^2\right)\Big\} \\
&\quad - \{f_2 \mathbf{dg_1} \cdot \boldsymbol{p} + (f_2 + g_2 u)\mathbf{dg_1} \cdot \boldsymbol{p} + g_1\left(\frac{\partial f_2}{\partial q_1} p_1 + \frac{\partial f_2}{\partial p_1}(f_1 + g_1 u) + \frac{\partial f_2}{\partial q_2} p_2 + \frac{\partial f_2}{\partial p_2}(f_2 + g_2 u)\right) \\
&\quad + p_2\left(\frac{\partial g_1}{\partial q_1}(f_1 + g_1 u) + \frac{\partial g_1}{\partial q_2}(f_2 + g_2 u)\right) + p_2\left(\frac{\partial^2 g_1}{\partial q_1^2} p_1^2 + 2\frac{\partial^2 g_1}{\partial q_1 \partial q_2} p_1 p_2 + \frac{\partial^2 g_1}{\partial q_2^2} p_2^2\right)\Big\}\Big] \\
&= \psi u + \lambda z_1 + c_1(z_2 - c_1 z_1 - \lambda \chi_1) + \phi
\end{aligned}
\tag{3.9}
$$

where,

$$
\begin{aligned}
\psi = g_2 - k\Big\{ & g_1 + g_1 g_2 \frac{\partial f_1}{\partial p_1} + g_2^2 \frac{\partial f_1}{\partial p_2} + g_1 \mathbf{dg_2} \cdot \boldsymbol{p} + p_1 \frac{\partial g_2}{\partial q_1} g_1 + p_1 \frac{\partial g_2}{\partial q_2} g_2 \\
& - g_1^2 \frac{\partial f_2}{\partial p_1} - g_1 g_2 \frac{\partial f_2}{\partial p_2} - g_2 \mathbf{dg_1} \cdot \boldsymbol{p} - p_2 \frac{\partial g_1}{\partial q_1} g_1 - p_2 \frac{\partial g_1}{\partial q_2} g_2 \Big\}
\end{aligned}
\tag{3.10}
$$

and

$$\phi = f_2 - k\left[\left\{f_1 + 2f_1 \boldsymbol{dg_2}\cdot\boldsymbol{p} + p_1\left(\frac{\partial g_2}{\partial q_1}f_1 + \frac{\partial g_2}{\partial q_2}f_2 + \frac{\partial^2 g_2}{\partial q_1^2}p_1^2 + 2\frac{\partial^2 g_2}{\partial q_1 \partial q_2}p_1 p_2 + \frac{\partial^2 g_2}{\partial q_2^2}p_2^2\right)\right\}\right.$$
$$+\left\{g_2\left(\frac{\partial f_1}{\partial q_1}p_1 + \frac{\partial f_1}{\partial q_2}p_2 + \frac{\partial f_1}{\partial p_1}f_1 + \frac{\partial f_1}{\partial p_2}f_2\right) - g_1\left(\frac{\partial f_2}{\partial q_1}p_1 + \frac{\partial f_2}{\partial q_2}p_2 + \frac{\partial f_2}{\partial p_1}f_1 + \frac{\partial f_2}{\partial p_2}f_2\right)\right\}$$
$$\left.-\left\{2f_2 \boldsymbol{dg_1}\cdot\boldsymbol{p} + p_2\left(\frac{\partial g_1}{\partial q_1}f_1 + \frac{\partial g_1}{\partial q_2}f_2\frac{\partial^2 g_2}{\partial q_1^2}p_1^2 + 2\frac{\partial^2 g_2}{\partial q_1 \partial q_2}p_1 p_2 + \frac{\partial^2 g_2}{\partial q_2^2}p_2^2\right)\right\}\right] \tag{3.11}$$

As stated earlier, the design Steps 1–3 has actually transformed the original state model of the underactuated system described in Eq. (3.1) into a strict feedback form. This approach has eventually yielded a convenient design of control law.

Step 4: It is the final step and it gives the control law u so as to attain the desired dynamics of the z_1 and z_2 i.e. $\dot{z}_1 = -\lambda_1\chi_1 - c_1 z_1 + z_2$ and $\dot{z}_2 = -z_1 - c_2 z_2$. The desired dynamics of z_2 is expressed in Eq. (3.11) as following:

$$\dot{z}_2 = -z_1 - c_2 z_2 \tag{3.12}$$

Please note that the dynamics z_1 as mentioned in Eq. (3.8) together with the desired dynamics of z_2 as shown in the above Eq. (3.12) describe the dynamics of a stable system, which resembles the state model of a second order stable system with two poles located at $-c_1$, and $-c_2$, respectively. State model of the reduced order system in z_1, z_2 coordinate is shown below:

$$\begin{aligned}\dot{z}_1 &= z_2 - c_1 z_1 - \lambda\chi_1\\ \dot{z}_2 &= -z_1 - c_2 z_2\end{aligned} \tag{3.13}$$

Consequently, from Eqs. (3.8) and (3.12), expression of the desired control law could be found out in the following manner:

$$\begin{aligned}&\psi u + \lambda z_1 + c_1(z_2 - c_1 z_1 - \lambda\chi_1) + \phi = -z_1 - c_2 z_2\\ &\text{or, } \psi u = -\lambda z_1 - c_1(z_2 - c_1 z_1 - \lambda\chi_1) - \phi - z_1 - c_2 z_2\\ &\text{or, } u = \psi^{-1}\left[-\left(1 - c_1^2 + \lambda\right)z_1 - (c_1 + c_2)z_2 + \lambda c_1\chi_1 - \phi\right]\end{aligned} \tag{3.14}$$

The proposed control law of Eq. (3.14) transforms the closed loop system in the state model of Eq. (3.13).

3.1.3 Zero Dynamics Analysis of 2-DOF Underactuated Mechanical System

Systematic derivation of the proposed control law for the 2-DOF UMS has been presented in Sect. 3.1.2. Expression of the control input is shown in Eq. (3.14). However, a minute observation on the proposed control law reveals that the control law [described in Eq. (3.14)] only ensures the stability of the transformed system in z_1, z_2 coordinate system [4]. Nonetheless, the algebraic state transformation has just converted the original fourth order underactuated state model of Eq. (3.1) into a reduced order state model (described by z_1 and z_2). Conversely, from the basic concepts of control engineering it can be stated that if a state model that does not contain any redundant state represents a system, it is impossible to reduce the dimension of that very system by means of any feasible state transformation! and herein lies the importance of internal dynamics. For an in-depth study on Internal Dynamics readers may refer to [2]. Actually, the proposed state transformation of Sect. 3.2.2 just has transfigured the system into a block-strict feedback form, while the $z_1 - z_2$ subsystem describes the system in strict feedback form, other two state variables (among q_1, q_2, p_1, and p_2) must be selected to represent the internal dynamics of the block-strict feedback form. In this case, q_1 and p_1 have been selected to represent the zero dynamics of the system. Needless to say, that the stability of internal dynamics can only be assessed by means of zero dynamics analysis [4]. Hence, in the subsequent section, zero dynamics state model will be utilized to represent the internal dynamics of the system.

In this research, during the derivation of zero dynamics, z_1 has been considered as a virtual output from the nonlinear system. Hence, it can be easily concluded that if someone wants to derive the zero dynamics for the above-mentioned nonlinear system, he must have to find out the expression of control input u that drives z_1 identically equal to zero. Subsequently, z_1, first time derivative of z_1, and second time derivative of z_1 have been found out to realize the desired expression of control law u that will drive z_1 identically equal to zero.

The first order differentiation of z_1 yields the dynamics of Eq. (3.15). Thus, the second order differentiation of z_1 results in the following dynamics.

$$\begin{aligned}\ddot{z}_1 &= \dot{z}_2 - c_1\dot{z}_1 - \lambda z_1 \\ &= \psi u + \lambda z_1 + c_1\dot{z}_1 + \vartheta - c_1\dot{z}_1 - \lambda z_1 \\ &= \psi u + \vartheta\end{aligned} \tag{3.15}$$

So it is quite evident from the above expression (3.15) that the two successive differentiations of z_1 establishes an explicit relationship between z_1 (output) and u (input). Therefore, if z_1 is treated as an output of the system then the relative degree of the overall underactuated system becomes *two* [4]. Hence, from the concept of output feedback linearization one can conclude that the state transformation described in Sect. 3.2.2, has yielded an unobservable internal dynamics of order two.

Since two successive differentiation of z_1 is required to establish an explicit relationship between input and output, the variable z_1, the first derivative of z_1 ($\dot{z}_1$) and second derivative of z_1 ($\ddot{z}_1$) must be equal to zero for the derivation of zero dynamics [4]. Now, in order to represent the system's internal dynamics in terms of q_1 and p_1, the other two variables q_2 and p_2 must be expressed in terms of q_1 and p_1. Therefore, from the following equations, it is possible to represent the zero dynamics of the system in terms of q_1 and p_1 as shown in the following equation set (3.16.a–3.16.c):

$$z_1 = q_2 - k(q_1 + p_1 - g_1 p_2) = 0 \Rightarrow q_2 = k(q_1 + p_1 - g_1 p_2) \tag{3.16.a}$$

$$\dot{z}_1 = p_2 - k(p_1 + f_1 - p_2 \mathrm{d}g_1 \cdot p) = 0 \Rightarrow p_2 = k(p_1 + f_1 - p_2 \mathrm{d}g_1 \cdot p)$$

$$p_2 = k(p_1 + f_1)/(1 + k\mathrm{d}g_1 \cdot p) \tag{3.16.b}$$

$$\ddot{z}_1 = \psi u + \vartheta = 0 \Rightarrow u = -\psi^{-1}\vartheta \tag{3.16.c}$$

Consequently, one can represent the dynamics of q_1, p_1 subsystem together with the input u of Eq. (3.16.c) as:

$$\begin{aligned} \dot{q}_1 &= p_1 \\ \dot{p}_1 &= f_1 + g_1 u = f_1 - g_1\left(\psi^{-1}\vartheta\right) = F(q_1, p_1) \end{aligned} \tag{3.17}$$

Now, if the parameter k is selected in such a manner to ensure the zero dynamics [vide Eq. (3.17)] stability of the transformed system, it will ensure the asymptotic convergences of q_1 and p_1 to their desired equilibriums. Now, convergences of z_1, q_1 and p_1, automatically ensure the asymptotic convergence of each of q_2 and p_2 to their desired equilibrium points.

Remark 3.1 The above formulation is not rigid or specific for a particular underactuated system. Similar type of control algorithms can be obtained by defining a new set of state variables like: $z_1 = q_2 - kq_1$.

Remark 3.2 The control law relies on the fact that ψ is invertible. In case of control law design for real-time implementations, it is always possible to select a value of k that will ensure the invertibility of ψ and the stability of the zero dynamics, simultaneously. In this context, it must be noted that although k is a crucial design factor and calculation of zero dynamics appeared to be a complicated one, yet the designers can always find out the value of parameter k offline, before the real-time run. Needless to say that this facility of evaluating the suitable value of controller parameter k by offline calculation, considerably simplifies the implementation of the proposed control law during practical applications.

Remark 3.3 The proposed control law asymptotically stabilizes the equilibrium of the original fourth order state model of the 2-DOF UMS in large.

Remark 3.4 The state model of the underactuated system shown in Eq. (3.3) is not in strict feedback form. Therefore, an algebraic transformation has been utilized to convert the system into a reduced order strict feedback form. The aforementioned transformation together with the control input u of Eq. (3.14) has resulted in the reduced order system of Eq. (3.13) and the zero dynamics equation of (3.17).

Remark 3.5 Another significant feature of the proposed block backstepping design is that the transformation of the system into block-strict feedback form is carried out during the design of control algorithm, which makes it more compact than its predecessor backstepping based approaches.

Remark 3.6 The integral action is incorporated into the proposed backstepping technique by modifying the conventional stabilizing function. Thus, the ultimate control input that is derived by the proposed modified block backstepping technique would enhance the steady state performance of the system.

3.2 Formulation of Generalized Block Backstepping Control Law for Underactuated Systems with *N* Degrees of Freedom

In this section, the systematic derivation of the control law for a generic n-DOF underactuated system is described. Similar to the earlier Sect. 3.1, here also at first the dynamics of a generalized UMS model is discussed, and then the formulation of a generalized block backstepping based control algorithm is described in a systematic manner.

3.2.1 Problem Formulation

The generic Lagrangian model of an n-DOF underactuated system is shown in Eq. (3.18)

$$\begin{aligned} m_{11}(\boldsymbol{q})\ddot{\boldsymbol{q}}_{\boldsymbol{1}} + m_{12}(\boldsymbol{q})\ddot{\boldsymbol{q}}_{\boldsymbol{2}} + \boldsymbol{h}_1(\boldsymbol{q},\boldsymbol{p}) &= 0 \\ m_{21}(\boldsymbol{q})\ddot{\boldsymbol{q}}_{\boldsymbol{1}} + m_{22}(\boldsymbol{q})\ddot{\boldsymbol{q}}_{\boldsymbol{2}} + \boldsymbol{h}_2(\boldsymbol{q},\boldsymbol{p}) &= B(\boldsymbol{q})\tau \end{aligned} \tag{3.18}$$

where, $\boldsymbol{q}_{\boldsymbol{1}} \in \mathbb{R}^{n_1}$, $\boldsymbol{q}_{\boldsymbol{2}} \in \mathbb{R}^{n_2}$ and $\boldsymbol{q} = col(\boldsymbol{q}_{\boldsymbol{1}}, \boldsymbol{q}_{\boldsymbol{2}}) \in \mathbb{R}^n$ is the configuration vector of nth degree of freedom UMS. In the above representation $\boldsymbol{q}_{\boldsymbol{1}}$ represents passive joint configuration variables, and $\boldsymbol{q}_{\boldsymbol{2}}$ represents active joint configuration variables. The dimension of the overall configuration manifold is $n_1 + n_2 = n$. The time derivative of the configuration vector $\boldsymbol{q}$ is expressed as $\boldsymbol{p} = \text{col}(\boldsymbol{p}_{\boldsymbol{1}}, \boldsymbol{p}_{\boldsymbol{2}}) \in \mathbb{R}^n$, and $\tau \in \mathbb{R}^{n_2}$ is the control input. In the above representation, $\boldsymbol{h}_1(\boldsymbol{q},\boldsymbol{p}) : \mathbb{R}^{2n} \rightarrow \mathbb{R}^{n_1}$ and $\boldsymbol{h}_2(\boldsymbol{q},\boldsymbol{p}) :$

$\mathbb{R}^{2n} \rightarrow \mathbb{R}^{n_2}$ contain the coriolis, centrifugal and gravity terms. Whereas, $m_{ij}(\boldsymbol{q})$ $q = 1, 2$, represents the components of the $n \times n$ inertia matrix, which is symmetric and positive definite for all $\boldsymbol{q}$. $B(\boldsymbol{q}) \in \mathbb{R}^{n_2 \times n_2}$ represents a full rank matrix. According to Spong, there exists an invertible change of the control input $\boldsymbol{\tau}$ as shown in Eq. (3.19) [5].

$$\tau = B^{-1}(\boldsymbol{q})\left(\left(\boldsymbol{h}_2(\boldsymbol{q},\boldsymbol{p}) - m_{21}(\boldsymbol{q})m_{11}^{-1}(\boldsymbol{q})\boldsymbol{h}_1(\boldsymbol{q},\boldsymbol{p})\right) + \left(m_{22}(\boldsymbol{q}) - m_{21}(\boldsymbol{q})m_{11}^{-1}(\boldsymbol{q})m_{12}(\boldsymbol{q})\right)\boldsymbol{u}\right) \tag{3.19}$$

that transforms the Lagrangian model of Eq. (3.18) into

$$\begin{aligned} \dot{\boldsymbol{q}}_1 &= \boldsymbol{p}_1 \\ \dot{\boldsymbol{q}}_2 &= \boldsymbol{p}_2 \\ \dot{\boldsymbol{p}}_1 &= \boldsymbol{f}(\boldsymbol{q},\boldsymbol{p}) + g(\boldsymbol{q})\boldsymbol{u} \\ \dot{\boldsymbol{p}}_2 &= \boldsymbol{u} \end{aligned} \tag{3.20}$$

where, $f(\boldsymbol{q},\boldsymbol{p}) : \mathbb{R}^{2n} \rightarrow \mathbb{R}^{n_1}$, $g(\boldsymbol{q}) \in \mathbb{R}^{n_1 \times n_2}$ are given by

$$\begin{aligned} \boldsymbol{f}(\boldsymbol{q},\boldsymbol{p}) &= -m_{11}^{-1}(\boldsymbol{q})\boldsymbol{h}_1(\boldsymbol{q},p) \\ g(\boldsymbol{q}) &= -m_{11}^{-1}(\boldsymbol{q})m_{12}(\boldsymbol{q}) \end{aligned} \tag{3.21}$$

The state vector can be expressed as $\boldsymbol{X} = [\boldsymbol{q}_1 \quad \boldsymbol{p}_1 \quad \boldsymbol{q}_2 \quad \boldsymbol{p}_2] \in \mathbb{R}^{2n}$. Now, the objective is to design a nonlinear state feedback control input $\boldsymbol{u}$ for the UMS of Eq. (3.21) by employing block backstepping technique such that it would ensure the asymptotic stability of the system. In other words, if the state error $\boldsymbol{E}$ is defined as $\boldsymbol{E} = \boldsymbol{X}(t) - \boldsymbol{X}_0$, where $\boldsymbol{X}(t)$ denotes the system states at time t and X_0 denotes the desired equilibrium point in the state space, then the goal of the control law $\boldsymbol{u}$ is to ensure that $|\boldsymbol{E}| \rightarrow 0$ as $t \rightarrow \infty$.

3.2.2 *Derivation of the Control Law for n-DOF Underactuated Mechanical Systems*

A minute observation of the state model, which is described in Eq. (3.20), reveals the fact that like 2-DOF underactuated system state model it also fails to satisfy the prerequisite condition of integrator backstepping. Hence, following the similar state transformation approach of last section, at first the state model of a n-DOF system has been transfigured [shown in (3.21)] into a reduced order state model in

block-strict form, and then the expression of control input $\boldsymbol{u}$ is found out to stabilize the reduced order system at its desired equilibrium. The derivation of the control algorithm is shown in the following steps 1–4 as given below:

Step 1: Following the same design philosophy, which the authors have introduced for 2-DOF underactuated system, the control law for n-DOF system has been derived. Therefore, a new control variable $\boldsymbol{z_1} \in \mathbb{R}^{n_2}$ has been defined to convert the state model of the system in block-strict form. Please note that the dimension of actuated configuration variable is also n_2. During this design, the authors have defined $\boldsymbol{z_1}$ in such a manner that dimension of $\boldsymbol{z_1}$ has also become n_2. Formal definition of $\boldsymbol{z_1}$ is shown below in Eq. (3.22)

$$\boldsymbol{z_1} = \boldsymbol{q_2} - K(\boldsymbol{q_1} + \boldsymbol{p_1} - g\boldsymbol{p_2}) \tag{3.22}$$

where, $K \in \mathbb{R}^{n_2 \times n_1}$ is a constant matrix such that $K_{ij} = k$ only when $i = j$ or $K_{ij} = 0$ otherwise. In the above equation, $g(\boldsymbol{q})$ is represented by g, and henceforth for the ease of representation, $\boldsymbol{f}(\boldsymbol{q},\boldsymbol{p})$ and $g(\boldsymbol{q})$ will be denoted by $\boldsymbol{f}$ and g, respectively. Construction of K matrix can be illustrated with the following examples of a six dimensional system where the dimension of actuated configuration variable is 4 $\left(\boldsymbol{q_2} \in \mathbb{R}^4\right)$, and the dimension of unactuated configuration variable is 2 $\left(\boldsymbol{q_1} \in \mathbb{R}^2\right)$. structure of K matrix is shown in Eq. (3.23)

$$K = \begin{bmatrix} k_1 & 0 \\ 0 & k_2 \\ 0 & 0 \\ 0 & 0 \end{bmatrix} \tag{3.23}$$

In order to find out the expression of stabilizing function, time derivative of $\boldsymbol{z_1}$ has been calculated as shown in the following Eq. (3.24):

$$\begin{aligned} \dot{\boldsymbol{z}}_1 &= \boldsymbol{p_2} - K(\boldsymbol{p_1} + \boldsymbol{f} + g\boldsymbol{u} - g\boldsymbol{u} - D(g)\boldsymbol{p_2}) \\ &= \boldsymbol{p_2} - K(\boldsymbol{p_1} + \boldsymbol{f} - D(g)\boldsymbol{p_2}) \end{aligned} \tag{3.24}$$

In above representation $D(g) \in \mathbb{R}^{n_1 \times n_2}$ represents the time differentiation of matrix $g(\boldsymbol{q})$, where any element of $D(g)$ can be expressed as $D\left(g_{ij}\right) = \sum_{k=1}^{n} \frac{\partial g_{ij}}{\partial q_k} p_k$, where i and j indicates the position of the elements of $D(g)$ matrix. Construction of $D(g)$ matrix is explained in the following example.

Consider a very simple underactuated system in which $q_2 \in \mathbb{R}^{n_2}$ and $q_1 \in \mathbb{R}$, the state model of the system can easily be represented by the following generic state model:

$$\begin{aligned}
\dot{q}_1 &= p_1 \\
\begin{bmatrix} \dot{q}_{21} \\ \dot{q}_{22} \end{bmatrix} &= \begin{bmatrix} p_{21} \\ p_{22} \end{bmatrix} \\
\dot{p}_1 &= f(\boldsymbol{q},\boldsymbol{p}) + [\, g_1(\boldsymbol{q}) \quad g_2(\boldsymbol{q}) \,] \begin{bmatrix} u_1 \\ u_2 \end{bmatrix} \\
\begin{bmatrix} \dot{p}_{21} \\ \dot{p}_{22} \end{bmatrix} &= \begin{bmatrix} u_1 \\ u_2 \end{bmatrix}
\end{aligned} \tag{3.25}$$

Please note that in the above state model two bracketed terms q_{21} and q_{22} basically represent the elements of $\boldsymbol{q_2}$ vector, similarly p_{21} and p_{22} represent the components of $\boldsymbol{p_2}$ vector. Clearly the above state model represents a 3-DOF underactuated system with two inputs and 3 outputs. Now if we try to realize the structure of $D(g)$ matrix then it will take the following shape as described in Eq. (3.26)

$$D(g) = \left[\frac{\partial g_1}{\partial q_1} p_1 + \frac{\partial g_1}{\partial q_{21}} p_{21} + \frac{\partial g_1}{\partial q_{22}} p_{22} \quad \frac{\partial g_2}{\partial q_1} p_1 + \frac{\partial g_2}{\partial q_{21}} p_{21} + \frac{\partial g_2}{\partial q_{22}} p_{22} \right] \tag{3.26}$$

Step 2: Similar to the previous case, stabilizing function for the $\boldsymbol{z_1}$ subsystem has been chosen to ensure the desired dynamics behavior of $\boldsymbol{z_1}$. Mathematical expression of the stabilizing function is shown in Eq. (3.27) below:

$$\boldsymbol{\alpha_1} = -c_1 \boldsymbol{z_1} - \lambda \boldsymbol{\chi_1} + K(\boldsymbol{p_1} + \boldsymbol{f} - D(g)\boldsymbol{p_2}) \tag{3.27}$$

Needless to say that the second term of the right hand side of the above equation denotes integral action ($\boldsymbol{\chi_1} = \int_0^t \boldsymbol{z_1} dt$ and λ is an arbitrary positive design constant) that has been incorporate to enhance the steady state performance. In above equation c_1 is a positive design constant that controls the rate of convergence of the regulated variables.

Step 3: Likewise the previous case, a second error variable $\boldsymbol{z_2} \in \mathbb{R}^{n_2}$ has been defined according to Eq. (3.28):

$$\boldsymbol{z_2} = \boldsymbol{p_2} - \boldsymbol{\alpha_1} \tag{3.28}$$

By virtue of the above definition of second control variable $\boldsymbol{z_2}$ variable, $\dot{\boldsymbol{z}}_1$ has become:

$$\dot{\boldsymbol{z}}_1 = \boldsymbol{z_2} - c_1 \boldsymbol{z_1} - \lambda \boldsymbol{\chi_1} \tag{3.29}$$

Dynamics of second error variable $\boldsymbol{z_2}$ can be expressed as:

$$\begin{aligned}\dot{\boldsymbol{z}}_2 &= \dot{\boldsymbol{p}}_2 - \dot{\boldsymbol{\alpha}}_1 \\ &= \boldsymbol{u} + c_1\dot{\boldsymbol{z}}_1 + \lambda \boldsymbol{z}_1 - K\left(\dot{\boldsymbol{p}}_1 + \dot{\boldsymbol{f}} - D(g)\dot{\boldsymbol{p}}_2 - D^2(g)\boldsymbol{p}_2\right) \\ &= \boldsymbol{u} + c_1(\boldsymbol{z}_2 - c_1\boldsymbol{z}_1 - \lambda\boldsymbol{\chi}_1) + \lambda\boldsymbol{z}_1 \\ &\quad - K\left[\boldsymbol{f} + g\boldsymbol{u} + Df_{q1}\boldsymbol{p}_1 + Df_{q2}\boldsymbol{p}_2 + Df_{p1}(\boldsymbol{f} + g\boldsymbol{u})\right. \\ &\quad \left. + Df_{p2}\boldsymbol{u} - D(g)\boldsymbol{u} - D^2(g)\boldsymbol{p}_2\right]\end{aligned} \tag{3.30}$$

In Eq. (3.30), $Df_{q1} \in \mathbb{R}^{n_1 \times n_1}$, $Df_{q2} \in \mathbb{R}^{n_1 \times n_2}$, $Df_{p1} \in \mathbb{R}^{n_1 \times n_1}$ and $Df_{p2} \in \mathbb{R}^{n_1 \times n_2}$ represent the matrices of partial derivatives of $\boldsymbol{f}$ vector with respect to different sub-component of state vector such as $\boldsymbol{q_1}$, $\boldsymbol{q_2}$, $\boldsymbol{p_1}$ and $\boldsymbol{p_2}$. In order to enhance the comprehensibility of this text, the authors have again considered the generic 3-DOF state model of Eq. (3.25) to explain the construction of the above-mentioned matrices. For the system of (3.25) they will take the following shape as shown in equation series (3.31.a–3.31.d) below:

$$Df_{q1} = \frac{\partial f}{\partial q_1} \tag{3.31.a}$$

$$Df_{q2} = \begin{bmatrix} \frac{\partial f}{\partial q_{21}} & \frac{\partial f}{\partial q_{22}} \end{bmatrix} \tag{3.31.b}$$

$$Df_{p1} = \frac{\partial f}{\partial p_1} \tag{3.31.c}$$

$$Df_{p2} = \begin{bmatrix} \frac{\partial f}{\partial p_{21}} & \frac{\partial f}{\partial p_{22}} \end{bmatrix} \tag{3.31.d}$$

$D_2(g) \in \mathbb{R}^{n_1 \times n_2}$ is given by $D^2(g) = \left[D_1^2(g) + D_2^2(g)\right]$. The definition of $D_1^2(g)$ and $D_2^2(g)$ are as follows:

$$D_1^2(g_{ij}) = \sum_{l=1}^{n}\sum_{k=1}^{n}\frac{\partial^2 g_{ij}}{\partial q_k \partial q_l}p_k p_l \tag{3.32}$$

$$D_2^2(g_{ij}) = \sum_{k=1}^{n}\frac{\partial g_{ij}}{\partial q_k}\dot{p}_k \tag{3.33}$$

In the above expression, p_k and p_l represents the individual elements of p vector. similar to the previous case, we can exemplify the structure of $D_1^2(g)$ and $D_2^2(g)$ matrix as shown in the following equation series (3.34.a, 3.34.b):

$$D_1^2(g) = \begin{bmatrix} \frac{\partial^2 g_1}{\partial q_1^2}p_1^2 + \frac{\partial^2 g_1}{\partial q_{21}^2}p_{21}^2 + \frac{\partial^2 g_1}{\partial q_2^2}p_{22}^2 + 2\frac{\partial^2 g_1}{\partial q_{21}q_1}p_1p_{21} + 2\frac{\partial^2 g_1}{\partial q_{22}q_1}p_1p_{22} + 2\frac{\partial^2 g_1}{\partial q_{21}q_{22}}p_{22}p_{21} \\ \frac{\partial^2 g_2}{\partial q_1^2}p_1^2 + \frac{\partial^2 g_2}{\partial q_{21}^2}p_{21}^2 + \frac{\partial^2 g_2}{\partial q_2^2}p_{22}^2 + 2\frac{\partial^2 g_2}{\partial q_{21}q_1}p_1p_{21} + 2\frac{\partial^2 g_2}{\partial q_{22}q_1}p_1p_{22} + 2\frac{\partial^2 g_2}{\partial q_{21}q_{22}}p_{22}p_{21} \end{bmatrix}^{\mathrm{T}} \tag{3.34.a}$$

$$D_2^2(g) = \begin{bmatrix} \frac{\partial g_1}{\partial q_1}\dot{p}_1 + \frac{\partial g_1}{\partial q_{21}}\dot{p}_{21} + \frac{\partial g_1}{\partial q_{22}}\dot{p}_{22} & \frac{\partial g_2}{\partial q_1}\dot{p}_1 + \frac{\partial g_2}{\partial q_{21}}\dot{p}_{21} + \frac{\partial g_2}{\partial q_{22}}\dot{p}_{22} \end{bmatrix} \tag{3.34.b}$$

Now, it is very clear from the construction of $D_2^2(g)$ that its element contains the elements of input vector. Therefore, proper measures should be taken to group the input vector elements together so as to find out a compact expression of the control law.

However, from the structure of $D_2^2(g)$ matrix it can be easily inferred that $D_2^2(g)\boldsymbol{p_2}$ can be further partitioned into three parts as shown in the following equation:

$$D_2^2(g)\boldsymbol{p_2} = D_{2p_1}^2(g)\boldsymbol{f} + D_{2p_1}^2(g)g\boldsymbol{u} + D_{2p_2}^2(g)\boldsymbol{u} \tag{3.35}$$

where the elements of each fragment are:

$$D_{2p_1}^2(g_{mr}) = \sum_{i=1}^{n_2}\frac{\partial g_{mi}}{\partial q_{1r}}p_{2i} \tag{3.36}$$

where $D_{2p_1}^2(g) \in \mathbb{R}^{n_1 \times n_1}$ and $m = 1,\ldots, n_1$ indicates the row index of g matrix, q_{1r} is the elements of the vector $\boldsymbol{q}_1$, where r denotes the index of the particular configuration variables and p_{2i} denotes element of $\boldsymbol{p}_2$ vector.

$$D_{2p_2}^2(g_{mr}) = \sum_{i=1}^{n_2}\frac{\partial g_{mi}}{\partial q_{2r}}p_{2i} \tag{3.37}$$

where $D_{2p_2}^2(g) \in \mathbb{R}^{n_1 \times n_2}$ $m = 1,\ldots, n_1$ indicates the row number of g matrix, q_{2r} is the elements of the vector $\boldsymbol{q}_2$, where r denotes the index of the particular configuration variables. Construction of the matrices that have been described in Eqs. (3.36) and (3.37) can also be explained with the help of the state model of Eq. (3.25).

$$D_2^2(g)\boldsymbol{p_2} = \begin{bmatrix} \frac{\partial g_1}{\partial q_1}\left(f + [\,g_1 \quad g_2\,]\begin{bmatrix} u_1 \\ u_2 \end{bmatrix}\right) + \frac{\partial g_1}{\partial q_{21}}u_1 + \frac{\partial g_1}{\partial q_{22}}u_2 \\ \frac{\partial g_2}{\partial q_1}\left(f + [\,g_1 \quad g_2\,]\begin{bmatrix} u_1 \\ u_2 \end{bmatrix}\right) + \frac{\partial g_2}{\partial q_{21}}u_1 + \frac{\partial g_2}{\partial q_{22}}u_2 \end{bmatrix}^{\mathrm{T}} \begin{bmatrix} p_{21} \\ p_{22} \end{bmatrix}$$
$$= \left[\left(\frac{\partial g_1}{\partial q_1}p_{21} + \frac{\partial g_2}{\partial q_1}p_{22}\right)\left(f + [\,g_1 \quad g_2\,]\begin{bmatrix} u_1 \\ u_2 \end{bmatrix}\right)\right.$$
$$\left. + \left(\frac{\partial g_1}{\partial q_{21}}p_{21} + \frac{\partial g_2}{\partial q_{21}}p_{22}\right)u_1 + \left(\frac{\partial g_1}{\partial q_{22}}p_{21} + \frac{\partial g_2}{\partial q_{22}}p_{22}\right)u_2\right] \tag{3.38}$$

Hence, with the above mentioned simplification technique, it is always possible to represent the time derivative of $\boldsymbol{z_2}$ in the following compact form as shown in Eq. (3.39)

$$\begin{aligned} \dot{\boldsymbol{z}}_2 &= \boldsymbol{u} + c_1(\boldsymbol{z_2} - c_1\boldsymbol{z_1} - \lambda\boldsymbol{\chi_1}) + \lambda\boldsymbol{z_1} \\ &\quad - K\left[\boldsymbol{f} + g\boldsymbol{u} + Df_{q_1}\boldsymbol{p_1} + Df_{q2}\boldsymbol{p_2} + Df_{p1}(\boldsymbol{f} + g\boldsymbol{u}) + Df_{p2}\boldsymbol{u}\right. \\ &\quad \left. - D(g)\boldsymbol{u} - D_1^2(g)\boldsymbol{p_2} - D_{2p_1}^2(g)\boldsymbol{f} - D_{2p_1}^2(g)g\boldsymbol{u} - D_{2p_2}^2(g)\boldsymbol{u}\right] \\ &= \psi\boldsymbol{u} + \lambda\boldsymbol{z_1} + c_1(\boldsymbol{z_2} - c_1\boldsymbol{z_1} - \lambda\boldsymbol{\chi_1}) + \boldsymbol{\Phi} \end{aligned} \tag{3.39}$$

where the expressions of $\psi \in \mathbb{R}^{n_2 \times n_2}$ and $\boldsymbol{\Phi} \in \mathbb{R}^{n_2}$ are shown in following equations:

$$\psi = \left[I - K\left(g + Df_{p_1}g + Df_{p_2} - D(g) - D_{2p_1}^2(g)g - D_{2p_2}^2(g)\right)\right] \tag{3.40}$$

and

$$\boldsymbol{\Phi} = -K\left[\boldsymbol{f} + Df_{q_1}\boldsymbol{p_1} + Df_{q_2}\boldsymbol{p_2} + Df_{p_1}\boldsymbol{f} - D_1^2(g)\boldsymbol{p_2} - D_{2p1}^2(g)\boldsymbol{f}\right] \tag{3.41}$$

In Eq. (3.40), I denotes an identity matrix of order n_2. Similar to the case of 2-DOF UMS (described in Sect. 3.2.2), above three steps transform the state model of an n-DOF underactuated system of (3.20) into the block-strict feedback form.

Step 4: The control law $\boldsymbol{u}$ is designed to ensure the desired dynamics for $\boldsymbol{z_2}$. The desired dynamics of $\boldsymbol{z_2}$ is expressed in Eq. (3.42) as following:

$$\dot{\boldsymbol{z}}_2 = -\boldsymbol{z_1} - c_2\boldsymbol{z_2} \tag{3.42}$$

where c_2 is an arbitrary positive design constant.

Consequently, from Eqs. (3.40) and (3.42) the desired control input can be derived in the following manner:
or,

$$\boldsymbol{u} = \psi^{-1}\left[-\left(1 - c_1^2 + \lambda\right)\boldsymbol{z_1} - (c_1 + c_2)\boldsymbol{z_2} + \lambda c_1 \boldsymbol{\chi_1} - \boldsymbol{\Phi}\right] \tag{3.43}$$

such choice of control input $\boldsymbol{u}$ results in the following dynamics:

$$\begin{aligned} \dot{\boldsymbol{z}}_1 &= \boldsymbol{z_2} - c_1 \boldsymbol{z_1} - \lambda \boldsymbol{\chi_1} \\ \dot{\boldsymbol{z}}_2 &= -\dot{\boldsymbol{z}}_1 - c_2 \boldsymbol{z_2} \end{aligned} \tag{3.44}$$

3.2.3 Zero Dynamics Analysis of n-DOF Underactuated Mechanical System

Similar to the analysis of zero dynamics stability presented in Sect. 3.2.3, it is also possible to analyze the stability of the zero dynamics for the n-DOF underactuated system (3.20). Akin to the previous case of 2 DOF UMS, two successive differentiation of $\boldsymbol{z_1}$ yields an explicit relationship between the input vector $\boldsymbol{u}$ and the output vector $\boldsymbol{z_1}$. From Eq. (3.32), one can write:

$$\begin{aligned} \ddot{\boldsymbol{z}}_1 &= \dot{\boldsymbol{z}}_2 - c_1 \dot{\boldsymbol{z}}_1 - \lambda z_1 \\ &= \psi \boldsymbol{u} + \lambda z_1 + c_1 \dot{\boldsymbol{z}}_1 + \boldsymbol{\Phi} - c_1 \dot{\boldsymbol{z}}_1 - \lambda \boldsymbol{z_1} \\ &= \psi \boldsymbol{u} + \boldsymbol{\Phi} \end{aligned} \tag{3.45}$$

Hence, one can proceed in a similar manner to derive the expressions of the zero dynamics system (here the authors have exactly followed Eqs. (3.16.a–3.16.c) to derive the expression of zero dynamics). As a result,

$$\boldsymbol{z_1} = 0 \Rightarrow \boldsymbol{q_2} = K(\boldsymbol{q_1} + \boldsymbol{p_1} - g\boldsymbol{p_2}) \tag{3.46.a}$$

$$\dot{z}_1 = \boldsymbol{p_2} - K(\boldsymbol{p_1} + \boldsymbol{f} - D(g)\boldsymbol{p_2}) = 0 \Rightarrow \boldsymbol{p_2} = K(\boldsymbol{p_1} + \boldsymbol{f} - D(g)\boldsymbol{p_2}) \tag{3.46.b}$$

$$\ddot{\boldsymbol{z}}_1 = \psi \boldsymbol{u} + \boldsymbol{\Phi} = 0 \Rightarrow \boldsymbol{u} = \psi^{-1}\boldsymbol{\Phi} \tag{3.46.c}$$

Consequently, one can represent the dynamics of $\boldsymbol{q_1}, \boldsymbol{p_1}$ subsystem together with the input $\boldsymbol{u}$ of Eq. (3.46.c) as:

$$\begin{aligned} \dot{\boldsymbol{q}}_1 &= \boldsymbol{p_1} \\ \dot{\boldsymbol{p}}_1 &= \boldsymbol{f} + g\boldsymbol{u} = \boldsymbol{f} - g\psi^{-1}\boldsymbol{\Phi} \end{aligned} \tag{3.47}$$

Furthermore, after a few algebraic manipulations, it is always possible to replace all the terms containing $\boldsymbol{q_2}$ and $\boldsymbol{p_2}$ by the expressions of Eqs. (3.46.a, 3.46.b),

respectively. Hence, it is possible to describe the dynamics of the transformed system with the reduced order model as shown in Eq. (3.47) and subsequently the zero dynamics model as shown in Eq. (3.48),

$$\begin{aligned} \dot{\boldsymbol{q}}_{\boldsymbol{1}} &= \boldsymbol{p}_{\boldsymbol{1}} \\ \dot{\boldsymbol{p}}_{\boldsymbol{1}} &= \boldsymbol{F}(\boldsymbol{q}_{\boldsymbol{1}}, \boldsymbol{p}_{\boldsymbol{1}})|\boldsymbol{z}_{\boldsymbol{1}} = \boldsymbol{0} \end{aligned} \tag{3.48}$$

The schematic diagram of the overall control system is shown in Fig. 3.1. Now, if the elements of matrix K is selected in such a manner that it can ensure zero dynamics [vide Eq. (3.48)] stability of the transformed system, then it will also ensure the asymptotic convergences of $\boldsymbol{q}_{\boldsymbol{1}}$ and $\boldsymbol{p}_{\boldsymbol{1}}$ to their desired equilibriums.

It is evident from the expressions of ψ, and $\boldsymbol{\Phi}$ of Eqs. (3.46.c) and (3.48) that the zero dynamics stability of the system depends on the choice of the elements (parameters) of K matrix. Therefore, K should be selected in a sensible manner to assure the stability of the zero dynamic system, which in turn would guarantee the global asymptotic stability of the entire system [shown in Eq. (3.22)].

Indeed, it is also clear from the expression of (3.44) that the controller parameters c_1 and c_2 control the rate of convergence of the regulated variables. It is also clear from Eq. (3.44) that c_1, c_2, and λ should be selected from the set of all positive real numbers $(\mathbb{R}_+)$ to ensure the asymptotic stability of the proposed control algorithm. Since a very high value of λ may generate some adverse affect on the controller performance, a comparatively small value of λ has been chosen to control the integral action.

Remark 3.7 The dimension of the reduced order system described by Eq. (3.44) is $2n_2$ and the dimension of the zero dynamics described in (3.48) is $2n_1$. The dimension of the overall system state model (3.20) is $2n$. Hence, the above results

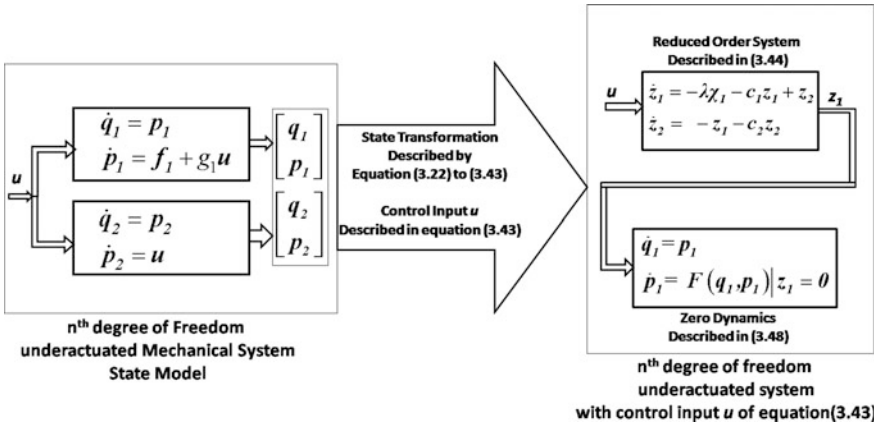

Fig. 3.1 Schematic diagram of the controlled system

corroborate the fact that the order of overall system ($2n$) = the order of reduced order system in $\boldsymbol{z_1}$, $\boldsymbol{z_2}$ ($2n_2$) +the order of zero dynamics ($2n_1$).

Remark 3.8 The stability of the zero dynamics system (3.48) ensures the asymptotic convergence of $\boldsymbol{q_1}$ and $\boldsymbol{p_1}$ to zero (i.e. $\boldsymbol{q}_1 \rightarrow \boldsymbol{0}$ and $\boldsymbol{p}_1 \rightarrow \boldsymbol{0}$, as $\boldsymbol{t} \rightarrow \infty$).

3.3 Analysis of Global Diffeomorphism of the Control Law

Previous section presents the systematic formulation of the proposed control law for 2-DOF system and n-DOF system, respectively. The algebraic state transformation, which is described in Sect. 3.2.2, has converted the original n-DOF UMS of Eq. (3.22) into a reduced order state model of Eq. (3.44). Since $\boldsymbol{X}$ is a $2n$ dimensional state vector, another $2n_1$ number components will be required to completely describe the diffeomorphic state transformation from $\boldsymbol{X}$ coordinate to $\boldsymbol{Z}$ coordinate. In this work, $\boldsymbol{q_1}$ and $\boldsymbol{p_1}$ have been chosen to be these two components. Consequently, the proposed diffeomorphic transformation can be expressed as shown in the Eq. (3.49) below:

$$\boldsymbol{Z} = T(\boldsymbol{X}) = \begin{bmatrix} \boldsymbol{z_1} \\ \boldsymbol{z_2} \\ \boldsymbol{z_3} \\ \boldsymbol{z_4} \end{bmatrix} = \begin{bmatrix} \boldsymbol{q_2} - K(\boldsymbol{q_1} + \boldsymbol{p_1} - g_1\boldsymbol{p_2}) \\ \boldsymbol{p_2} + c_1 z_1 + \lambda \boldsymbol{\chi_1} - K(\boldsymbol{p_1} + \boldsymbol{f} - D(g)\boldsymbol{p_2}) \\ \boldsymbol{q_1} \\ \boldsymbol{p_1} \end{bmatrix} \tag{3.49}$$

In order to verify the fact that $T(\boldsymbol{X})$ is indeed a global diffeomorphism, the Jacobian of the proposed state transformation $T(\boldsymbol{X})$ has been computed as shown below:

$$\frac{\partial T}{\partial \boldsymbol{X}} = \begin{bmatrix} -K + K\frac{\partial g}{\partial \boldsymbol{q_1}}\boldsymbol{p_2} & -K & 1 + K\frac{\partial g}{\partial \boldsymbol{q_2}}\boldsymbol{p_2} & Kg \\ -K\left(c_1 + \frac{\partial D(g)}{\partial \boldsymbol{q_1}}\boldsymbol{p_2} + \frac{\partial f}{\partial \boldsymbol{q_1}} - c_1\frac{\partial g}{\partial \boldsymbol{q_1}}\boldsymbol{p_2}\right) & -K(1 + c_1 + \frac{\partial f}{\partial \boldsymbol{p_1}} + \frac{\partial D(g)}{\partial p_2}) & c_1 + K\left(c_1\frac{\partial g}{\partial \boldsymbol{q_2}}\boldsymbol{p_2} - \frac{\partial f}{\partial \boldsymbol{q_2}} - \frac{\partial D(g)}{\partial \boldsymbol{q_2}}\boldsymbol{p_2}\right) & K\left(c_1 g - \frac{\partial f}{\partial \boldsymbol{p_2}} + D(g) + \frac{\partial D(g)}{\partial \boldsymbol{p_2}}\boldsymbol{p_2}\right) \\ 1 & 0 & 0 & 0 \\ 0 & 1 & 0 & 0 \end{bmatrix} \tag{3.50}$$

Therefore, determinant of $\frac{\partial T}{\partial \boldsymbol{X}}$ can be expressed as:

$$\begin{aligned} \Delta = & \left(1 + K\frac{\partial g}{\partial \boldsymbol{q_2}}\boldsymbol{p_2}\right)K\left(c_1 g - \frac{\partial f}{\partial \boldsymbol{p_2}} + D(g) + \frac{\partial D(g)}{\partial \boldsymbol{p_2}}\right) \\ & - \left(c_1 + K\left(c_1\frac{\partial g}{\partial \boldsymbol{q_2}}\boldsymbol{p_2} - \frac{\partial f}{\partial \boldsymbol{q_2}} - \frac{\partial D(g)}{\partial \boldsymbol{q_2}}\boldsymbol{p_2}\right)\right)kg \end{aligned} \tag{3.51}$$

Consequently, it can be inferred that the full rank of the Jacobian $\frac{\partial T}{\partial X}$ implies a nonzero Δ. Hence, global invertibility of $\frac{\partial T}{\partial X}$ implies the state transformation described in Eq. (3.51) is a global diffeomorphism. Equation (3.51) reveals that the nonsingularity of the Jacobian $\frac{\partial T}{\partial X}$ depends on the controller parameter K, but the other controller parameters (e.g. c_1, c_2, λ) do not alter the rank of the Jacobian $\frac{\partial T}{\partial X}$.

3.4 Stability Analysis of the Proposed Controller

In this section, stability of the proposed control algorithm is analyzed using Lyapunov's stability criterion. At first, the stability of the reduced order system of equation is proved using the Barbalat's Lemma (3.38)

Theorem 3.1 *If the underactuated system is represented by the state model of Eq. (3.22), then the system can be transformed into a block-strict feedback form by a global state transformation as described by Eqs. (3.22)–(3.27). Moreover, there exists a state feedback control law as given in Eq. (3.43), which ensures the global stabilization of the equilibrium for the underactuated system.*

Proof The first part of the theorem (i.e. the transformation of the underactuated system in block-strict feedback form) can be proved by direct calculation. Since it has already been established in the last section that global diffeomorphism is automatically ensured, it can be concluded that the invertibility of ψ ensures existence of the proposed state feedback control law. Now, the proof of the stabilizing property of the control law is given below.

The proposed control law of Eq. (3.43) transforms the closed loop system in the closed loop forms of Eq. (3.44).

Now, the following Lyapunov function has been defined for the transformed system as described in the following Eq. (3.44):

$$V = \frac{1}{2}\lambda \boldsymbol{\chi}_1^{\mathrm{T}} \boldsymbol{\chi}_1 + \frac{1}{2} z_1^{\mathrm{T}} z_1 + \frac{1}{2} z_2^{\mathrm{T}} z_2 \tag{3.52}$$

The derivative of the Lyapunov Function can be computed as:

$$\begin{aligned} \dot{V} &= \lambda \boldsymbol{\chi}_1^{\mathrm{T}} z_1 + z_1^{\mathrm{T}}(z_2 - c_1 z_1 - \lambda \boldsymbol{\chi}_1) + z_2^{\mathrm{T}}(z_1 - c_2 z_2) \\ &= -c_1 z_1^{\mathrm{T}} z_1 - c_2 z_2^{\mathrm{T}} z_2 \end{aligned} \tag{3.53}$$

The expression of Eq. (3.53) reveals the negative-definiteness of $\dot{V}$ and also implies the fact that $V(t) \leq V(0)$. Therefore, it ensures the boundedness of z_1 and z_2.

Now, define the following function:

$$N(t) = c_1 z_1^{\mathrm{T}} z_1 + c_2 z_2^{\mathrm{T}} z_2 \tag{3.54}$$

Integration of Eq. (3.53) results the following expression:

$$\begin{aligned} V(t) &= V(\boldsymbol{\chi_1}(0), \boldsymbol{z_1}(0), \boldsymbol{z_2}(0)) + \int_0^t \dot{V}(\tau)\mathrm{d}\tau \\ &= V(\boldsymbol{\chi_1}(0), \boldsymbol{z_1}(0), \boldsymbol{z_2}(0)) - \int_0^t N(\tau)\mathrm{d}\tau \end{aligned} \tag{3.55}$$

Thus,

$$\int_0^t N(\tau)\mathrm{d}\tau = V(\boldsymbol{\chi_1}(0), \boldsymbol{z_1}(0), \boldsymbol{z_2}(0)) - V(t) \tag{3.56}$$

Considering $\dot{V}(t) \leq 0$ and $V(t) \geq 0$, the following results can be obtained easily:

$$\lim_{t\to\infty} \int_0^t N(\tau)\mathrm{d}\tau \leq \infty \tag{3.57}$$

The derivative of $\dot{V}$ can be expressed as

$$\ddot{V} = \left[2c_1 z_1^{\mathrm{T}} \dot{\boldsymbol{z}}_1 + 2c_2 z_2^{\mathrm{T}} \dot{z}_2\right] \tag{3.58}$$

Since $\boldsymbol{z_1}, z_2, \dot{\boldsymbol{z}}_1, \dot{z}_2$ are bounded, Eq. (3.58) implies the fact that $\dot{V}(t)$ is a continuous function of time. Hence, with the application of Barbalat's Lemma it can be proved that $\boldsymbol{z_1}$ and $\boldsymbol{z_2}$ converge to zero as $t \to \infty$.

Theorem 3.2 *The global asymptotic stability of the reduced order system of (3.44) together with the global asymptotic stability of the zero dynamics system (3.48) ensures the global asymptotic stability of the original underactuated system of (3.20).*

Proof The global asymptotic stability of the reduced order system of Eq. (3.44) ensures that the state vectors of the reduced order system (i.e. $\boldsymbol{z_1}$, $\boldsymbol{z_2}$) will asymptotically converge to the desired equilibrium. That is $\boldsymbol{z_1}$ will asymptotically converge to zero as $t \to \infty$.

$$\boldsymbol{z_1} = \boldsymbol{q_2} - K(\boldsymbol{q_1} + \boldsymbol{p_1} - g\boldsymbol{p_2}) \to 0 \tag{3.59}$$

In addition, the global asymptotic stability of the zero dynamic system [vide Eq. (3.42)] ensures that the $\boldsymbol{q_1}$ and $\boldsymbol{p_1}$ will asymptotically converge to zero as $t \to \infty$ (Vide Remark 3.8).

That is, with $t \to \infty$

$$\boldsymbol{q_1} \to 0 \text{ and } \boldsymbol{p}_1 \to 0 \tag{3.60}$$

Therefore, $t \to \infty$ results in,

$$\boldsymbol{q_2} + Kg\boldsymbol{p_2} \to 0 \tag{3.61}$$

The above Eq. (3.52) reveals the fact that $\boldsymbol{q_2} + Kg\boldsymbol{p_2}$ must converge to zero when $\boldsymbol{z_1}$ converges to the zero.

Now according to the definition of the state model of Eq. (3.20) $\dot{\boldsymbol{q}}_2 = \boldsymbol{p_2}$. Consequently, it can be concluded that the state $\boldsymbol{q_2}$ and $\boldsymbol{p_2}$ are orthogonal to each other. In addition, K is a constant matrix. Furthermore, by definition, $g(q)$ is not a null matrix [vide Eq. (3.21)].

Therefore, asymptotic convergence of $\boldsymbol{q_2} + Kg\boldsymbol{p_2}$ to zero clearly implies that the individual element $\boldsymbol{q_2}$ and $\boldsymbol{p_2}$ must converge to zero when $t \to \infty$. Hence, the proposed control law ensures the global stabilization of the original n-DOF underactuated system [as shown in Eq. (3.20)].

3.5 Notes

A theoretical framework is presented for designing a block backstepping controller for nonlinear UMSs. The proposed control algorithm can ensure the global asymptotic stability of the origin of the underactuated system. At the onset of the design, a global change of coordinates is introduced to transform the state model of the underactuated system into a block-strict feedback form, which is convenient for backstepping design for MIMO systems. Thereafter, a nonlinear block backstepping control law is designed for the generic underactuated system. Integral action is incorporated in the control law to enhance the steady state performance of the controller. In addition, the zero dynamic stability of the controller is thoroughly analyzed to ensure the global asymptotic stability of the overall nonlinear system. Furthermore, global diffeomorphism of the control law is analyzed to ensure the fact that the proposed state transformation will work well for any initial value of state ordinate. Therefore, in a nutshell it can be inferred that the proposed control law will ensure global asymptotic stability of the system.

References

1. Krstic M, Kanellakopoulos I, Kokotovic PV (1995) Nonlinear and adaptive control design. Wiley Interscience, New York
2. Kokotovic PV, Arcak M (2001) Constructive nonlinear control: a historical perspective. Automatica 37(5):637–662
3. Olfati Saber R (2001) Nonlinear control of underactuated mechanical systems with application to robotics and aerospace vehicles, Ph.D. thesis, Department of Electrical Engineering and Computer, Massachusetts Institute of Technology
4. Rudra S, Barai RK, Maitra M (2014) Nonlinear state feedback controller design for underactuated mechanical system: a modified block backstepping approach. ISA Trans 53 (2):317–326
5. Spong MW (1998) Underactuated mechanical systems. In Control problems in robotics and automation, vol 230. Springer, Berlin, pp 135–150
6. Yu H, Liu Y (2013) A survey of underactuated mechanical systems. IET Control Theory Appl 7 (7):921–935

Chapter 4
Applications of the Block Backstepping Algorithm on 2-DOF Underactuated Mechanical Systems: Some Case Studies

Abstract Before dealing with the actual content of this chapter, the authors would like to refer the definition of engineering from Merriam-Webster dictionary. It defines engineering as "the application of science and mathematics by which the properties of matter and the sources of energy in nature are made useful to people." Indeed, engineers should deal with the practical problem instead of spending time in analyzing theoretical issues. In order to make the book compatible as well as a primed one for engineering readers, applications of the proposed control law on different members of underactuated mechanical system (UMS) family have been presented in a systematic manner. Several important UMSs such as acrobot, pendubot, Translational oscillator and rotational actuator (TORA), Furuta pendulum, Inertia wheel pendulum (IWP), inverted pendulum, single dimensional overhead crane fall under the category of two degrees of freedom UMSs. Quite often 2-DOF systems are being used as a standard laboratory test bed to gain physical insight of the complicated real-time systems [37, 38]. In addition, several higher order nonlinear systems can be represented as a cascade combination of 2-DOF systems. Keeping in view the immense importance of 2-DOF underactuated mechanical systems, this chapter presents systematic formulations of the proposed control algorithm on seven different 2-DOF systems. For the sake of better comprehensibility, at first, the system with most simple construction (having simple Lagrangian dynamic model) has been selected for demonstrating application of the proposed control law on an UMS. Thereafter, based on the constructional complexity of the other family members of the same class (i.e., 2-DOF underactuated mechanical systems) one after another system has been selected for the aforesaid purpose. Prime objective of this chapter is to ensure the fact that regardless of configuration of the concerned UMS, proposed control law is versatile enough to offer a satisfactory stabilizing performance for any kind of 2-DOF underactuated mechanical systems. Authors are very much confident with the fact that lucid treatment of this chapter would be able to convince the readers to implement the control law on different 2-DOF underactuated mechanical systems. Since the Inertia wheel

Electronic supplementary material The online version of this article (doi:10.1007/978-981-10-1956-2_4) contains supplementary material, which is available to authorized users.

S. Rudra et al., *Block Backstepping Design of Nonlinear State Feedback Control Law for Underactuated Mechanical Systems*, DOI 10.1007/978-981-10-1956-2_4

pendulum (IWP) possesses a comparatively simple dynamic model, at the onset, a comprehensive description of the application of proposed control law on an IWP is presented in Sect. 4.1 for better comprehensibility. However, for the sake of brevity, demonstrations of the control law on other 2-DOF systems are succinctly presented in the subsequent sections.

4.1 Application on the Inertia Wheel Pendulum[1]

Stabilization of an inertia wheel pendulum [IWP] is being considered as an active research area for control system engineers [17, 21, 24, 39]. The system comprises of a rigid mass link that is connected to the base at a pivot point, with one free moving spinning wheel attached to its free end. IWP falls under the category of flat holonomic underactuated systems. Nowadays, inertia wheel system has received a significant amount of research attention from control theorists [17, 40]. Indeed, IWP resembles the control problem of an underactuated spacecraft [16]. Therefore, during early days of research while designing a control law for spaceship, control engineers used to utilize it lab scale model to formulate the control law for the actual system [21]. Needless to say that the interaction between two different configuration variables makes the control problem pretty complicated. Out-of-the-way, set point control of IWP has been being considered as an active area of research since the time of its invention [16, 21, 39]. Needless to say that the control design of IWP is more complicated than that of a fully actuated system. A schematic diagram of the system is shown in Fig. 4.1.

State model of the system can be described by the following Eq. (4.1.a). (Detailed state model of the system is derived in Appendix A.1.)

$$\begin{aligned} \dot{q}_1 &= p_1 \\ \dot{p}_1 &= f + gu \\ \dot{q}_2 &= p_2 \\ \dot{p}_2 &= u \end{aligned} \tag{4.1.a}$$

where

$$f = \frac{m_{21} m_0 \boldsymbol{g}}{m_{11}} \sin(q_1) \tag{4.1.b}$$

[1]This section 4.1 is based on "Global Stabilization of a Flat Underactuated Inertia Wheel: A Block Backstepping Approach," by S. Rudra, R.K. Barai, M. Maitra, D. Mandal, S. Ghosh, S. Dam, P. Bhattacharyya, and A. Dutta, appeared in Proc. of 2nd International Conference Computer Communication and Informatics, 2013, pp. 1–4. (C) 2013 IEEE. Permission obtained from IEEE.

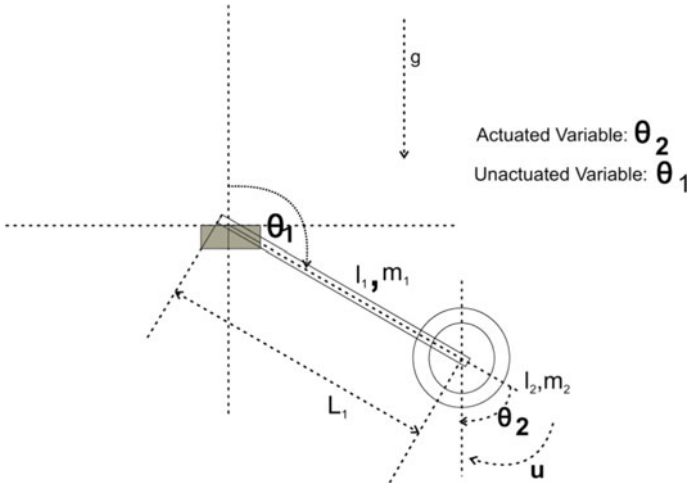

Fig. 4.1 Schematic diagram of the inertia wheel pendulum

$$g = -\frac{m_{12}}{m_{11}} \tag{4.1.c}$$

Salient Features of Inertia Wheel Pendulum: *Actuated shape variable system, flat underactuated system, holonomic constraint.*

Control Objective: *The control objective is to ensure the asymptotic stabilization of the inertia wheel system. That is, the control algorithm is required to ensure the asymptotic convergence of all the state variables toward their equilibrium* [21, 39, 40].

4.1.1 Derivation of the Control Law for Inertia Wheel Pendulum

During derivation of control law for IWP, the authors have precisely followed the design procedure of Chap. 3. At first, the first error variable z_1 has been defined as shown in the following Eq. (4.2):

$$z_1 = q_2 - k(q_1 + p_1 - gp_2) \tag{4.2}$$

Thereafter, the time derivative of z_1 has been computed accordingly:

$$\dot{z}_1 = p_2 - k(p_1 + f - p_2 dg \cdot p) \tag{4.3}$$

After that, the stabilizing function has been defined according to Eq. (3.5) as shown in Eq. (4.4):

$$\alpha_1 = -c_1 z_1 - \lambda \chi_1 + k(p_1 + f - p_2 dg \cdot p), \tag{4.4}$$

where $\chi_1 = \int_0^t z_1 dt$ and c_1, λ are two arbitrary positive design constant.

Now, the second error variable z_2 has been defined in accordance with Eq. (3.7) as shown in the following Eq. (4.5):

$$z_2 = p_1 - \alpha_1 \tag{4.5}$$

Subsequently, the time derivative of z_2 has become

$$\dot{z}_2 = u + c_1(z_2 - c_1 z_1) - k\left[\left\{f + gu + df\dot{X} - udg \cdot p + p_2\left(\frac{\partial g}{\partial q_1}(f + gu) + \frac{\partial g}{\partial q_2}(u)\right) + p_2\left(\frac{\partial^2 g}{\partial q_1^2}p_1^2 + 2\frac{\partial^2 g}{\partial q_1 \partial q_2}p_1 p_2 + \frac{\partial^2 g}{\partial q_2^2}p_2^2\right)\right\}\right] \tag{4.6}$$

Hence, comparison of Eq. (4.6) with Eq. (3.9) has yielded the following expression for ψ and ϕ:

$$\psi = 1 - k\left\{g + g\frac{\partial f}{\partial p_1} + \frac{\partial f}{\partial p_2} - dg \cdot p - p_2\frac{\partial g}{\partial q_1}g - p_2\frac{\partial g}{\partial q_2}\right\} \tag{4.7}$$

$$\phi = -k\left[f + \frac{\partial f}{\partial q_1}p_1 + \frac{\partial f}{\partial q_2}p_2 + \frac{\partial f}{\partial p_1}f - \left\{p_2\frac{\partial g}{\partial q_1}f + p_2\left(\frac{\partial^2 g}{\partial q_1^2}p_1^2 + 2\frac{\partial^2 g}{\partial q_1 \partial q_2}p_1 p_2 + \frac{\partial^2 g}{\partial q_2^2}p_2^2\right)\right\}\right] \tag{4.8}$$

The above choices of ψ and ϕ have resulted in the compact expression of control input as shown below:

$$\ddot{z}_2 = \psi u + \lambda z_1 + c_1(z_2 - c_1 z_1 - \lambda \chi_1) + \phi \tag{4.9}$$

However, the desired dynamics of z_2 can be found out from Eq. (3.12) as shown below:

$$\dot{z}_2 = -z_1 - c_2 z_2 \tag{4.10}$$

Similar to the method described in Sect. 3.1.2, comparison of the above equation of $\dot{z}_2$ with the desired dynamics of z_2 yields:

$$u = \psi^{-1}\left[-\left(1 - c_1^2 + \lambda\right)z_1 - (c_1 + c_2)z_2 + \lambda c_1 \chi_1 - \phi\right] \tag{4.11}$$

In the above expressions the differentials can be calculated as follows:

$$\frac{\partial f}{\partial p_1} = 0 \tag{4.12}$$

$$\frac{\partial f}{\partial p_2} = 0 \tag{4.13}$$

$$\frac{\partial g}{\partial q_1} = 0 \tag{4.14}$$

$$\frac{\partial g}{\partial q_2} = 0 \tag{4.15}$$

$$\frac{\partial f}{\partial q_1} = \frac{m_{21} m_0 \boldsymbol{g}}{m_{11}} \cos(q_1) \tag{4.16}$$

$$\frac{\partial f}{\partial q_2} = 0 \tag{4.17}$$

(Detailed description of the variables, which are used in the above equations, can be found in Appendix A.1.) As it has already been stated in Sect. 3.1.3, Eqs. (3.16.a)–(3.16.c) represent the zero dynamics structure for a 2-DOF under-actuated mechanical system. *Consequently, in the special case of the IWP* $z_1 = 0$ and $\dot{z}_1 = 0$ *has resulted in the following expression of* q_2 *and* p_2.

$$z_1 = q_2 - k(q_1 + p_1 - g p_2) = 0 \Rightarrow q_2 = k(q_1 + p_1 - g p_2) \tag{4.18.a}$$

$$\dot{z}_1 = p_2 - k(p_1 + f - p_2 dg \cdot p) = 0 \Rightarrow p_2 = k(p_1 + f - p_2 dg \cdot p) \tag{4.18.b}$$

Now, if the q_2 and p_2 terms of f, g, ψ, and ϕ could be replaced by the expressions of (4.18.a) and (4.18.b), respectively, then the equations of zero dynamics for the inertia wheel pendulum will take the following form:

$$\begin{aligned} \dot{q}_1 &= p_1 \\ \dot{p}_1 &= f(q_1, p_1) - g(q_1, p_1)\psi^{-1}(q_1, p_1)\varphi(q_1, p_1) \end{aligned} \tag{4.18.c}$$

In Eq. (4.18.c), $f(q_1, p_1), g(q_1, p_1), \psi^{-1}(q_1, p_1)$ and $\varphi(q_1, p_1)$ represent the same functions f, g, ψ^{-1} and φ, with the only difference that the last equation, all the q_2 and p_2 terms have been replaced by the expression of (4.18.a) and (4.18.b), respectively. Constant k has been selected in such a manner that it could ensure the stability of the zero dynamics system. Following Lyapunov function has been defined to analyze stability of the internal dynamics of Eq. (4.18.c)

$$V_z = \frac{1}{2}q_1^2 + \frac{1}{2}p_1^2 \tag{4.19}$$

Now, time derivative of the above Lyapunov function V_z has resulted in:

$$\dot{V}_z = q_1 p_1 + p_1 F \tag{4.20}$$

Now, the controller parameter k has been selected in a judicial manner to ensure the negative definiteness of the $\dot{V}_z$. The other three controller parameters do not alter the negative definiteness of $\dot{V}_z$ [27]. However, they have been chosen in a manner so that they could satisfy the condition $c_1 > 0$, $c_2 > 0$ and $\lambda > 0$. (Detailed criteria of controller parameter selection have been discussed in Chap. 3, Sect. 3.2.3.)

4.1.2 Simulation Results and Performance Analysis

The effectiveness of the proposed control law has been verified after simulating the closed-loop system in MATLAB® (version: 7.14) Simulink (version: 7.9) environment. In this section, stepwise development of the proposed control law on IWP is systematically described in detail so that the reader can carry out the similar design process for other 2-DOF underactuated mechanical systems. During the simulation study, the authors have used the parameters of Table 4.1 to simulate the state model of IWP system's model in the simulation environment. Initial value of the state variables, which have been chosen for simulation experiment, are as following: $q_1 = \pi/6, q_2 = \pi/3, p_1 = 0$ and $p_2 = 0$.

Now for IWP, the elements of mass matrix can be expressed as shown in Eq. (4.21):

$$M = \begin{bmatrix} 4.45 \times 10^{-3} & 24.95 \times 10^{-6} \\ 24.95 \times 10^{-6} & 24.95 \times 10^{-6} \end{bmatrix} \tag{4.21}$$

Therefore, according to Eqs. (4.1.b) and (4.1.c) one can write:

$$f = 1.99 \times 10^{-3} \sin(q_1) \tag{4.22.a}$$

$$g = -5.60 \times 10^{-3} \tag{4.22.b}$$

Table 4.1 Parameters of the inertia wheel system (SI unit)

m_1	m_2	I_1	I_2	l_1	l_2
0.2164	0.0850	0.0002233	0.00002495	0.1173	0.1270

Therefore, from Eq. (3.47), equation of zero dynamics can be derived as shown in Eq. (4.23):

$$\begin{aligned}\dot{q}_1 &= p_1 \\ \dot{p}_1 &= 1.99 \times 10^{-3} \sin q_1 + \frac{5.6 \times 10^{-3} \times k \times 1.99 \times 10^{-3}(\sin q_1 + \cos q_1)}{1 - 5.6 \times 10^{-3} \times k}\end{aligned} \tag{4.23}$$

Consequently, the $\dot{V}_1$ (as described in Eq. 4.20) has become

$$\dot{V}_1 = p_1\left(q_1 + 1.99 \times 10^{-3} \sin q_1 + \frac{5.6 \times 10^{-3} \times k \times 1.99 \times 10^{-3}(\sin q_1 + \cos q_1)}{1 - 5.6 \times 10^{-3} \times k}\right) \tag{4.24}$$

Variation of the time derivative of V_1 is plotted for $k = 0.9$ as shown in Fig. 4.2.

Minute observation of Fig. 4.2 reveals that the value of parameter $k = 0.9$ *ensures negative definiteness of the* $\dot{V}_1$. Parameters of the proposed block backstepping controllers are tabulated in Table 4.2. (Please note that the stability of internal dynamics does not depend on any other controller's parameters.)

Variation of the state variables q_1 and p_1 are shown in Figs. 4.3 and 4.4.

It can be inferred from Figs. 4.3 and 4.4 that the proposed control law can ensure the global asymptotic stabilization of the state variables q_1 (i.e., angle of the base

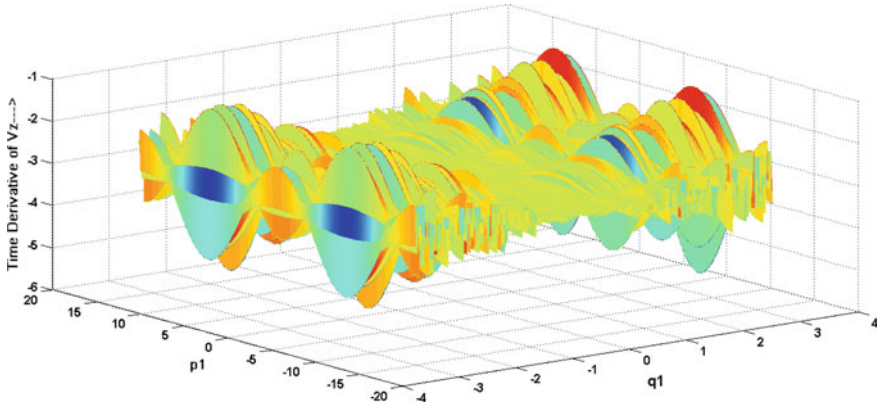

Fig. 4.2 Variation of the time derivative of V_1 for different values of k

Table 4.2 Parameters of the proposed block backstepping controller

c_1	c_2	k	λ
8	8	0.9	0.05

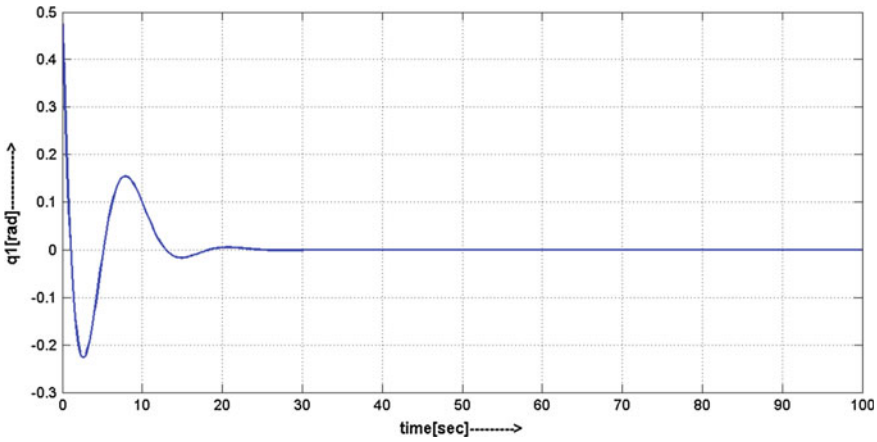

Fig. 4.3 Variation of the state variable q_1 with time

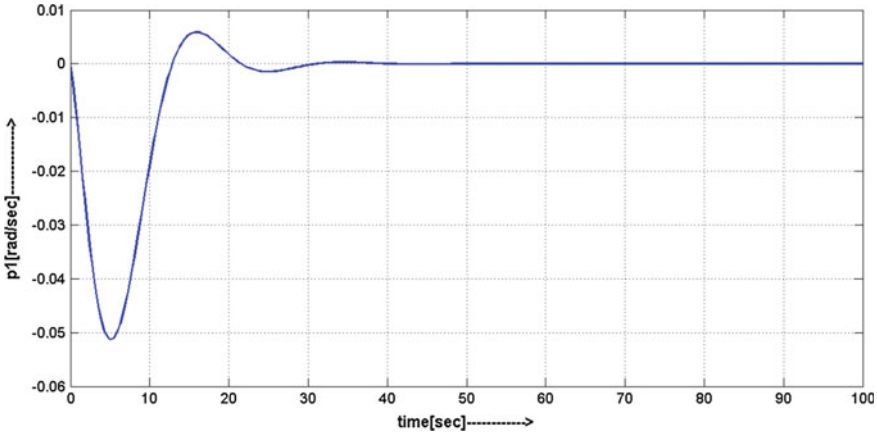

Fig. 4.4 Variation of the state variable p_1 with time

link) and p_1 (i.e., angular velocity of the base link). Convergence of the state variables, q_1 and p_1, has corroborated the fact that the asymptotic stability of the zero dynamics ensures the asymptotic convergence of q_1 and p_1 at their desired equilibrium.

It can be inferred from Figs. 4.5 and 4.6 that the control input u could ensure the global asymptotic stabilization of the actuated state variables. Proposition of theorem 2 (Chap. 3, Sect. 3.4), which states the global asymptotic stability of the reduced order system together with the global asymptotic stability of the internal dynamics ensures asymptotic stabilization of the actuated shape variables, has been corroborated by the stabilization of the actuated state variables.

Being a flat underactuated mechanical system, inertia wheel pendulum requires smooth control input for its stabilization. Figure 4.7 reveals the fact that the

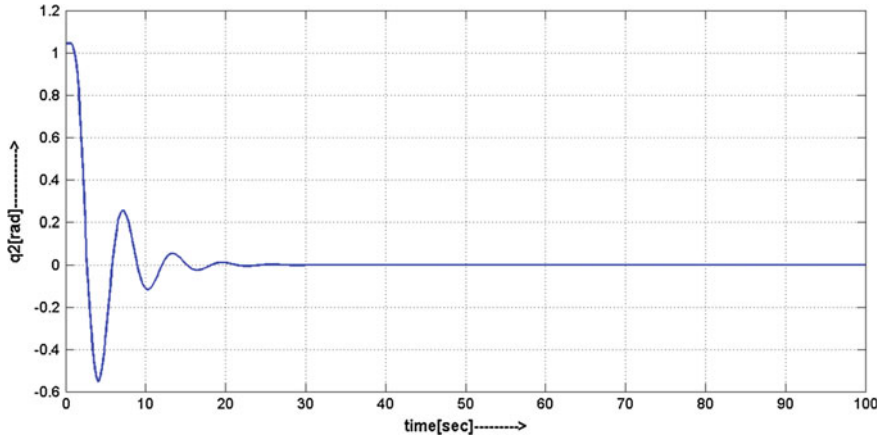

Fig. 4.5 Variation of the state variable q_2 with time

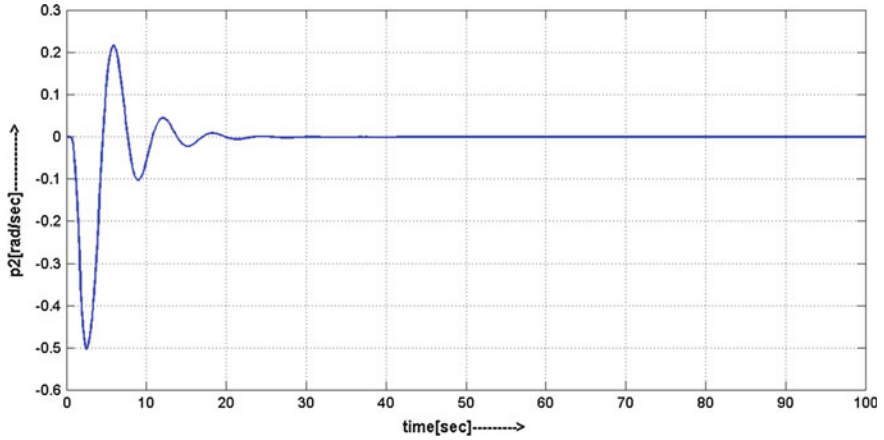

Fig. 4.6 Variation of the state variable p_2 with time

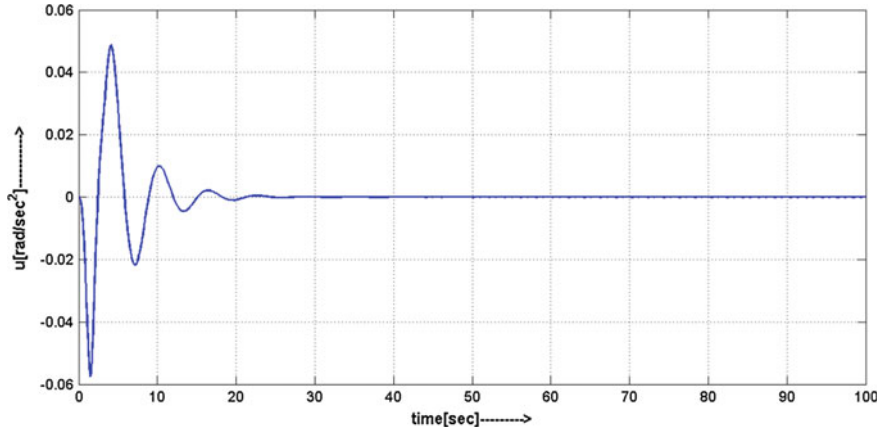

Fig. 4.7 Variation of the control input u with time

proposed control law generates a smooth control input for the stabilization of inertia wheel pendulum.

Authors are very much confident with the fact that the lucid presentation of devising control law for 2-DOF flat underactuated IWP will definitely help the reader to understand the concepts, and it will encourage them to apply the same on the control problems of other 2-DOF underactuated mechanical systems. In the next section, formulation of control law for TORA (Translational Oscillator with a Rotational Actuator) system and its implementation on the same test bench will be discussed in a systematic manner.

4.2 Application on the TORA System[2]

TORA system possesses just a bit more complicated dynamics than that of IWP [21]. Due to its actuation pattern and complicated nonlinear dynamics TORA system has been drawing conspicuous amount of research attention for the last three decades [2, 9]. Indeed, TORA system resembles the complex control problem of a dual-spin aircraft [21]. Needless to say, the interaction between spin and nutation complicates the algorithm design task for the control system engineers [11–13]. However, it is a quite difficult task to verify the versatility of a control algorithm on an actual dual-spin aircraft, and it may even lead to a catastrophic system failure. Therefore, during the developmental stage, quite often control engineers used to implement the same control law on a lab scale TORA system model to check its suitability for the intended real-time applications.

Nonetheless, not only TORA is being used to resemble the dynamics of dual-spin aircraft; moreover, stabilization of TORA is also considered as a benchmark problem in the literature of control system engineering [2, 9, 11–13]. Consequently, devising an efficient control algorithm for a TORA system remains as an active area of research [26]. Needless to say that the control design of a TORA system is more complicated than that of a fully actuated system [9, 11]. Furthermore, coupling action between translational motion of the cart and angular rotation of the eccentric mass makes the control design task more complicated [2, 9, 26].

Figure 4.8 illustrates the top view of this nonlinear benchmark mechanical system in which the rotational motion of an eccentric mass controls the translational oscillations of the platform. Assuming that the platform moves in the horizontal plane, the dynamics of the system can be described by the following state equations of (4.25.a). (Detailed state model of the system is derived in Appendix A.2.)

[2]Section 4.2 is based on " Design of Nonlinear State Feedback Control Law for Underactuated TORA System: A Block Backstepping Approach," by S. Rudra, R.K. Barai, M. Maitra, D. Mandal, S. Ghosh, S. Dam, P. Bhattacharyya, A. Dutta, appeared in Proc. of 7th International Conference on Intelligent Systems and Control, 2013, pp. 93–98. (C) IEEE 2013. Permission obtained from IEEE.

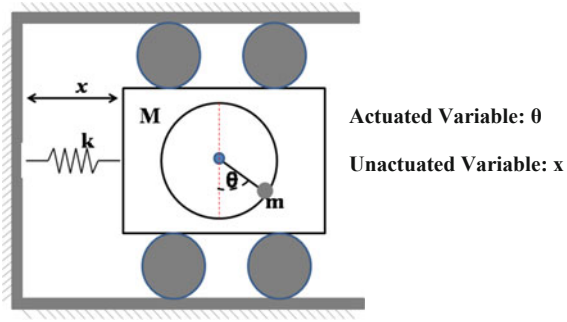

Fig. 4.8 Schematic diagram of the TORA system

$$\begin{aligned}\dot{q}_1 &= p_1 \\ \dot{p}_1 &= f + gu \\ \dot{q}_2 &= p_2 \\ \dot{p}_2 &= u\end{aligned} \tag{4.25.a}$$

where

$$f = -k_3 q_1 + k_2 \sin(q_2) p_1^2 \tag{4.25.b}$$

$$g = -k_2 \cos(q_2) \tag{4.25.c}$$

$$k_2 = m_2 r/(m_1 + m_2) \tag{4.25.d}$$

$$k_3 = -K/(m_1 + m_2) \tag{4.25.e}$$

Salient Features: *Holonomic constraint, actuated shape variable, badly damped equilibrium.*

Control Objective: *In case of a TORA system, prime objective of the controller design is to devise an elegant control law that would ensure smooth convergence of the state variables of the TORA system* [21, 40] *to their desired equilibrium.*

4.2.1 Derivation of the Control Law for TORA System

Indeed, for the TORA system, authors have followed the same design steps that had been utilized during formulation of the control law for IWP. At first, the first error variable z_1 has been defined as shown in the following Eq. (4.26):

Similar to Eq. (4.2), the first state variable z_1 has been defined as shown in the following Eq. (4.26):

$$z_1 = q_2 - k(q_1 + p_1 - gp_2) \tag{4.26}$$

Consequently, the time derivative of z_1 has taken the form of Eq. (4.27):

$$\dot{z}_1 = p_2 - k(p_1 + f - p_2 dg \cdot p) \tag{4.27}$$

Since *TORA system is also a member of actuated configuration variables type UMS like the IWP*, similar to the previous case one can define the stabilization function for TORA system (in case of the given model $f_1 = f, g_1 = g, f_2 = 0, g_2 = 1$) as shown in Eq. (4.28):

$$\alpha_1 = -c_1 z_1 - \lambda \chi_1 + k(p_1 + f - p_2 dg \cdot p) \tag{4.28}$$

Indeed, $\chi_1 = \int_0^t z_1 \mathrm{d}t$ represents the integral action in the feedback law.

Following Eq. (4.5), the second error variable z_2 has been defined to ensure the desired expression for $\dot{z}_1$. Definition of z_2 is shown in Eq. (4.29):

$$z_2 = p_2 - \alpha_1 \tag{4.29}$$

Obtaining time derivative of z_2 has resulted in the following expression of Eq. (4.30):

$$\dot{z}_2 = u + c_1(z_2 - c_1 z_1 - \lambda \chi_1) - k\left[\left\{f + gu + \frac{\partial f}{\partial q_1}p_1 + \frac{\partial f}{\partial q_2}p_2 + \frac{\partial f}{\partial p_1}f + g\frac{\partial f}{\partial p_1}u + \frac{\partial f}{\partial p_2}u - udg \cdot p - p_2\left(\frac{\partial g}{\partial q_1}(f + gu) + \frac{\partial g}{\partial q_2}(u)\right) - p_2\left(\frac{\partial^2 g}{\partial q_1^2}p_1^2 + 2\frac{\partial^2 g}{\partial q_1 \partial q_2}p_1 p_2 + \frac{\partial^2 g}{\partial q_2^2}p_2^2\right)\right\}\right] \tag{4.30}$$

Hence, comparison of Eq. (4.30) with Eq. (3.9) has yielded the following expression for ψ and ϕ:

$$\psi = 1 - k\left\{g + g\frac{\partial f}{\partial p_1} + \frac{\partial f}{\partial p_2} - dg \cdot p - p_2\frac{\partial g}{\partial q_1}g - p_2\frac{\partial g}{\partial q_2}\right\} \tag{4.31}$$

$$\phi = -k\left[f + \frac{\partial f}{\partial q_1}p_1 + \frac{\partial f}{\partial q_2}p_2 + \frac{\partial f}{\partial p_1}f - \left\{p_2\frac{\partial g}{\partial q_1}f + p_2\left(\frac{\partial^2 g}{\partial q_1^2}p_1^2 + 2\frac{\partial^2 g}{\partial q_1 \partial q_2}p_1 p_2 + \frac{\partial^2 g}{\partial q_2^2}p_2^2\right)\right\}\right] \tag{4.32}$$

The above definitions of ψ and ϕ have resulted in the compact expression of control input as shown in Eq. (4.33):

$$\dot{z}_2 = \psi u + \lambda z_1 + c_1(z_2 - c_1 z_1 - \lambda \chi_1) + \phi \tag{4.33}$$

However, the desired dynamics of z_2 is

$$\dot{z}_2 = -z_1 - c_2 z_2 \tag{4.34}$$

Similar to the method described in Sect. 3.1.2, comparison of the above equation of $\dot{z}_2$ with the desired dynamics of z_2 has resulted in:

$$u = \psi^{-1}\left[-\left(1 - c_1^2 + \lambda\right)z_1 - (c_1 + c_2)z_2 + \lambda c_1 \chi_1 - \phi\right] \tag{4.35}$$

In the above expressions the differentials can be calculated as follows:

$$\frac{\partial f}{\partial p_1} = 2k_2 \sin(q_2)p_1 \tag{4.36}$$

$$\frac{\partial f}{\partial p_2} = 0 \tag{4.37}$$

$$\frac{\partial g}{\partial q_1} = 0 \tag{4.38}$$

$$\frac{\partial g}{\partial q_2} = -k_2 \cos(q_2) \tag{4.39}$$

$$\frac{\partial f}{\partial q_1} = -k_3 \tag{4.40}$$

$$\frac{\partial f}{\partial q_2} = k_2 \cos(q_2)p_1^2 \tag{4.41}$$

$$\frac{\partial^2 g}{\partial q_2^2} = k_2 \sin(q_2) \tag{4.42}$$

(Detailed description of the variables, which are used in above equations, can be found in Appendix A.2.) As it has already been mentioned in Sect. 3.1.3, Eqs. (3.16.a)–(3.16.c) depict the zero dynamics structure for a 2-DOF underactuated mechanical system. Consequently, in the special case of the TORA ($z_1 = 0$ and $\dot{z}_1 = 0$) has yielded the following expression of q_2 and p_2.

$$z_1 = q_2 - k(q_1 + p_1 - gp_2) = 0 \Rightarrow q_2 = k(q_1 + p_1 - gp_2) \tag{4.43.a}$$

$$\dot{z}_1 = p_2 - k(p_1 + f - p_2 dg \cdot p) = 0 \Rightarrow p_2 = k(p_1 + f - p_2 dg \cdot p) \tag{4.43.b}$$

Now, if the q_2 and p_2 terms of f, g, ψ and ϕ has been replaced by the expressions of (4.43.a) and (4.43.b), respectively, then the equations of zero dynamics for the TORA system has taken the following form:

$$\begin{aligned}\dot{q}_1 &= p_1 \\ \dot{p}_1 &= f(q_1,p_1) - g(q_1,p_1)\psi^{-1}(q_1,p_1)\varphi(q_1,p_1)\end{aligned} \tag{4.43.c}$$

In Eq. (4.43.c), $f(q_1,p_1), g(q_1,p_1), \psi^{-1}(q_1,p_1)$ and $\varphi(q_1,p_1)$ have represented the same functions f, g, ψ^{-1}, and φ, where all the terms which contain q_2 and p_2 terms have been replaced by the expressions of (4.43.a) and (4.43.b), respectively. Constant k has been selected in such a manner that it would ensure the stability of the zero dynamic system of (4.43.c). The detailed procedure of calculating parameter k has already been described in Sect. 4.1.2. Following Lyapunov function has been defined to analyze stability of the internal dynamics of Eq. (4.43.c) as shown in Eq. (4.44):

$$V_z = \frac{1}{2}q_1^2 + \frac{1}{2}p_1^2 \tag{4.44}$$

Consequently, time derivative of the above Lyapunov function V_z has resulted in:

$$\dot{V}_z = q_1 p_1 + p_1 F \tag{4.45}$$

Now, the controller parameter k has been selected in a judicial manner to ensure the negative definiteness of the $\dot{V}_z$. The other three controller parameters do not alter the negative definiteness of $\dot{V}_z$ (Rudra et al.). However, they have been chosen in a manner so that they satisfy the conditions $c_1 > 0$, $c_2 > 0$, and $\lambda > 0$. (Detailed criteria of controller parameter selection have been discussed in Chap. 3, Sect. 3.2.3.)

4.2.2 Simulation Results and Performance Analysis

In order to verify the effectiveness of the proposed control law on TORA system, at first the state model has been developed in MATLAB® (version: 7.14) Simulink (version: 7.9) environment. During the simulation study, parameters of Table 4.3 have been used to replicate the model of TORA system in the simulation environment. The controller parameters are tabulated in Table 4.4. Initial value of the state variables, which have been chosen for simulation experiment, are as follows: $q_1 = 1, q_2 = \pi/3, p_1 = 0$ and $p_2 = 0$.

Table 4.3 Parameters of TORA system (SI unit)

M	K	l_1	m	R	l_2
2.7	300	0.1	0.2	0.18	0.148

Table 4.4 Parameters of the proposed block backstepping controller

c_1	c_2	k	λ
5	5	0.5	0.05

It is clearly evident from Figs. 4.9 and 4.10 that the control law ensures convergence of the state variables q_1 (i.e., longitudinal displacement of the cart) and p_1 (i.e., cart velocity) to their desired value. Detailed study on the topic reveals that the stability of zero dynamics ensures the convergence of the variables q_1 and p_1 to their desired values. Asymptotic convergence of the state variables, q_1 and p_1, have corroborated the fact that the asymptotic stability of the zero dynamics would ensure the asymptotic convergence of q_1 and p_1 at their desired equilibrium.

On the other hand, Figs. 4.11 and 4.12 the actuated configuration variable q_2 and its derivative p_2 converge to their desired value, which in turn implies that the stability of reduced order system together with the stability of zero dynamics ensure

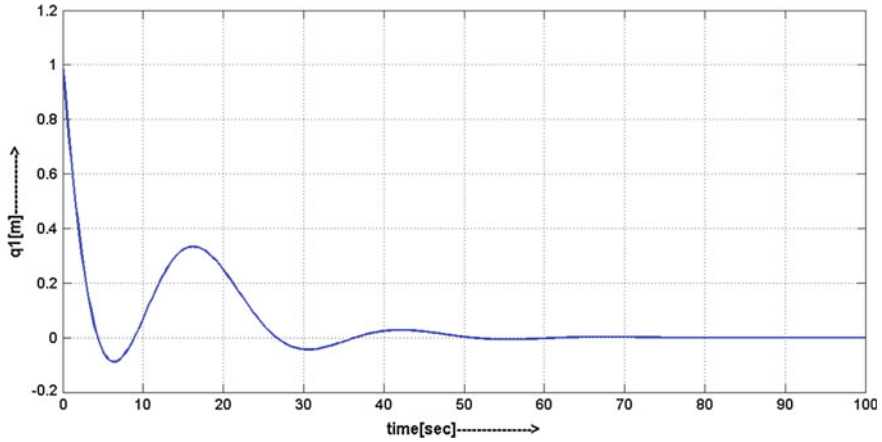

Fig. 4.9 Variation of the state variable q_1 with time

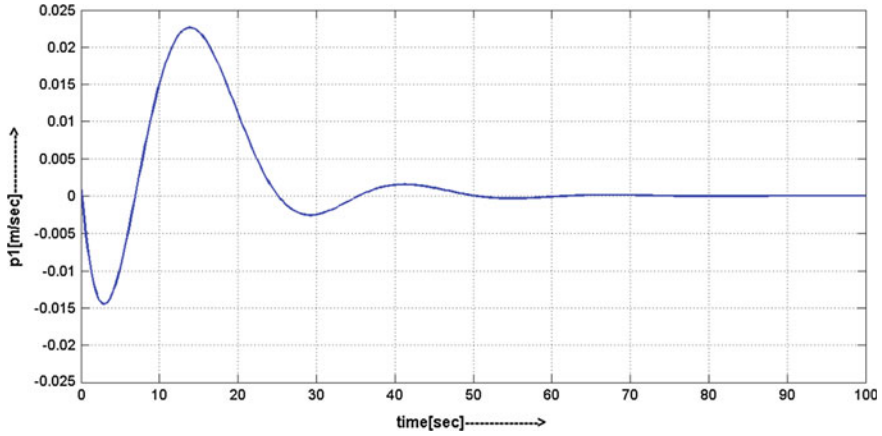

Fig. 4.10 Variation of the state variable p_1 with time

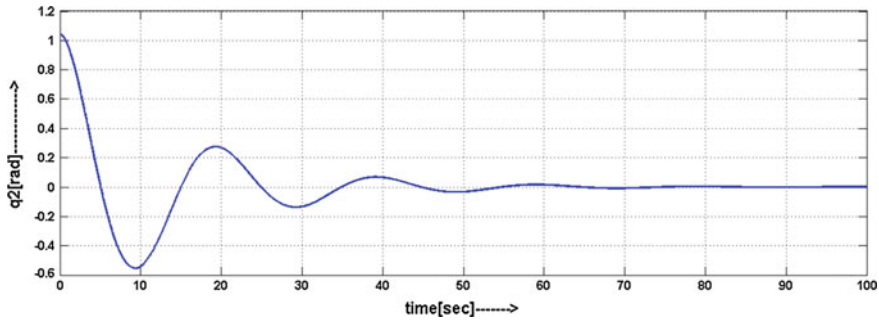

Fig. 4.11 Variation of the state variable q_2 with time

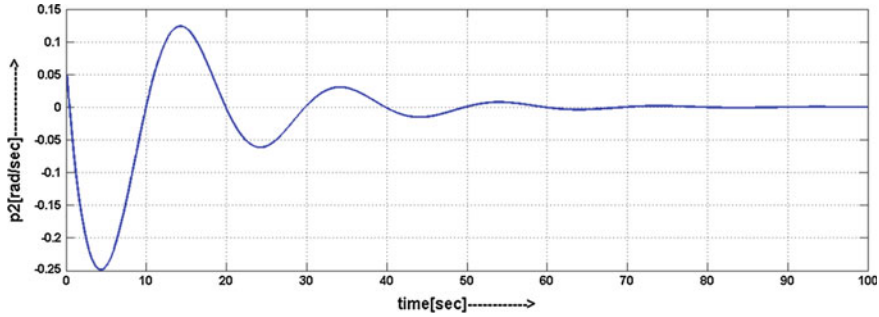

Fig. 4.12 Variation of the state variable p_2 with time

the convergence of the actuated variable toward their desired value. The above findings corroborate the assertion of the theorem 2 of Sect. 3.4, which states the global asymptotic stability of the reduced order system together with the global asymptotic stability of the internal dynamics ensures asymptotic stabilization of the actuated shape variables.

Since TORA system belongs to the category of a holonomic system, it does not require nonsmooth input for its stabilization purpose. Figure 4.13 reveals the fact that the proposed control law generates a smooth control input for the stabilization of the TORA system.

In the next section, application of the present control law on Furuta Pendulum will be presented in a systematic matter. Since Furuta Pendulum belongs to a group of nonholonomic UMSs, it requires either nonsmooth or time-varying control action for its stabilization. Therefore, aptness of the proposed control law can be verified on the platform of Furuta Pendulum to study the suitability and applicability of the same on control problems of nonholonomic systems.

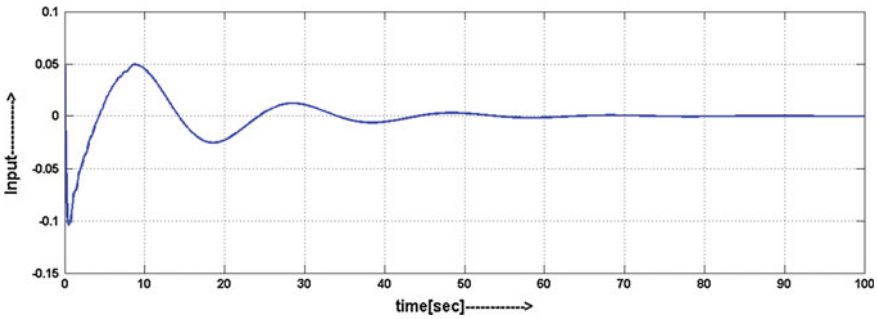

Fig. 4.13 Variation of the control input u with time

4.3 Application on the Furuta Pendulum[3]

Furuta Pendulum was invented by Katsuhisa Furuta and his colleagues in 1992 at Tokyo Institute of Technology, and since then it has been being used as an important test bed for 2-DOF nonlinear UMSs [3, 6, 8]. Early research activities on Furuta Pendulum were initiated by the need of designing an elegant controller that could address the balance of the rockets during a vertical takeoff [6, 8, 16]. Being a member of nonholonomic underactuated mechanical systems, Furuta pendulum fails to satisfy the *Brocket condition of feedback linearization* [21]. *Therefore, it needs time-varying or nonsmooth control law for stabilization* [16, 20, 21]. Indeed, Furuta pendulum executes rotational motion in two different planes, which in turn makes the control problem more complicated than other ordinary 2-DOF nonholonomic systems that usually executes rotary motion only in a single plane [28, 35]. Therefore, in this section application of the proposed control law on Furuta Pendulum is described to verify its aptness for other nonholonomic underactuated systems.

The Furuta pendulum system consists of an inverted pendulum connected to a moving shaft, which is able to execute a rotational motion in horizontal plane (Fig. 4.14). The controller is required to serve a twofold control objective. First objective is to stabilize the pole in its upright position, and the second objective is to ensure the proper orientation control of the shaft $(q_1 = \varphi)$. The state model of the Furuta pendulum can be described by the following equation $\left(q_1 = \varphi, p_1 = \dot{\varphi}, q_2 = \theta, p_2 = \dot{\theta}\right)$ (4.46.a). (Detailed derivation of the state model is given in Appendix A.3.)

[3]Setion 4.3. is based on "Stabilization of Furuta Pendulum: A Backstepping Based Hierarchical Sliding Mode Approach with Disturbance Estimation," by S. Rudra, R.K. Barai, M. Maitra, D. Mandal, S. Ghosh, S. Dam, P. Bhattacharyya, and A. Dutta, appeared in Proc. of 7th International Conference on Intelligent Systems and Control, 2013, pp. 99–105. (C) IEEE 2013. Permission obtained from IEEE.

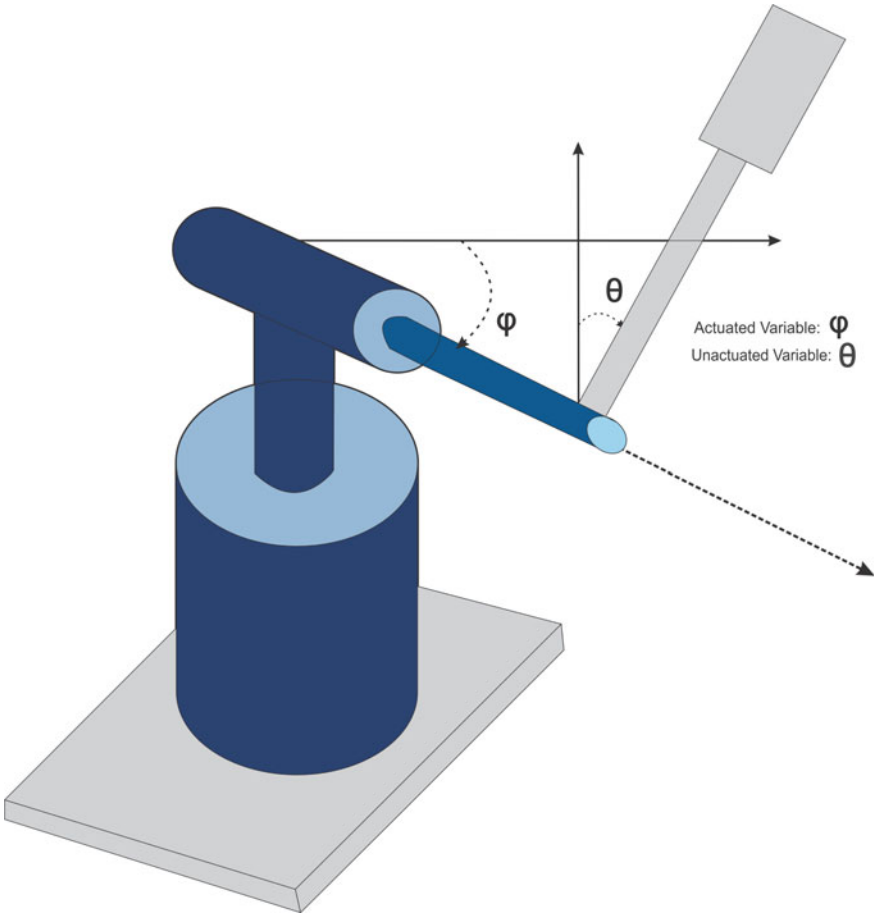

Fig. 4.14 Schematic diagram of Furuta pendulum

$$\begin{aligned} \dot{q}_1 &= p_1 \\ \dot{p}_1 &= u \\ \dot{q}_2 &= p_2 \\ \dot{p}_2 &= f + gu \end{aligned} \tag{4.46.a}$$

where

$$f = k_2 \tan(q_2) + k_3 \sin(q_2) p_1^2 \tag{4.46.b}$$

$$g = -k_1 / \cos(q_2) \tag{4.46.c}$$

$$k_1 = \left(J_2 + m_2 l_2^2\right)/m_2 l_1 l_2 \tag{4.46.d}$$

$$k_2 = \boldsymbol{g} l_1 / L_1 l_2 \tag{4.46.e}$$

$$k_3 = l_2 / L_1 \tag{4.46.f}$$

Salient Features of the Rotating Pendulum: *Unactuated Shape Variable, 2nd order nonholonomic constraints, unstable equilibrium.*

Control Objective: *The goal of the control design is to ensure the asymptotic stabilization of the underactuated rotating Pendulum in its upright position as well as the control law should ensure the proper orientation control of the movable shaft* [35].

4.3.1 Derivation of the Control Law for Furuta Pendulum System

Although Furuta Pendulum is a member of 2-DOF underactuated systems like IWP and TORA, yet its control problem is more complicated than that of the previously mentioned systems. Furuta Pendulum falls under the category of systems with unactuated shape variables; therefore, the definition of first error variable of z_1 has also been modified according to Eq. (4.47) as shown below:

$$z_1 = q_1 - k(q_2 + p_2 - g p_1) \tag{4.47}$$

Unlike the previous two cases where the systems belong to the class of UMSs with actuated shape variable, while defining the variable z_1, the authors have altered the position of configuration variables, and their corresponding derivatives according to the actuation pattern of the system. As a matter of fact, time derivative of z_1 has taken the form of Eq. (4.48):

$$\dot{z}_1 = p_1 - k(p_2 + f - p_1 dg \cdot p) \tag{4.48}$$

Likewise the previous two cases, the stabilizing function has been defined as shown in Eq. (4.49):

$$\alpha_1 = -c_1 z_1 - \lambda \chi_1 + k(p_1 + f - p_1 dg \cdot p) \tag{4.49}$$

where $\chi_1 = \int_0^t z_1 \mathrm{d}t$ and c_1, λ are two arbitrary positive design constant.

Since in this case q_1 is the actuated configuration, the second error variable z_2 has been defined according to Eq. (4.50):

$$z_2 = p_1 - \alpha_1 \tag{4.50}$$

Consequently, the time derivative of z_2 has become:

$$\dot{z}_2 = u + c_1(z_2 - c_1 z_1) - k\left[\left\{f + gu + \frac{\partial f}{\partial q_1}p_1 + \frac{\partial f}{\partial q_2}p_2 + \frac{\partial f}{\partial p_1}f + g\frac{\partial f}{\partial p_1}u + \frac{\partial f}{\partial p_2}u - udg \cdot p - p_1\left(\frac{\partial g}{\partial q_1}(u) + \frac{\partial g}{\partial q_2}(f + gu)\right) - p_1\left(\frac{\partial^2 g}{\partial q_1^2}p_1^2 + 2\frac{\partial^2 g}{\partial q_1 \partial q_2}p_1 p_2 + \frac{\partial^2 g}{\partial q_2^2}p_2^2\right)\right\}\right] \tag{4.51}$$

Hence, comparison of Eq. (4.51) with Eq. (3.9) have yielded the following expression for ψ and ϕ:

$$\psi = 1 - k\left\{g + g\frac{\partial f}{\partial p_1} + \frac{\partial f}{\partial p_2} - dg \cdot p - p_1\frac{\partial g}{\partial q_1}g - p_1\frac{\partial g}{\partial q_2}\right\} \tag{4.52}$$

$$\phi = -k\left[f + \frac{\partial f}{\partial q_1}p_1 + \frac{\partial f}{\partial q_2}p_2 + \frac{\partial f}{\partial p_1}f - \left\{p_1\frac{\partial g}{\partial q_1}f + p_1\left(\frac{\partial^2 g}{\partial q_1^2}p_1^2 + 2\frac{\partial^2 g}{\partial q_1 \partial q_2}p_1 p_2 + \frac{\partial^2 g}{\partial q_2^2}p_2^2\right)\right\}\right] \tag{4.53}$$

The above choice of ψ and ϕ have resulted in the compact expression of $\dot{z}_2$ as follows

$$\dot{z}_2 = \psi u + \lambda z_1 + c_1(z_2 - c_1 z_1 - \lambda\chi_1) + \phi \tag{4.54}$$

However, as it has been already mentioned in the earlier sections that the desired dynamics of z_2 is

$$\dot{z}_2 = -z_1 - c_2 z_2 \tag{4.55}$$

Similar to the method described in Sect. 3.1.2, comparison of the Eq. (4.54) with the desired dynamics of z_2 [as shown in Eq. (4.55)] has resulted in the following expression of the control input

$$u = \psi^{-1}\left[-\left(1 - c_1^2 + \lambda\right)z_1 - (c_1 + c_2)z_2 + \lambda c_1\chi_1 - \phi\right] \tag{4.56}$$

In the above expressions the differentials can be calculated as follows

$$\frac{\partial f}{\partial p_1} = 2k_3 \sin(q_2)p_1 \tag{4.57}$$

$$\frac{\partial f}{\partial p_2} = 0 \tag{4.58}$$

$$\frac{\partial g}{\partial q_1} = 0 \tag{4.59}$$

$$\frac{\partial g}{\partial q_2} = -k_1 \sec q_2 \tan q_2 \tag{4.60}$$

$$\frac{\partial f}{\partial q_1} = 0 \tag{4.61}$$

$$\frac{\partial f}{\partial q_2} = k_2 \sec^2(q_2) + k_3 \cos(q_2) p_1^2 \tag{4.62}$$

$$\frac{\partial^2 g}{\partial q_2^2} = k_1 \sec q_2 \left(\tan^2 q_2 + \sec^2 q_2\right) \tag{4.63}$$

(Detailed description of the variables, which are used in above equations, can be found in Appendix A.3.) Since Furuta pendulum belongs to the class of unactuated shape variables, definition of zero dynamics has to be modified suitably to find the controller gain k.

$$z_1 = q_1 - k(q_2 + p_2 - g p_1) = 0 \Rightarrow q_1 = k(q_2 + p_2 - g p_1) \tag{4.64.a}$$

$$\dot{z}_1 = p_1 - k(p_2 + f - p_1 dg \cdot P) = 0 \Rightarrow p_1 = k(p_2 + f - p_1 dg \cdot p) \tag{4.64.b}$$

Now, if the q_1 and p_1 terms of f, g, ψ, and ϕ could be replaced by the expressions of (4.64.a) and (4.64.b), respectively, then the equations of zero dynamics for the Furuta pendulum will take the following form:

$$\begin{aligned} \dot{q}_2 &= p_2 \\ \dot{p}_2 &= f(q_2, p_2) - g(q_2, p_2)\psi^{-1}(q_2, p_2)\phi(q_2, p_2) \end{aligned} \tag{4.64.c}$$

In Eq. (4.64.c), $f(q_2, p_2)$, $g(q_2, p_2)$, $\psi^{-1}(q_2, p_2)$ and $\phi(q_2, p_2)$ have represented the same functions f, g, ψ^{-1} and ϕ, with all the q_1 and p_1 terms of the expressions have been replaced by the expressions of (4.64.a) and (4.64.b), respectively. Constant k has been selected in such a manner that it can ensure the stability of the zero dynamic system of (4.64.c). Following Lyapunov function has been defined to analyze stability of the internal dynamics of Eq. (4.64.c)

$$V_z = \frac{1}{2} q_2^2 + \frac{1}{2} p_2^2 \tag{4.65}$$

Now time derivative of the above Lyapunov function V_z has resulted in:

Table 4.5 Parameters of the Furuta pendulum (SI unit)

J_1	I_1	m_1	l_1	J_2	I_2	m_2	l_2
3.127×10^{-2}	0.1	0.08	0.150	2.169×10^{-3}	0.148	0.098	0.215

Table 4.6 Parameters of the proposed block backstepping controller

c_1	c_2	k	λ
15	15	1.35	0.05

$$\dot{V}_z = q_2 p_2 + p_2 F \tag{4.66}$$

Hence, the controller parameter k has been selected in a judicial manner to ensure the negative definiteness of the $\dot{V}_z$. The other three controller parameters do not alter the negative definiteness of $\dot{V}_z$ [27]. However, they have been chosen in a manner so that they could satisfy the condition $c_1 > 0$, $c_2 > 0$ and $\lambda > 0$. (Detailed criteria of controller parameter selection have been discussed in Chap. 3, Sect. 3.2.3.)

4.3.2 Simulation Results and Performance Analysis

Effectiveness of the proposed control law has been verified after simulating the closed-loop system in MATLAB® (version: 7.14) Simulink (version: 7.9) environment. Indeed from the discussion of the previous section, it is clearly evident that no such significant alteration is required to make the control law applicable for unactuated shape variable systems. Although the theoretical analysis has already established the fact that proposed control law can ensure global asymptotic stability of the system, yet in order to corroborate the same in simulation environment the authors have used the parameters of Table 4.5. The controller parameters are tabulated in Table 4.6. Initial value of the state variables that have been chosen for simulation experiment, are as follows: $q_1 = \pi/3, q_2 = \pi/6, p_1 = 0$ and $p_2 = 0$.

In case of IWP and TORA, at first time variation of the unactuated configuration variable and its derivative (namely q_1 and p_1) have been shown to assure that zero dynamics stability ensure convergence of the unactuated state variable toward their desired equilibrium state. Since in case of the Furuta pendulum q_2 and p_2 represent unactuated configuration variable, the authors have first shown variation of the above-mentioned variables.

It is clear from Figs. 4.15 and 4.16 that judicial selection of k, which is able to ensure stability of the zero dynamics, also ensure convergence of the unactuated variable and its derivative to their desired state coordinate. Now, the time variation of actuated variables is shown in the following Figs. 4.17 and 4.18.

It can be inferred from Figs. 4.17 and 4.18 that the control input u can also ensure the global asymptotic stabilization of the actuated state variables.

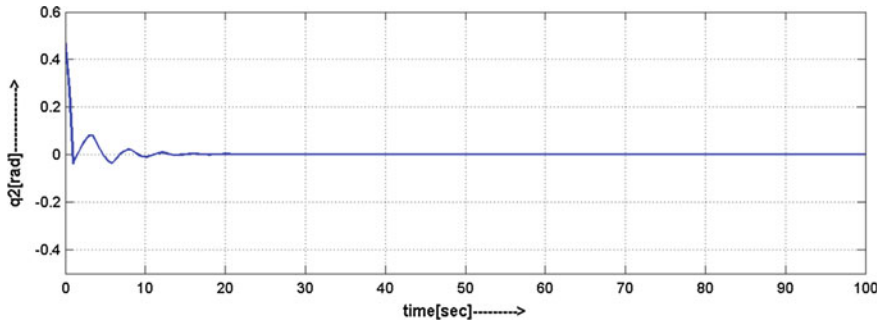

Fig. 4.15 Variation of the state variable q_2 with time

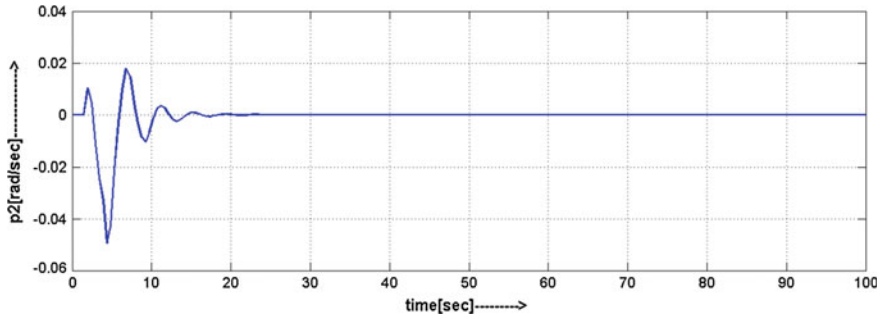

Fig. 4.16 Variation of the state variable p_2 with time

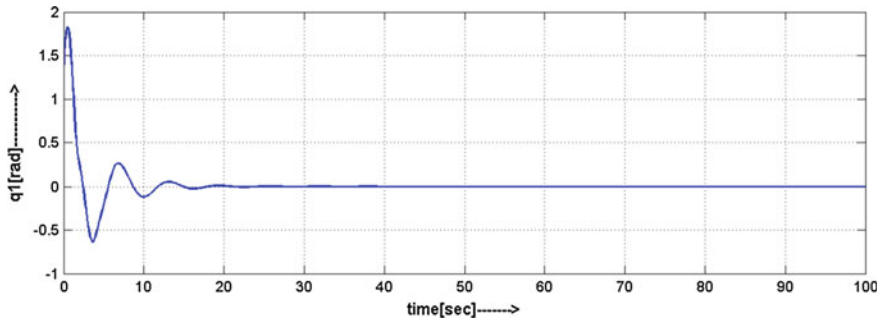

Fig. 4.17 Variation of the state variable q_1 with time

Convergence of the actuated shape variables to their desired value, which in turn corroborates the fact that stability of the reduced order system together with the stability of zero dynamics ensure convergence of the actuated variable toward their desired value. The above findings substantiate the assertion of the theorem 2 of

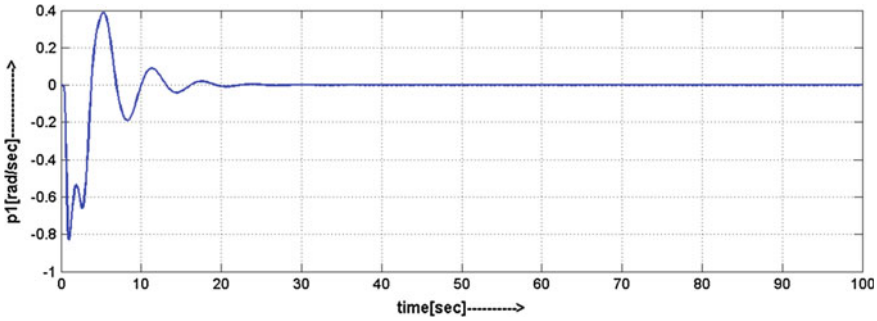

Fig. 4.18 Variation of the state variable p_1 with time

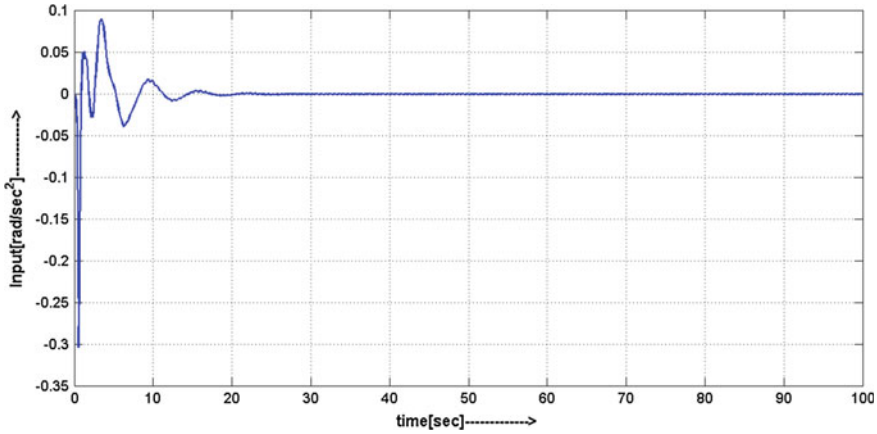

Fig. 4.19 Variation of the control input u with time

Sect. 3.4, which states the global asymptotic stability of the reduced order system together with the global asymptotic stability of the internal dynamics ensures asymptotic stabilization of the actuated shape variables.

Indeed it has been mentioned earlier that Furuta pendulum falls under the system with nonholonomic motion constraints; therefore, they requires nonsmooth or time-varying state feedback for their stabilization. Now, it is clear from Eq. (4.56) and the partial derivatives of (4.57)–(4.63) that the control law generates nonsmooth actuating signal. In the following Fig. 4.19 variation of control input with time as shown below.

Indeed, all the three above-mentioned systems possess different dynamics, and aptness of the proposed control law has already established its versatility and suitability for different UMSs. However, the authors think without validating the application of proposed control law on two different benchmark underactuated systems, namely acrobot and pendubot, which have been invented by the great

scientist M.W. Spong himself; this demonstration would not take a complete shape. Therefore, in the subsequent sections, application of the proposed control law on acrobot and pendubot will be explained in a systematic manner.

4.4 Application on the Acrobot System

An acrobot is a typical example of an underactuated mechanical system with two degrees of freedom (DOF) [10, 15, 18]. It executes planar motion in the vertical plane and resembles a gymnast on a high bar where the first and second joint can be thought of as the mechanical analog of the gymnast's hands and hips respectively [18, 29–34]. In the acrobat, an actuator is mounted only at the second joint although it is a 2-DOF mechanical system, leaving its first joint without any actuation [21, 29]. A common control objective for an acrobot is to swing it up from the straight down position and stabilize it at the straight up position, which imitates the motion of a gymnast going from a natural hanging position to a handstand on the bar [21, 29–34]. One of the important control problems for acrobot is the set point control (regulation or stabilization) of acrobot at vertical upright position [21, 22]. During the last two decades, several research articles have been published on the design of the swing up and stabilizing controller for the acrobot system [21, 22]. An acrobot is a complicated nonlinear underactuated system with a second-order nonholonomic constraint (SNC) and is not a full-state feedback linearizable system [13, 22]. Consequently, its controller design is being considered as a challenging problem [13, 21].

The nonlinear two-link planar robot considered in this section, popularly known as acrobot system, was first introduced by M.W. Spong [23, 29–31]. Figure 4.20 illustrates the schematic diagram of the geometrical structure of this nonlinear benchmark robotic system in which the rotational motion of the elbow joint controls the motions of the two links of the robot. Assuming the robot links are made up of rigid elements, the following mathematical model can be used to describe the dynamics of the acrobot system. (Detailed mathematical model is derived in Appendix A, Sect. A.4.)

The state model of the acrobot is shown in following Eqs. (4.67.a)–(4.67.c). (For detailed derivation of the state model, please refer Appendix A.4.)

$$\begin{aligned} \dot{q}_1 &= p_1 \\ \dot{p}_1 &= f + gu \\ \dot{q}_2 &= p_2 \\ \dot{p}_2 &= u \end{aligned} \tag{4.67.a}$$

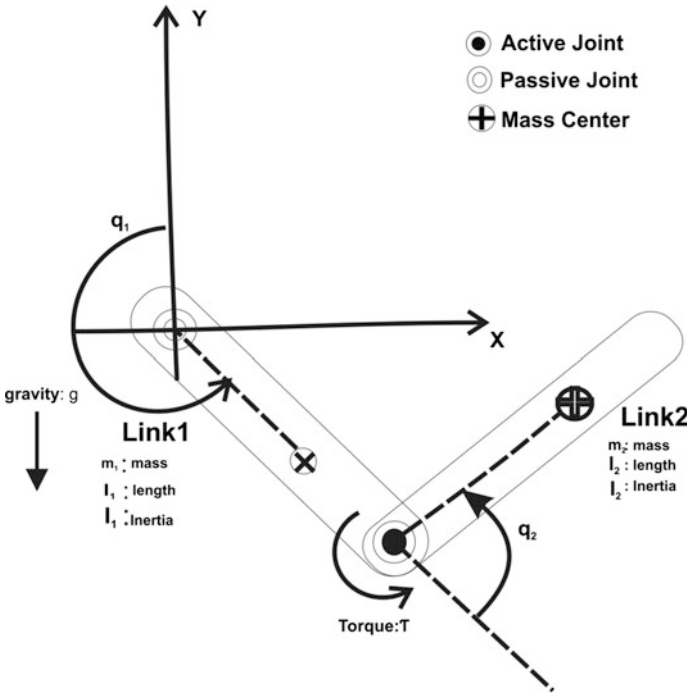

Fig. 4.20 Schematic diagram of the acrobot

where

$$f = -\left(\frac{h_1}{m_{11}} + \frac{\phi_1}{m_{11}}\right) \tag{4.67.b}$$

$$g = -\frac{m_{12}}{m_{11}} \tag{4.67.c}$$

Salient Features of Acrobot: *Actuated shape variable system, unstable equilibrium, second-order nonholonomic motion constraint.*

Control Objective: *Stabilize the acrobot at its vertical upright position.*

4.4.1 Derivation of the Control Law for Acrobot System

Since the system belongs to a class of actuated shape variable systems, the first error variable z_1 has been defined like the authors have defined it for IWP and TORA system. Definition of first error variable is shown in the following Eq. (4.68):

$$z_1 = q_2 - k(q_1 + p_1 - gp_2) \tag{4.68}$$

The derivative of z_1 has been computed as shown in the following Eq. (4.69):

$$\dot{z}_1 = p_2 - k(p_1 + f - p_2 dg \cdot p) \tag{4.69}$$

The stabilizing function has been defined as

$$\alpha_1 = -c_1 z_1 - \lambda \chi_1 + k(p_1 + f - p_2 dg \cdot p) \tag{4.70}$$

where $\chi_1 = \int_0^t z_1 \mathrm{d}t$ and c_1, λ are two arbitrary positive design constant.

Now, the second error variable z_2 has been defined

$$z_2 = p_2 - \alpha_1 \tag{4.71}$$

Subsequently, the time derivative of z_2 has taken the shape of Eq. (4.72):

$$\dot{z}_2 = u + c_1(z_2 - c_1 z_1 - \lambda \chi_1) - k\left[\left\{f + gu + \frac{\partial f}{\partial q_1}p_1 + \frac{\partial f}{\partial q_2}p_2 + \frac{\partial f}{\partial p_1}f + g\frac{\partial f}{\partial p_1}u + \frac{\partial f}{\partial p_2}u - udg \cdot p - p_2\left(\frac{\partial g}{\partial q_1}(f + gu) + \frac{\partial g}{\partial q_2}(u)\right) - p_2\left(\frac{\partial^2 g}{\partial q_1^2}p_1^2 + 2\frac{\partial^2 g}{\partial q_1 \partial q_2}p_1 p_2 + \frac{\partial^2 g}{\partial q_2^2}p_2^2\right)\right\}\right] \tag{4.72}$$

Hence, comparison of Eq. (4.72) with Eq. (3.9) has resulted in the following expression for ψ and ϕ:

$$\psi = 1 - k\left\{g + g\frac{\partial f}{\partial p_1} + \frac{\partial f}{\partial p_2} - dg \cdot p - p_2\frac{\partial g}{\partial q_1}g - p_2\frac{\partial g}{\partial q_2}\right\} \tag{4.73}$$

$$\phi = -k\left[f + \left(\frac{\partial f}{\partial q_1}p_1 + \frac{\partial f}{\partial q_2}p_2 + \frac{\partial f}{\partial p_1}f\right) - \left\{p_2\frac{\partial g}{\partial q_1}f + p_2\left(\frac{\partial^2 g}{\partial q_1^2}p_1^2 + 2\frac{\partial^2 g}{\partial q_1 \partial q_2}p_1 p_2 + \frac{\partial^2 g}{\partial q_2^2}p_2^2\right)\right\}\right] \tag{4.74}$$

The above choice of ψ and ϕ has yielded the compact expression of control input as follows:

$$\ddot{z}_2 = \psi u + \lambda z_1 + c_1(z_2 - c_1 z_1 - \lambda \chi_1) + \phi \tag{4.75}$$

However, the desired dynamics of z_2 is

$$\dot{z}_2 = -z_1 - c_2 z_2 \tag{4.76}$$

Similar to the method described in Sect. 3.1.2, comparison of the above equation of $\dot{z}_2$ with the desired dynamics of z_2 has resulted in:

$$u = \psi^{-1}\left[-\left(1 - c_1^2 + \lambda\right)z_1 - (c_1 + c_2)z_2 + \lambda c_1 \chi_1 - \phi\right] \tag{4.77}$$

In the above expressions, the differentials can be calculated as shown below:

$$\frac{\partial f}{\partial p_1} = \frac{2M_l \sin(q_2)p_2}{m_{11}} \tag{4.78}$$

$$\frac{\partial f}{\partial p_2} = \frac{-4M_l \sin(q_2)(p_2 - p_1)}{m_{11}} \tag{4.79}$$

$$\frac{\partial g}{\partial q_1} = 0 \tag{4.80}$$

$$\frac{\partial g}{\partial q_2} = -\frac{M_1(M_2 + M_l)\sin(q_2)}{m_{11}^2} \tag{4.81}$$

$$\frac{\partial f}{\partial q_1} = \left(\frac{\phi' \sin(q_1) + \phi'' \sin(q_1 + q_2)}{m_{11}}\right) \tag{4.82}$$

$$\frac{\partial f}{\partial q_2} = \frac{M_l \cos(q_2)\left(p_2^2 - 2p_2p_1\right) + \phi'' \sin(q_1 + q_2) + 2M_l \sin(q_2)f}{m_{11}} \tag{4.83}$$

$$\frac{\partial^2 g}{\partial q_2^2} = \frac{2(1 + 2g)M_l^2 \sin^2(q_2) + m_{11}(1 + 2g)M_l \cos(q_2)}{m_{11}^2} \tag{4.84}$$

(Calculation of all the partial differential equations are shown in Appendix A.4.) As it has already been stated in Sect. 3.1.3, Eqs. (3.16.a)–(3.16.c) depict the zero dynamics structure for a 2-DOF underactuated mechanical system. Therefore, in the special case of the acrobot $z_1 = 0$ and $\dot{z}_1 = 0$ has yielded the following expressions of q_2 and p_2:

$$z_1 = q_2 - k(q_1 + p_1 - gp_2) = 0 \Rightarrow q_2 = k(q_1 + p_1 - gp_2) \tag{4.85.a}$$

$$\dot{z}_1 = p_2 - k(p_1 + f - p_2 dg \cdot p) = 0 \Rightarrow p_2 = k(p_1 + f - p_2 dg \cdot p) \tag{4.85.b}$$

Now, if the q_2 and p_2 terms of f_1, g_1, ψ, and ϕ have been replaced by the expressions of (4.85.a) and (4.85.b), respectively, then the equations of zero dynamics for the acrobot has taken the following form:

$$\begin{aligned} \dot{q}_1 &= p_1 \\ \dot{p}_1 &= f(q_1, p_1) - g_1(q_1, p_1)\psi^{-1}(q_1, p_1)\varphi(q_1, p_1) \end{aligned} \tag{4.85.c}$$

In Eq. (4.85.c), $f(q_1, p_1)$, $g(q_1, p_1)$, $\psi^{-1}(q_1, p_1)$ and $\varphi(q_1, p_1)$ have represented the same functions f_1, g_1, ψ^{-1}, and φ, where all the q_2 and p_2 terms have been

replaced by the expression of (4.85.a) and (4.85.b), respectively. Constant k has been selected in such a manner that it can ensure the stability of the zero dynamic system of (4.85.c). Following Lyapunov function has been defined to analyze stability of the internal dynamics of Eq. (4.85.c):

$$V_z = \frac{1}{2}q_1^2 + \frac{1}{2}p_1^2 \tag{4.86}$$

Now, time derivative of the above Lyapunov function V_z has shown in the following equation:

$$\dot{V}_z = q_1 p_1 + p_1 F \tag{4.87}$$

It is clear from the above discussion that the controller parameter k has been selected in a judicial manner to ensure the negative definiteness of the $\dot{V}_z$. The other three controller parameters do not alter the negative definiteness of $\dot{V}_z$ [27]. However, they have been chosen in a manner so that they satisfy the condition $c_1 > 0$, $c_2 > 0$ and $\lambda > 0$. (Detailed criteria of controller parameter selection have been discussed in Chap. 3, Sect. 3.2.3.)

4.4.2 Simulation Results and Performance Analysis

Effectiveness of the proposed control law has been verified after simulating the closed-loop system in MATLAB® (version: 7.14) Simulink (version: 7.9) environment. During the simulation study, parameters of Table 4.7 have been used to develop the model of the acrobot system in simulation environment. Parameters of the proposed controller are tabulated in Table 4.8. Initial value of the state variables, which have been chosen for the present simulation experiment, are as follows: $q_1 = \pi/3, q_2 = \pi/4, p_1 = 0$ and $p_2 = 0$.

Variation of the state variable q_1 with time is shown in Fig. 4.21, and time variation of p_1 is shown in the following Fig. 4.22.

It can be inferred from Figs. 4.21 and 4.22 that the proposed control law could ensue the global asymptotic stabilization of the state variable q_1 (i.e., angle of the base link), and p_1 (i.e., angular velocity of the base link). Asymptotic convergence of the state variables, q_1 and p_1, has corroborated the fact that the asymptotic

Table 4.7 Parameters of the acrobot (SI unit)

m_1	m_2	l_1	l_2	l_{c1}	l_{c2}	I_1	I_2	G
1	1	1	2	0.5	1	0.083	0.33	9.8

Table 4.8 Parameters of the proposed block backstepping controller

c_1	c_2	K	λ
10	10	0.9	0.05

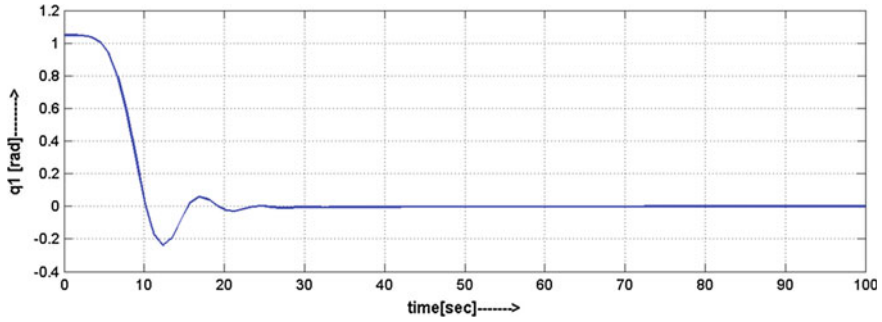

Fig. 4.21 Variation of the state variable q_1 with time

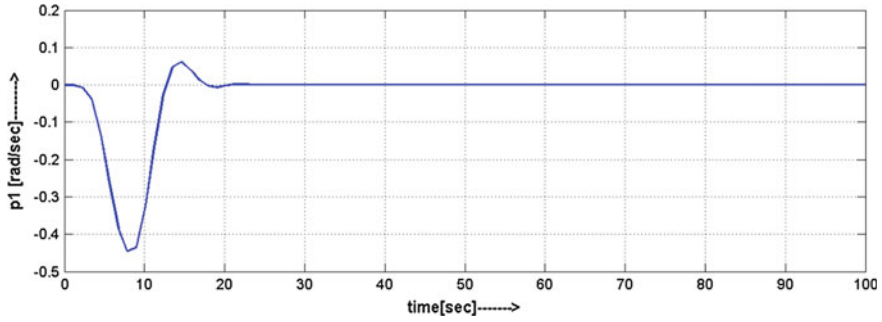

Fig. 4.22 Variation of the state variable p_1 with time

stability of the zero dynamics would ensure the asymptotic convergence of q_1 and p_1 at their desired equilibrium.

Similar to Figs. 4.21 and 4.22, variation of the state variable q_2 is shown in Fig. 4.23 and variation of the state variable p_2 is shown in Fig. 4.24.

It can be inferred that Figs. 4.23 and 4.24 that the control input u can ensure the asymptotic stabilization of the actuated state variables. Proposition of theorem 2 (Chap. 3, Sect. 3.4), which states the global asymptotic stability of the reduced order system together with the global asymptotic stability of the internal dynamics ensures asymptotic stabilization of the actuated shape variables which have been corroborated by the stabilization of the actuated state variables.

Being a nonholonomic mechanical system, acrobot fails to satisfy the Brockets' condition of feedback linearization [23]. Therefore, it requires a nonsmooth control input for its stabilization. Figure 4.25 reveals the fact that the proposed control law can generate a nonsmooth control input for the stabilization of acrobot system. In the next section, application of control law on pendubot will be demonstrated in a systematic manner.

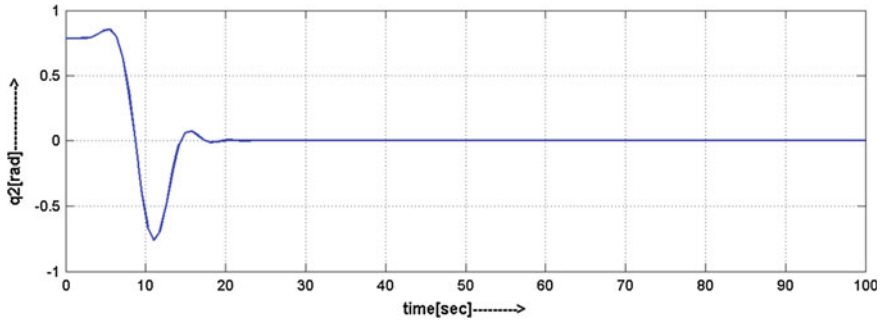

Fig. 4.23 Variation of the state variable q_2 with time

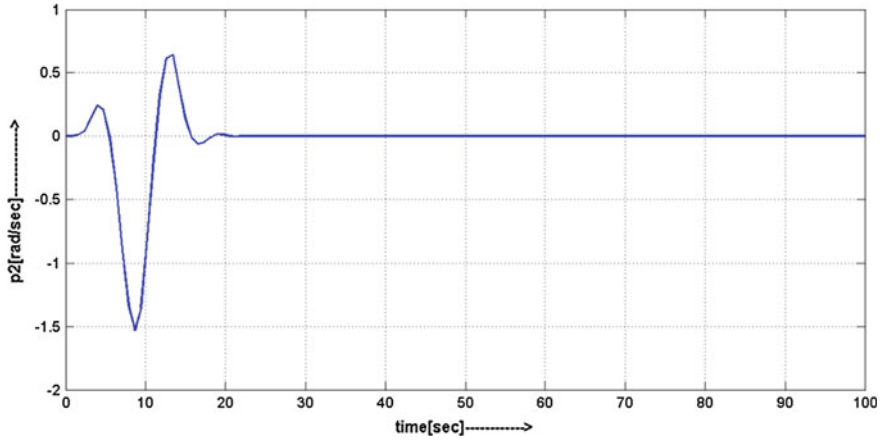

Fig. 4.24 Variation of the state variable p_2 with time

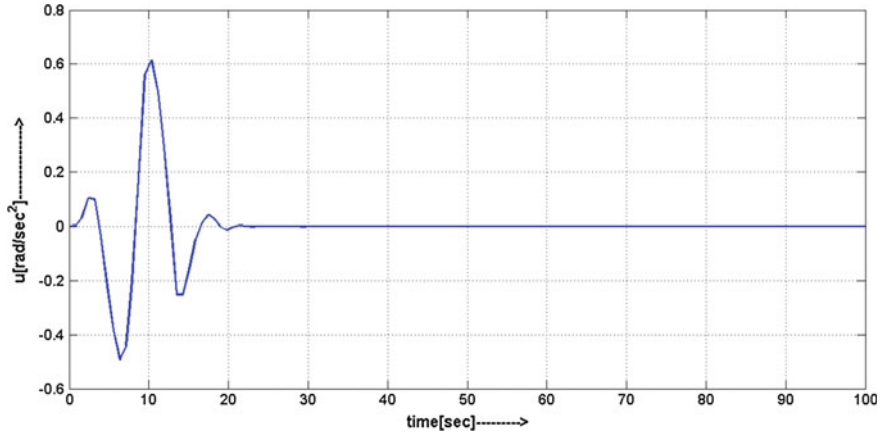

Fig. 4.25 Variation of the control input u with time

4.5 Application on the Pendubot System[4]

A pendubot is a two-link planar robot, whose first link is actuated and second link is unactuated [1, 3, 7]. It is a complicated 2-DOF underactuated mechanical system [7, 18, 21, 39]. Schematic diagram of the pendubot is shown in Fig. 4.26. The construction of pendubot is almost similar to that of acrobot. However, in case of pendubot the actuated joint is the base joint, as a result the system becomes an unactuated shape variable system. Hence, the control problem of pendubot becomes more complicated than that of the previous one [13, 21]. In order to feedback stabilize the pendubot to its vertical upright position, swing up control is frequently used to move the pendubot close to the equilibrium position, and thereafter a balance control action is activated to keep the pendubot at its vertical upright position [18, 21]. Over the past few decades, several research endeavors have been made to devise a proper swing up control algorithm for the pendubot system [1, 7]. In addition, several researchers have dealt with the stabilizing control problem of pendubot at its vertical upright position [29–32]. Spong has used a linear quadratic regulator (LQR) and pole placement controller for the balancing and stabilizing controller for the stabilization of the Pendubot [33]. Fantoni, Lozano and Spong have devised another type of swing up and balancing controller for pendubot using energy based control approach [5, 18]. Pendubot also possesses some unique construction features that make the controller design task for the system more challenging than that of the other 2-DOF underactuated mechanical systems [18, 39]. Similar to acrobot, pendubot also belongs to the class of nonholonomic underactuated systems, and hence it is not possible to stabilize the system using smooth feedback law [16, 21]. However, unlike acrobot, pendubot belongs to the class of unactuated shape variable 2-DOF underactuated mechanical systems [15, 16, 18]. As a result, control problem of pendubot is considered to be more challenging than that of acrobot system [16, 21].

The nonlinear state model of pendubot considered in this section was first introduced by M.W. Spong [29–32]. Figure 4.26 illustrates the schematic diagram of the geometrical structure of this nonlinear benchmark robotic system in which the rotational motion of the base joint controls the motions of the two links of the robot. Assuming the robot links are made up of rigid elements, following mathematical model can be used to describe the dynamics of the pendubot system. The state model of pendubot is shown in Eq. (4.88.a). (The detailed mathematical modeling of pendubot could be found in Appendix A.5.)

[4]Section 4.5 is based on Design of block backstepping based nonlinear state feedback controller for pendubot by S. Rudra and R.K. Barai, appeared in Proc. of Conference on IEEE First International Conference on Control, Measurement and Instrumentation (CMI), 2016, pp. 1–5. (C) IEEE 2016. Permission obtained from IEEE.

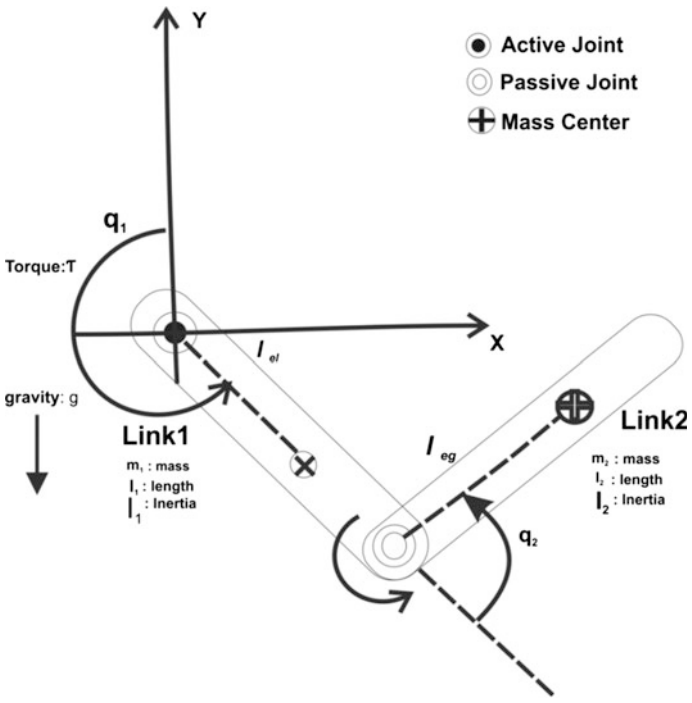

Fig. 4.26 Schematic diagram of the pendubot

$$\begin{aligned}\dot{q}_1 &= p_1\\ \dot{p}_1 &= u\\ \dot{q}_2 &= p_2\\ \dot{p}_2 &= f + gu\end{aligned} \tag{4.88.a}$$

where

$$f = -\left(\frac{h_2}{m_{22}} + \frac{\phi_2}{m_{22}}\right) \tag{4.88.b}$$

$$g = -\frac{m_{21}}{m_{22}} \tag{4.88.c}$$

Salient features of Pendubot: *Unactuated shape variable systems, second-order nonholonomic constraints, and unstable equilibrium point.*

Control Objective: *Stabilize the pendubot at its vertical upright position.*

4.5.1 Derivation of the Control Law for Pendubot System

At first, state variable z_1 has been defined according to Eq. (4.89):

$$z_1 = q_1 - k(q_2 + p_2 - gp_1) \tag{4.89}$$

Since pendubot also belongs to the class of unactuated shape variable system like Furuta pendulum, first error variable for pendubot has also been defined in a similar fashion.

Therefore, time derivative of z_1 has been computed as shown in Eq. (4.90):

$$\dot{z}_1 = p_1 - k(p_2 + f - p_1 dg \cdot p) \tag{4.90}$$

Accordingly, the stabilizing function has been defined as shown in the following Eq. (4.91):

$$\alpha_1 = -c_1 z_1 - \lambda \chi_1 + k(p_2 + f - p_1 dg \cdot p) \tag{4.91}$$

where $\chi_1 = \int_0^t z_1 \mathrm{d}t$ and c_1, λ are two arbitrary positive design constant.

Like Furuta pendulum, the second error variable z_2 has also been defined in accordance with Eq. (4.50), which is shown in Eq. (4.92):

$$z_2 = p_1 - \alpha_1 \tag{4.92}$$

Subsequently, the derivative of z_2 has become:

$$\dot{z}_2 = u + c_1(z_2 - c_1 z_1 - \lambda \chi_1) - k\left[\left\{f + gu + \frac{\partial f}{\partial q_1}p_1 + \frac{\partial f}{\partial q_2}p_2 + \frac{\partial f}{\partial p_1}f + g\frac{\partial f}{\partial p_1}u + \frac{\partial f}{\partial p_2}u - udg \cdot p - p_1\left(\frac{\partial g}{\partial q_1}(u) + \frac{\partial g}{\partial q_2}(f + gu)\right) - p_1\left(\frac{\partial^2 g}{\partial q_1^2}p_1^2 + 2\frac{\partial^2 g}{\partial q_1 \partial q_2}p_1 p_2 + \frac{\partial^2 g}{\partial q_2^2}p_2^2\right)\right\}\right] \tag{4.93}$$

Hence, comparison of Eq. (4.93) with Eq. (3.9) has yielded the following expression for ψ and ϕ:

$$\psi = 1 - k\left\{g + g\frac{\partial f}{\partial p_1} + \frac{\partial f}{\partial p_2} - dg \cdot p - p_1\frac{\partial g}{\partial q_1} - p_1\frac{\partial g}{\partial q_2}g_2\right\} \tag{4.94}$$

$$\phi = -k\left[f + \left(\frac{\partial f}{\partial q_1}p_1 + \frac{\partial f}{\partial q_2}p_2 + \frac{\partial f}{\partial p_1}f\right) - \left\{p_1\frac{\partial g}{\partial q_1}f + p_1\left(\frac{\partial^2 g}{\partial q_1^2}p_1^2 + 2\frac{\partial^2 g}{\partial q_1 \partial q_2}p_1 p_2 + \frac{\partial^2 g}{\partial q_2^2}p_2^2\right)\right\}\right] \tag{4.95}$$

The above choice of ψ and ϕ has resulted in the compact expression of control input as shown in the following Eq. (4.96):

$$\ddot{z}_2 = \psi u + \lambda z_1 + c_1(z_2 - c_1 z_1 - \lambda\chi_1) + \phi \tag{4.96}$$

Likewise the previous design case, desired dynamics of z_2 can be defined as:

$$\dot{z}_2 = -z_1 - c_2 z_2 \tag{4.97}$$

Similar to the method described in Sect. 3.1.2, comparison of the Eq. (4.96) with the desired dynamics of z_2 has resulted in:

$$u = \psi^{-1}\left[-\left(1 - c_1^2 + \lambda\right)z_1 - (c_1 + c_2)z_2 + \lambda c_1 \chi_1 - \phi\right] \tag{4.98}$$

In the above expressions the differentials can be calculated as follows:

$$\frac{\partial f}{\partial p_1} = \frac{2M_l \sin(q_2)p_2}{m_{11}} \tag{4.99}$$

$$\frac{\partial f}{\partial p_2} = \frac{-4M_l \sin(q_2)(p_2 - p_1)}{m_{11}} \tag{4.100}$$

$$\frac{\partial g}{\partial q_1} = 0 \tag{4.101}$$

$$\frac{\partial g}{\partial q_2} = -\frac{M_1(M_2 + M_l)\sin(q_2)}{m_{11}^2} \tag{4.102}$$

$$\frac{\partial f}{\partial q_1} = \left(\frac{\phi' \sin(q_1) + \phi'' \sin(q_1 + q_2)}{m_{11}}\right) \tag{4.103}$$

$$\frac{\partial f}{\partial q_2} = \frac{M_l \cos(q_2)\left(p_2^2 - 2p_2 p_1\right) + \phi'' \sin(q_1 + q_2) + 2M_l \sin(q_2) f}{m_{11}} \tag{4.104}$$

$$\frac{\partial^2 g}{\partial q_2^2} = \frac{2(1 + 2g)M_l^2 \sin^2(q_2) + m_{11}(1 + 2g)M_l \cos(q_2)}{m_{11}^2} \tag{4.105}$$

(Calculation of all the above-mentioned partial derivatives are shown in Appendix A.5.) As it has already been stated in Sect. 3.1.3, Eqs. (3.16.a)–(3.16.c) represent the zero dynamics structure for a 2-DOF underactuated mechanical system. Consequently, in special case of the pendubot $z_1 = 0$ and $\dot{z}_1 = 0$ has yielded the following expression of q_1 and p_1.

$$z_1 = q_1 - k(q_2 + p_2 - gp_1) = 0 \Rightarrow q_1 = k(q_2 + p_2 - gp_1) \tag{4.106.a}$$

$$\dot{z}_1 = p_1 - k(p_2 + f - p_1 dg \cdot P) = 0 \Rightarrow p_1 = k(p_2 + f - p_1 dg \cdot p) \tag{4.106.b}$$

Now, if the q_1 and p_1 terms of f, g, ψ and ϕ have been replaced by the expressions of (4.106.a) and (4.106.b), respectively, then the equations of zero dynamics for the pendubot has taken the following form:

$$\begin{aligned} \dot{q}_2 &= p_2 \\ \dot{p}_2 &= f(q_2, p_2) - g(q_2, p_2)\psi^{-1}(q_2, p_2)\phi(q_2, p_2) \end{aligned} \tag{4.106.c}$$

In Eq. (4.106.c), $f(q_2, p_2)$, $g(q_2, p_2)$, $\psi^{-1}(q_2, p_2)$ and $\phi(q_2, p_2)$ have represented the same functions f, g, ψ^{-1} and ϕ, with the only difference that all the q_1 and p_1 terms of the equations have been replaced by the expressions of (4.106.a) and (4.106.b), respectively. Therefore, constant k has been selected in such a manner that it would ensure the stability of the zero dynamic system of Eq. (4.106.c). Following Lyapunov function has been defined to analyze stability of the internal dynamics of Eq. (4.106.c)

$$V_z = \frac{1}{2}q_2^2 + \frac{1}{2}p_2^2 \tag{4.107}$$

Now, time derivative of the above Lyapunov function V_z has shown in the following equation:

$$\dot{V}_z = q_2 p_2 + p_2 F \tag{4.108}$$

Now, the controller parameter k has been selected in a judicial manner to ensure the negative definiteness of the $\dot{V}_z$. The other three controller parameters do not alter the negative definiteness of $\dot{V}_z$ [27]. However, they have been chosen in a manner so that they satisfy the condition $c_1 > 0$, $c_2 > 0$ and $\lambda > 0$. (Detailed criteria of controller parameter selection have been discussed in Chap. 3, Sect. 3.2.3.)

Table 4.9 Parameters of the pendubot (SI unit)

m_1	m_2	l_1	l_2	l_{c1}	l_{c2}	I_1	I_2	g
1	1	1	2	0.5	1	0.083	0.33	9.8

Table 4.10 Parameters of the proposed block backstepping controller

c_1	c_2	K	λ
5	5	1.5	0.05

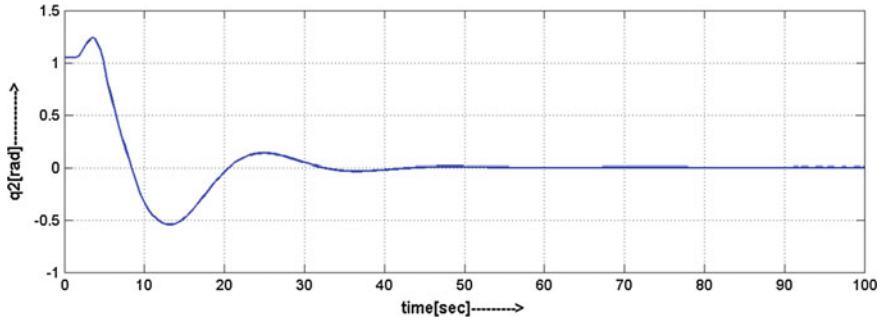

Fig. 4.27 Variation of the state variable q_2 with time

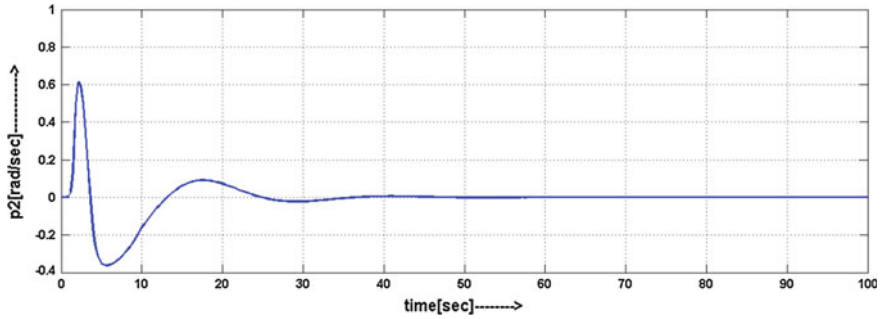

Fig. 4.28 Variation of the state variable p_2 with time

4.5.2 Simulation Results and Performance Analysis

Effectiveness of the proposed control law has been verified after simulating the closed-loop system in MATLAB® (version: 7.14) Simulink (version: 7.9) environment. During the present simulation study, parameters of Table 4.9 have been used to develop the model of pendubot in simulation environment. Parameters of the proposed controller are tabulated in Table 4.10. Initial value of the state variables, which have been chosen for simulation experiment, are as following: $q_1 = \pi/4, q_2 = \pi/3, p_1 = 0$ and $p_2 = 0$.

Similar to the case of Furuta pendulum at first the variation of unactuated configuration variable (q_2) and its derivative (p_2) have been shown in Figs. 4.27 and 4.28.

It is clear from Figs. 4.27 and 4.28 that judicial selection of k, which is able to ensure stability of the zero dynamics, also ensure convergence of the unactuated variable and its derivative to their desired state coordinate. Now, the time variation of actuated variables is shown in the following Figs. 4.29 and 4.30.

It can be inferred from Figs. 4.29 and 4.30 that the control input u can ensure the global asymptotic stabilization of the actuated state variables. Proposition of

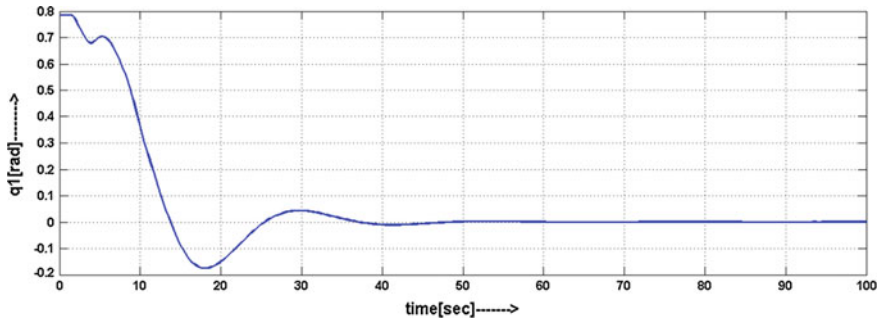

Fig. 4.29 Variation of the state variable q_1 with time

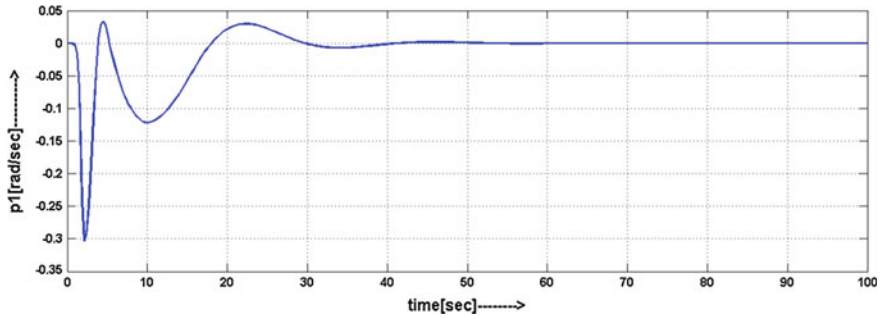

Fig. 4.30 Variation of the state variable p_1 with time

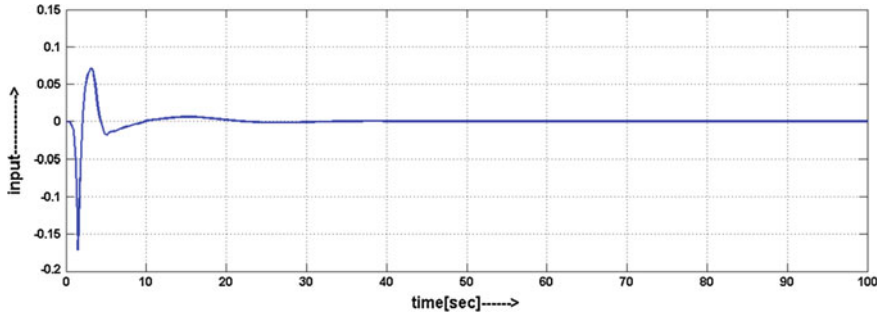

Fig. 4.31 Variation of the control input u with time

theorem 2 (Chap. 3, Sect. 3.5), which states the global asymptotic stability of the reduced order system together with the global asymptotic stability of the internal dynamics ensures asymptotic stabilization of the actuated shape variables has been corroborated by the stabilization of the actuated state variables.

Being a nonholonomic mechanical system, pendubot fails to satisfy the Brockets' condition of feedback linearization [21]. Therefore, it requires nonsmooth control input for its stabilization. Figure 4.31 reveals the fact that the proposed control law generates a nonsmooth control input for the stabilization of pendubot system.

Indeed, the authors have already demonstrated applications of the proposed control law on five different underactuated systems. It is also important to note that all of them possess some unique constructional features, and each of the systems is having their unique dynamic models. Moreover, all the above-mentioned systems belong to different classes of mechanical systems like flat, holonomic, nonholonomic, etc. As a matter of fact, their control problems become quite unique in nature with their individual design constraints. Since the proposed control law has successfully addressed their control problems in simulation environment, without any loss of generality, one can assume that the same is versatile enough to address the control problem of most of the 2-DOF systems in simulation environment. However, the zeal of engineering lies in performing the real-time experiments, not in the rigorous analysis of complicated mathematical formulations. The authors have also realized the same, and they have applied the proposed control law on a real-time platform to verify the efficacy of the proposed law during practical applications. The authors have selected the test bed of digital inverted pendulum for the said purpose, which will be described in the following two Sects. 4.6 and 4.7.

4.6 Application on the Inverted Pendulum[5]

The inverted pendulum on cart has been treated as an interesting and classical control problem for control system engineers since 1950 [3, 16, 19, 21]. Balancing or stabilization control of such an inverted pendulum in the vertical upright position (which is its unstable equilibrium point) has become a very popular benchmark control problem for the derivation of advanced control algorithms for inherently unstable nonlinear systems [4, 14, 17, 19]. Dynamics of the inverted pendulum resembles the dynamics of numerous other systems of interest [4, 16, 21, 25]. Therefore, inverted pendulum has been a popular test rig for the research and illustration of various control methods like feedback stabilization, variable structure control, and passivity based control, backstepping and forwarding control, nonlinear observer, friction compensation, task oriented control, hybrid system control, and chaotic system control [35, 41]. It is quite interesting to note that biped walking robot control resembles the inverted pendulum control problem [4, 21]. The main control objectives of the most of the research contributions were to control the

[5]Section 4.6 is based on "Nonlinear state feedback controller design for underactuated mechanical system: A modified block backstepping approach" by Shubhobrata Rudra, Ranjit Kumar Barai, and Madhubanti Maitra, which appeared in ISA Transactions, vol 53, issue 2, pp 317–326, March 2014, Copyright © 2013 ISA. Published by Elsevier Ltd. Permission obtained from Elsevier.

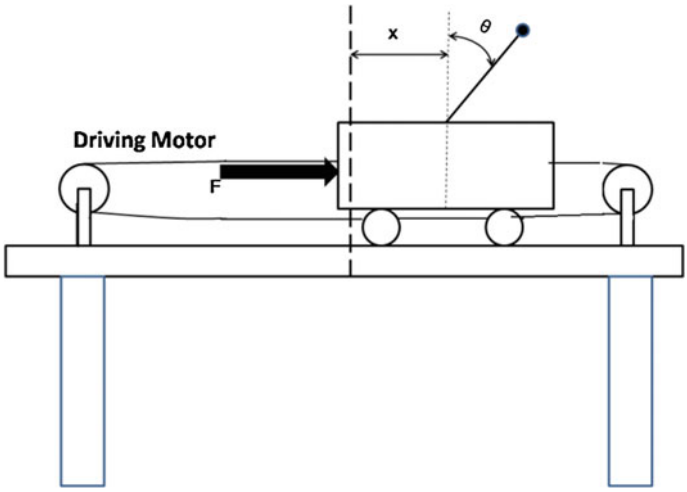

Fig. 4.32 Schematic diagram of the inverted pendulum

inverted pendulum on the cart so that the unstable equilibrium point could be stabilized [39, 41]. Inverted pendulum also provides a simple model for stabilization control of rockets when it is being launched [4, 27]. It has two equilibrium points: vertical upright equilibrium point and downward equilibrium point [16, 27]. The vertical upright equilibrium point is inherently unstable, as any small disturbance may cause the pendulum to fall on the either side when the cart is at rest [21, 27]. However, this equilibrium can be maintained indefinitely by properly controlling the motion of the cart [21, 27]. Schematic diagram of the inverted pendulum is shown in Fig. 4.32.

The state model of the cart-pole system is shown in Eq. (4.109) (where $x_1 = x$ and $x_2 = \theta$). (Detailed modeling of the inverted pendulum can be found in Appendix A.6.) In the following state model, $\mu = l(M+m)\, d = J + \mu l \sin^2 x_2$ and $a = l^2 + \frac{J}{M+m}$, where M is the mass of the cart, m is the mass of the pendulum bob, l represents the length of the rod, J represents the moment of inertia, and b represents the coefficient of viscous friction between cart's wheels and rails.

$$\begin{aligned}
\dot{x}_1 &= x_3 \\
\dot{x}_2 &= x_4 \\
\dot{x}_3 &= \frac{\mu g l \sin 2x_2}{2d} - \frac{\mu x_4^2 \sin x_2}{d} - \frac{b x_3}{d} + \frac{au}{d} \\
\dot{x}_4 &= \frac{\mu g \sin 2x_2}{2d} - \frac{\mu x_4^2 \sin x_2}{d} - \frac{b x_3}{d} + \frac{lu}{d}
\end{aligned} \tag{4.109}$$

Salient features of 1-D inverted pendulum: *Unactuated shape variable, holonomic motion constraint, complex nonlinear dynamics, and unstable equilibrium.*

Control Objective: *Stabilize the pendulum at vertical upright position, while stabilize the motion of the cart at any desired equilibrium manifold. Unlike the previous cases, state model of the inverted pendulum has been derived from Newtonian modeling equation. Therefore, the control law should be derived according to derivation process of* Sect. 3.1, *which was intended for solving control problems of 2-DOF system equation derived from Newtonian equation.*

4.6.1 Derivation of the Control Law for Inverted Pendulum

In case the above state model of Eq. (4.109) is compared with the standard state model of 2-DOF underactuated system shown in Eq. (3.1), then the state variables can be written as $x_1 = q_1, x_2 = q_2, x_3 = p_1, x_4 = p_2$.

The drift vector field for x_3 and x_4 are as shown below:

$$f_1 = \frac{\mu g l \sin 2x_2}{2d} - \frac{\mu x_4^2 \sin x_2}{d} - \frac{b x_3}{d} \tag{4.110}$$

$$f_2 = \frac{\mu g \sin 2x_2}{2d} - \frac{\mu x_4^2 \sin x_2}{d} - \frac{b x_3}{d} \tag{4.111}$$

The control fields are given by, $g_1 = \frac{a}{d}$ and $g_2 = \frac{l}{d}$. Moreover,

$$\dot{d} = \mu l x_4 \sin 2x_2 \tag{4.112}$$

$$\ddot{d} = 2\mu l x_4^2 \cos 2x_2 + \mu l \dot{x}_4 \sin 2x_2 \tag{4.113}$$

$$\dot{f}_1 = \frac{\mu g l \cos 2x_2}{d} x_4 - \frac{2\mu x_4 \sin x_2}{d}\left(f_2 + \frac{lu}{d}\right) - \frac{\mu x_4^3 \cos x_2}{d} - \frac{b}{d}\left(f_1 + \frac{au}{d}\right) \tag{4.114}$$

and

$$\dot{f}_2 = \frac{\mu g \cos 2x_2}{d} x_4 - \frac{2\mu x_4 \sin x_2}{d}\left(f_2 + \frac{lu}{d}\right) - \frac{\mu x_4^3 \cos x_2}{d} - \frac{b}{d}\left(f_1 + \frac{au}{d}\right) \tag{4.115}$$

Please note that as stated earlier, the state model of the inverted pendulum (4.109) has been derived from Newtonian equation, and it resembles the state models of Eq. (3.1). Therefore, z_1 can be defined according to Eq. (3.2) (here $g_1 = \frac{a}{d}$ and $g_2 = \frac{l}{d}$). Hence, z_1 has been defined in accordance with Eq. (3.2), as shown below:

$$z_1 = x_2 - k(x_1 + ldx_3 - adx_4) \tag{4.116}$$

Hence, the dynamics of z_1-has become

$$\dot{z}_1 = x_4 - k\big(x_3 + \dot{d}(lx_3 - ax_4) + d(lf_1 - af_2)\big) \tag{4.117}$$

The stabilization function α_1 has been defined as shown in Eq. (4.118):

$$\alpha_1 = -\lambda\chi_1 - c_1 z_1 + k\big(x_3 + \dot{d}(lx_3 - ax_4) + d(lf_1 - af_2)\big) \tag{4.118}$$

The second control variable z_2 has been defined as $z_2 = x_4 - \alpha_1$. Hence, the time derivative of z_2 can be computed as shown in the following Eq. (4.119):

$$\begin{aligned}\dot{z}_2 = {} & f_2 + \frac{lu}{d} + \lambda z_1 + c_1(z_2 - c_1 z_1 - \lambda\chi_1) - k\Big[f_1 + \frac{au}{d} + 2\mu l x_4^2 \cos 2x_2 (lx_3 - ax_4) + \mu \boldsymbol{g} l^2 x_4 \cos 2x_2 \\ & + 2\mu l x_4 \sin 2x_2 (lf_1 - af_2) + \mu l \sin 2x_2 \left(f_2 + \frac{lu}{d}\right) - 2\mu l x_4 \sin x_2 \left(f_2 + \frac{lu}{d}\right) - \mu l x_4^3 \cos x_2 - blf_1 \\ & - \frac{blau}{d} - \mu a \boldsymbol{g} x_4 \cos x_2 - 2\mu a x_4 \sin x_2 \left(f_2 + \frac{lu}{d}\right) - \mu a x_4^3 \cos x_2 - baf_1 - \frac{ba^2 u}{d}\Big]\end{aligned} \tag{4.119}$$

Hence, comparison of Eq. (4.119) with Eq. (3.9) has resulted in the following expression for ψ and ϕ:

$$\psi = \frac{l}{d} - k\left(\frac{a}{d} + \frac{\mu l^2 \sin 2x_2}{d} - \frac{2\mu l^2 \sin x_2 x_4}{d} - \frac{ba}{d}(l - a) + \frac{2\mu a l x_4 \sin x_2}{d}\right) \tag{4.120}$$

$$\begin{aligned}\phi = {} & f_2 - k\big[f_1 + 2\mu l x_4^2 \cos 2x_2 (lx_3 - ax_4) + 2\mu l x_4 \sin 2x_2 (lf_1 - af_2) + \mu \boldsymbol{g} l^2 x_4 \cos 2x_2 \\ & - 2\mu l x_4 \sin x_2 f_2 - \mu l x_4^3 \cos x_2 - blf_1 - \mu a \boldsymbol{g} x_4 \cos x_2 + 2\mu a x_4 \sin x_2 f_2 \\ & + \mu a x_4^3 \cos x_2 + baf_1 + \mu l f_2 \sin 2x_2\big]\end{aligned} \tag{4.121}$$

The above choice of ψ and ϕ has yielded following compact expression of the control input:

$$= \psi u + \lambda z_1 + c_1(z_2 - c_1 z_1 - \lambda\chi_1) + \phi \tag{4.122}$$

However, the desired dynamics of z_2 can be defined according to Eq. (4.123):

$$\dot{z}_2 = -z_1 - c_2 z_2 \tag{4.123}$$

Similar to the method describe in Sect. 3.1.2, comparison of Eq. (4.123) with the desired dynamics of z_2 (described in Eq. (4.119) has resulted in:

$$u = \psi^{-1}\left[-\left(1 - c_1^2 + \lambda\right)z_1 - (c_1 + c_2)z_2 + \lambda c_1 \chi_1 - \phi\right] \tag{4.124}$$

As it has already been stated in Sect. 3.1.3, Eqs. (3.16.a)–(3.16.c) depict the zero dynamics structure for a 2-DOF system. Consequently, in the special case of the inverted pendulum ($z_1 = 0$ and $\dot{z}_1 = 0$) has yielded the following expressions of x_2 and x_4:

$$x_2 = k\left[1 - \frac{adk^2\mu g(l^2 - a)}{1 + kda + ak^2 d\mu g(l^2 - a)}\right]x_1 + k\left[ld - \frac{1 + dl + b(a - l) + lk\mu gd}{1 + kda + ak^2 d\mu g(l^2 - a)}\right]x_3 \tag{4.125.a}$$

$$x_4 = \frac{k^2\mu g(l^2 - a)x_1 + k[1 + dl + b(a - l) + lk\mu gd]x_3}{1 + kda + ak^2 d\mu g(l^2 - a)} \tag{4.125.b}$$

Now, the x_2 and x_4 terms of f_1, ψ, and ϕ have been replaced by the expressions of (4.125.a) and (4.125.b), respectively, then the equations of zero dynamics for the inverted pendulum has taken the following form:

$$\begin{aligned} \dot{x}_1 &= x_3 \\ \dot{x}_3 &= f_1(x_1, x_3) - g_1(x_1, x_3)\psi^{-1}(x_1, x_3)\phi(x_1, x_3) \end{aligned} \tag{4.125.c}$$

In Eq. (4.125.c), $f_1(x_1, x_3)$, $g_1(x_1, x_3)$, $\psi^{-1}(x_1, x_3)$ and $\phi(x_1, x_3)$ represent the same functions f_1, g_1, ψ^{-1} and ϕ, with all the x_2 and x_4 terms have been replaced by the expressions of (4.125.a) and (4.125.b), respectively. The gain k has been

Fig. 4.33 Real-time experimental setup of the inverted pendulum

Table 4.11 Parameters of the proposed block backstepping controller

c_1	c_2	λ	K
10	10	0.001	1

selected in such a manner that it will ensure the stability of the zero dynamic system of (4.125.c).

4.6.2 Results Obtained from Real-Time Experiments

The real-time experimental setup of an inverted pendulum is shown in Fig. 4.33. The length and weight of the pendulum are 0.402 m and 0.095 kg. The cart mass is 1.12 kg. The moment of inertia of the inverted pendulum is 0.014 kg m^2. The dynamic friction coefficient between cart and rail is 0.05 kg/s. These values of the physical parameters of the digital pendulum setup are obtained from Rudra et al. [27]. Although the maximum force that can be applied on the Cart is 16.5N, the maximum control force actually applied on the cart has been limited to 6N for smooth operation of actuator. The resolution of the encoder is 2048 increments per one revolution.

The experiment has been performed for 100 s. MATLAB® (version 6.5), Simulink (version 5.2) environment and real-time windows target has been used to implement and test the proposed control algorithm in real time. The control algorithm has been developed as a Simulink model and then it has been passed through the "Build" operation to create all the executable files that are necessary for the real-time implementation.

The control input u has been defined according to Eq. (3.9). The design parameters c_1, c_2, λ have been chosen in such a manner that the condition $c_1 > 0$, $c_2 > 0$, and $\lambda > 0$ has been satisfied. Constant k has been selected in such a manner that it ensures the stability of the zero dynamic system of (4.125.c). (Detailed criteria of controller parameter selection have been discussed in Chap. 3, Sect. 3.2.3.) The control parameters values are shown in Table 4.11.

Since inverted pendulum is also a type of unactuated shape variable system like Furuta pendulum, and Pendubot, like the previous design studies here also at first time variation of the unactuated configuration variables q_2 and p_2 have been shown in Fig. 4.34a, b.

It is clear from Fig. 4.34a, b that judicial selection of k, which is able to ensure stability of the zero dynamics, also ensure convergence of the unactuated variable and its derivative to their desired state coordinate. Now, the time variation of actuated variables is shown in the following Fig. 4.35a, b.

In order to verify the effectiveness of this proposed controller in real situation, an external disturbance has been introduced by applying an impulse force on the pendulum after 47 s in an experimental run while it was in the vertical upright

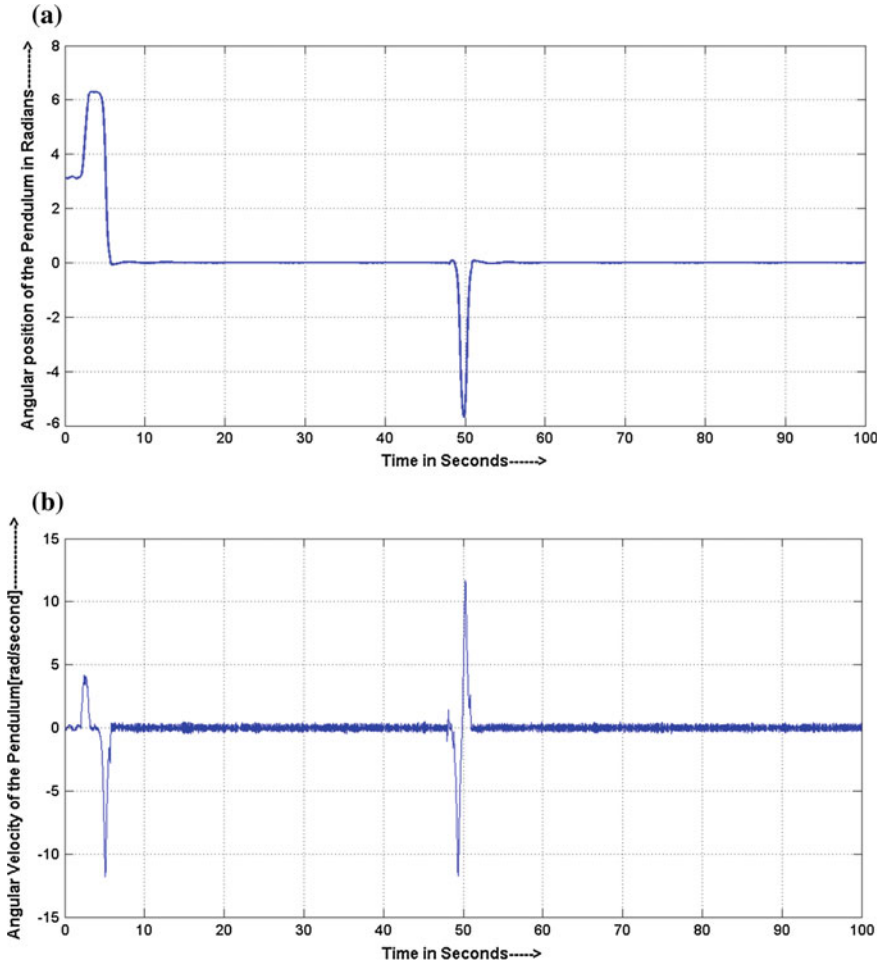

Fig. 4.34 **a** Pendulum angle variation with time. **b** Pendulum angular velocity

position. It is clear that the proposed control law is quite robust against such bounded external impact.

The variation of the input voltage on the driving motor terminal is shown in Fig. 4.36. From these results, it can be observed that just after the application of external impact, the cart was quickly executing a to and fro motion to reduce the impact of the disturbance on the pendulum. Another noticeable feature of the proposed approach that after application of external impact, within a few seconds the cart was able to follow its desired trajectory. Moreover, the control input to the system (the voltage applied on the dc motor armature) was varying within a safe limit. Therefore, it is easy to understand that the proposed control law can ensure

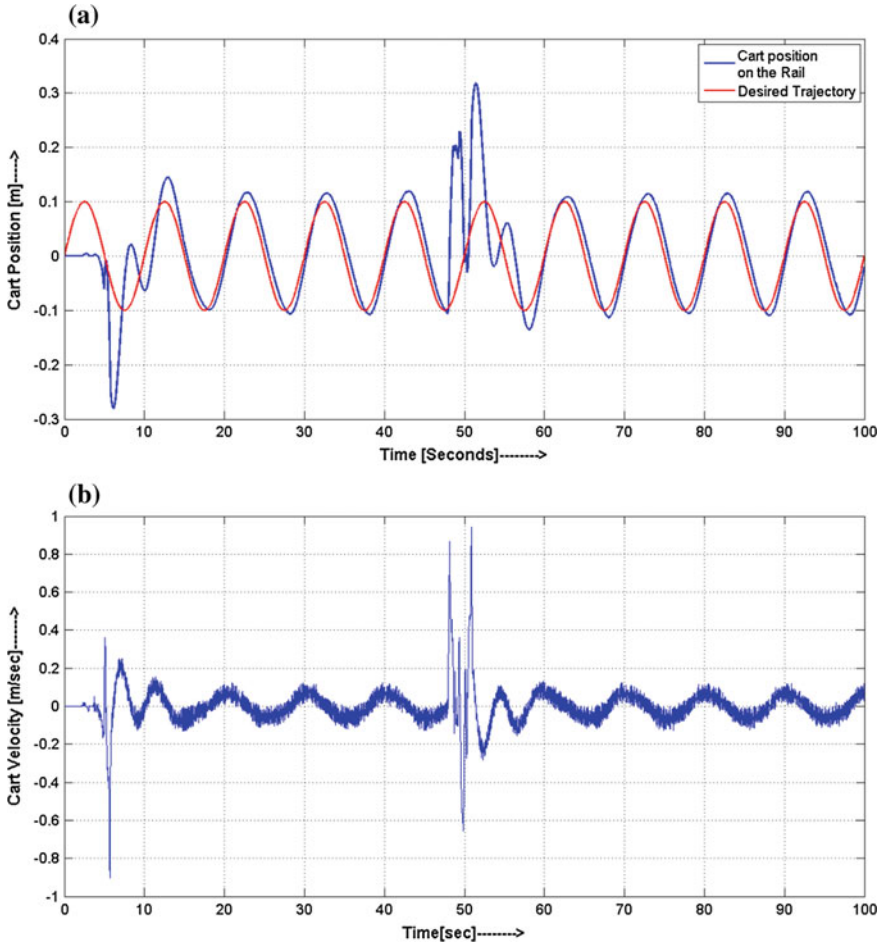

Fig. 4.35 **a** Motion of the cart on the rail. **b** Velocity of the cart

that the control input will never generate high stress on the associated mechanical accessories.

Unlike the other case studies of stabilization problems of different underactuated mechanical systems, in this case the control algorithm has been used to address the tracking control problem of inverted pendulum system. Experimental results have revealed the fact that the proposed control law can ensure a guaranteed tracking of actuated variable of the holonomic underactuated systems. In this case, the actuated configuration variable (i.e., motion of the cart) has smoothly tracked the reference trajectory. Further observation has unveiled the fact that proposed control law can ensure guaranteed tracking performance even in the presence of bounded external impact. Therefore, it can be concluded from the above experimental results that the

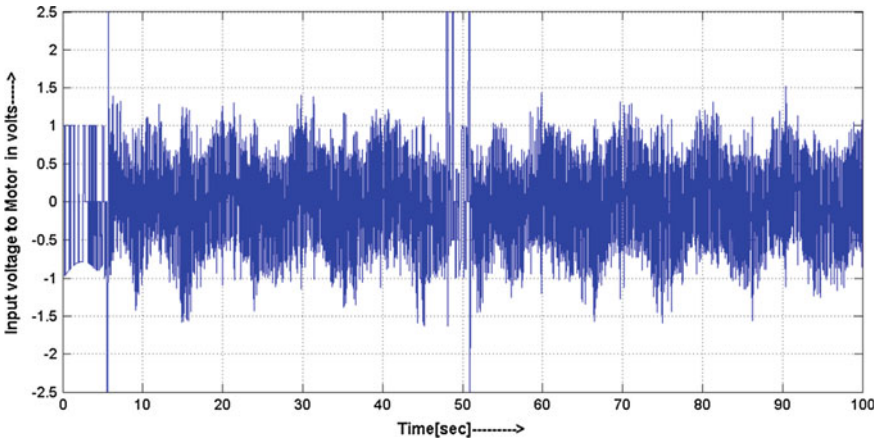

Fig. 4.36 Variation of the control input with time

proposed control algorithm can be used as a tracking control algorithm for holonomic underactuated system.

4.7 Application on the Single Dimension Granty Crane

Indeed, in the last six sections, authors have described the application of control law on different complicated underactuated systems. However, without considering the case of single dimension overhead crane, discussion on 2-DOF underactuated mechanical systems does not take a complete shape. Therefore, in this section a concise description of real-time application of proposed control law on overhead Granty crane is presented.

The fundamental motions of a Granty crane consist of travel, load hoisting, and load lowering. The control problem of a crane is a typical example of the underactuated motion control problems [16, 21]. Noteworthy feature of a gantry crane is that all motions are performed simultaneously at relatively high speed [16, 21]. Crane travel and transverse motions, especially when starting or stopping, induce undesirable swinging of the suspended load [16, 21]. Therefore, a crane designer should seek a satisfactory control method to suppress the unwanted load swing during transport [36, 39]. In this demonstration, control of the single dimension crane model has been considered to verify the effectiveness of the proposed control algorithm. The same experimental setup of inverted pendulum has been used as a setup of single dimension crane.

The state model of the single dimension Granty crane is shown below (where $x_1 = x$ and $x_2 = \theta$). (For detailed modeling please refer Appendix A.6.)

$$\begin{aligned}\dot{x}_1 &= x_3\\ \dot{x}_2 &= x_4\\ \dot{x}_3 &= \frac{\mu g l \sin 2x_2}{2d} + \frac{\mu x_4^2 \sin x_2}{d} - \frac{bx_3}{d} + \frac{au}{d}\\ \dot{x}_4 &= \frac{\mu g \sin 2x_2}{2d} + \frac{\mu x_4^2 \sin x_2}{d} - \frac{bx_3}{d} + \frac{lu}{d}\end{aligned} \tag{4.126}$$

In the above state model, $\mu = l(M+m)\, d = J + \mu l \sin^2 x_2$ and $a = l^2 + \frac{J}{M+m}$, where M is the mass of the cart and m represents the mass of the payload bob, l represents the length of the rod, J represents the moment of inertia, and b represents the coefficient of viscous friction between cart's wheels and rails.

Salient features of 1-D crane: *Unactuated shape variable, holonomic motion constraint, complex nonlinear dynamics, badly damped system (payload dynamics).*

Control Objective: *Minimize the oscillation of the payload during load hoisting, stabilization of the cart to a desired manifold.*

4.7.1 Derivation of the Control Law for Granty Crane System

In case, the above state model of Eq. (4.126) is compared with the standard state model of 2-DOF underactuated system shown in Eq. (3.1), then the state variables can be written as $x_1 = q_1, x_2 = q_2, x_3 = p_1, x_4 = p_2$

The drift vector field for x_3 and x_4 are as follows:

$$f_1 = \frac{\mu g l \sin 2x_2}{2d} + \frac{\mu x_4^2 \sin x_2}{d} - \frac{bx_3}{d} \tag{4.127}$$

$$f_2 = \frac{\mu g \sin 2x_2}{2d} + \frac{\mu x_4^2 \sin x_2}{d} - \frac{bx_3}{d} \tag{4.128}$$

The control fields are given by, $g_1 = \frac{a}{d}$ and $g_2 = \frac{l}{d}$. Moreover,

$$\dot{d} = \mu l x_4 \sin 2x_2 \tag{4.129}$$

$$\ddot{d} = 2\mu l x_4^2 \cos 2x_2 + \mu l \dot{x}_4 \sin 2x_2 \tag{4.130}$$

$$\dot{f}_1 = \frac{\mu g l \cos 2x_2}{d} x_4 + \frac{2\mu x_4 \sin x_2}{d}\left(f_2 + \frac{lu}{d}\right) + \frac{\mu x_4^3 \cos x_2}{d} - \frac{b}{d}\left(f_1 + \frac{au}{d}\right) \tag{4.131}$$

and

$$\dot{f}_2 = \frac{\mu \boldsymbol{g} \cos 2x_2}{d} x_4 + \frac{2\mu x_4 \sin x_2}{d}\left(f_2 + \frac{lu}{d}\right) + \frac{\mu x_4^3 \cos x_2}{d} - \frac{b}{d}\left(f_1 + \frac{au}{d}\right) \quad (4.132)$$

Now, z_1 has been defined as shown in the following Eq. (4.133):

$$z_1 = x_2 - k(x_1 + ldx_3 - adx_4) \quad (4.133)$$

Hence, the derivative of z_1-has taken the shape of Eq. (4.134):

$$\dot{z}_1 = x_4 - k\big(x_3 + \dot{d}(lx_3 - ax_4) + d(lf_1 - af_2)\big) \quad (4.134)$$

The stabilization function α_1 has been defined according to Eq. (4.135):

$$\alpha_1 = -\lambda\chi_1 - c_1 z_1 + k\big(x_3 + \dot{d}(lx_3 - ax_4) + d(lf_1 - af_2)\big) \quad (4.135)$$

The second control variable z_2 has been defined as $z_2 = x_4 - \alpha_1$. Consequently, the time derivative of z_2 can be computed as shown in the following Eq. (4.136):

$$\begin{aligned}\dot{z}_2 = {} & f_2 + \frac{lu}{d} + \lambda z_1 + c_1(z_2 - c_1 z_1 - \lambda\chi_1) - k\Big[f_1 + \frac{au}{d} + 2\mu l x_4^2 \cos 2x_2 (lx_3 - ax_4) + \mu g l^2 x_4 \cos 2x_2 \\ & + 2\mu l x_4 \sin 2x_2 (lf_1 - af_2) + \mu l \sin 2x_2 \left(f_2 + \frac{lu}{d}\right) - 2\mu l x_4 \sin x_2 \left(f_2 + \frac{lu}{d}\right) - \mu l x_4^3 \cos x_2 - blf_1 \\ & - \frac{blau}{d} - \mu a g x_4 \cos x_2 - 2\mu a x_4 \sin x_2 \left(f_2 + \frac{lu}{d}\right) - \mu a x_4^3 \cos x_2 - baf_1 - \frac{ba^2 u}{d}\Big]\end{aligned} \quad (4.136)$$

Hence, comparison of Eq. (4.136) with Eq. (3.9) has resulted in the following expression for ψ and ϕ:

$$\psi = \frac{l}{d} - k\left(\frac{a}{d} + \frac{\mu l^2 \sin 2x_2}{d} - \frac{2\mu l^2 \sin x_2 x_4}{d} - \frac{ba}{d}(l - a) + \frac{2\mu a l x_4 \sin x_2}{d}\right) \quad (4.137)$$

$$\begin{aligned}\phi = {} & f_2 - k\big[f_1 + 2\mu l x_4^2 \cos 2x_2 (lx_3 - ax_4) + 2\mu l x_4 \sin 2x_2 (lf_1 - af_2) + \mu \boldsymbol{g} l^2 x_4 \cos 2x_2 \\ & - 2\mu l x_4 \sin x_2 f_2 - \mu l x_4^3 \cos x_2 - blf_1 - \mu a \boldsymbol{g} x_4 \cos x_2 + 2\mu a x_4 \sin x_2 f_2 \\ & + \mu a x_4^3 \cos x_2 + baf_1 + \mu l f_2 \sin 2x_2\big]\end{aligned} \quad (4.138)$$

The above choice of ψ and ϕ has resulted in the compact expression of control input as follows

$$= \psi u + \lambda z_1 + c_1(z_2 - c_1 z_1 - \lambda\chi_1) + \phi \quad (4.139)$$

However, the desired dynamics of z_2 is

$$\dot{z}_2 = -z_1 - c_2 z_2 \tag{4.140}$$

Similar to the method describe in Sect. 3.1.3, comparison of Eq. (4.140) with the desired dynamics of z_2 has resulted in the following Eq. (4.141):

$$u = \psi^{-1}\left[-\left(1 - c_1^2 + \lambda\right)z_1 - (c_1 + c_2)z_2 + \lambda c_1 \chi_1 - \phi\right] \tag{4.141}$$

As it has already been stated in Sect. 3.1.3, Eqs. (3.16.a)–(3.16.c) depict the zero dynamics structure for a 2-DOF system. Therefore, in this case of Granty crane the zero dynamics equation can be derived in a similar manner. Like the previous cases, $z_1 = 0$ and $\dot{z}_1 = 0$ has yielded the following expressions of x_2 and x_4:

$$x_2 = k\left[1 - \frac{adk^2\mu g(l^2 - a)}{1 + kda + ak^2 d\mu g(l^2 - a)}\right]x_1 + k\left[ld + \frac{1 + dl + b(a - l) + lk\mu g d}{1 + kda + ak^2 d\mu g(l^2 - a)}\right]x_3 \tag{4.142.a}$$

$$x_4 = \frac{k^2\mu g(l^2 - a)x_1 + k[1 - dl + b(a - l) + lk\mu g d]x_3}{1 + kda + ak^2 d\mu g(l^2 - a)} \tag{4.142.b}$$

Fig. 4.37 Real-time experimental setup of single dimensional Granty crane

Table 4.12 Parameters of the proposed block backstepping controller

c_1	c_2	λ	k
4	4	0.001	0.75

Now, if the x_2 and x_4 terms of f_1, ψ, and ϕ can be replaced by the expressions of (4.142.a) and (4.142.b), respectively, then the equations of zero dynamics for the crane will take the following form:

$$\begin{aligned}\dot{x}_1 &= x_3 \\ \dot{x}_3 &= f_1(x_1, x_3) - g_1(x_1, x_3)\psi^{-1}(x_1, x_3)\phi(x_1, x_3)\end{aligned} \tag{4.142.c}$$

In Eq. (4.142.c), $f_1(x_1, x_3), g_1(x_1, x_3), \psi^{-1}(x_1, x_3)$ and $\phi(x_1, x_3)$ represent the same functions f_1, g_1, ψ^{-1}, and ϕ, with all the terms of last equation, all the x_2 and x_4 terms have been replaced by the expression of (4.142.a) and (4.142.b), respectively. The gain k has been selected in such a manner that it will ensure the stability of the zero dynamic system of (4.142.c).

4.7.2 Results Obtained from Real-Time Experiments

The real-time experimental setup of an inverted pendulum is shown in Fig. 4.37. The link length and weight of the payload are 0.402 m and 0.095 kg. The cart mass is 1.12 kg. The moment of inertia of the payload is 0.014 kg m^2. The dynamic friction coefficient between cart and rail is 0.05 kg/s. These values of the physical parameters of the digital pendulum setup are obtained from Rudra et al. [27]. Although the maximum force that can be applied on the cart is 16.5N, the maximum control force actually applied on the cart has been limited to 6N for smooth operation of actuator. The resolution of the encoder is 2048 increments per one revolution.

The experiment has been performed for 100 s. MATLAB® Simulink environment and Real-time Windows Target has been used to implement and test the proposed control algorithm in real time. The control algorithm has been developed as a Simulink model and then it has been passed through the "Build" operation to create all the executable files that are necessary for the real-time implementation. Parameters of the proposed controller are shown in Table 4.12.

In order to verify the effectiveness of this proposed controller in real situation, an external disturbance has been introduced by applying an impulse force on the payload after 40 s. The dynamic responses of the payload for the angular position in space and angular velocity are shown in Fig. 4.38a, b, respectively, during the application of this impulse disturbance. Position of the cart on the rail and the velocity of the cart during the application of the impact disturbance are shown in

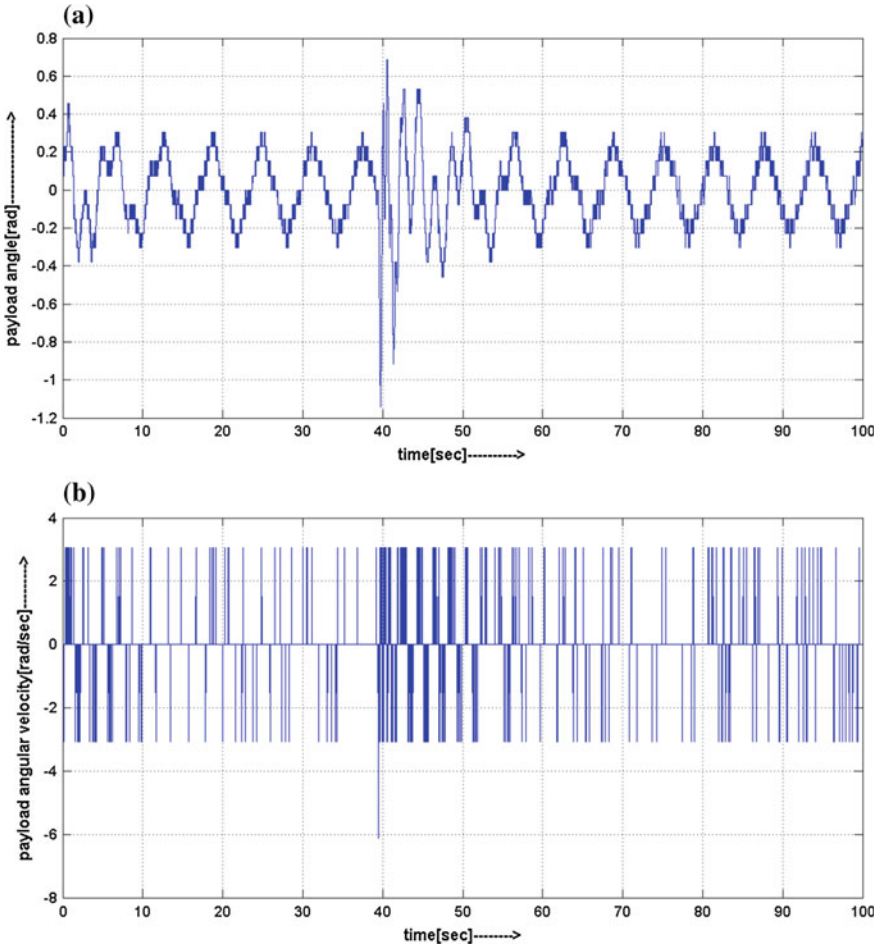

Fig. 4.38 **a** Payload angle variation with time. **b** Payload angular velocity

Fig. 4.39a, b, respectively. The variation of the input voltage on the driving motor terminal is shown in Fig. 4.40.

From these results, it can be observed that the cart was moving quickly to reduce the impact of the disturbance on the payload. In addition, it can be observed that after application of the external impact within a few seconds the cart was able to follow its desired trajectory. Moreover, the control input to the system (the voltage applied on the dc motor armature) was varying within a safe limit, which has established the fact that the control input will never generate high stress on the associated mechanical accessories. Thus, the block backstepping controller with integral action has manifested a very fast response during the motion control of the single dimension overhead crane system, and has maintained the stability of the payload even in the face of bounded external disturbance.

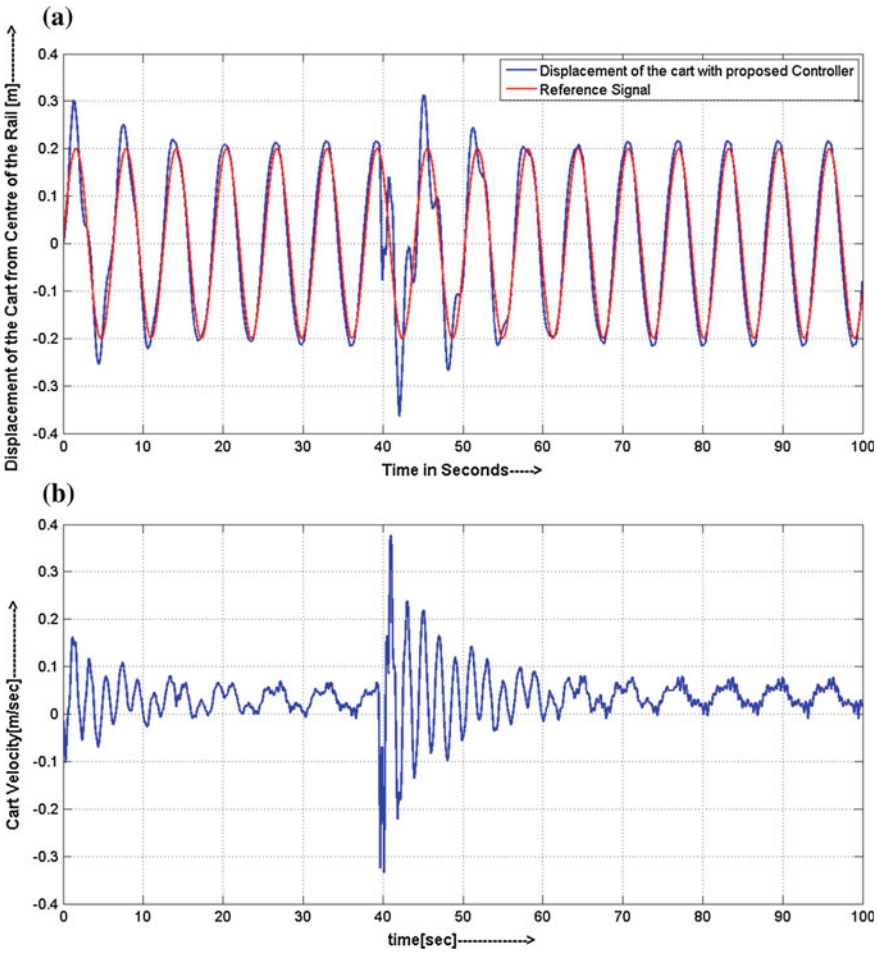

Fig. 4.39 **a** Motion of the cart on the rail. **b** Velocity of the cart

4.8 Notes

This chapter presents the detailed implementation of the proposed control law on seven 2-DOF underactuated mechanical systems. It can be inferred from the foregoing discussions that the proposed control law is versatile enough to address the control problem of any 2-DOF underactuated system without any significant modifications. Simplicity and generalized nature are the two distinctive features of the proposed control law. Extensive simulation studies have revealed that the proposed control law can successfully address the control problems of different 2-DOF underactuated mechanical systems, which belong to different classes of UMSs. Along with verification of the proposed control law in simulation

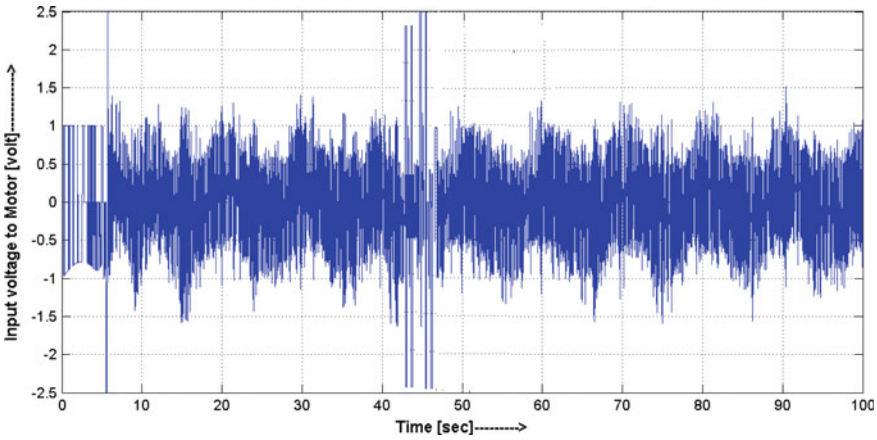

Fig. 4.40 Variation of the control input with time

environment, it has also been applied on the real-time test bed (inverted pendulum setup and granty crane model) to corroborate the theoretical findings of the present proposition. Experimental results have established that the theoretical design of the control law is apt for real-time applications. In addition, it can be observed from real-time results that the proposed control algorithm can also address the tracking control problem of holonomic UMSs. However, it is important to note that not all the UMSs are 2-DOF in nature, rather in reality most of the times engineers have to deal with more complicated systems having more degrees of freedom. Therefore, in the next chapter, application of the proposed control law on different important higher order UMSs will be described in a systematic manner. Authors are quite confident with the fact that reader has already gained an insightful view of designing control law for 2-DOF underactuated mechanical systems. All being well, after going through the next chapter, reader will gain enough confidence to design control law for any UMSs.

References

1. Albahkali T, Mukherjee R, Das T (2009) Swing-up control of the pendubot: an impulse momentum approach. IEEE Trans Rob 25(4):975–982
2. Avis JM, Nersesov SG, Nathan R, Ashrafiuon H, Muske KR (2010) A comparison study of nonlinear control techniques for the RTAC system. Nonlinear Anal Real World Appl 11 (4):2647–2658
3. Chang DE (2010) Stabilizability of controlled Lagrangian systems of two degrees of freedom and one degree of under-actuation by the energy-shaping method. IEEE Trans Autom Control 55(8):1888–1893
4. Chatterjee D, Patra A, Joglekar HK (2002) Swing-up and stabilization of a cart pendulum system under restricted cart track length. Syst Control Lett 47(4):355–364

5. Fantoni I, Lozano R, Spong MW (2000) Energy based control of the pendubot. IEEE Trans Autom Control 45(4):725–729
6. Fantoni I, Lozano R (2001) Nonlinear control for underactuated mechanical systems. Springer, London
7. Fantoni I, Lozano R (2002) Stabilization of the Furuta pendulum around its homoclinic orbit. Int J Control 75(6):390–398
8. Freidovich L, Shiriaev A, Gordillo F, Gomez-Estern F, Aracil J (2009) Partial-energy shaping control for orbital stabilization of high-frequency oscillations of the Furuta pendulum. IEEE Trans Control Syst Technol 17(4):853–858
9. Gao A, Zhang X, Chen H, Zhao J (2009) Energy-based control design of an underactuated 2-dimensional TORA system. Paper presented at the IEEE/RSJ international conference on intelligent robots and systems, St. Louis, USA, pp 1296–1301
10. Jafari R, Mathis FB, Mukherjee R (2011) Swing-up control of the acrobot: an impulse momentum approach. Paper presented at American control conference, San Francisco, CA, USA, pp 262–267
11. Jankovic M, Fontaine D, Kokotovic PV (1996) TORA example: cascade and passivity based control designs. IEEE Trans Control Syst Technol 4(3):292–297
12. Jiang ZP, Hill DJ, Guo Y (1998) Stabilization and tracking via output feedback for the nonlinear benchmark system. Automatica 34(7):907–915
13. Jiang ZP, Kanellakopoulos I (2000) Global output-feedback tracking for a benchmark nonlinear system. IEEE Trans Autom Control 45(5):1023–1027
14. Kim Y, Kim SH, Kwak YK (2005) Dynamic analysis of a nonholonomic two-wheeled inverted pendulum robot. J Intell Rob Syst 44(1):25–46
15. Lai XZ, She JH, Yang SX, Wu M (2009) Comprehensive unified control strategy for underactuated two-link manipulators. IEEE Trans Syst Man Cybern 39(2):389–398
16. Liu Y, Yu H (2013) A survey of underactuated mechanical systems. IET Control Theory Appl 7(7):921–935
17. Lopez-Martinez M, Acosta JA, Cano JM (2010) Non-linear sliding mode surfaces for a class of underactuated mechanical systems. IET Control Theory Appl 4(10):2195–2204
18. Luca Ad, Mattone R, Orilo G (1996) Control of underactuated mechanical systems: application to the planar 2R robot. Paper presented at the international conference on decision and control, Kobe, Japan, pp 1455–1460
19. Mori S, Nishiharaa H, Furuta K (1976) Control of unstable mechanical system control of pendulum. Int J Control 23(5):673–692
20. Nair S, Leonard NE (2002) A normal form for energy shaping: application to the Furuta pendulum. Paper presented at the 41th international conference on decision and control, vol 1, pp 516–521
21. Olfati-Saber R (2001) Nonlinear control of underactuated mechanical systems with application to robotics and aerospace vehicles, Ph.D. thesis, Department of Electrical Engineering and Computer, Massachusetts Institute of Technology
22. Olfati-Saber R, Megretski A (1998) Controller design for a class of underactuated nonlinear systems. Paper presented at the 37th international conference on decision and control, vol 4. Tampa, FL, pp 4182–4187
23. Oriolo G, Nakamura T (1991) Control of mechanical systems with second-order nonholonomic constraints: underactuated manipulators. Paper presented at the international conference on decision and control, Brighton, UK, pp 2398–2403
24. Ortega R, Spong MW, Gómez-Estern F, Blankenstein G (2002) Stabilization of a class of underactuated mechanical systems via interconnection and damping assignment. IEEE Trans Autom Control 8(47):1218–1232
25. Pathak K, Franch J, Agrawal SK (2005) Velocity and position control of a wheeled inverted pendulum by partial feedback linearization. IEEE Trans Rob 21(3):505–513
26. Pavlov A, Janssen B, van de Wouw N, Nijmeijer H (2007) Experimental output regulation for a nonlinear benchmark system. IEEE Trans Control Syst Technol 15(4):786–793

27. Rudra S, Barai RK, Maitra M (2014) Nonlinear state feedback controller design for underactuated mechanical system: a modified block backstepping approach. ISA Trans 53 (2):317–326
28. Shiriaev AS, Freidovich LB, Robertsson A, Johansson R, Sandberg A (2007) Virtual holonomic-constraints-based design of stable oscillations of Furuta pendulum: theory and experiments. IEEE Trans Rob 23(4):827–832
29. Spong MW (1994) Partial feedback linearization of underactuated mechanical systems. Paper presented at IEEE/RSJ/GI international conference on intelligent robots and systems, Munich, Germany, pp 314–321
30. Spong M (1995) The swing-up control problem for the acrobot. IEEE Control Syst Mag 47 (1):49–55
31. Spong MW (1996) Energy based control of a class of underactuated mechanical systems. Paper presented at the IFAC world congress, San Francisco, CA, USA, pp 431–435
32. Spong M, Praly L (1996) Control of underactuated mechanical systems using switching and saturation. In: Morse AS (ed) Paper presented on control using logic-based switching (lecture notes no. 222). Springer, Berlin, Germany, pp 162–172
33. Spong MW (1998) Underactuated mechanical systems, control problems in robotics and automation, vol 230. Springer, pp 135–150
34. Viola G, Ortega R, Banavar R, Acosta JA, Astolfi A (2007) Total energy shaping control of mechanical systems: simplifying the matching equations via coordinate changes. IEEE Trans Autom Control 52(6):1093–1099
35. Wan J, Bernstein DS, Coppola VT (1994) Global stabilization of the oscillating eccentric rotor. Paper presented at the international conference on decision and control, Orlando, USA, pp 4024–4029
36. Wang WJ, Lin HR (1999) Fuzzy control design for the trajectory tracking on uncertain nonlinear systems. IEEE Trans Fuzzy Syst 7(1):53–62
37. Wang W, Yi J, Zhao D, Liu D (2004) Design of a stable sliding mode controller for a class of second-order underactuated systems. IEEE Proc Control Theory Apr 151(6):683–690
38. White WN, Foss M, Guo X (2006) A direct Lyapunov approach for a class of underactuated mechanical systems. Paper presented at the American control conference, Minneapolis, MN, USA, pp 103–110
39. Ye H, Wang H (2007) Stabilization of a PVTOL aircraft and an inertia wheel pendulum using saturation technique. IEEE Trans Control Syst Technol 15(6):1143–1150
40. Zhang M, Tarn T (2002) Hybrid control of the pendubot. IEEE/ASME Trans Mechatron 7 (1):79–86
41. Zhao J, Spong MW (2001) Hybrid control for global stabilization of the cart-pendulum system. Automatica 37(12):1941–1951

Chapter 5
Applications of the Block Backstepping Algorithm on Underactuated Mechanical Systems with Higher Degrees of Freedom: Some Case Studies

Abstract Applications of the proposed control algorithm on 2-DOF underactuated mechanical systems (UMS) have already been discussed in the previous chapter. Needless to say that during real-life applications, most of the practical UMSs that comes in the scenario has more degrees of freedom. Therefore, only dealing with the 2-DOF systems would not give readers full working knowledge. Keeping in view the immense importance of higher order UMSs, authors dedicate this chapter to describe the applications of the proposed control algorithm on the same in a systematic manner. Following the similar presentation approach of Chap. 4, at the onset, a very simple flat 3-DOF system model is considered to demonstrate the controller design procedure for higher order systems. Since flat UMS has most simple dynamic characteristics than that of the other UMSs, it is always easy to deal with the control problems for such type of systems. Application of the proposed control algorithm on a vertical-takeoff-landing air craft (VTOL), which is also a type of flat UMS, is described in the first section. Thereafter, Sect. 5.2 describes application of control law on underactuated surface vessel (USV). Being a member of nonholonomic systems, it fails to satisfy the Brocket's condition of feedback linearization. Therefore, USV requires nonsmooth or time varying control input for its stabilization. Needless to say that designing a control law for USV is more difficult than that of other holonomic UMS (e.g., VTOL). Nonetheless, without considering robotic applications, discussions on UMSs would not be able to take its complete shape. Therefore, at the end, Sect. 5.3 demonstrates application of the control law on the robotic manipulator. Like USV, 3-DOF manipulator also belongs to the class of nonholonomic systems; however, unlike USV it possesses interacting control inputs. Hence, it is easy to understand that control law design for the same is more difficult than that of USV. Like the previous chapter, here also the reader will observe that no such significant modification is required to recast the control law for individual systems. Proposed control law is generalized enough that it can address the control problems of most of the higher order UMSs. All being well after going

Electronic supplementary material The online version of this article (doi:10.1007/978-981-10-1956-2_5) contains supplementary material, which is available to authorized users.

S. Rudra et al., *Block Backstepping Design of Nonlinear State Feedback Control Law for Underactuated Mechanical Systems*, DOI 10.1007/978-981-10-1956-2_5

through this chapter, the readers will find themselves ready to design control law for any practical underactuated systems.

5.1 Application on the VTOL

The VTOL aircraft has a strong coupling between rolling moments and lateral acceleration, and thereby the stabilization control of the center of mass in the lateral direction tends to cause rolling of the aircraft [1, 2]. Needless to say that interacting control input makes the control law designing task quite complicated [3, 4]. Further research on VTOL has revealed that the system possesses unstable zero dynamics, and thereby it could be treated as a type of nonminimum phase nonlinear systems [5–10]. Consequently, several design methods have been proposed to stabilize the system at its equilibrium [11–13]. In recent years, trajectory tracking and configuration stabilization of the VTOL has been extensively studied by many researchers [14, 15]. A few researchers have relied on output feedback controller for the tracking of VTOL [16]. Nonetheless, the control laws that they have conceived can ensure only local stability of the VTOL system [17, 18], but have failed to ensure global stability. On the other hand, a robust optimal control law has been designed by the authors of [8] to address the hovering control problem of a VTOL aircraft. Not only that a few researchers have also exploited the concept of dynamic inversion and robust control techniques to deal with the nonminimum phase dynamics [2]. In the recent past, a dynamic high-gain approach-based control law has also been proposed to ensure the global tracking of a reference trajectory [11]. Nevertheless, all this previously proposed approaches have devised several elegant control algorithms to address the stabilization control problem of VTOL, yet those methods often become too complex for real-time implementation [9, 10]. Therefore, stabilization problem of VTOL is still being considered as an open research problem [1, 6], and that is why the authors have chosen it as a standard test bed to demonstrate their proposed control algorithm on the same. The present section describes application of the proposed control law on nonminimum phase, underactuated VTOL system. Schematic diagram of the VTOL is shown in Fig. 5.1.

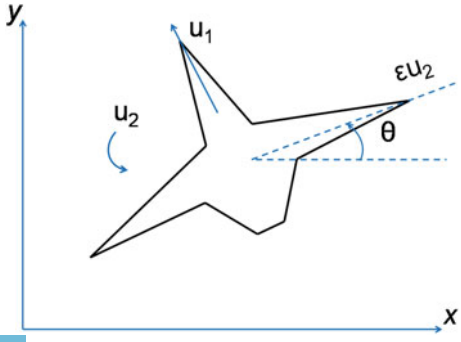

Fig. 5.1 Schematic diagram of the VTOL

The dynamic equation of the VTOL is described in Eq. (5.1). With the following choice of state variables: $x_1 = x, x_2 = v_x,\ x_3 = y, x_4 = v_y,\ x_5 = \theta, x_6 = \omega$. The nonlinear state equation of the VTOL takes the structure of state model that is described in following Eq. (5.1).

$$\begin{aligned}
\dot{x}_1 &= x_2 \\
\dot{x}_2 &= v_1 \\
\dot{x}_3 &= x_4 \\
\dot{x}_4 &= v_2 \\
\dot{x}_5 &= x_6 \\
\dot{x}_6 &= \frac{\lambda}{\varepsilon}[v_1 \cos x_5 + v_2 \sin x_5 + g\ \sin x_5]
\end{aligned} \tag{5.1}$$

However, the case of strong input coupling has been considered during this demonstration that yields $\varepsilon \neq 0$. The above-stated model can be rearranged with the following definitions of Eq. (5.2.a), so that it will take the shape of a 3-DOF system as shown in Eq. (5.2.b):

$$\begin{aligned}
q_1 &= x_5 \\
p_1 &= x_6 \\
q_2 &= [x_1 \quad x_3]^T \\
p_2 &= [x_2 \quad x_4]^T
\end{aligned} \tag{5.2.a}$$

and,

$$\begin{aligned}
\dot{q}_1 &= p_1 \\
\dot{q}_2 &= p_2 \\
\dot{p}_1 &= f + gu \\
\dot{p}_2 &= u
\end{aligned} \tag{5.2.b}$$

where

$$f = \frac{\lambda}{\varepsilon} g\ \sin x_5 \tag{5.2.c}$$

$$g = [g_1 \quad g_2] = \frac{\lambda}{\varepsilon}[\cos x_5 \quad \sin x_5] \tag{5.2.d}$$

(Detailed description of the state model is given in Appendix A.8).

Salient Control Features of VTOL Aircraft: *Actuated Shape variable, interacting input configuration, flat underactuated system, nonminimum phase zero dynamics.*

Control Objective: *Stabilize the aircraft at a desired configuration point.*

5.1.1 Derivation of the Control Law for VTOL

Step 1: Following the design procedure of Sect. 3.2.2, a new control variable $z_1 \in \mathbb{R}^2$ has been defined according to Eq. (3.22). The new control variable has taken the form of Eq. (5.3) below:

$$z_1 = q_2 - K(q_1 + p_1 - gp_2) \tag{5.3}$$

where, $K \in \mathbb{R}^{2\times 1}$ is a constant matrix such that $K = [k \quad 0]$. In the above equation, $g(q)$ is represented by g.

Time derivative of z_1 has been computed as shown in the following Eq. (5.4):

$$\dot{z}_1 = p_2 - K(p_1 + f - D(g)p_2) \tag{5.4}$$

In above representation $D(g) \in \mathbb{R}^{1\times 2}$ represents the time differentiation of matrix $g(q)$, where any element of $D(g)$ can be expressed as $D(g_{ij}) = \sum_{k=1}^{n} \frac{\partial g_{ij}}{\partial q_k} p_k$, where i and j indicate the position of the elements of $D(g)$ matrix. (Please note that $g \in \mathbb{R}^{1\times 2}$.) Therefore, construction of $D(g)$ matrix can be simply explained with the following Eq. (5.5):

$$D(g) = \left[\frac{\partial g_1}{\partial q_1}p_1 + \frac{\partial g_1}{\partial q_{21}}p_{21} + \frac{\partial g_1}{\partial q_{22}}p_{22} \quad \frac{\partial g_2}{\partial q_1}p_1 + \frac{\partial g_2}{\partial q_{21}}p_{21} + \frac{\partial g_2}{\partial q_{22}}p_{22}\right] \tag{5.5}$$

Further simplification has resulted in

$$D(g) = \frac{\lambda}{\varepsilon}\left[\sum_{k=1}^{3}\frac{\partial \cos x_5}{\partial q_k}p_k \quad \sum_{k=1}^{3}\frac{\partial \ sinx_5}{\partial q_k}p_k\right] = \frac{\lambda}{\varepsilon}\left[-\sin x_5 x_6 \quad \cos x_5 x_6\right] \tag{5.6}$$

Step 2: The stabilizing function has been defined in accordance with Eq. (3.27) to ensure the desired dynamic behavior of z_1. Expression of the stabilizing function has been shown in Eq. (5.7)

$$\alpha = -c_1 z_1 - \lambda \chi_1 + K(p_1 + f - D(g)p_2) \tag{5.7}$$

Step 3: Following Eq. (3.28), the second error variable $z_2 \in \mathbb{R}^2$ has been defined according to Eq. (5.8) as shown below

$$z_2 = p_2 - \alpha \tag{5.8}$$

with the above definition of second control variable, the dynamics of first error variable has become:

$$\dot{\boldsymbol{z}}_{\boldsymbol{1}} = \boldsymbol{z}_{\boldsymbol{2}} - c_1\boldsymbol{z}_{\boldsymbol{1}} - \lambda\boldsymbol{\chi}_{\boldsymbol{1}} \tag{5.9}$$

Consequently, time derivative of the second error variable z_2 is as shown in Eq. (5.10) below

$$\begin{aligned}\dot{\boldsymbol{z}}_{\boldsymbol{2}} &= \dot{\boldsymbol{p}}_{\boldsymbol{2}} - \dot{\boldsymbol{\alpha}} \\ &= \boldsymbol{u} + c_1(\boldsymbol{z}_{\boldsymbol{2}} - c_1\boldsymbol{z}_{\boldsymbol{1}} - \lambda\boldsymbol{\chi}_1) + \lambda\boldsymbol{z}_{\boldsymbol{1}} \\ &\quad - K\big[\boldsymbol{f} + g\boldsymbol{u} + Df_{q1}\boldsymbol{p}_{\boldsymbol{1}} + Df_{q2}\boldsymbol{p}_{\boldsymbol{2}} + Df_{p1}(\boldsymbol{f} + g\boldsymbol{u}) \\ &\quad + Df_{p2}\boldsymbol{u} - D(g)\boldsymbol{u} - D^2(g)\boldsymbol{p}_{\boldsymbol{2}}\big]\end{aligned} \tag{5.10}$$

In Eq. (5.10), $Df_{q1} \in \mathbb{R}^{1\times1}$, $Df_{q2} \in \mathbb{R}^{1\times2}$, $Df_{p1} \in \mathbb{R}^{1\times1}$ and $Df_{p2} \in \mathbb{R}^{1\times2}$ represent the matrices of partial derivatives of $\boldsymbol{f}$ vector with respect to different sub-component of state vector such as $\boldsymbol{q_1}$, $\boldsymbol{q_2}$, $\boldsymbol{p_1}$ and $\boldsymbol{p_2}$ as shown below:

$$Df_{q1} = \frac{\partial f}{\partial q_1} \tag{5.11.a}$$

$$Df_{q2} = \begin{bmatrix}\dfrac{\partial f}{\partial q_{21}} & \dfrac{\partial f}{\partial q_{22}}\end{bmatrix} \tag{5.11.b}$$

$$Df_{p1} = \frac{\partial f}{\partial p_1} \tag{5.11.c}$$

$$Df_{p2} = \begin{bmatrix}\dfrac{\partial f}{\partial p_{21}} & \dfrac{\partial f}{\partial p_{22}}\end{bmatrix} \tag{5.11.d}$$

$D_2(g) \in \mathbb{R}^{n_1\times n_2}$ is given by $D^2(g) = \left[D_1^2(g) + D_2^2(g)\right]$. The definition of $D_1^2(g)$ and $D_2^2(g)$ are shown in the following equations:

$$D_1^2(g_{ij}) = \sum_{l=1}^{n}\sum_{k=1}^{n}\frac{\partial^2 g_{ij}}{\partial q_k \partial q_l}p_k p_l \tag{5.12}$$

$$D_2^2(g_{ij}) = \sum_{k=1}^{n}\frac{\partial g_{ij}}{\partial q_k}\dot{p}_k \tag{5.13}$$

In the above expression, p_k and p_l represent the individual elements of $\boldsymbol{p}$ vector. Similar to the previous case, one can represent the structure of $D_1^2(g)$ and $D_2^2(g)$ matrix as shown in the following equation series (5.14.a, 5.14.b):

$$D_1^2(g) = \begin{bmatrix} \frac{\partial^2 g_1}{\partial q_1^2}p_1^2 + \frac{\partial^2 g_1}{\partial q_{21}^2}p_{21}^2 + \frac{\partial^2 g_1}{\partial q_2^2}p_{22}^2 + 2\frac{\partial^2 g_1}{\partial q_{21}q_1}p_1p_{21} + 2\frac{\partial^2 g_1}{\partial q_{22}q_1}p_1p_{22} + 2\frac{\partial^2 g_1}{\partial q_{21}q_{22}}p_{22}p_{21} \\ \frac{\partial^2 g_2}{\partial q_1^2}p_1^2 + \frac{\partial^2 g_2}{\partial q_{21}^2}p_{21}^2 + \frac{\partial^2 g_2}{\partial q_2^2}p_{22}^2 + 2\frac{\partial^2 g_2}{\partial q_{21}q_1}p_1p_{21} + 2\frac{\partial^2 g_2}{\partial q_{22}q_1}p_1p_{22} + 2\frac{\partial^2 g_2}{\partial q_{21}q_{22}}p_{22}p_{21} \end{bmatrix}^T \tag{5.14.a}$$

$$D_2^2(g) = \begin{bmatrix} \frac{\partial g_1}{\partial q_1}\dot{p}_1 + \frac{\partial g_1}{\partial q_{21}}\dot{p}_{21} + \frac{\partial g_1}{\partial q_{22}}\dot{p}_{22} & \frac{\partial g_2}{\partial q_1}\dot{p}_1 + \frac{\partial g_2}{\partial q_{21}}\dot{p}_{21} + \frac{\partial g_2}{\partial q_{22}}\dot{p}_{22} \end{bmatrix} \tag{5.14.b}$$

However, from the structure of $D_2^2(g)$ matrix it can be easily inferred that $D_2^2(g)\boldsymbol{p_2}$ can be further partitioned into three parts as shown in the following equation:

$$D_2^2(g)\boldsymbol{p_2} = D_{2\boldsymbol{p_1}}^2(g)\boldsymbol{f} + D_{2\boldsymbol{p_1}}^2(g)g\boldsymbol{u} + D_{2\boldsymbol{p_2}}^2(g)\boldsymbol{u} \tag{5.15}$$

where the elements of each components are

$$D_{2p_1}^2(g_{mr}) = \sum_{i=1}^{n_2} \frac{\partial g_{mi}}{\partial q_{1r}} p_{2i} \tag{5.16}$$

where $D_{2p_1}^2(g) \in \mathbb{R}^{n_1 \times n_1}$ and $m = 1,\ldots, n_1$ indicates the row index of g matrix, q_{1r} is the elements of vector $\boldsymbol{q}_1$, where r denotes the index of the particular configuration variables and p_{2i} denotes the element of $\boldsymbol{p}_2$ vector.

$$D_{2p_2}^2(g_{mr}) = \sum_{i=1}^{n_2} \frac{\partial g_{mi}}{\partial q_{2r}} p_{2i} \tag{5.17}$$

where $D_{2p_2}^2(g) \in \mathbb{R}^{n_1 \times n_2}$ $m = 1,\ldots, n_1$ indicates the row number of g matrix, q_{2r} belongs to the vector $\boldsymbol{q}_2$, where r denotes the index of the particular configuration variables. Construction of the matrices that are described in Eqs. (5.16) and (5.17) can also be explained with the help of the state model of Eqs. (5.2.a–5.2.d).

$$\begin{aligned} D_2^2(g)\boldsymbol{p_2} &= \begin{bmatrix} \frac{\partial g_1}{\partial q_1}\left(f + [g_1 g_2]\begin{bmatrix} u_1 \\ u_2 \end{bmatrix}\right) + \frac{\partial g_1}{\partial q_{21}}u_1 + \frac{\partial g_1}{\partial q_{22}}u_2 \\ \frac{\partial g_2}{\partial q_1}\left(f + [g_1 g_2]\begin{bmatrix} u_1 \\ u_2 \end{bmatrix}\right) + \frac{\partial g_2}{\partial q_{21}}u_1 + \frac{\partial g_2}{\partial q_{22}}u_2 \end{bmatrix}^T \begin{bmatrix} p_{21} \\ p_{22} \end{bmatrix} \\ &= \left[\left(\frac{\partial g_1}{\partial q_1}p_{21} + \frac{\partial g_2}{\partial q_1}p_{22}\right)\left(f + [g_1 g_2]\begin{bmatrix} u_1 \\ u_2 \end{bmatrix}\right) + \left(\frac{\partial g_1}{\partial q_{21}}p_{21} + \frac{\partial g_2}{\partial q_{21}}p_{22}\right)u_1 + \left(\frac{\partial g_1}{\partial q_{22}}p_{21} + \frac{\partial g_2}{\partial q_{22}}p_{22}\right)u_2\right] \end{aligned} \tag{5.18}$$

Hence, with the above mentioned simplification technique, it is always possible to represent the time derivative of $\boldsymbol{z_2}$ in the following compact form as shown in Eq. (5.19)

$$\begin{aligned}\dot{\boldsymbol{z}}_{\boldsymbol{2}} &= \boldsymbol{u} + c_1(\boldsymbol{z}_{\boldsymbol{2}} - c_1\boldsymbol{z}_{\boldsymbol{1}} - \lambda\boldsymbol{\chi}_{\boldsymbol{1}}) + \lambda\boldsymbol{z}_{\boldsymbol{1}} \\ &\quad - K\left[\boldsymbol{f} + g\boldsymbol{u} + Df_{q_1}\boldsymbol{p}_{\boldsymbol{1}} + Df_{q2}\boldsymbol{p}_{\boldsymbol{2}} + Df_{p1}(\boldsymbol{f} + g\boldsymbol{u}) + Df_{p2}\boldsymbol{u}\right. \\ &\quad \left. - D(g)\boldsymbol{u} - D_1^2(g)\boldsymbol{p}_{\boldsymbol{2}} - D_{2p_1}^2(g)\boldsymbol{f} - D_{2p_1}^2(g)g\boldsymbol{u} - D_{2p_2}^2(g)\boldsymbol{u}\right] \\ &= \psi\boldsymbol{u} + \lambda\boldsymbol{z}_{\boldsymbol{1}} + c_1(\boldsymbol{z}_{\boldsymbol{2}} - c_1\boldsymbol{z}_{\boldsymbol{1}} - \lambda\boldsymbol{\chi}_{\boldsymbol{1}}) + \boldsymbol{\Phi}\end{aligned} \tag{5.19}$$

where the expressions of $\psi \in \mathbb{R}^{n_2 \times n_2}$ and $\boldsymbol{\Phi} \in \mathbb{R}^{n_2}$ are shown in following equations:

$$\psi = \left[I - K\left(g + Df_{p1}g + Df_{p2} - D(g) - D_{2p_1}^2(g)g - D_{2p_2}^2(g)\right)\right] \tag{5.20}$$

and

$$\boldsymbol{\Phi} = -K\left[\boldsymbol{f} + Df_{q1}\boldsymbol{p}_{\boldsymbol{1}} + Df_{q2}\boldsymbol{p}_{\boldsymbol{2}} + Df_{p1}\boldsymbol{f} - D_1^2(g)\boldsymbol{p}_{\boldsymbol{2}} - D_{2p1}^2(g)\boldsymbol{f}\right] \tag{5.21}$$

In Eq. (5.20), I denotes an identity matrix of order n_2. Similar to the case of 2-DOF UMSs (described in the previous chapter), above three steps have transformed the state model of an n-DOF underactuated system of (5.1) into the block-strict feedback form.

Step 4: The control law $\boldsymbol{u}$ has been designed to ensure the desired dynamics for $\boldsymbol{z_2}$. The desired dynamics of $\boldsymbol{z_2}$ has been defined in the following Eq. (5.22) as shown below:

$$\dot{\boldsymbol{z}}_{\boldsymbol{2}} = -\boldsymbol{z}_{\boldsymbol{1}} - c_2\boldsymbol{z}_{\boldsymbol{2}} \tag{5.22}$$

where c_2 is an arbitrary positive design constant.

Consequently, from Eqs. (5.20) and (5.22) the desired control input has been derived in the following manner:

$$\boldsymbol{u} = \psi^{-1}\left[-\left(1 - c_1^2 + \lambda\right)\boldsymbol{z}_{\boldsymbol{1}} - (c_1 + c_2)\boldsymbol{z}_{\boldsymbol{2}} + \lambda c_1\boldsymbol{\chi}_{\boldsymbol{1}} - \boldsymbol{\Phi}\right] \tag{5.23}$$

such choice of control input $\boldsymbol{u}$ has resulted in the following dynamics:

$$\begin{aligned}\dot{\boldsymbol{z}}_{\boldsymbol{1}} &= \boldsymbol{z}_{\boldsymbol{2}} - c_1\boldsymbol{z}_{\boldsymbol{1}} - \lambda\boldsymbol{\chi}_{\boldsymbol{1}} \\ \dot{\boldsymbol{z}}_{\boldsymbol{2}} &= -\boldsymbol{z}_{\boldsymbol{1}} - c_2\boldsymbol{z}_{\boldsymbol{2}}\end{aligned} \tag{5.24}$$

The partial differential terms of the above Eq. (5.19) are shown below

$$Df_{q1} = \frac{\lambda}{\varepsilon}g\cos x_5 \tag{5.25}$$

$$Df_{q2} = [0 \quad 0] \tag{5.26}$$

$$Df_{p1} = 0 \tag{5.27}$$

$$Df_{p2} = [0 \quad 0] \tag{5.28}$$

$$D_{p1}^2(g) = \frac{\lambda}{\varepsilon}\left[\sum_{i=1}^{2}\frac{\partial \cos x_5}{\partial x_5}p_{2i}\right] = -\frac{\lambda}{\varepsilon}\sin x_5(x_2 + x_4) \tag{5.29}$$

$$D_{p2}^2(g) = \left[\frac{\partial(\cos x_5)}{\partial x_1}x_2 + \frac{\partial(\sin x_5)}{\partial x_1}x_4 \quad \frac{\partial(\cos x_5)}{\partial x_2}x_2 + \frac{\partial(\sin x_5)}{\partial x_2}x_4\right] = [0 \quad 0] \tag{5.30}$$

As it has already been stated in Sect. 3.2.3, Eqs. (3.46.a)–(3.46.c) depict the zero dynamics structure for an n degrees of freedom system. Consequently, in the special case of the VTOL $z_1 = 0\, and\, \dot{z}_1 = 0$ yield the following expression of q_2 and p_2.

$$\boldsymbol{z_1} = \boldsymbol{q_2} - K(q_1 + p_1 - g\boldsymbol{p_2}) = 0 \Rightarrow \boldsymbol{q_2} = K(q_1 + p_1 - g\boldsymbol{p_2}) \tag{5.31.a}$$

$$\dot{\boldsymbol{z}}_{\boldsymbol{1}} = \boldsymbol{p_2} - K(p_1 + f - D(g)\boldsymbol{p_2}) = 0 \Rightarrow \boldsymbol{p_2} = K(p_1 + f - D(g)\boldsymbol{p_2}) \tag{5.31.b}$$

$$\mathbb{k}_{\boldsymbol{1}} = \psi \boldsymbol{u} + \boldsymbol{\Phi} = \boldsymbol{0} \Rightarrow \boldsymbol{u} = \psi^{-1}\boldsymbol{\Phi} \tag{5.31.c}$$

Now, q_2 and p_2 terms of f, ψ, and Φ have been replaced by the expressions of (5.31.a) and (5.31.b), respectively, then the equations of zero dynamics for the VTOL has taken the following form of Eq. (5.32):

$$\begin{aligned} \dot{q}_1 &= p_1 \\ \dot{p}_1 &= f(q_1, p_1) - g(q_1, p_1)\psi^{-1}(q_1, p_1)\Phi(q_1, p_1) \end{aligned} \tag{5.32}$$

In Eq. (5.32), $f(q_1, p_1), g(q_1, p_1), \psi^{-1}(q_1, p_1)$ and $\varphi(q_1, p_1)$ represent the same functions f, g, ψ^{-1}, and φ, with the only difference being that the last equation, all the q_2 and p_2 terms have been replaced by the expression of (5.31.a) and (5.31.b), respectively. Constant k has to be selected in such a manner that it would ensure the stability of the zero dynamics system. Following Lyapunov function has been defined to analyze stability of the internal dynamics of Eq. (5.33)

$$V_z = \frac{1}{2}q_1^2 + \frac{1}{2}p_1^2 \tag{5.33}$$

Now, time derivative of the above Lyapunov function V_z results in

$$\dot{V}_z = q_1 p_1 + p_1 F \tag{5.34}$$

Now, the controller parameter k has been selected in a judicial manner to ensure the negative definiteness of the $\dot{V}_z$. The other three controller parameters do not alter the negative definiteness of $\dot{V}_z$. However, they have been chosen in a manner so that

they could satisfy the condition $c_1 > 0$, $c_2 > 0$, and $\lambda > 0$. (Detailed criteria of controller parameter selection have been discussed in Chap. 3, Sect. 3.2.3).

5.1.2 Simulation Results and Performance Analysis

Effectiveness of the proposed control law has been verified after simulating the closed-loop system in Matlab® (version: 7.14) Simulink (version: 7.9) environment. Parameters of Table 5.1 have been used to develop a virtual model of VTOL in the simulation environment. Parameters of the block backstepping controller are mentioned in Table 5.2. Initial value of the state variables that have been chosen for simulation experiment are as follows: $q_1 = 2, q_2 = [4 \quad \pi/3], p_1 = 3$ and $p_2 = [1 \quad 0]$

Figure 5.2 shows the variation of state variable x with time, whereas the time variation of the state variable $\dot{x}$ (the time derivative of x) is shown in Fig. 5.3. Similarly, Fig. 5.4 shows the variation of state variable y with time, while the time variation of the state variable $\dot{y}$ (the time derivative of y) has been shown in Fig. 5.5. Figure 5.6 shows the variation of state variable θ with time, whereas the variation of the state variable $\dot{\theta}$ (the time derivative of θ) is shown in Fig. 5.7. Following the representation style of Chap. 4, at first, time variation of the

Table 5.1 Parameters of the VTOL (SI unit)

M	J	λ	E	g
392	1.617	1	1	9.8

Table 5.2 Parameters of the proposed

c_1	c_2	λ	K
10	10	0.01	$[0.9 \quad 0]^T$

Block backstepping controller

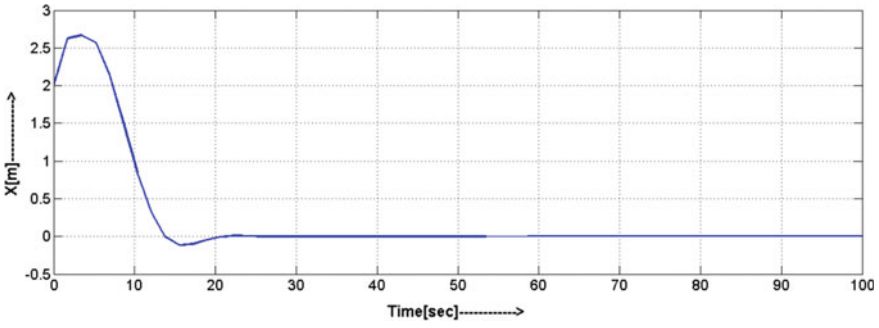

Fig. 5.2 Variation of the state variable x with time

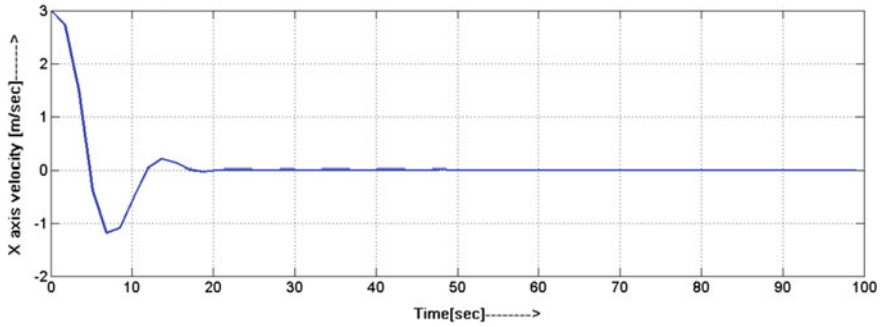

Fig. 5.3 Variation of the state variable $\dot{x}$ with time

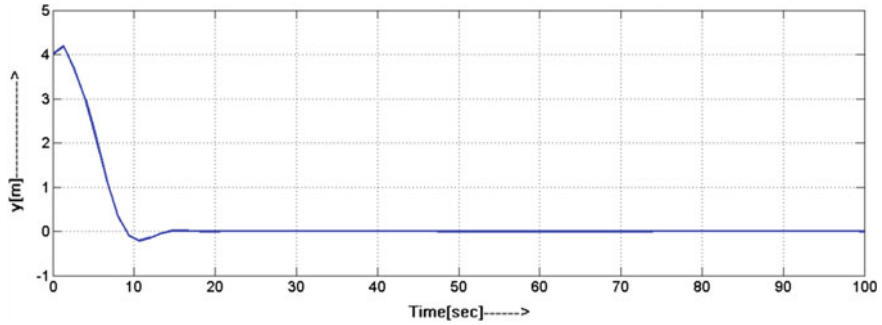

Fig. 5.4 Variation of the state variable y with time

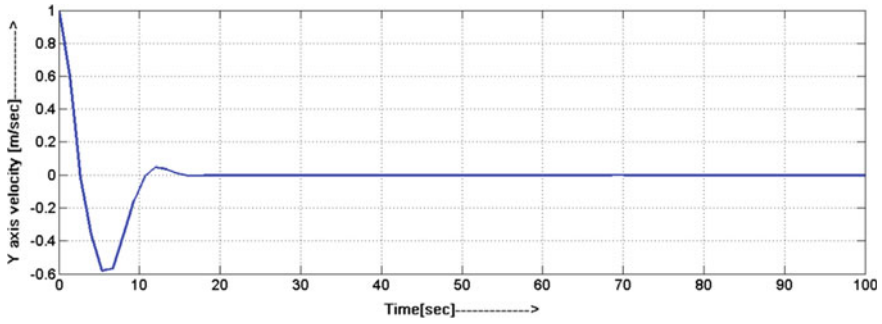

Fig. 5.5 Variation of the state variable $\dot{y}$ with time

unactuated configuration variable and corresponding velocity component variation with time are presented to investigate the zero dynamics stability of the system. Thereafter, time variations of the actuated variables are presented to corroborate the theoretical findings.

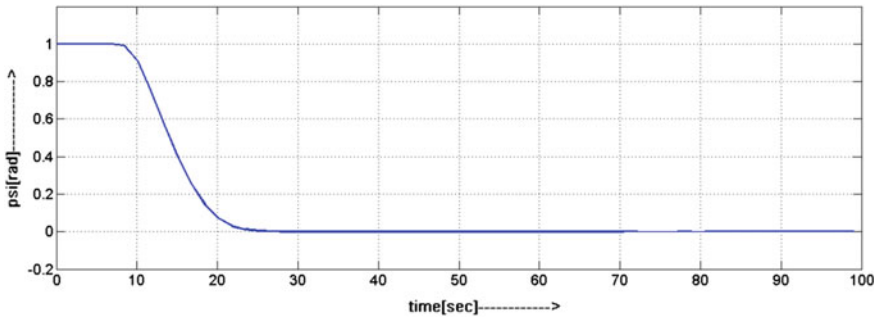

Fig. 5.6 Angular displacement of the VTOL

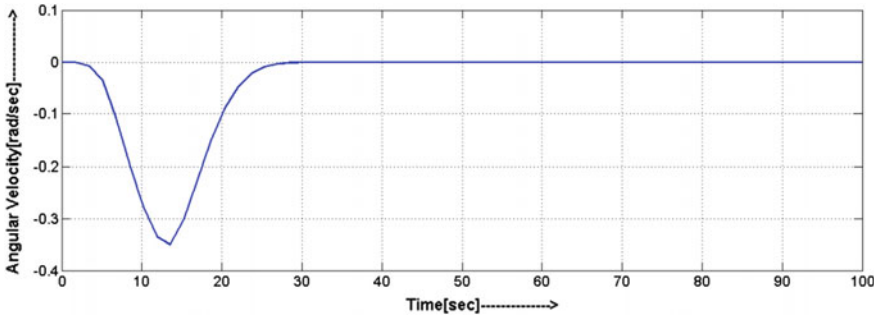

Fig. 5.7 Angular velocity of the VTOL

It can be inferred from the above figures that the proposed control law can ensure the global asymptotic stabilization of the unactuated state variables. Consequently, it has corroborated the fact that asymptotic stability of the zero dynamics ensures the asymptotic convergence of *unactuated state variables to zero*.

Convergences of the actuated variables are shown in Figs. 5.4, 5.5, 5.6 and 5.7. Hence, it is quite clear from the above simulation studies that the proposed control law is able to ensure the global asymptotic stability of the VTOL system. Proposition of theorem 2 (Chap. 3, Sect. 3.4), which states the global asymptotic stability of the reduced order system together with the global asymptotic stability of the internal dynamics ensures asymptotic stabilization of the actuated shape variables, has also been corroborated by the stabilization of the actuated state variables.

Figure 5.8 shows the variation of control input v_1 of VTOL, and Fig. 5.9 shows the control input v_2 of VTOL. Figures 5.8 and 5.9 reveal the fact that the proposed control law is capable of generating adequate control action to stabilize the configuration variable of a nonminimum phase, strongly coupled, flat underactuated system. In the next section, formulation of control law for USV (Underactuated surface vessel) system and its implementation on the same test bench will be discussed in a systematic manner.

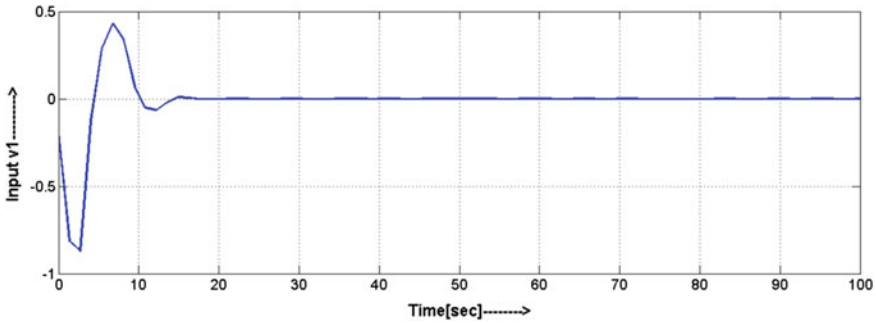

Fig. 5.8 Variation of control input v_1 with time

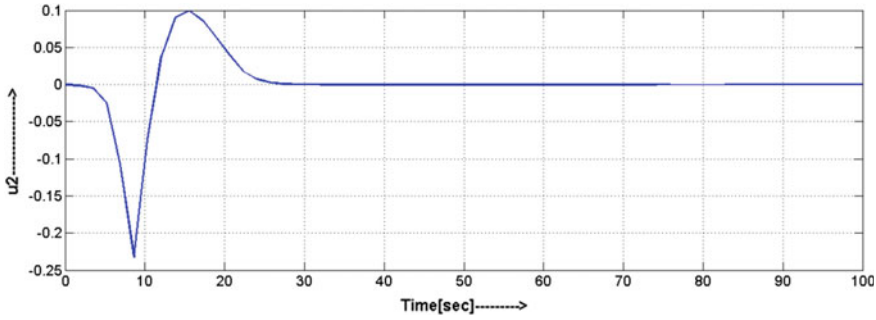

Fig. 5.9 Variation of control input v_2 with time

5.2 Application on the USV

Over the past few decades, stabilization problem of USV have drawn conspicuous amount of research attentions from control theorist and engineers [19–21]. The authors of [22–25] have shown that the dynamics of USV fails to satisfy the Brocket's necessary condition of feedback linearization. As a matter of fact the system requires nonsmooth or time varying control input for its asymptotic stabilization [12, 13]. In order to provide nonsmooth control input to the system, the authors of [26] and [27] have proposed a discontinuous feedback control law to ensure exponential stability of the system. However, the control law can only ensure local stability of the system. On the other hand, a time varying feedback control law has been devised by a group of researchers to ensure exponential stability of the desired equilibrium point [19]. Indeed, several research articles have

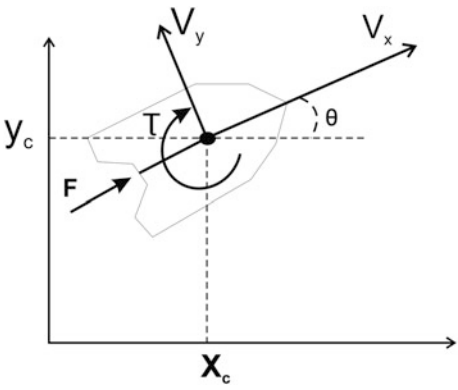

Fig. 5.10 Schematic diagram of the USV

proposed in the last few years to address the stabilization problem of USV, yet none of them could ensure ultimate performance for the system. Only they have achieved a tradeoff between different performance requirements, and thereby designing a control law for the USV is still being considered as an open research problem in the literature of nonlinear control engineering. Therefore, authors have also considered the stabilization problem of USV for demonstrating the versatility of the proposed control approach.

The schematic diagram of the USV is shown in Fig. 5.10. The dynamic equation of the USV is described in Eq. (5.35). With the following choice of state variables: $x_1 = x, x_2 = \theta, x_3 = y,\ \ x_4 = v_x, x_5 = \omega, x_6 = v_y$. Consequently, nonlinear state equation of the USV has taken the structure of state model as described in the following Eq. (5.35)

$$\begin{aligned}
\dot{x}_1 &= x_4 \\
\dot{x}_2 &= x_5 \\
\dot{x}_3 &= x_6 \\
\dot{x}_4 &= u_1 \\
\dot{x}_5 &= u_2 \\
\dot{x}_6 &= u_1 \tan x_2 + \frac{c_y}{m}(x_4 \tan x_2 - x_6)
\end{aligned} \tag{5.35}$$

In the above representation, x_1 and x_2 represent the actuated variable, where x_3 represents unactuated variable. Similarly, x_4 and x_5 represent the actuated velocity components, whereas x_6 is the unactuated velocity components. Two control inputs to the system are longitudinal acceleration and angular acceleration, denoted by u_1 and u_2, respectively.

However, the above state model can be represented as higher order UMS as shown below

$$\begin{aligned} q_1 &= x_3 \\ p_1 &= x_6 \\ q_2 &= [\,x_1 \quad x_2\,]^T \\ p_2 &= [\,x_4 \quad x_5\,]^T \end{aligned} \tag{5.36.a}$$

and,

$$\begin{aligned} \dot{q}_1 &= p_1 \\ \dot{q}_2 &= p_2 \\ \dot{p}_1 &= f + gu \\ \dot{p}_2 &= u \end{aligned} \tag{5.36.b}$$

where

$$f = \frac{c_y}{m}(x_4 \tan x_2 - x_6) \tag{5.36.c}$$

$$g = [\,\tan x_2 \quad 0\,] \tag{5.36.d}$$

(Detailed derivation of the state model is given in Appendix A.8).

Salient Control Features of USV: *Actuated Shape Variables, noninteracting inputs, 2*nd*-order nonholonomic systems.*

Control Objective: *Stabilize the USV at any desired equilibrium point (parking at a desired configuration).*

5.2.1 Derivation of the Control Law for USV

Step 1: Following the design procedure of VTOL, a new control variable $\boldsymbol{z_1} \in \mathbb{R}^2$ has been defined according to Eq. (5.37) as shown below

$$\boldsymbol{z_1} = \boldsymbol{q_2} - K(\boldsymbol{q_1} + \boldsymbol{p_1} - g\boldsymbol{p_2}) \tag{5.37}$$

where, $K \in \mathbb{R}^{2\times 1}$ is a constant matrix such that $K = [\,k \quad 0\,]$. In the above equation, $g(\boldsymbol{q})$ is represented by g.

Similar to the previous design case, time derivative of $\boldsymbol{z}_1$ has been computed as shown in the following Eq. (5.38):

$$\dot{\boldsymbol{z}}_1 = \boldsymbol{p_2} - K(\boldsymbol{p_1} + \boldsymbol{f} - D(g)\boldsymbol{p_2}) \tag{5.38}$$

In the above representation $D(g) \in \mathbb{R}^{1\times 2}$ represents the time differentiation of matrix $g(\boldsymbol{q})$, where any element of $D(g)$ can be expressed as $D(g_{ij}) = \sum_{k=1}^{n} \frac{\partial g_{ij}}{\partial q_k} p_k$,

where i and j indicate the position of the elements of $D(g)$ matrix. (Please note that $g \in \mathbb{R}^{1\times 2}$). Therefore, construction of $D(g)$ matrix can be simply explained with the following Eq. (5.39):

$$D(g) = \begin{bmatrix} \frac{\partial g_1}{\partial q_1}p_1 + \frac{\partial g_1}{\partial q_{21}}p_{21} + \frac{\partial g_1}{\partial q_{22}}p_{22} & \frac{\partial g_2}{\partial q_1}p_1 + \frac{\partial g_2}{\partial q_{21}}p_{21} + \frac{\partial g_2}{\partial q_{22}}p_{22} \end{bmatrix} \tag{5.39}$$

Further simplification has resulted in:

$$D(g) = \begin{bmatrix} \sum_{k=1}^{3} \frac{\partial \tan x_2}{\partial q_k} p_k & 0 \end{bmatrix} = \begin{bmatrix} \sec^2 x_2 & 0 \end{bmatrix} \tag{5.40}$$

Step 2: The stabilizing function has been defined in accordance with Eq. (3.27) to ensure the desired dynamic behavior of $\boldsymbol{z_1}$. Expression of the stabilizing function has been shown in Eq. (5.41)

$$\boldsymbol{\alpha} = -c_1\boldsymbol{z_1} - \lambda\boldsymbol{\chi_1} + K(\boldsymbol{p_1} + \boldsymbol{f} - D(g)\boldsymbol{p_2}) \tag{5.41}$$

Step 3: Following Eq. (3.28), the second error variable $\boldsymbol{z_2} \in \mathbb{R}^2$ has been defined that is shown in Eq. (5.42) below:

$$\boldsymbol{z_2} = \boldsymbol{p_2} - \boldsymbol{\alpha} \tag{5.42}$$

with the above definition of second control variable, the dynamics of first error variable has become

$$\dot{\boldsymbol{z}}_{\boldsymbol{1}} = \boldsymbol{z_2} - c_1\boldsymbol{z_1} - \lambda\boldsymbol{\chi_1} \tag{5.43}$$

Consequently, time derivative of the second error variable z_2 can be expressed as shown in Eq. (5.44) below

$$\begin{aligned} \dot{\boldsymbol{z}}_{\boldsymbol{2}} &= \dot{\boldsymbol{p}}_{\boldsymbol{2}} - \dot{\boldsymbol{\alpha}} \\ &= \boldsymbol{u} + c_1(\boldsymbol{z_2} - c_1\boldsymbol{z_1} - \lambda\boldsymbol{\chi}_1) + \lambda\boldsymbol{z_1} \\ &\quad - K\big[\boldsymbol{f} + g\boldsymbol{u} + Df_{q1}\boldsymbol{p_1} + Df_{q2}\boldsymbol{p_2} + Df_{p1}(\boldsymbol{f} + g\boldsymbol{u}) \\ &\quad + Df_{p2}\boldsymbol{u} - D(g)\boldsymbol{u} - D^2(g)\boldsymbol{p_2}\big] \end{aligned} \tag{5.44}$$

In Eq. (5.44), $Df_{q1} \in \mathbb{R}^{1\times 1}$, $Df_{q2} \in \mathbb{R}^{1\times 2}$, $Df_{p1} \in \mathbb{R}^{1\times 1}$ and $Df_{p2} \in \mathbb{R}^{1\times 2}$ represent the matrices of partial derivatives of $\boldsymbol{f}$ vector with respect to different sub-component of state vector such as $\boldsymbol{q_1}$, $\boldsymbol{q_2}$, $\boldsymbol{p_1}$, and $\boldsymbol{p_2}$ as shown below

$$Df_{q1} = \frac{\partial f}{\partial q_1} \tag{5.45.a}$$

$$Df_{q2} = \begin{bmatrix} \dfrac{\partial f}{\partial q_{21}} & \dfrac{\partial f}{\partial q_{22}} \end{bmatrix} \tag{5.45.b}$$

$$Df_{p1} = \frac{\partial f}{\partial p_1} \tag{5.45.c}$$

$$Df_{p2} = \begin{bmatrix} \dfrac{\partial f}{\partial p_{21}} & \dfrac{\partial f}{\partial p_{22}} \end{bmatrix} \tag{5.45.d}$$

$D_2(g) \in \mathbb{R}^{n_1 \times n_2}$ is given by $D^2(g) = \left[D_1^2(g) + D_2^2(g)\right]$. The definition of $D_1^2(g)$ and $D_2^2(g)$ are shown in the following equations:

$$D_1^2(g_{ij}) = \sum_{l=1}^{n} \sum_{k=1}^{n} \frac{\partial^2 g_{ij}}{\partial q_k \partial q_l} p_k p_l \tag{5.46}$$

$$D_2^2(g_{ij}) = \sum_{k=1}^{n} \frac{\partial g_{ij}}{\partial q_k} \dot{p}_k \tag{5.47}$$

In the above expression, p_k and p_l represent the individual elements of $\boldsymbol{p}$ vector. Similar to the previous case, one can represent the structure of $D_1^2(g)$ and $D_2^2(g)$ matrix as shown in the following equation series (5.48.a, 5.48.b):

$$D_1^2(g) = \begin{bmatrix} \dfrac{\partial^2 g_1}{\partial q_1^2} p_1^2 + \dfrac{\partial^2 g_1}{\partial q_{21}^2} p_{21}^2 + \dfrac{\partial^2 g_1}{\partial q_2^2} p_{22}^2 + 2\dfrac{\partial^2 g_1}{\partial q_{21} q_1} p_1 p_{21} + 2\dfrac{\partial^2 g_1}{\partial q_{22} q_1} p_1 p_{22} + 2\dfrac{\partial^2 g_1}{\partial q_{21} q_{22}} p_{22} p_{21} \\ \dfrac{\partial^2 g_2}{\partial q_1^2} p_1^2 + \dfrac{\partial^2 g_2}{\partial q_{21}^2} p_{21}^2 + \dfrac{\partial^2 g_2}{\partial q_2^2} p_{22}^2 + 2\dfrac{\partial^2 g_2}{\partial q_{21} q_1} p_1 p_{21} + 2\dfrac{\partial^2 g_2}{\partial q_{22} q_1} p_1 p_{22} + 2\dfrac{\partial^2 g_2}{\partial q_{21} q_{22}} p_{22} p_{21} \end{bmatrix}^T \tag{5.48.a}$$

$$D_2^2(g) = \begin{bmatrix} \dfrac{\partial g_1}{\partial q_1}\dot{p}_1 + \dfrac{\partial g_1}{\partial q_{21}}\dot{p}_{21} + \dfrac{\partial g_1}{\partial q_{22}}\dot{p}_{22} & \dfrac{\partial g_2}{\partial q_1}\dot{p}_1 + \dfrac{\partial g_2}{\partial q_{21}}\dot{p}_{21} + \dfrac{\partial g_2}{\partial q_{22}}\dot{p}_{22} \end{bmatrix} \tag{5.48.b}$$

However, from the structure of $D_2^2(g)$ matrix it can be easily inferred that $D_2^2(g)\boldsymbol{p_2}$ can be further partitioned into three parts as shown in the following equation:

$$D_2^2(g)\boldsymbol{p_2} = D_{2\boldsymbol{p_1}}^2(g)\boldsymbol{f} + D_{2\boldsymbol{p_1}}^2(g)g\boldsymbol{u} + D_{2\boldsymbol{p_2}}^2(g)\boldsymbol{u} \tag{5.49}$$

where the elements of each components are

$$D_{2p_1}^2(g_{mr}) = \sum_{i=1}^{n_2} \frac{\partial g_{mi}}{\partial q_{1r}} p_{2i} \tag{5.50}$$

where $D^2_{2p_1}(g) \in \mathbb{R}^{n_1 \times n_1}$ and $m = 1, \ldots, n_1$ indicates the row index of g matrix, q_{1r} is the elements of the vector $\boldsymbol{q}_1$, where r denotes the index of the particular configuration variables and p_{2i} denotes element of $\boldsymbol{p}_2$ vector.

$$D^2_{2p_2}(g_{mr}) = \sum_{i=1}^{n_2} \frac{\partial g_{mi}}{\partial q_{2r}} p_{2i} \tag{5.51}$$

where $D^2_{2p_2}(g) \in \mathbb{R}^{n_1 \times n_2}$ $m = 1, \ldots, n_1$ indicates the row number of g matrix, q_{2r} is the elements of the vector $\boldsymbol{q}_2$, where r denotes the index of the particular configuration variables. Construction of the matrices that have been described in Eqs. (5.50) and (5.51) can also be explained with the help of the state model of Eq. (5.35).

$$\begin{aligned} D^2_2(g)\boldsymbol{p_2} &= \begin{bmatrix} \frac{\partial g_1}{\partial q_1}\left(f + [g_1 g_2]\begin{bmatrix} u_1 \\ u_2 \end{bmatrix}\right) + \frac{\partial g_1}{\partial q_{21}}u_1 + \frac{\partial g_1}{\partial q_{22}}u_2 \\ \frac{\partial g_2}{\partial q_1}\left(f + [g_1 g_2]\begin{bmatrix} u_1 \\ u_2 \end{bmatrix}\right) + \frac{\partial g_2}{\partial q_{21}}u_1 + \frac{\partial g_2}{\partial q_{22}}u_2 \end{bmatrix}^T \begin{bmatrix} p_{21} \\ p_{22} \end{bmatrix} \\ &= \left[\left(\frac{\partial g_1}{\partial q_1}p_{21} + \frac{\partial g_2}{\partial q_1}p_{22}\right)\left(f + [g_1 g_2]\begin{bmatrix} u_1 \\ u_2 \end{bmatrix}\right) + \left(\frac{\partial g_1}{\partial q_{21}}p_{21} + \frac{\partial g_2}{\partial q_{21}}p_{22}\right)u_1 + \left(\frac{\partial g_1}{\partial q_{22}}p_{21} + \frac{\partial g_2}{\partial q_{22}}p_{22}\right)u_2\right] \end{aligned} \tag{5.52}$$

Hence, with the above mentioned simplification technique, it is always possible to represent the time derivative of $\boldsymbol{z_2}$ in the following compact form as shown in Eq. (5.53)

$$\begin{aligned} \dot{\boldsymbol{z}}_2 &= \boldsymbol{u} + c_1(\boldsymbol{z_2} - c_1\boldsymbol{z_1} - \lambda\boldsymbol{\chi_1}) + \lambda\boldsymbol{z_1} \\ &\quad - K\left[\boldsymbol{f} + g\boldsymbol{u} + Df_{q_1}\boldsymbol{p_1} + Df_{q2}\boldsymbol{p_2} + Df_{p1}(\boldsymbol{f} + g\boldsymbol{u}) + Df_{p2}\boldsymbol{u}\right. \\ &\quad \left. - D(g)\boldsymbol{u} - D^2_1(g)\boldsymbol{p_2} - D^2_{2p_1}(g)\boldsymbol{f} - D^2_{2p_1}(g)g\boldsymbol{u} - D^2_{2p_2}(g)\boldsymbol{u}\right] \\ &= \psi\boldsymbol{u} + \lambda\boldsymbol{z_1} + c_1(\boldsymbol{z_2} - c_1\boldsymbol{z_1} - \lambda\boldsymbol{\chi_1}) + \boldsymbol{\Phi} \end{aligned} \tag{5.53}$$

where the expressions of $\psi \in \mathbb{R}^{n_2 \times n_2}$ and $\boldsymbol{\Phi} \in \mathbb{R}^{n_2}$ are shown in following equations:

$$\psi = \left[I - K\left(g + Df_{p1}g + Df_{p2} - D(g) - D^2_{2p_1}(g)g - D^2_{2p_2}(g)\right)\right] \tag{5.54}$$

and

$$\boldsymbol{\Phi} = -K\left[\boldsymbol{f} + Df_{q1}\boldsymbol{p_1} + Df_{q2}\boldsymbol{p_2} + Df_{p1}\boldsymbol{f} - D^2_1(g)\boldsymbol{p_2} - D^2_{2p1}(g)\boldsymbol{f}\right] \tag{5.55}$$

In Eq. (5.54), I denotes an identity matrix of order n_2. Similar to the case of 2-DOF UMS (described in previous Chap. 4), above three steps have transformed

the state model of an n-DOF underactuated system of (5.35) into the block-strict feedback form.

Step 4: The control law $\boldsymbol{u}$ has been designed to ensure the desired dynamics for $\boldsymbol{z_2}$. The desired dynamics of $\boldsymbol{z_2}$ has been expressed in Eq. (5.56) as following:

$$\dot{z}_2 = -z_1 - c_2 z_2 \tag{5.56}$$

where c_2 is an arbitrary positive design constant.

Consequently, from Eq. (5.53) and (5.56) the desired control input has been derived in the following manner: or,

$$\boldsymbol{u} = \psi^{-1}\left[-\left(1 - c_1^2 + \lambda\right)\boldsymbol{z_1} - (c_1 + c_2)\boldsymbol{z_2} + \lambda c_1 \boldsymbol{\chi_1} - \boldsymbol{\Phi}\right] \tag{5.57}$$

such choice of control input $\boldsymbol{u}$ has resulted in the following dynamics:

$$\begin{aligned} \dot{z}_1 &= z_2 - c_1 z_1 - \lambda \boldsymbol{\chi_1} \\ \dot{z}_2 &= -z_1 - c_2 z_2 \end{aligned} \tag{5.58}$$

The partial differential terms of the above Eq. (5.57) are shown below

$$Df_{q1} = \frac{c_y}{m}\left(\frac{\partial}{\partial x_3}(x_4 \tan x_2 - x_6)\right) = 0 \tag{5.59}$$

$$Df_{q2} = \frac{c_y}{m}\left[\frac{\partial}{\partial x_1}(x_4 \tan x_2 - x_6) \quad \frac{\partial}{\partial x_2}(x_4 \tan x_2 - x_6)\right] = \frac{c_y}{m}\left[0 \quad x_4 \sec^2 x_2\right] \tag{5.60}$$

$$Df_{p1} = \frac{c_y}{m}\left(\frac{\partial}{\partial x_6}(x_4 \tan x_2 - x_6)\right) = -\frac{c_y}{m} \tag{5.61}$$

$$Df_{p2} = \frac{c_y}{m}\left[\frac{\partial}{\partial x_4}(x_4 \tan x_2 - x_6) \quad \frac{\partial}{\partial x_5}(x_4 \tan x_2 - x_6)\right] = \frac{c_y}{m}\left[\tan x_2 \quad 0\right] \tag{5.62}$$

$$D^2_{2p1}(g) = \left[\frac{\partial \tan x_2}{\partial x_3} x_4 + \frac{\partial 0}{\partial x_3} x_5\right] = 0 \tag{5.63}$$

$$D^2_{2p2}(g) = \left[\frac{\partial \tan x_2}{\partial x_1} x_4 + \frac{\partial (0)}{\partial x_1} x_5 \quad \frac{\partial \tan x_2}{\partial x_2} x_4 + \frac{\partial (0)}{\partial x_2} x_5\right] = \left[0 \quad \sec^2 x_2 x_4\right] \tag{5.64}$$

As it has already been stated in Sect. 3.2.3, Eqs. (3.46.a)–(3.46.c) depict the zero dynamics structure for n degrees of freedom system. Consequently, in the special case of the USV $z_1 = 0\, and\, \dot{z}_1 = 0$ yield the following expression of q_2 and p_2.

$$z_1 = q_2 - K(q_1 + p_1 - gp_2) = 0 \Rightarrow q_2 = K(q_1 + p_1 - gp_2) \tag{5.65.a}$$

$$\dot{z}_1 = p_2 - K(p_1 + f - D(g)p_2) = 0 \Rightarrow p_2 = K(p_1 + f - D(g)p_2) \tag{5.65.b}$$

$$\ddot{z}_1 = \psi u + \Phi = 0 \Rightarrow u = \psi^{-1}\Phi \tag{5.65.c}$$

Now, if the q_2 and p_2 terms of f, ψ, and Φ have been replaced by the expressions of (5.65.a) and (5.65.b), respectively, then the equations of zero dynamics for the USV has taken the following form:

$$\begin{aligned} \dot{q}_1 &= p_1 \\ \dot{p}_1 &= f(q_1, p_1) - g(q_1, p_1)\psi^{-1}(q_1, p_1)\Phi(q_1, p_1) \end{aligned} \tag{5.66}$$

In Eq. (5.66), $f(q_1, p_1), g(q_1, p_1), \psi^{-1}(q_1, p_1)$ and $\varphi(q_1, p_1)$ represent the same functions f, g, ψ^{-1}, and φ, with the only difference being that the last equation, all the q_2 and p_2 terms have been replaced by the expression (5.65.a) and (5.65.b), respectively. Constant k has been selected in such a manner that it would ensure the stability of the zero dynamics system. Following Lyapunov function has been defined to analyze stability of the internal dynamics of Eq. (5.67)

$$V_z = \frac{1}{2}q_1^2 + \frac{1}{2}p_1^2 \tag{5.67}$$

Now, time derivative of the above Lyapunov function V_z has resulted in

$$\dot{V}_z = q_1 p_1 + p_1 F \tag{5.68}$$

Now, the controller parameter k has been selected in a judicial manner to ensure the negative definiteness of the $\dot{V}_z$. The other three controller parameters do not alter the negative definiteness of $\dot{V}_z$. However, they have been chosen in a manner so that they can satisfy the condition $c_1 > 0$, $c_2 > 0$ and $\lambda > 0$. (Detailed criteria of controller parameter selection have been discussed in Chap. 3, Sect. 3.2.3).

5.2.2 *Simulation Results and Performance Analysis*

Effectiveness of the proposed control law has been verified after simulating the closed-loop system in Matlab® (version: 7.14) Simulink (version: 7.9) environment. During simulation study the parameters of Table 5.3 have been used to construct the model of USV in simulation environment. Parameters of the controller are listed in Table 5.4. Initial values of the state variables that have been chosen for the simulation experiment are as follows: $q_1 = 0.8, q_2 = [-0.19 \quad \pi/2], p_1 = 0.1$ and $p_2 = [1.6 \quad \pi/2]$

Table 5.3 Parameters of the USV (SI unit)

m_x	m_y	I	c_x	c_y	c_z
200	200	80	70	100	50

Table 5.4 Parameters of the proposed

c_1	c_2	λ	K
5	5	0.01	$[1.15 \quad 0]^T$

Block backstepping controller

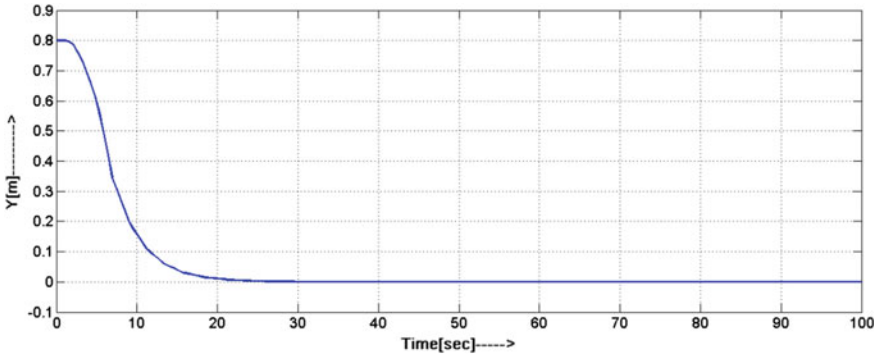

Fig. 5.11 Lateral displacement of the USV

Likewise the previous case of VTOL, here also authors follow the same representation style of demonstrating the time variation of unactuated state variable y at first in Fig. 5.11, while the time variation of another unactuated state variable $\dot{y}$ is shown in Fig. 5.12.

It can be inferred from the above Figs. 5.11 and 5.12 that the proposed control law can ensure the global asymptotic stabilization of the state variable q_1 (i.e., lateral displacement), and p_1 (i.e., lateral velocity). Convergence of the state variables, q_1 and p_1, have corroborated the fact that the asymptotic stability of the zero dynamics ensures the asymptotic convergence of q_1 and p_1 at their desired equilibrium.

Similar to the previous case of VTOL, after demonstrating unactuated variables, time variation of actuated variables are presented in Figs. 5.13, 5.14, 5.15 and 5.16. Figure 5.13 shows the variation of state variable x with time, whereas the time variation of the state variable $\dot{x}$ has been shown in Fig. 5.14. Figure 5.15 shows the

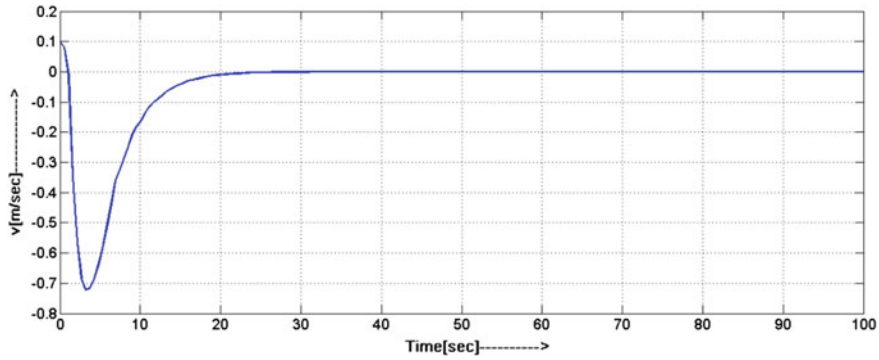

Fig. 5.12 Lateral velocity of the USV

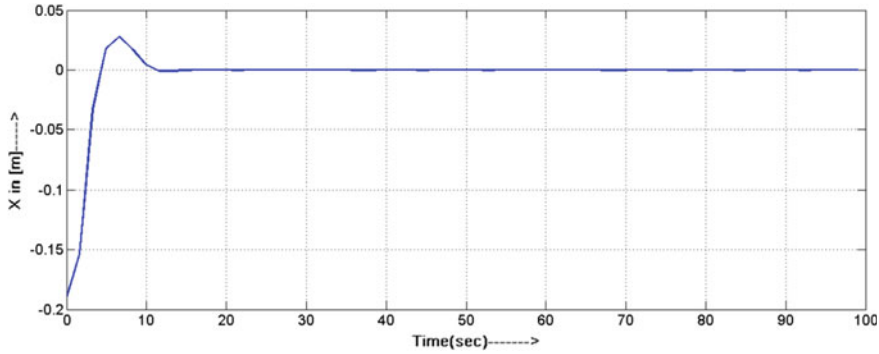

Fig. 5.13 Longitudinal displacement of the USV

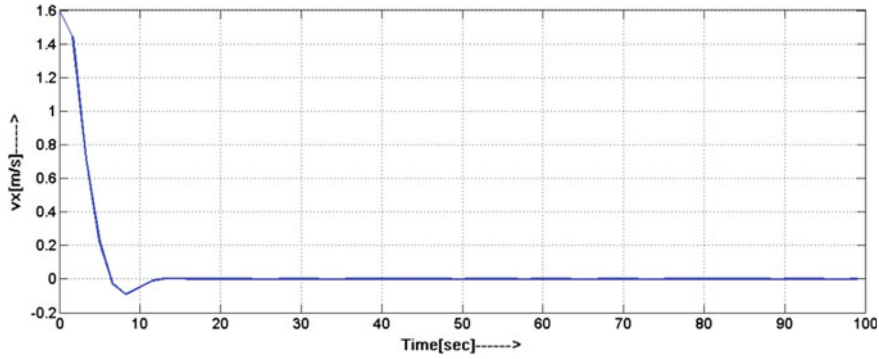

Fig. 5.14 Longitudinal velocity of the USV

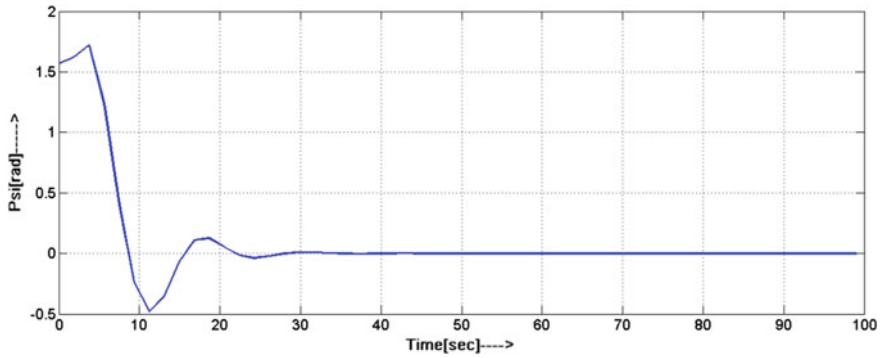

Fig. 5.15 Angular displacement of the USV

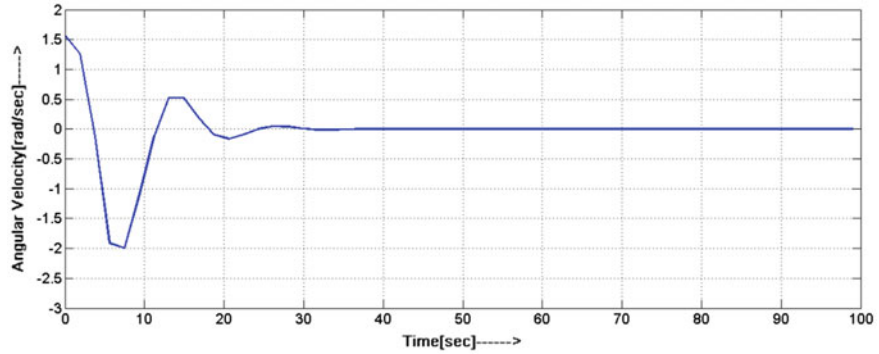

Fig. 5.16 Angular velocity of the USV

variation of state variable θ with time, while the time variation of the state variable $\dot{\theta}$ is shown in Fig. 5.16.

Figures 5.11 and 5.12 corroborate the fact that the asymptotic stability of zero dynamics (described by Eq. (5.65)) of the closed-loop system yields the convergence of the state variables q_1 and p_1 to their desired equilibrium. Convergences of the actuated variables have already been shown in Figs. 5.13, 5.14, 5.15 and 5.16. Therefore, it can be inferred that the above control inputs u_1 and u_2 can ensure the asymptotic stabilization of the actuated state variables. Proposition of theorem 2 (Chap. 3, Sect. 3.4), which states the global asymptotic stability of the reduced order system together with the global asymptotic stability of the internal dynamics ensures asymptotic stabilization of the actuated shape variables, have been cor-

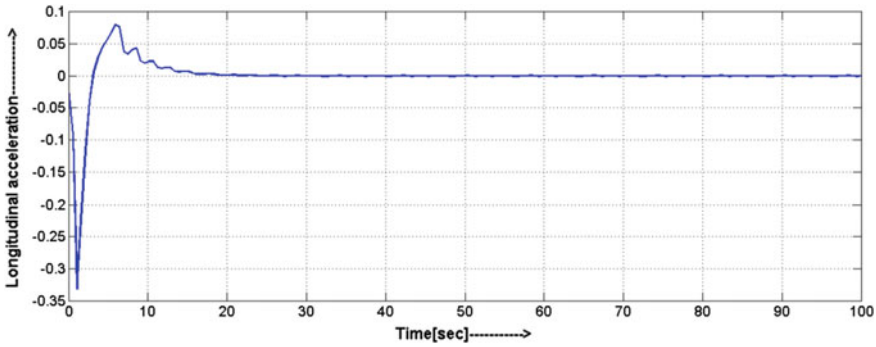

Fig. 5.17 Control input applied to USV (longitudinal acceleration)

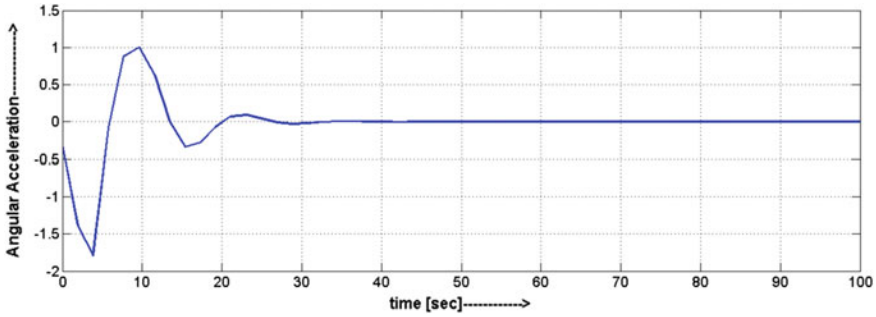

Fig. 5.18 Control input applied to USV (angular acceleration)

roborated by the stabilization of the actuated state variables. Hence, it is quite clear from the above simulation studies that the proposed controller is able to ensure the global asymptotic stability of the USV system.

Being a nonholonomic system USV fails to satisfy the Brockets' condition of feedback linearization [19, 20]. Therefore, it requires nonsmooth control input for its stabilization. Figure 5.17 shows the longitudinal acceleration input, and Fig. 5.18 shows the angular acceleration input. Figures of 5.17 and 5.18 reveal the fact that the proposed control law has generated a nonsmooth control input for the stabilization of USV system. However, as stated before without demonstrating application of the control law on a robotic system this chapter would not take its complete shape, in the next section a 3-DOF manipulator example is considered.

5.3 Application on Three Degree of Freedom Redundant Manipulator

A planar 3-DOF robot arm is a particular type of robot manipulator with two prismatic and one revolute joint, moving on a horizontal plane. The two prismatic joints are rigid, whereas the revolute joint is coupled to the end-effectors through an elastic degree of freedom. In addition, all the prismatic joints are actuated [5].

An idealized model of this manipulator is shown in Fig. 5.19. The model consists of a base body, which can translate and rotate freely in the plane, and a mass-less arm at the tip of which the end effector is attached [5]. The base body is connected to the mass-less arm by a linear torsional spring whose neutral position is $\varphi = 0$ [28]. The Cartesian position of the base body as well as the angle through which the base body is rotated can be controlled [28]. The variable φ measures the deviation of the mass-less arm from the assigned (φ = 0) value [28]. Whenever the variable is displaced from zero, it induces a restoring torque $-K\varphi$, where K denotes the torsional spring constant. The state model of 3-DOF manipulator is shown in following Eq. (5.69). The following state variables are chosen to represent the dynamics of 3-DOF manipulator: $x_1 = x, x_2 = \theta$, $x_3 = y, x_4 = v_x$, $x_5 = \omega, x_6 = v_y$

$$\begin{aligned}
\dot{x}_1 &= x_4 \\
\dot{x}_2 &= x_5 \\
\dot{x}_3 &= x_6 \\
\dot{x}_4 &= u_1 \\
\dot{x}_5 &= u_2 \\
\dot{x}_6 &= u_1 \tan x_2
\end{aligned} \tag{5.69}$$

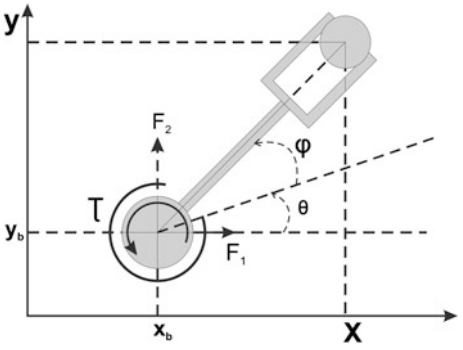

Fig. 5.19 Schematic diagram of the three degree of freedom redundant manipulator

Salient Control Features of 3 DOF Redundant Planar Robot: *Actuated Shape variable, interacting input configuration, 2nd order nonholonomic system.*

Control Objective: *Stabilize the robot arm at a desired configuration.*

Please note that 3-DOF system possesses interacting control inputs, as well as it belongs to the class of nonholonomic systems. Therefore, it is easy to understand that designing a control law for the same is a more difficult job than the previous demonstration.

The state model of Eq. (5.69) can be represented as higher order UMS as shown below:

$$\begin{aligned} q_1 &= x_3 \\ p_1 &= x_6 \\ q_2 &= [x_1 \quad x_2]^T \\ p_2 &= [x_4 \quad x_5]^T \end{aligned} \tag{5.70.a}$$

and,

$$\begin{aligned} \dot{q}_1 &= p_1 \\ \dot{q}_2 &= p_2 \\ \dot{p}_1 &= f + gu \\ \dot{p}_2 &= u \end{aligned} \tag{5.70.b}$$

where,

$$f = 0 \tag{5.70.c}$$

$$g = [\tan x_2 \quad 0] \tag{5.70.d}$$

5.3.1 Derivation of the Control Law for 3-DOF Robotic Manipulator

Step 1: Following the design procedure of Sect. 3.2.2, a new control variable $z_1 \in \mathbb{R}^2$ has been defined according to Eq. (3.22). The new control variable is shown in Eq. (5.71) below:

$$z_1 = q_2 - K(q_1 + p_1 - gp_2) \tag{5.71}$$

where, $K \in \mathbb{R}^{2\times 1}$ is a constant matrix such that $K = [k \quad 0]$. In the above equation, $g(q)$ is represented by g.

Similar to the previous design case, time derivative of z_1 has been computed as shown in the following Eq. (5.72):

$$\dot{z}_1 = p_2 - K(p_1 + f - D(g)p_2) \tag{5.72}$$

In above representation $D(g) \in \mathbb{R}^{1\times 2}$ represents the time differentiation of matrix $g(q)$, where any element of $D(g)$ can be expressed as $D(g_{ij}) = \sum_{k=1}^{n} \frac{\partial g_{ij}}{\partial q_k} p_k$, where i and j indicate the position of the elements of $D(g)$ matrix. (Please note that $g \in \mathbb{R}^{1\times 2}$). Therefore, construction of $D(g)$ matrix can be simply explained with the following Eq. (5.73):

$$D(g) = \begin{bmatrix} \frac{\partial g_1}{\partial q_1} p_1 + \frac{\partial g_1}{\partial q_{21}} p_{21} + \frac{\partial g_1}{\partial q_{22}} p_{22} & \frac{\partial g_2}{\partial q_1} p_1 + \frac{\partial g_2}{\partial q_{21}} p_{21} + \frac{\partial g_2}{\partial q_{22}} p_{22} \end{bmatrix} \tag{5.73}$$

Further simplification has resulted in

$$D(g) = \begin{bmatrix} \sum_{k=1}^{3} \frac{\partial \tan x_2}{\partial q_k} p_k & 0 \end{bmatrix} = \begin{bmatrix} \sec^2 x_2 x_5 & 0 \end{bmatrix} \tag{5.74}$$

Step 2: The stabilizing function has been defined in accordance with Eq. (3.27) to ensure the desired dynamic behavior of z_1. Expression of the stabilizing function has been shown in Eq. (5.75)

$$\alpha = -c_1 z_1 - \lambda \chi_1 + K(p_1 + f - D(g)p_2) \tag{5.75}$$

Step 3: Following Eq. (3.28), the second error variable $z_2 \in \mathbb{R}^2$ has been defined that is shown in Eq. (5.76) below

$$z_2 = p_2 - \alpha \tag{5.76}$$

with the above definition of second control variable, the dynamics of first error variable has become

$$\dot{z}_1 = z_2 - c_1 z_1 - \lambda \chi_1 \tag{5.77}$$

Consequently, time derivative of the second error variable z_2 can be expressed as shown in Eq. (5.78) below

$$\begin{aligned}\dot{\boldsymbol{z}}_{\boldsymbol{2}} &= \dot{\boldsymbol{p}}_{\boldsymbol{2}} - \dot{\boldsymbol{\alpha}} \\ &= \boldsymbol{u} + c_1(\boldsymbol{z}_{\boldsymbol{2}} - c_1\boldsymbol{z}_{\boldsymbol{1}} - \lambda\boldsymbol{\chi}_{\boldsymbol{1}}) + \lambda\boldsymbol{z}_{\boldsymbol{1}} \\ &\quad - K\left[\boldsymbol{f} + g\boldsymbol{u} + Df_{q1}\boldsymbol{p}_{\boldsymbol{1}} + Df_{q2}\boldsymbol{p}_{\boldsymbol{2}} + Df_{p1}(\boldsymbol{f} + g\boldsymbol{u})\right. \\ &\quad \left. + Df_{p2}\boldsymbol{u} - D(g)\boldsymbol{u} - D^2(g)\boldsymbol{p}_{\boldsymbol{2}}\right]\end{aligned} \tag{5.78}$$

In Eq. (5.78), $Df_{q1} \in \mathbb{R}^{1\times1}$, $Df_{q2} \in \mathbb{R}^{1\times2}$, $Df_{p1} \in \mathbb{R}^{1\times1}$ and $Df_{p2} \in \mathbb{R}^{1\times2}$ represent the matrices of partial derivatives of $\boldsymbol{f}$ vector with respect to different sub-component of state vector such as $\boldsymbol{q_1}$, $\boldsymbol{q_2}$, $\boldsymbol{p_1}$ and $\boldsymbol{p_2}$ as shown below:

$$Df_{q1} = \frac{\partial f}{\partial q_1} \tag{5.79.a}$$

$$Df_{q2} = \begin{bmatrix}\frac{\partial f}{\partial q_{21}} & \frac{\partial f}{\partial q_{22}}\end{bmatrix} \tag{5.79.b}$$

$$Df_{p1} = \frac{\partial f}{\partial p_1} \tag{5.79.c}$$

$$Df_{p2} = \begin{bmatrix}\frac{\partial f}{\partial p_{21}} & \frac{\partial f}{\partial p_{22}}\end{bmatrix} \tag{5.79.d}$$

$D_2(g) \in \mathbb{R}^{n_1\times n_2}$ is given by $D^2(g) = \left[D_1^2(g) + D_2^2(g)\right]$. The definition of $D_1^2(g)$ and $D_2^2(g)$ are shown in the following equations:

$$D_1^2(g_{ij}) = \sum_{l=1}^{n}\sum_{k=1}^{n}\frac{\partial^2 g_{ij}}{\partial q_k \partial q_l}p_k p_l \tag{5.80}$$

$$D_2^2(g_{ij}) = \sum_{k=1}^{n}\frac{\partial g_{ij}}{\partial q_k}\dot{p}_k \tag{5.81}$$

In the above expression, p_k and p_l represent the individual elements of $\boldsymbol{p}$ vector. similar to the previous case, one can represent the structure of $D_1^2(g)$ and $D_2^2(g)$ matrix as shown in the following equation series (5.82.a, 5.82.b):

$$D_1^2(g) = \begin{bmatrix}\frac{\partial^2 g_1}{\partial q_1^2}p_1^2 + \frac{\partial^2 g_1}{\partial q_{21}^2}p_{21}^2 + \frac{\partial^2 g_1}{\partial q_2^2}p_{22}^2 + 2\frac{\partial^2 g_1}{\partial q_{21}q_1}p_1p_{21} + 2\frac{\partial^2 g_1}{\partial q_{22}q_1}p_1p_{22} + 2\frac{\partial^2 g_1}{\partial q_{21}q_{22}}p_{22}p_{21} \\ \frac{\partial^2 g_2}{\partial q_1^2}p_1^2 + \frac{\partial^2 g_2}{\partial q_{21}^2}p_{21}^2 + \frac{\partial^2 g_2}{\partial q_2^2}p_{22}^2 + 2\frac{\partial^2 g_2}{\partial q_{21}q_1}p_1p_{21} + 2\frac{\partial^2 g_2}{\partial q_{22}q_1}p_1p_{22} + 2\frac{\partial^2 g_2}{\partial q_{21}q_{22}}p_{22}p_{21}\end{bmatrix}^T \tag{5.82.a}$$

$$D_2^2(g) = \begin{bmatrix}\frac{\partial g_1}{\partial q_1}\dot{p}_1 + \frac{\partial g_1}{\partial q_{21}}\dot{p}_{21} + \frac{\partial g_1}{\partial q_{22}}\dot{p}_{22} & \frac{\partial g_2}{\partial q_1}\dot{p}_1 + \frac{\partial g_2}{\partial q_{21}}\dot{p}_{21} + \frac{\partial g_2}{\partial q_{22}}\dot{p}_{22}\end{bmatrix} \tag{5.82.b}$$

However, from the structure of $D_2^2(g)$ matrix it can be easily inferred that $D_2^2(g)\boldsymbol{p_2}$ can be further partitioned into three parts as shown in the following equation:

$$D_2^2(g)\boldsymbol{p_2} = D_{2\boldsymbol{p_1}}^2(g)\boldsymbol{f} + D_{2\boldsymbol{p_1}}^2(g)g\boldsymbol{u} + D_{2\boldsymbol{p_2}}^2(g)\boldsymbol{u} \tag{5.83}$$

where the elements of each components are:

$$D_{2p_1}^2(g_{mr}) = \sum_{i=1}^{n_2} \frac{\partial g_{mi}}{\partial q_{1r}} p_{2i} \tag{5.84}$$

where $D_{2p_1}^2(g) \in \mathbb{R}^{n_1 \times n_1}$ and $m = 1, \ldots, n_1$ indicates the row index of g matrix, q_{1r} is the elements of the vector $\boldsymbol{q}_1$, where r denotes the index of the particular configuration variables and p_{2i} denotes element of $\boldsymbol{p}_2$ vector.

$$D_{2p_2}^2(g_{mr}) = \sum_{i=1}^{n_2} \frac{\partial g_{mi}}{\partial q_{2r}} p_{2i} \tag{5.85}$$

where $D_{2p_2}^2(g) \in \mathbb{R}^{n_1 \times n_2}$ $m = 1, \ldots, n_1$ indicates the row number of g matrix, q_{2r} is the elements of the vector $\boldsymbol{q}_2$, where r denotes the index of the particular configuration variables. Construction of the matrices that have been described in Eqs. (5.84) and (5.85) can also be explained with the help of the state model Eqs. (5.70.a–5.70.d).

$$\begin{aligned} D_2^2(g)\boldsymbol{p_2} &= \begin{bmatrix} \frac{\partial g_1}{\partial q_1}\left(f + [g_1 g_2]\begin{bmatrix} u_1 \\ u_2 \end{bmatrix}\right) + \frac{\partial g_1}{\partial q_{21}}u_1 + \frac{\partial g_1}{\partial q_{22}}u_2 \\ \frac{\partial g_2}{\partial q_1}\left(f + [g_1 g_2]\begin{bmatrix} u_1 \\ u_2 \end{bmatrix}\right) + \frac{\partial g_2}{\partial q_{21}}u_1 + \frac{\partial g_2}{\partial q_{22}}u_2 \end{bmatrix}^T \begin{bmatrix} p_{21} \\ p_{22} \end{bmatrix} \\ &= \left[\left(\frac{\partial g_1}{\partial q_1}p_{21} + \frac{\partial g_2}{\partial q_1}p_{22}\right)\left(f + [g_1 g_2]\begin{bmatrix} u_1 \\ u_2 \end{bmatrix}\right) + \left(\frac{\partial g_1}{\partial q_{21}}p_{21} + \frac{\partial g_2}{\partial q_{21}}p_{22}\right)u_1 + \left(\frac{\partial g_1}{\partial q_{22}}p_{21} + \frac{\partial g_2}{\partial q_{22}}p_{22}\right)u_2\right] \end{aligned} \tag{5.86}$$

Hence, with the above-mentioned simplification technique, it is always possible to represent the time derivative of $\boldsymbol{z_2}$ in the following compact form as shown in Eq. (5.87)

$$\begin{aligned} \dot{\boldsymbol{z}}_2 &= \boldsymbol{u} + c_1(\boldsymbol{z_2} - c_1\boldsymbol{z_1} - \lambda\boldsymbol{\chi_1}) + \lambda\boldsymbol{z_1} \\ &\quad - K\big[\boldsymbol{f} + g\boldsymbol{u} + Df_{q1}\boldsymbol{p_1} + Df_{q2}\boldsymbol{p_2} + Df_{p1}(\boldsymbol{f} + g\boldsymbol{u}) + Df_{p2}\boldsymbol{u} \\ &\quad - D(g)\boldsymbol{u} - D_1^2(g)\boldsymbol{p_2} - D_{2p_1}^2(g)\boldsymbol{f} - D_{2p_1}^2(g)g\boldsymbol{u} - D_{2p_2}^2(g)\boldsymbol{u}\big] \\ &= \psi\boldsymbol{u} + \lambda\boldsymbol{z_1} + c_1(\boldsymbol{z_2} - c_1\boldsymbol{z_1} - \lambda\boldsymbol{\chi_1}) + \boldsymbol{\Phi} \end{aligned} \tag{5.87}$$

where the expressions of $\psi \in \mathbb{R}^{n_2 \times n_2}$ and $\boldsymbol{\Phi} \in \mathbb{R}^{n_2}$ are shown in following equations:

$$\psi = \left[I - K\left(g + Df_{p1} g + Df_{p2} - D(g) - D^2_{2p_1}(g) g - D^2_{2p_2}(g) \right) \right] \tag{5.88}$$

and

$$\boldsymbol{\Phi} = -K\left[\boldsymbol{f} + Df_{q1} \boldsymbol{p_1} + Df_{q2} \boldsymbol{p_2} + Df_{p1} \boldsymbol{f} - D^2_1(g) \boldsymbol{p_2} - D^2_{2p1}(g) \boldsymbol{f} \right] \tag{5.89}$$

In Eq. (5.88), I denotes an identity matrix of order n_2. Similar to the case of 2-DOF UMS (described in previous Chap. 4), above three steps have transformed the state model of an n-DOF underactuated system of (5.89) into the block-strict feedback form.

Step 4: The control law $\boldsymbol{u}$ has been designed to ensure the desired dynamics for $\boldsymbol{z_2}$. The desired dynamics of $\boldsymbol{z_2}$ has been expressed in Eq. (5.90) as following:

$$\dot{z}_2 = -z_1 - c_2 z_2 \tag{5.90}$$

where c_2 is an arbitrary positive design constant.

Consequently, from Eq. (5.87) and (5.90) the desired control input has been derived in the following manner: or,

$$\boldsymbol{u} = \psi^{-1}\left[-\left(1 - c_1^2 + \lambda\right) \boldsymbol{z_1} - (c_1 + c_2) \boldsymbol{z_2} + \lambda c_1 \boldsymbol{\chi_I} - \boldsymbol{\Phi} \right] \tag{5.91}$$

such choice of control input $\boldsymbol{u}$ has resulted in the following dynamics:

$$\begin{aligned} \dot{z}_1 &= z_2 - c_1 z_1 - \lambda \boldsymbol{\chi_1} \\ \dot{z}_2 &= -z_1 - c_2 z_2 \end{aligned} \tag{5.92}$$

The partial differential terms of the above Eq. (5.57) are shown below

$$Df_{q1} = 0 \tag{5.93}$$

$$Df_{q2} = 0 \tag{5.94}$$

$$Df_{p1} = 0 \tag{5.95}$$

$$Df_{p2} = 0 \tag{5.96}$$

$$D^2_{2p1}(g) = \left[\frac{\partial \tan x_2}{\partial x_3} x_4 + \frac{\partial 0}{\partial x_3} x_5 \right] = 0 \tag{5.97}$$

$$D_{2p2}^{2}(g)=\left[\frac{\partial \tan x_2}{\partial x_1}x_4+\frac{\partial(0)}{\partial x_1}x_5 \quad \frac{\partial \tan x_2}{\partial x_2}x_4+\frac{\partial(0)}{\partial x_2}x_5\right]=\begin{bmatrix}0 & \sec^2 x_2 x_4\end{bmatrix} \tag{5.98}$$

As it has already been stated in Sect. 3.2.3, Eqs. (3.46.a)–(3.46.c) depict the zero dynamics structure for an n degrees of freedom system. Consequently, in the special case of the manipulator $z_1 = 0 \, and \, \dot{z}_1 = 0$ has yielded the following expression of q_2 and p_2.

$$\boldsymbol{z_1} = \boldsymbol{q_2} - K(q_1 + p_1 - g\boldsymbol{p_2}) = 0 \Rightarrow \boldsymbol{q_2} = K(q_1 + p_1 - g\boldsymbol{p_2}) \tag{5.99.a}$$

$$\dot{\boldsymbol{z}}_{\boldsymbol{1}} = \boldsymbol{p_2} - K(p_1 + f - D(g)\boldsymbol{p_2}) = 0 \Rightarrow \boldsymbol{p_2} = K(p_1 + f - D(g)\boldsymbol{p_2}) \tag{5.99.b}$$

$$\ddot{\boldsymbol{z}}_{\boldsymbol{1}} = \psi \boldsymbol{u} + \boldsymbol{\Phi} = \boldsymbol{0} \Rightarrow \boldsymbol{u} = \psi^{-1}\boldsymbol{\Phi} \tag{5.99.c}$$

Now, the q_2 and p_2 terms of f, ψ, and Φ have been replaced by the expressions of (5.99.a) and (5.99.b), respectively, then the equations of zero dynamics for the USV will take the following form:

$$\begin{aligned}\dot{q}_1 &= p_1 \\ \dot{p}_1 &= f(q_1, p_1) - g(q_1, p_1)\psi^{-1}(q_1, p_1)\Phi(q_1, p_1)\end{aligned} \tag{5.100}$$

In Eq. (5.100), $f(q_1, p_1), g(q_1, p_1), \psi^{-1}(q_1, p_1)$ and $\varphi(q_1, p_1)$ represent the same functions f, g, ψ^{-1}, and φ, with the only difference being that the last equation, all the q_2 and p_2 terms have been replaced by the expression of (5.99.a) and (5.99.b), respectively. Constant k has to be selected in such a manner that it would ensure the stability of the zero dynamics system. Following Lyapunov function has been defined to analyze stability of the internal dynamics of Eq. (5.101)

$$V_z = \frac{1}{2}q_1^2 + \frac{1}{2}p_1^2 \tag{5.101}$$

Now, time derivative of the above Lyapunov function V_z has resulted in:

$$\dot{V}_z = q_1 p_1 + p_1 F \tag{5.102}$$

Now, the controller parameter k has to be selected in a judicial manner to ensure the negative definiteness of the $\dot{V}_z$. The other three controller parameters do not alter the negative definiteness of $\dot{V}_z$. However, they have been chosen in a manner so that they could satisfy the condition $c_1 > 0$, $c_2 > 0$ and $\lambda > 0$. (Detailed criteria of controller parameter selection have been discussed in Chap. 3, Sect. 3.2.3).

5.3.2 Simulation Results and Performance Analysis

Effectiveness of the proposed control law has been verified after simulating the closed-loop system in MATLAB® (version: 7.14) Simulink (version: 7.9) environment. Initial value of the state variables are chosen for simulation experiment is as following: $q_1 = 0.755, q_2 = [1 \quad \pi/4], p_1 = 0.5$ and $p_2 = [0.5 \quad 0]$

Figure 5.20 shows the variation of state variable y with time, whereas the time variation of the state variable $\dot{y}$ (the time derivative of y) is shown in Fig. 5.21. Similarly, Fig. 5.22 shows the time variation of state variable x, while the time variation of the state variable $\dot{x}$ (the time derivative of x) is shown in Fig. 5.23. Figure 5.24 shows the variation of state variable θ with time, and the time variation of the state variable $\dot{\theta}$ (the time derivative of θ) is shown in Fig. 5.25 (The parameter of the robot is not appearing into the state model description. Therefore, for the sake of simplicity, the authors have assumed values of all the parameters are equal to one (Table 5.5).

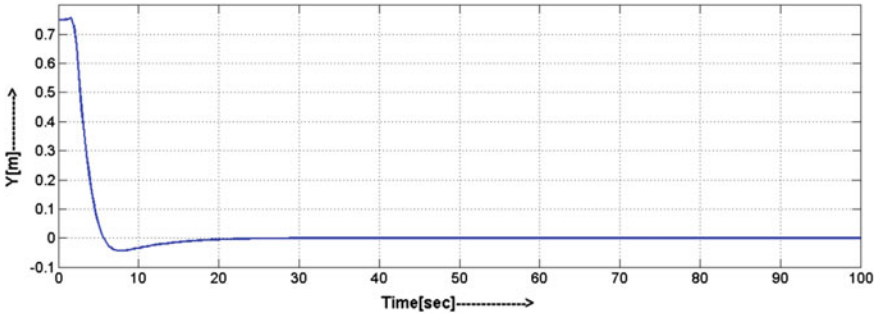

Fig. 5.20 Variation of the state variable y with time

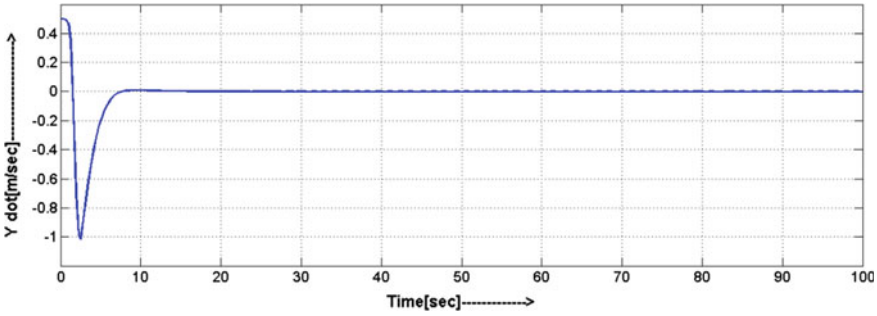

Fig. 5.21 Variation of the state variable $\dot{y}$ with time

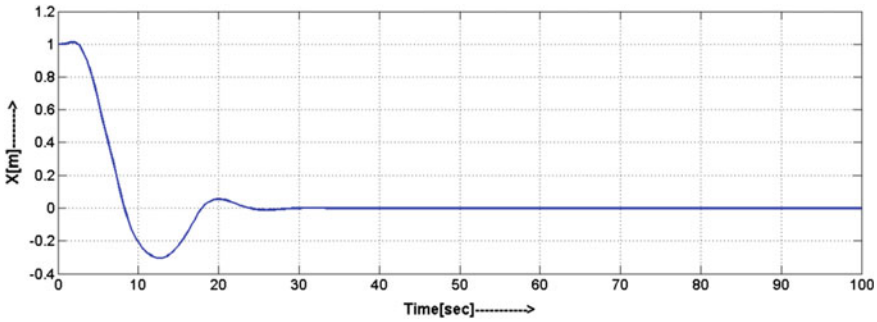

Fig. 5.22 Variation of state variable x with time

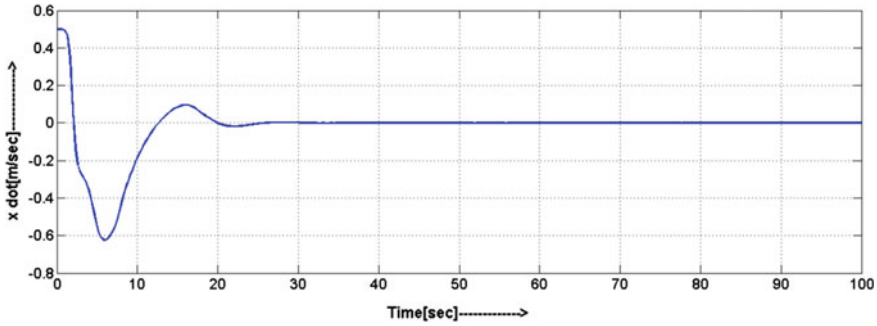

Fig. 5.23 Variation of state variable $\dot{x}$ with time

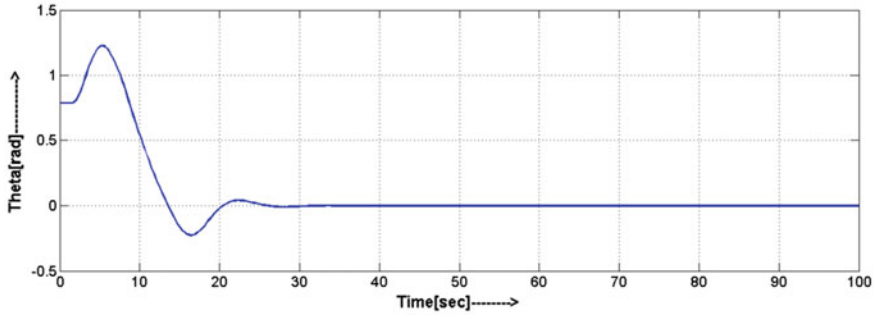

Fig. 5.24 Variation of state variable θ with time

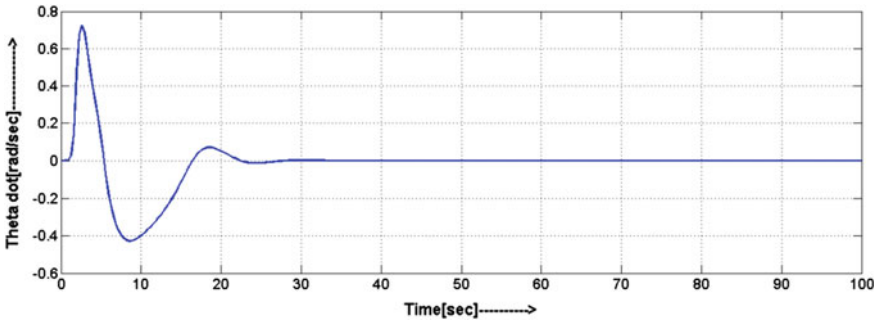

Fig. 5.25 Variation of state variable $\dot{\theta}$ with time

Table 5.5 Parameters of the proposed Block backstepping controller

c_1	c_2	λ	K
10	10	0.01	$[0.57 \quad 0]^T$

Figures 5.20 and 5.21 corroborate the fact that the asymptotic stability of zero dynamics (described by Eq. (5.100)) of the closed-loop system yields the convergence of the state variables q_1 and p_1 to their desired equilibrium. Convergences of the actuated variables are shown in Figs. 5.22, 5.23, 5.24 and 5.25. Hence, it is quite clear from the above simulation studies that the proposed controller is able to ensure the global asymptotic stability of the 3-DOF redundant manipulator system. Proposition of theorem 2 (Chap. 3, Sect. 3.4), which states the global asymptotic stability of the reduced order system together with the global asymptotic stability of the internal dynamics ensures asymptotic stabilization of the actuated shape variables, has been corroborated by the stabilization of the actuated state variables.

Figure 5.26 shows the variation of control input u_1, and Fig. 5.27 shows the control input u_2. Figures 5.26 and 5.27 reveal the fact that the proposed control law

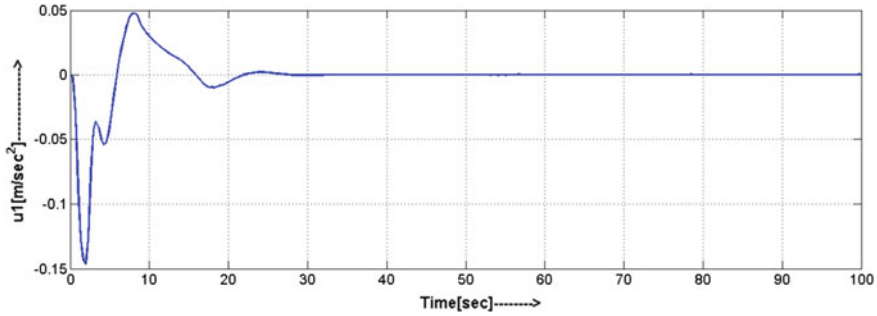

Fig. 5.26 Control input u_1

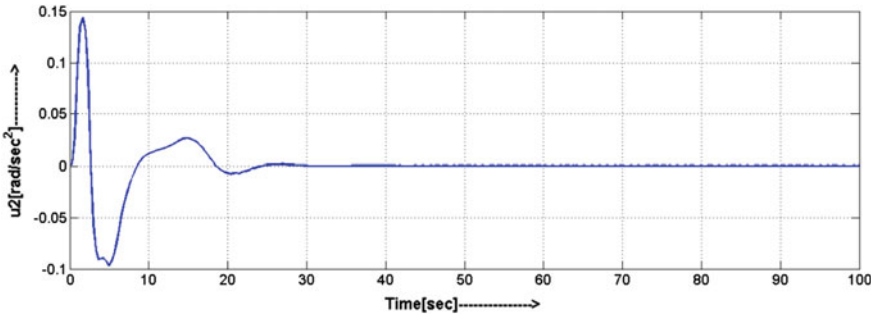

Fig. 5.27 Control input u_2

is capable of generating adequate control action to stabilize the configuration variables of a nonholonomic system with 2nd-order nonholonomic constraint. Unlike USV, 3-DOF redundant manipulator possesses interacting control inputs. Indeed, the proposed algorithm is so generalized that it can address the control problem of 3-DOF system without any significant modifications.

5.4 Notes

This chapter demonstrates the detailed implementation of proposed control law on three different higher-order UMSs, namely VTOL, USV, 3-DOF manipulator. Although VTOL belongs to the family of flat UMSs, yet interacting control input makes the control law design quite complicated. On the other hand, USV system possesses two noninteracting inputs, but it falls within the class of nonholonomic systems, and thereby it has got its own set of motion constraints. Finally, in case of 3-DOF robotic manipulator, it is a nonholonomic system, and also possesses interacting control inputs. Therefore, it is easy to understand that design a control law for the 3-DOF redundant manipulator is always a more complicated problem than the previous two cases. Indeed, extensive simulation studies, which have been carried out on three different systems, have substantiated the fact that proposed control law can effectively address the control problems of the higher order UMSs without any significant modifications. Another noteworthy feature of the control algorithm is that the proposed control law automatically modifies itself according to the dynamics of the system. Hence, in a nutshell, it can be concluded that the proposed control law is versatile enough to stabilize the control problem of any higher order UMS. Authors are quite confident about the fact that after going through this chapter, the readers will definitely be able to design control law for the same class of systems.

References

1. Abdessameuda A, Tayebi A (2010) Global trajectory tracking control of VTOL-UAVs without linear velocity measurements. Automatica 46(6):1053–1059
2. Al-Hiddabi SA, McClamroch NH (2002) Tracking and maneuver regulation control for nonlinear non-minimum phase systems: application to flight control. IEEE Trans Control Syst Technol 10(6):780–792
3. Consolini L, Maggiore M, Nielsen C, Tosques M (2010) Path following for the PVTOL aircraft. Automatica 46(8):1284–1296
4. Consolini L, Tosques M (2007) On the VTOL exact tracking with bounded internal dynamics via a Poincare map approach. IEEE Trans Autom Control 52(9):1757–1762
5. De Luca RMA, Iannitti S, Oriolo G (2001) Control problems in underactuated manipulators Paper presented at IEEE/ASME international conference on advanced intelligent mechatronics, Como, Italy, pp 8–12
6. Gruszka A, Malisoff, M, Mazenc F (2011) On tracking for the PVTOL model with bounded feedbacks. Paper presented at American control conference, San Francisco, CA, USA, pp 1428–1433
7. Hauser J, Sastry S, Meyer G (1992) Nonlinear control design for slightly non-minimum phase systems. Automatica 28(4):665–679
8. Lin F, Zhang W, Brandt RD (1999) Robust hovering control of a PVTOL aircraft. IEEE Trans Control Syst Technol 7(3):343–351
9. Lozano R, Castillo P, Dzul A (2004) Global stabilization of the PVTOL: real-time application to a mini-aircraft. Int J Control 77(8):735–740
10. Yu R, Zhu Q, Xia G, Liu Z (2012) Sliding mode tracking control of an underactuated surface vessel. IET Control Theory Appl 6(3):461–466
11. Do KD, Jiang ZP, Pan j (2003) On global tracking control of a VTOL aircraft without velocity measurements. IEEE Trans Autom Control 48(12):2212–2217
12. Marconi L, Isidori A, Serrani A (2002) Autonomous vertical landing on an oscillating platform: an internal-model based approach. Automatica 38(1):21–32
13. Martin P, Devasia S, Paden B (1996) A different look at output tracking: control of a VTOL aircraft. Automatica 32(1):101–107
14. Notarstefano G, Hauser J, Frezza R (2005) Trajectory manifold exploration for the PVTOL aircraft. Paper presented at IEEE conference on decision and control and European control conference, Seville, Spain, pp 5848–5853
15. Olfati-Saber R (2002) Global configuration stabilization for the VTOL aircraft with strong input coupling. IEEE Trans Autom Control 47(11):1949–1952
16. Setlur P, Dawson D, Fang Y, Costic B (2001) Nonlinear tracking control of the VTOL aircraft. Paper presented at the international conference on decision and control, Orlando, USA, pp 4592–4597
17. Wood R, Cazzolato B (2007) An alternative nonlinear control law for the global stabilization of the PVTOL vehicle. IEEE Trans Autom Control 52(7):1282–1287
18. Zavala-Rio A, Fantoni I, Lozano R (2003) Global stabilization of a PVTOL aircraft model with bounded inputs. Int J Control 76(18):1833–1844
19. Aguiar AP, Hespanha JP (2003) Position tracking of underactuated vehicles. Paper presented at American control conference, Denver, CO, 3, pp 1988–1993
20. Bi FY, Wei YJ, Zhang JZ, Cao W (2010) Position-tracking control of underactuated autonomous underwater vehicles in the presence of unknown ocean currents. IET Control Theory Appl 4(11):2369–2380
21. Do KD, Jiang ZP, Pan J (2002) Underactuated ship global tracking under relaxed conditions. IEEE Trans Autom Control 47(9):1529–1536
22. Dong W, Farrell JA (2008) Formation control of multiple underactuated surface vessels. IET Control Theory Appl 2(2):1077–1085

23. Egeland O, Dalsmo M, Sordalen OJ (1996) Feedback control of a nonholonomic underwater vehicle with constant desired configuration. Int J Robot Res 15(1):24–35
24. Fahimi F (2007) Sliding-mode formation control for underactuated surface vessels. IEEE Trans Robot 23(3):617–622
25. Ghommam J, Mnif F, Derbel N (2010) Global stabilisation and tracking control of underactuated surface vessels. IET Control Theory Appl 4(1):71–88
26. McNich LC, Ashrafiuon H, Muske KR (2010) Sliding mode set-point control of an underactuated surface vessel: simulation and experiment. Paper presented at American control conference, Baltimore, MD, USA, pp 5212–5217
27. Pettersen KY, Nijmeijer H (1996) Tracking control of an underactuated surface vessel. Paper presented at the international conference on decision and control, Florida, USA, pp 4561–4566
28. Reyhanoglul M, van der Schaft AJ, Harris McClamroch N, Kolmanovsky I (1996) Nonlinear control of a class of underactuated systems. Paper presented at 35th conference on decision and control, Kobe, Japan December, pp 1682–1687
29. Zhixiang T, Hongtao W, Chun F (2010) Hierarchical adaptive backstepping sliding mode control for under actuated space robot. In: International conference on informatics in control, automation and robotics, pp 500–503

Chapter 6
Challenges and New Frontiers in the Field of Underactuated Mechanical Systems Control

This concluding chapter epitomizes the major work described in this book. Comprehensive analysis on the generalized formulation of a novel block backstepping control law, and detailed description of its applications on ten different underactuated systems have been studied in the last three chapters. Nonetheless, a concise discussion at the end always assists the readers to feel the zest. Therefore, in this chapter, the authors briefly reiterate all the pros and cons of the present research endeavor. Finally, a few plausible directions in the field of UMS control problems are discussed to assist the prospective researchers.

6.1 Different Aspects of the Proposed Control Law

Over the past few decades, several research endeavors have been carried out to address the stabilization problem of the UMSs [1–11]. Owing to its practical relevance such as stabilization of robot arm, parking of underactuated vehicles, etc., this field of study has drawn significant research interests from the modern industry [5, 7]. On the other hand, captivated by the complex mathematical formulation of such problem, applied mathematicians have devoted their sincere efforts to address the same set of problems from completely different perspectives [6]. As stated earlier, nonholonomic systems fail to satisfy the Brocket's condition of feedback linearization, and thereby it is impossible to stabilize such systems using a smooth time-invariant feedback law. Since most of the UMSs fall under the nonholonomic systems, naïve approaches of nonlinear control theory often fail to address the stabilization problem of such systems [5–7, 12, 13]. As a result, devising a controller that would ensure global asymptotic stability of the generic UMSs is being considered as a quite challenging problem in the literature of control engineering [6–8, 14–21]. In addition, different aspects of the practical implementations such as compactness of the control law, complexity of the mathematical operations, total computation time, etc., make the design problem more complicated during real-time

S. Rudra et al., *Block Backstepping Design of Nonlinear State Feedback Control Law for Underactuated Mechanical Systems*, DOI 10.1007/978-981-10-1956-2_6

applications [3, 22–25]. A control law, which seems to be foolproof in the theoretical framework, quite often fails to produce a plausible control input for real-time applications. On contrary, a meticulously designed application-oriented approach frequently becomes too intended to a particular application that it fails to address the similar type of control problem of other practical systems [6, 15]. Keeping in view the aspects of generality in the theoretical framework as well as different prerequisites of practical implementation, this book has described a novel block backstepping control algorithm to address the stabilization control problem of generic UMS. The control algorithm is truly novel in the sense that it does not adhere to several unrealistic assumptions, and yet it can ensure the global asymptotic stability for a large class of the UMSs. Furthermore, another significant feature of the proposed control algorithm is that it is quite compact and perfectly suitable for real-world applications.

As mentioned earlier, backstepping is a recursive design approach that simplifies the control problem of an nth order nonlinear system by treating it as a control problem of the n numbers of cascade connected first-order systems [6, 7, 15]. Therefore, from the time of its inception, it has been being preferred by the control theorist, especially during the controller design task for complicated real-life systems [15]. However, a drawback of integrator backstepping is it relies on the conjecture that system under consideration is in strict feedback form. Needless to say, the complicated nonlinear state model of a UMS quite often fails to satisfy the prerequisite of backstepping approach [6, 7, 15]. Hence, in order to extend the advantageous features of backstepping to address the control problems of the UMSs, an algebraic state transformation has been utilized to convert the state model of such systems into a convenient feedback form [15]. Indeed, the proposed algebraic state transformation converts the system into a block-strict feedback form. Simply stated, it decomposes the state model of the n-DOF UMS into two parts, while the first part is represented by a reduced order strict feedback state model, the other part is used to represent the "internal dynamics" of the transformed system [15]. Thereafter, integrator backstepping algorithm has been utilized to derive the complete expression of the control law for the entire nonlinear system [15]. In addition, integral action has been incorporated with the control law to enhance the steady-state performance of the control law [15]. Since stability of the entire block backstepping controller depends on the stability of the zero dynamics of the transformed system, stability of the zero dynamics has thoroughly been analyzed to ensure the global asymptotic stability of the overall system at its desired equilibrium point [15]. In a nutshell, it can be inferred that the proposed algorithm is generalized enough to address the control problem of the large class of UMSs, as well as it yields a compact expression of control law for real-time applications [15].

Indeed, the merit of a theoretical proposition could only be assessed by analyzing its performance during practical applications. Hence, applications of the proposed control algorithm on different UMS have been discussed in this book. Since most of the important UMS belong to the category of two degree of freedom system [6], five different 2-DOF mechanical systems having different system dynamics have been selected to verify the theoretical claims of the present

proposition. Extensive simulation studies have revealed the fact that the proposed algorithm can ensure global asymptotic stability of the different UMS without significant modifications. In addition, the proposed control law has been applied on two real-time systems to corroborate the stabilization ability of the block backstepping algorithm during real-time applications.

Similar to the case of 2-DOF UMS, the block backstepping control law has been applied to higher order UMSs to justify the generalized nature of the proposed control algorithm. Consequently, it applications have been studied on three different higher order UMSs, namely USV, VTOL, and 3-DOF redundant manipulator. Extensive simulation studies have corroborated the fact that the proposed control law can ensure global asymptotic stability of the higher order UMSs. Hence, it can be concluded that the proposed algorithm is generalized enough to address the control problem of UMSs.

6.2 Major Inferences

(I) A novel block backstepping control algorithm has been devised to address the control problem of a generic underactuated mechanical systems.
(II) Proposed control algorithm utilizes an algebraic state transformation to convert the state model of the UMS into a system having two cascaded blocks; the reduced order system modeled and depicted in strict feedback form followed by a dynamic block that actually represents the unobservable internal dynamics of the transformed system.
(III) Stability of the internal dynamics can easily be analyzed using the concept of zero dynamics.
(IV) In this work, a control law has been devised that can ensure the global asymptotic stability for a large class of UMSs.
(V) Use of simple algebraic state transformation makes the control law amenable to real-time implementation.
(VI) Control law, which has been described in this book, can successfully address the stabilization problems of different UMSs (including holonomic, nonholonomic, "actuated shape variable," "unactuated shape variable," and flat underactuated mechanical systems).
(VII) Real-time experiments have revealed the fact that the proposed control law can be used to address the tracking control problem of the holonomic underactuated mechanical system.

6.3 Scope of the Future Work

In this section, a few active areas of research on the UMSs are explored to assist the budding researchers. They are as follows:

6.3.1 Robust Adaptive Block Backstepping Design for Underactuated Mechanical Systems

Design of a novel block backstepping control law has been presented in Chap. 3. Although the proposition is versatile enough to provide a plausible solution to the control problems a large class of UMSs, yet further advancement of the same could make it more flexible to deal with the control problem of uncertain systems. Therefore, future research can be pursued to develop a robust adaptive block backstepping control law for such class of systems.

Similar to the present method, an algebraic transformation could be utilized to convert the system in a block-strict feedback form, and thereafter an adaptive version of the same control law could be devised to address the control problem of UMSs. Concept of *tuning function* can be exploited to circumvent the problem of over parameterization, which commonly occurred with certainty equivalence-type adaption law. The prime design advantage offered by the tuning function approach is the reduction of dynamic order of the controller to its minimum. The number of parameter estimations becomes exactly equal to the number of unknown parameters. The minimum order design is advantageous not only for implementation but also because it ensures the strongest achievable stability and convergence properties. In the tuning function design, the parameter update law is designed recursively. At each consecutive step, designers utilize a tuning function as a potential update law. In contrary with normal adaptive backstepping, these intermediate update laws are not implemented, only the controller uses them to compensate the effect of parameter estimation transients. Eventually, the final tuning function is used for the parameter update law. Hence, the conventional adaptive block backstepping control law that utilizes certainty equivalence adaptation law should be redesigned using the concept of tuning function.

However, uncertainty is an intractable issue in real-time design problem. In case of practical applications, where the knowledge of the parameters of an underactuated mechanical system is incomplete, approximation errors may creep into the feedback loop. Needless to say, such type of approximation errors quite often leads to a very high rate of adaptation, which eventually destabilizes the performance of the entire control system. Therefore, the control law should be judicially redesigned to maintain a desirable adaptation rate for the entire nonlinear system. One may employ the concept of σ-switching function to make the controller robust against such type of unmodeled dynamics. Switching function can be incorporated in the tuning function to control the high rate of adaptation. Subsequently, a robust adaptive block backstepping control law could be designed to address the control problems of UMSs.

6.3.2 Industrial Needs

Owing to their cost-effective operation, nowadays UMSs are widely being used in manufacturing and transportation industry. Examples of these systems include USV, underwater autonomous vehicle, VTOL, helicopter, mobile robot, space platform, capsubot, robotic manipulator, flexible joint robot, etc. As stated in the foregoing discussion that most of the control law performs well in the well-structured environment [6]. However, due to presence of structured and nonstructured uncertainties during practical implementation, it becomes quite difficult to address the control problem of UMSs [26]. Concept of robust adaptive control law has been put forward in the previous subsection. However, a feasible solution, which considers all the aspects of real-time implementation like fuel optimization, actuator saturation, and many others issues, is still an open research problem. Soft computing approach may be considered to fulfill the needs for a few applications [26]. On the other hand, an adaptive higher order sliding mode is also a good option to deal with such kinds of control problems. Although lots of research contributions from practicing engineers have already published on the said topics, yet none of them can be claimed to be impeccable [6, 26]. Moreover, with the advent of modern technology one can always expect a more self-sufficient operation from UMSs in an unstructured and dynamically changing environment. Thus, design a control law that can satisfy all these needs is still an active area of research.

6.3.3 High-DOF Complex UMS

Since the UMSs use fewer numbers of actuators to generate the required input, the overall design of the system becomes more compact and lightweight. Use of fewer actuators not only reduces the weight, it also reduces the fuel consumption of the overall system. All these distinctive features of UMSs make it more amenable to real-time applications than that of fully actuated MIMO systems. However, when the degrees of freedom of a particular UMS increase, it affects the reliability of the overall system. One may consider the case of a 6-DOF autonomous vehicle or a 6-DOF haptic device, which uses a large number of control loops [26]. Indeed, most of the times they are intended to operate in an uncertain environment. Robust design of control law can always yield a solution in face of model uncertainties and external disturbances. However, one must consider the economic constraints, as well as feasibility of implementing an advanced control law at the time of practical applications.

6.3.4 Fault Tolerant Deduction and Control

Failure of an actuator makes a fully actuated MIMO system a UMS one, even more it may convert a strongly coupled UMS to a UMS having more unactuated degrees of freedom than that of the actuating inputs [26]. On the other hand, sensor failure results in unavailability of feedback signal that further affects the tracking performance of the overall system. Keeping in view the chances of actuator and sensor failure during real-time operation, an elegant backup control plan should be ready to avoid the catastrophic accidents [26]. Moreover, an efficacious switching strategy must be designed to activate the fault tolerant mechanism. Therefore, designing of a suitable control law that could provide a plausible solution during occurrence of faults, is currently an active area of research.

6.3.5 Networked UMS

Different issues that arise from networking of several UMSs while operating in a group, is also an open area of research. Nowadays, mobile robots are being used in rescue operation, and surveillance [26]. Ensuring proper communication and coordination between all the team members while the operating environment may also differ considerably for individual members, is a popular topic of distributed control [26]. Packet loss and communication delays may also eventually result in an undesirable situation. Therefore, new research could be pursued to devise an elegant control law that is robust as well as can yield an efficacious performance in distributed environment [26].

6.4 Notes

Indeed, UMS is an important class of mechanical systems that has treasured it applications in the different corners of modern civic life. Needless to say that covering up the entire research areas in a single book is quite a difficult task, and also beyond the scope of this present discussion. Only a particular control design approach and its application on several systems are being discussed here in this book. The authors are quite hopeful that this presentation would be able to impart subtle yet sufficient knowledge about mathematical and implementation-oriented approaches toward control of the underactuated nonlinear systems. However, in order to understand the breadth and depth of the UMSs control problems, readers may refer the references [1–66].

References

1. Chatterjee D, Patra A, Joglekar HK (2002) Swing-up and stabilization of a cart pendulum system under restricted cart track length. Syst Control Lett 47(4):355–364
2. Fantoni I, Lozano R (2002) Stabilization of the Furuta pendulum around its homoclinic orbit. Int J Control 75(6):390–398
3. Freidovich L, Shiriaev A, Gordillo F, Gómez-Estern F, Aracil J (2009) Partial-energy shaping control for orbital stabilization of high-frequency oscillations of the Furuta pendulum. IEEE Trans Control Syst Technol 17(4):853–858
4. Jiang ZP, Hill DJ, Guo Y (1998) Stabilization and tracking via output feedback for the nonlinear benchmark system. Automatica 34(7):907–915
5. Luca AD, Mattone R, Orilo G (1996) Control of underactuated mechanical systems: application to the planar 2R robot. Paper presented at the international conference on decision and control, Kobe, Japan, pp 1455–1460
6. Notarstefano G, Hauser J, Frezza R (2005) Trajectory manifold exploration for the PVTOL aircraft. Paper presented at IEEE conference on decision and control and European control conference, Seville, Spain, pp 5848–5853
7. Olfati RS (2001) Nonlinear control of underactuated mechanical systems with application to robotics and aerospace vehicles, Ph.D. thesis, Department of Electrical Engineering and Computer, Massachusetts Institute of Technology
8. Oriolo G, Nakamura T (1991) Control of mechanical systems with second-order nonholonomic constraints: Underactuated manipulators. Paper presented at the international conference on decision and control, Brighton, UK, pp 2398–2403
9. Viola G, Ortega R, Banavar R, Acosta JA, Astolfi A (2007) Total energy shaping control of mechanical systems: simplifying the matching equations via coordinate changes. IEEE Trans Autom Control 52(6):1093–1099
10. White WN, Foss M, Guo X (2006) A direct Lyapunov approach for a class of underactuated mechanical systems. Paper presented at the American control conference, Minneapolis, Minnesota, USA 103–110:2006
11. Wood R, Cazzolato B (2007) An alternative nonlinear control law for the global stabilization of the PVTOL vehicle. IEEE Trans Autom Control 52(7):1282–1287
12. Egeland O, Dalsmo M, Sordalen OJ (1996) Feedback control of a nonholonomic underwater vehicle with constant desired configuration. Int J Robot Res 15(1):24–35
13. Kim Y, Kim SH, Kwak YK (2005) Dynamic analysis of a nonholonomic two-wheeled inverted pendulum robot. J Intell Robot Syst 44(1):25–46
14. Olfati-Saber R, Megretski A (1998) Controller design for a class of underactuated nonlinear systems. Paper presented at the 37th international conference on decision and control, Tampa, FL, vol 4, pp 4182–4187
15. Pavlov A, Janssen B, van de Wouw N, Nijmeijer H (2007) Experimental output regulation for a nonlinear benchmark system. IEEE Trans Control Syst Technol 15(4):786–793
16. Shiriaev AS, Freidovich LB, Robertsson A, Johansson R, Sandberg A (2007) Virtual holonomic-constraints-based design of stable oscillations of Furuta pendulum: theory and experiments. IEEE Trans Robot 23(4):827–832
17. Spong MW (1994) Partial feedback linearization of underactuated mechanical systems. Paper presented at IEEE/RSJ/GI international conference on intelligent robots and systems, Munich, Germany, pp 314–321
18. Spong M (1995) The swing-up control problem for the Acrobot. IEEE Control Syst Mag 47(1):49–55
19. Spong MW (1996) Energy based control of a class of underactuated mechanical systems. Paper presented at the IFAC world congress, San Francisco, CA, USA, pp 431–435
20. Spong M, Praly L (1996) Control of underactuated mechanical systems using switching and saturation. In Morse AS (ed) Paper presented on control using logic-based switching (Lecture Notes no. 222). Springer, Berlin, pp 162–172

21. Wang WJ, Lin HR (1999) Fuzzy control design for the trajectory tracking on uncertain nonlinear systems. IEEE Trans Fuzzy Syst 7(1):53–62
22. Albahkali T, Mukherjee R, Das T (2009) Swing-up control of the pendubot: an impulse momentum approach. IEEE Trans Robot 25(4):975–982
23. Al-Hiddabi SA, McClamroch NH (2002) Tracking and maneuver regulation control for nonlinear non-minimum phase systems: application to flight control. IEEE Trans Control Syst Technol 10(6):780–792
24. Jankovic M, Fontaine D, Kokotovic PV (1996) TORA example: cascade and passivity based control designs. IEEE Trans Control Syst Technol 4(3):292–297
25. Pathak K, Franch J, Agrawal SK (2005) Velocity and position control of a wheeled inverted pendulum by partial feedback linearization. IEEE Trans Robot 21(3):505–513
26. Liu Y, Yu H (2013) A survey of underactuated mechanical systems. IET Control Theory Appl 7(7):921–935
27. Abdessameuda A, Tayebi A (2010) Global trajectory tracking control of VTOL-UAVs without linear velocity measurements. Automatica 46(6):1053–1059
28. Aguiar AP, Hespanha JP (2003) Position tracking of underactuated vehicles. Paper presented at American control conference, Denver, Co, 3, 1988–1993
29. Avis JM, Nersesov SG, Nathan R, Ashrafiuon H, Muske KR (2010) A comparison study of nonlinear control techniques for the RTAC system. Nonlinear Anal Real World Appl 11(4):2647–2658
30. Bi FY, Wei YJ, Zhang JZ, Cao W (2010) Position-tracking control of underactuated autonomous underwater vehicles in the presence of unknown ocean currents. IET Control Theory Appl 4(11):2369–2380
31. Chang DE (2010) Stabilizability of controlled Lagrangian systems of two degrees of freedom and one degree of under-actuation by the energy-shaping method. IEEE Trans Autom Control 55(8):1888–1893
32. Consolini L, Maggiore M, Nielsen C, Tosques M (2010) Path following for the PVTOL aircraft. Automatica 46(8):1284–1296
33. Consolini L, Tosques M (2007) On the VTOL exact tracking with bounded internal dynamics via a Poincar´e map approach. IEEE Trans Autom Control 52(9):1757–1762
34. De Luca RMA, Iannitti S, Oriolo G (2001) Control problems in underactuated manipulators. Paper presented at IEEE/ASME international conference on advanced intelligent mechatronics, Como, Italy, pp 8–12
35. Do KD, Jiang ZP, Pan J (2002) Underactuated ship global tracking under relaxed conditions. IEEE Trans Autom Control 47(9):1529–1536
36. Do KD, Jiang ZP, Pan J (2003) On global tracking control of a VTOL aircraft without velocity measurements. IEEE Trans Autom Control 48(12):2212–2217
37. Dong W, Farrell JA (2008) Formation control of multiple underactuated surface vessels. IET Control Theory Appl 2(2):1077–1085
38. Fahimi F (2007) Sliding-mode formation control for underactuated surface vessels. IEEE Trans Robot 23(3):617–622
39. Fantoni I, Lozano R, Spong MW (2000) Energy based control of the Pendubot. IEEE Trans Autom Control 45(4):725–729
40. Fantoni I, Lozano R (2001) Nonlinear control for underactuated mechanical systems. Springer-Verlag, London
41. Gao A, Zhang X, Chen H, Zhao J (2009) Energy-based control design of an underactuated 2-dimensional TORA system. Paper presented at the IEEE/RSJ international conference on intelligent robots and systems, St. Louis, USA, pp 1296–1301
42. Ghommam J, Mnif F, Derbel N (2010) Global stabilisation and tracking control of underactuated surface vessels. IET Control Theory Appl 4(1):71–88
43. Gruszka A, Malisoff, M, Mazenc F (2011) On tracking for the PVTOL model with bounded feedbacks. Paper presented at American control conference, San Francisco, CA, USA, pp 1428–1433

44. Jafari R, Mathis FB, Mukherjee R (2011) Swing-up control of the acrobot: an impulse momentum approach. Paper presented at American control conference, San Francisco, CA, USA, pp 262–267
45. Jiang ZP, Kanellakopoulos I (2000) Global output-feedback tracking for a benchmark nonlinear system. IEEE Trans Autom Control 45(5):1023–1027
46. Lai XZ, She JH, Yang SX, Wu M (2009) Comprehensive unified control strategy for underactuated two-link manipulators. IEEE Trans Syst Man Cybern B 39(2):389–398
47. Lopez-Martinez M, Acosta JA, Cano JM (2010) Non-linear sliding mode surfaces for a class of underactuated mechanical systems. IET Control Theory Appl 4(10):2195–2204
48. Lozano R, Castillo P, Dzul A (2004) Global stabilization of the PVTOL: real-time application to a mini-aircraft. Int J Control 77(8):735–740
49. Yu R, Zhu Q, Xia G, Liu Z (2012) Sliding mode tracking control of an underactuated surface vessel. IET Control Theory Appl 6(3):461–466
50. Marconi L, Isidori A, Serrani A (2002) Autonomous vertical landing on an oscillating platform: an internal-model based approach. Automatica 38(1):21–32
51. Martin P, Devasia S, Paden B (1996) A different look at output tracking: control of a VTOL aircraft. Automatica 32(1):101–107
52. McNich LC, Ashrafiuon H, Muske KR (2010) Sliding mode set-point control of an underactuated surface vessel: simulation and experiment. Paper presented at American control conference, Baltimore, MD, USA, pp 5212–5217
53. Mori S, Nishiharaa H, Furuta K (1976) Control of unstable mechanical system Control of pendulum. Int J Control 23(5):673–692
54. Nair S, Leonard NE (2002) A normal form for energy shaping: application to the Furuta pendulum. Paper presented at the 41th international conference on decision and control, vol 1, pp 516–521
55. Ortega R , Spong MW, G´omez-Estern F, Blankenstein G (2002) Stabilization of a class of underactuated mechanical systems via interconnection and damping assignment, IEEE Trans Autom Control (47)8:1218–1232
56. Rudra S, Barai RK, Maitra M (2014) Nonlinear state feedback controller design for underactuated mechanical system: a modified block backstepping approach. ISA Trans 53(2):317–326
57. Van der Schaft J (1999) L2-Gain and passivity in nonlinear control. Springer-Verlag, New York
58. Setlur P, Dawson D, Fang Y, Costic B (2001) Nonlinear tracking control of the VTOL aircraft. Paper presented at the international conference on decision and control, Orlando, USA, pp 4592–4597
59. Spong MW (1998) Underactuated mechanical systems, control problems in robotics and automation, vol 230. Springer-Verlag, Berlin, pp 135–150
60. Wan J, Bernstein DS, Coppola VT (1994) Global stabilization of the oscillating eccentric rotor. Paper presented at the international conference on decision and control, Orlando, USA, pp 4024–4029
61. Wang W, Yi J, Zhao D, Liu D (2004) Design of a stable sliding mode controller for a class of second-order underactuated systems. IEEE Proc Control Theory April 151(6):683–690
62. Ye H, Wang H (2007) Stabilization of a PVTOL aircraft and an inertia wheel pendulum using saturation technique. IEEE Trans Control Syst Technol 15(6):1143–1150
63. Zavala-Rio A, Fantoni I, Lozano R (2003) Global stabilization of a PVTOL aircraft model with bounded inputs. Int J Control 76(18):1833–1844
64. Zhixiang T, Hongtao W, Chun F (2010) Hierarchical adaptive backstepping sliding mode control for under actuated space robot. In: International conference on informatics in control, automation and robotics, pp 500–503
65. Zhang M, Tarn T (2002) Hybrid control of the Pendubot. IEEE/ASME Trans Mechatronics 7(1):79–86
66. Zhao J, Spong MW (2001) Hybrid control for global stabilization of the cart-pendulum system. Automatica 37(12):1941–1951

Appendix
Modeling of Different Underactuated Mechanical Systems

A.1 Mathematical Modeling of Inertia Wheel Pendulum

Schematic diagram of the inertia wheel pendulum is shown in Fig. A.1.

The Lagrangian model of the inertia wheel system has been shown below:

$$m_{11}\ddot{q}_1 + m_{12}\ddot{q}_2 + h_1(q,\dot{q}) = 0 \tag{A.1}$$

$$m_{21}\ddot{q}_1 + m_{22}\ddot{q}_2 = \tau \tag{A.2}$$

where,

$$m_{12} = m_{21} = m_{22} = I_2 \tag{A.3}$$

$$h_1 = -m_0 g \sin q_1 \tag{A.4}$$

$$|M| = m_{11}m_{22} - m_{12}m_{21} \tag{A.5}$$

The use of the following global feedback yields the following state feedback structure

$$\tau = \left(m_{22} - \frac{m_{21}m_{12}}{m_{11}}\right)u + \left(\frac{m_{21}m_0}{m_{11}}\right)\sin(q_1) \tag{A.6}$$

One may able to realize the following state model structure for underactuated mechanical system

$$\begin{aligned} \dot{q}_1 &= p_1 \\ \dot{p}_1 &= f + gu \\ \dot{q}_2 &= p_2 \\ \dot{p}_2 &= u \end{aligned} \tag{A.7}$$

S. Rudra et al., *Block Backstepping Design of Nonlinear State Feedback Control Law for Underactuated Mechanical Systems*, DOI 10.1007/978-981-10-1956-2

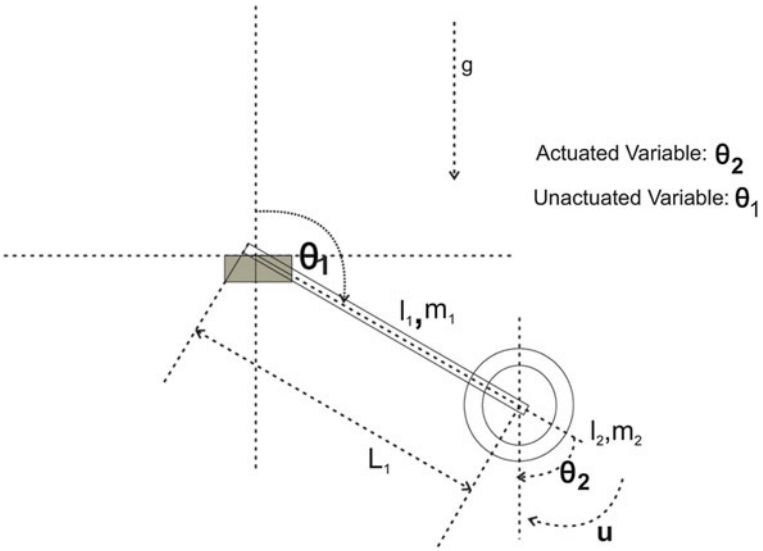

Fig. A.1 Inertia wheel system

where,

$$f = \frac{m_{21} m_0 g}{m_{11}} \sin(q_1) \tag{A.8}$$

$$g = -\frac{m_{12}}{m_{11}} \tag{A.9}$$

A.2 Mathematical Modeling of TORA System

Figure A.5 illustrates the top view of this nonlinear benchmark mechanical system in which the rotational motion of an eccentric mass controls the translational oscillations of the platform. Assuming that the platform moves in the horizontal plane, the dynamics of the system are described by Fig. A.2.

The Lagrangian model of the TORA system has been shown below:

$$\begin{aligned} m_{11}\ddot{q}_1 + m_{12}\ddot{q}_2 + h_1(q, \dot{q}) &= 0 \\ m_{21}\ddot{q}_1 + m_{22}\ddot{q}_2 + h_2(q, \dot{q}) &= \tau \end{aligned} \tag{A.10}$$

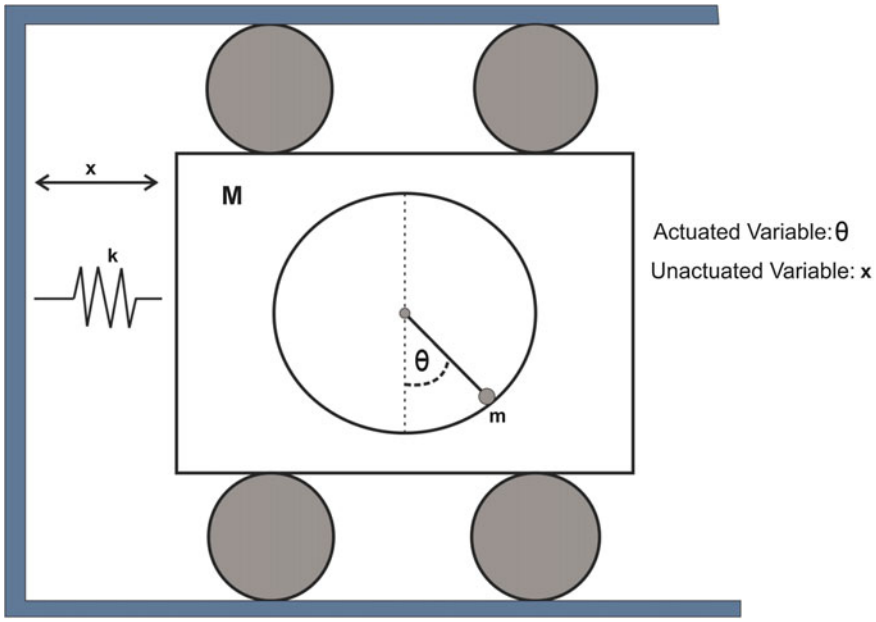

Fig. A.2 The TORA system

where,

$$m_{11} = M + m \tag{A.11}$$

$$m_{12} = m_{21} = mr\cos\theta \tag{A.12}$$

$$m_{22} = I + mr^2 \tag{A.13}$$

$$h_1 = -mr\sin\theta\dot{\theta}^2 + kx \tag{A.14}$$

$$h_2 = -m_2 gr\sin q_2 \tag{A.15}$$

$$\Delta = m_{11}m_{22} - m_{12}m_{21} \tag{A.16}$$

Applying the following feedback law:

$$u = \frac{\tau}{\Delta} - m_2^2 r^2 \sin(2q_2)p_2^2 + kq_1 m_2 r\cos(q_2) - m_2 gr\sin(q_2)(m_1 + m_2) \tag{A.17}$$

One may able to realize the following state model structure for underactuated mechanical system

$$\begin{aligned}\dot{q}_1 &= p_1\\ \dot{p}_1 &= f + gu\\ \dot{q}_2 &= p_2\\ \dot{p}_2 &= u\end{aligned} \tag{A.18}$$

where,

$$f = -k_3 q_1 + k_2 \sin(q_2) p_1^2 \tag{A.19}$$

$$g = -k_2 \cos(q_2) \tag{A.20}$$

$$k_2 = m_2 r/(m_1 + m_2) \tag{A.21}$$

$$k_3 = -k_1/(m_1 + m_2) \tag{A.22}$$

A.3 Mathematical Modeling of Furuta Pendulum

Schematic diagram of Furuta Pendulum is shown in Fig. A.3.

The Lagrangian model of the Furuta pendulum system has been shown below:

$$\begin{aligned}m_{11}\ddot{q}_1 + m_{12}\ddot{q}_2 + h_1(q,\dot{q}) + g_1(q) &= \tau\\ m_{21}\ddot{q}_1 + m_{22}\ddot{q}_2 + h_2(q,\dot{q}) + g_2(q) &= 0\end{aligned} \tag{A.23}$$

where

$$m_{11} = J_1 + m_2 l_1^2 + m_2 l_2^2 \sin^2(q_2) \tag{A.24}$$

$$m_{12} = m_{21} = m_2 L_1 l_2 \cos(q_2) \tag{A.25}$$

$$m_{22} = J_2 + m_2 l_2^2 \tag{A.26}$$

$$h_1 = 2m_2 l_2^2 \sin(q_2)\cos(q_2)\dot{q}_1\dot{q}_2 - m_2 L_1 l_2 \sin(q_2)\dot{q}_2^2 \tag{A.27}$$

$$h_2 = -m_2 l_2^2 \sin(q_2)\cos(q_2)\dot{q}_1^2 \tag{A.28}$$

$$g_1 = 0 \tag{A.29}$$

$$g_2 = -m_2 g l_1 \sin(q_2) \tag{A.30}$$

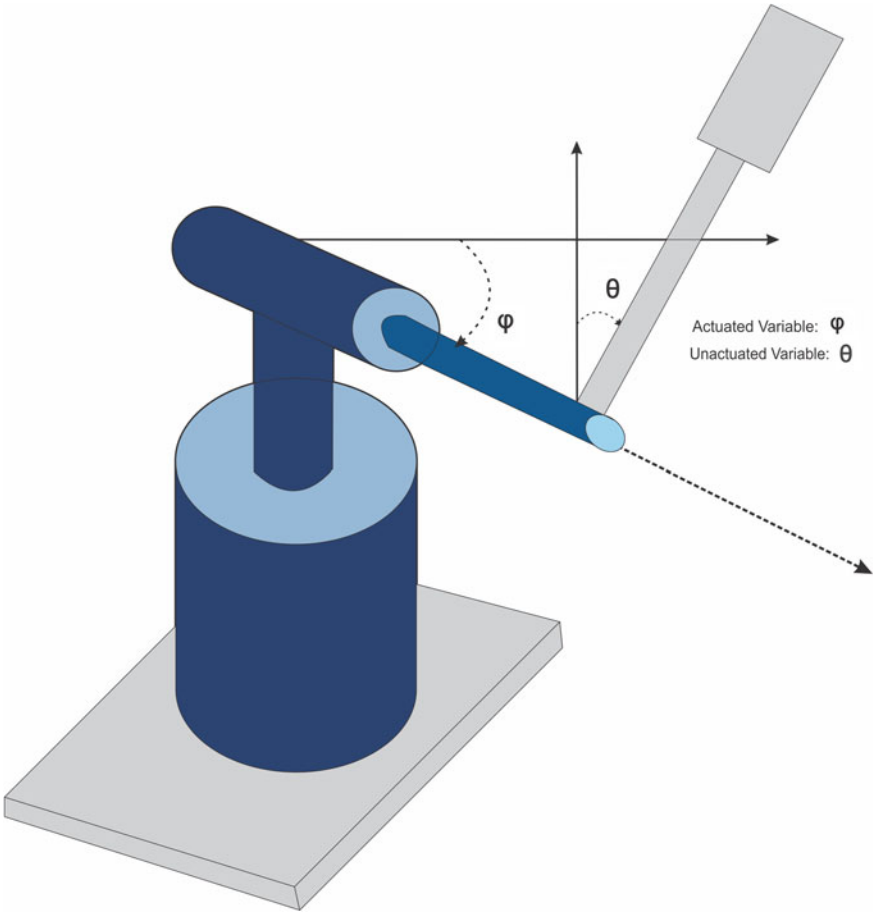

Fig. A.3 Furuta pendulum system

$$\Delta = m_{11}m_{22} - m_{12}m_{21} \tag{A.31}$$

Noting that $\cos(q_2) \neq 0$ $(q_2 \in (-\pi/2, \pi/2))$, and applying the following feedback law:

$$\tau = -\frac{\Delta}{m_{12}}u - \frac{m_{11}}{m_{12}}h_2 + h_1 - \frac{m_{11}}{m_{12}}g_2 \tag{A.32}$$

One may able to realize the following state model structure for underactuated mechanical system as follows

$$\begin{aligned}\dot{q}_1 &= p_1\\ \dot{p}_1 &= f + g u\, k_2 \tan(q_2) + k_3 \sin(q_2) p_1^2 - k_1 u/\cos(q_2)\\ \dot{q}_2 &= p_2\\ \dot{p}_2 &= u\end{aligned} \tag{A.33}$$

where,

$$f = k_2 \tan(q_2) + k_3 \sin(q_2) p_1^2 \tag{A.34}$$

$$g = -k_1 \cos(q_2) \tag{A.35}$$

$$k_1 = \left(J_2 + m_2 l_2^2\right)/m_2 l_1 l_2 \tag{A.36}$$

$$k_2 = g l_1 / L_1 l_2 \tag{A.37}$$

$$k_3 = l_2 / L_1 \tag{A.38}$$

A.4 Mathematical Modeling of Acrobot

Referring to Fig. A.4, the Lagrangian model of the acrobot system can be described by the following equations:

$$\begin{aligned} m_{11}\ddot{q}_1 + m_{12}\ddot{q}_2 + h_1(q,\dot{q}) + \phi_1(q) &= 0\\ m_{21}\ddot{q}_1 + m_{22}\ddot{q}_2 + h_2(q,\dot{q}) + \phi_2(q) &= \tau\end{aligned} \tag{A.39}$$

where,

$$m_{11} = m_1 l_{c1}^2 + m_2\left(l_1^2 + l_{c2}^2 + 2 l_1 l_{c2}\cos(q_2)\right) + I_1 + I_2 \tag{A.40}$$

$$m_{12} = m_{21} = m_2\left(l_{c2}^2 + l_1 l_{c2}\cos(q_2)\right) + I_2 \tag{A.41}$$

$$m_{22} = m_2 l_{c2}^2 + I_2 \tag{A.42}$$

$$h_1 = -m_2 l_1 l_{c2}\sin(q_2)\dot{q}_2^2 - 2 m_2 l_1 l_{c2}\sin(q_2)\dot{q}_2\dot{q}_1 \tag{A.43}$$

$$h_2 = m_2 l_1 l_{c2}\sin(q_2)\dot{q}_1^2 \tag{A.44}$$

$$\phi_1 = (m_1 l_{c1} + m_2 l_1) g\cos(q_1) + m_2 l_{c2} g\cos(q_1 + q_2) \tag{A.45}$$

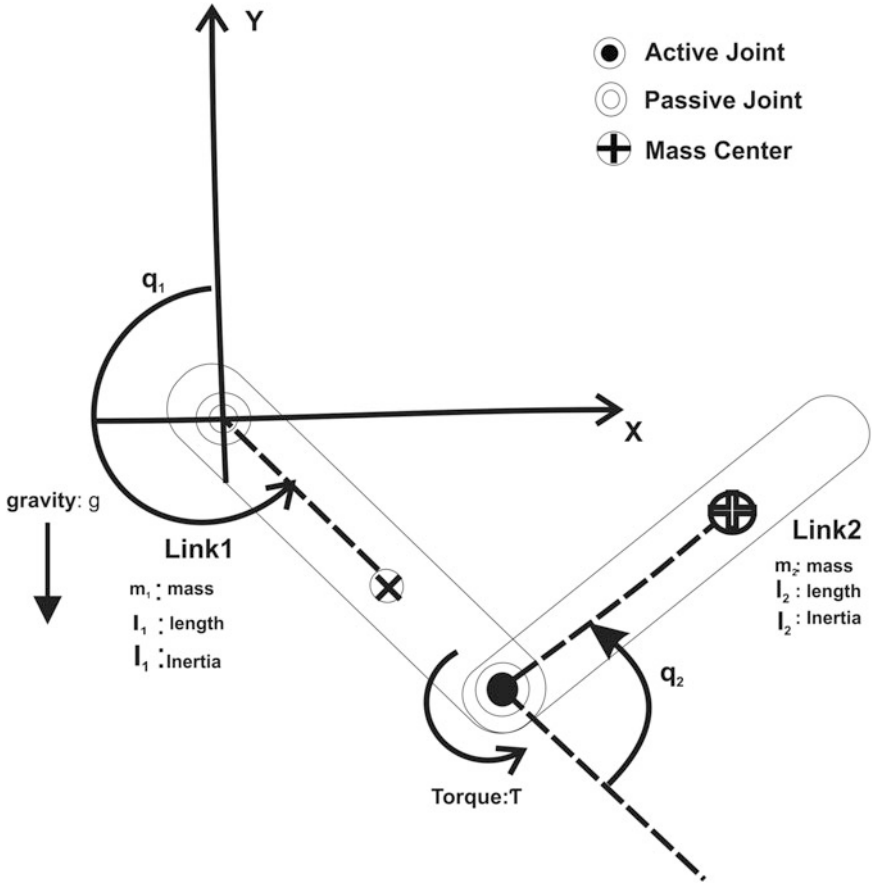

Fig. A.4 Schematic diagram of acrobot

$$\phi_2 = m_2 l_{c2} g \cos(q_1 + q_2) \tag{A.46}$$

$$\Delta = m_{11} m_{22} - m_{12} m_{21} \tag{A.47}$$

$$M_l = m_2 l_1 l_{c2} \tag{A.48}$$

$$M_1 = m_{11} - 2M_l \cos(q_2) \tag{A.49}$$

$$M_2 = m_2 l_{c2}^2 + I_2 \tag{A.50}$$

$$\phi' = (m_1 l_{c1} + m_2 l_1) g \tag{A.51}$$

$$\phi'' = m_2 l_{c2} g \tag{A.52}$$

The parameters m_i, l_i, l_{ci}, and I_i denote the mass, link length, distance of the mass center of the link from their respective joint end, and moment of inertia of the ith link respectively.

Applying the following feedback control input as shown in equation (A.53), one may be able to formulate the state model structure for the underactuated acrobot system as shown in equation (A.54.a).

$$\tau = \frac{m_{11}}{\Delta}\left(\frac{m_{11}h_2 - m_{21}h_1 + m_{11}\phi_2 - m_{21}\phi_1}{m_{11}} + \frac{\Delta}{m_{11}}u\right) \tag{A.53}$$

With the above choice of state feedback, the state model of the acrobot system becomes:

$$\begin{aligned} \dot{q}_1 &= p_1 \\ \dot{p}_1 &= f_1 + g_1 u \\ \dot{q}_2 &= p_2 \\ \dot{p}_2 &= u \end{aligned} \tag{A.54.a}$$

where

$$f_1 = -\left(\frac{h_1}{m_{11}} + \frac{\phi_1}{m_{11}}\right) \tag{A.54.b}$$

$$g_1 = -\frac{m_{12}}{m_{11}} \tag{A.54.c}$$

A.5 Mathematical Modeling of Pendubot

Referring to Fig. A.5, the Lagrangian model of the Pendubot system can be described by the following equations:

$$\begin{aligned} m_{11}\ddot{q}_1 + m_{12}\ddot{q}_2 + h_1(q,\dot{q}) + \phi_1(q) &= \tau \\ m_{21}\ddot{q}_1 + m_{22}\ddot{q}_2 + h_2(q,\dot{q}) + \phi_2(q) &= 0 \end{aligned} \tag{A.55}$$

where,

$$m_{11} = m_1 l_{c1}^2 + m_2\left(l_1^2 + l_{c2}^2 + 2l_1 l_{c2}\cos(q_2)\right) + I_1 + I_2 \tag{A.56}$$

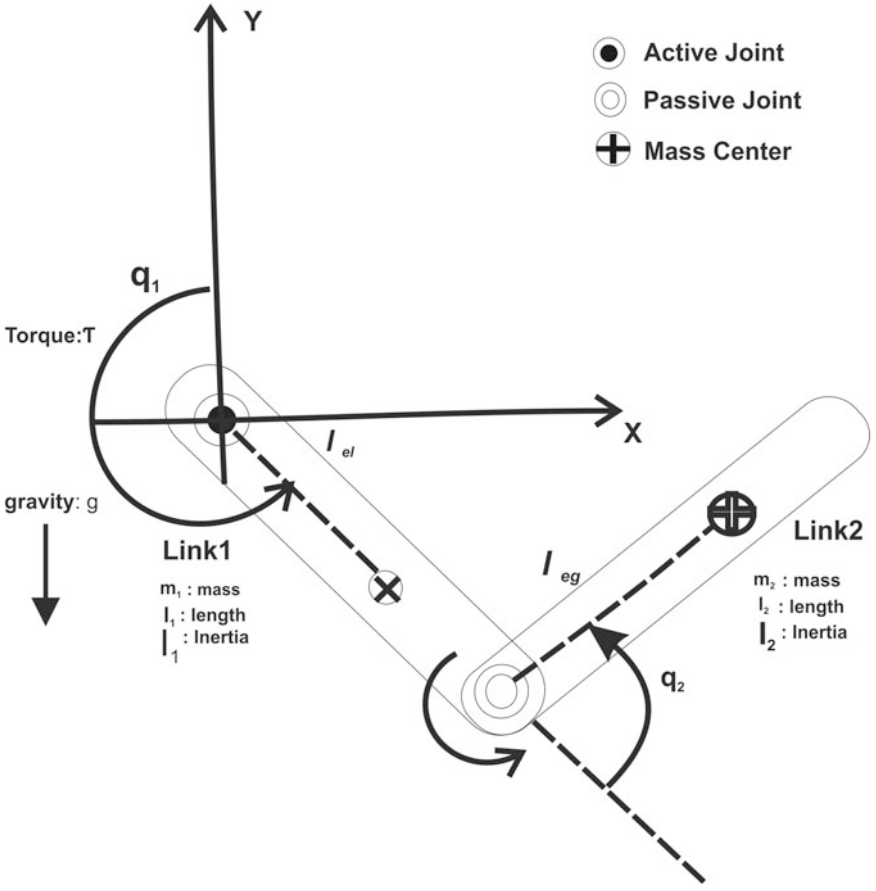

Fig. A.5 The Schematic diagram of pendubot

$$m_{12} = m_{21} = m_2\left(l_{c2}^2 + l_1 l_{c2}\cos(q_2)\right) + I_2 \tag{A.57}$$

$$m_{22} = m_2 l_{c2}^2 + I_2 \tag{A.58}$$

$$h_1 = -m_2 l_1 l_{c2}\sin(q_2)\dot{q}_2^2 - 2m_2 l_1 l_{c2}\sin(q_2)\dot{q}_2\dot{q}_1 \tag{A.59}$$

$$h_2 = m_2 l_1 l_{c2}\sin(q_2)\dot{q}_1^2 \tag{A.60}$$

$$\phi_1 = (m_1 l_{c1} + m_2 l_1)g\cos(q_1) + m_2 l_{c2} g\cos(q_1 + q_2) \tag{A.61}$$

$$\phi_2 = m_2 l_{c2} g\cos(q_1 + q_2) \tag{A.62}$$

$$\Delta = m_{11}m_{22} - m_{12}m_{21} \tag{A.63}$$

$$M_l = m_2 l_1 l_{c2} \tag{A.64}$$

$$M_1 = m_{11} - 2M_l \cos(q_2) \tag{A.65}$$

$$M_2 = m_2 l_{c2}^2 + I_2 \tag{A.66}$$

$$\phi' = (m_1 l_{c1} + m_2 l_1)g \tag{A.67}$$

$$\phi'' = m_2 l_{c2} g \tag{A.68}$$

The parameters m_i, l_i, l_{ci}, and I_i denote the mass, link length, distance of the mass center of the link from their respective joint end, and moment of inertia of the ith link respectively.

Applying the following feedback control input as shown in equation (A.69), one may be able to formulate the state model structure for the underactuated Pendubot system as shown in equation (A.70.a).

$$\tau = \frac{m_{22}}{\Delta}\left(\frac{m_{11}h_2 - m_{21}h_1 + m_{11}\phi_2 - m_{21}\phi_1}{m_{22}} + \frac{\Delta}{m_{22}}u\right) \tag{A.69}$$

With the above choice of state feedback, the state model of the acrobot system becomes:

$$\begin{aligned} \dot{q}_1 &= p_1 \\ \dot{p}_1 &= u \\ \dot{q}_2 &= p_2 \\ \dot{p}_2 &= f + gu \end{aligned} \tag{A.70.a}$$

where

$$f_1 = -\left(\frac{h_1}{m_{11}} + \frac{\phi_1}{m_{11}}\right) \tag{A.70.b}$$

$$g_1 = -\frac{m_{12}}{m_{11}}. \tag{A.70.c}$$

A.6 Mathematical Modeling of Cart-Pole System

The model of a digital inverted pendulum has been shown in Fig. A.6, where θ is the angle of the pendulum, x is the displacement of the cart, and F is the control force, parallel to the rail, applied to the cart.

The dynamic equation of the system can be derived based on the second law of Newton. The following equation of motions can be obtained using force law of Newton

$$(M+m)\frac{d^2}{dt^2}(x - l\sin\theta) = F - T \tag{A.71}$$

$$(M+m)\frac{d^2}{dt^2}(l\cos\theta) = V - (M+m)g \tag{A.72}$$

$$J\frac{d^2\theta}{dt^2} = (F - T)l\cos\theta + Vl\sin\theta \tag{A.73}$$

The masses of the cart and the pendulum are denoted by M and m. In particular, l is the distance from axis of rotation to the center of mass of the inverted pendulum. J is the moment of inertia of the inverted pendulum with respect to the center of masses. The force of reaction of the rail V acts vertically on the cart. T denotes the friction between cart and the rail. Here, it is assumed that $T = fx_3$, where f is the friction coefficient of the cart with the rail. Combining the above three equations, it is possible to realize the state model of the pendulum cart system which is given below

$$\dot{x}_1 = x_3 \tag{A.74}$$

$$\dot{x}_2 = x_4 \tag{A.75}$$

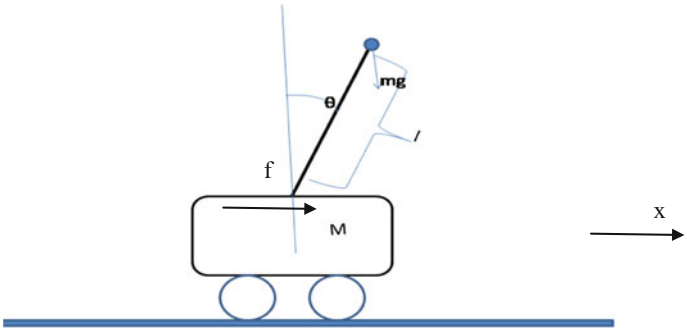

Fig. A.6 Dynamics of cart pole system

$$\dot{x}_3 = \frac{a(F - T - \mu x_4^2 \sin x_2) + l \cos x_2 \mu g \sin x_2}{J + \mu l \sin^2 x_2} \tag{A.76}$$

$$\dot{x}_3 = \frac{l(F - T - \mu x_4^2 \sin x_2) + \mu g \sin x_2}{J + \mu l \sin^2 x_2} \tag{A.77}$$

where $a = l^2 + \frac{J}{M+m}$ and $\mu = l(M+m)$. The state vector of the system is consisting of four state variables as $X = [x_1, x_2, x_3, x_4]^{\mathrm{T}}$. In the above representation, x_1 is the cart position (distance from the center of the rail), x_2 is the pendulum angle between the upright vertical and the axis of the centre of mass of the pendulum, measured counter-clockwise from the cart $x_3$is the cart velocity, and x_4 is the angular velocity of the pendulum. The same state model can be used as a state model for crane.

A.7 Mathematical Modeling of VTOL

Here we consider a very simplified PVTOL (Planar Vertical Take-off and Landing) aircraft (see Fig. A.7). Let $(\vec{i}, \vec{j}, \vec{k})$ be a fixed inertial frame and $(\overrightarrow{i_b}, \overrightarrow{j_b}, \overrightarrow{k_b})$, with $\overrightarrow{j_b} = \vec{j}$ be a moving frame attached to the aircraft (body axes). The forces acting on the system are (Fig. A.7):

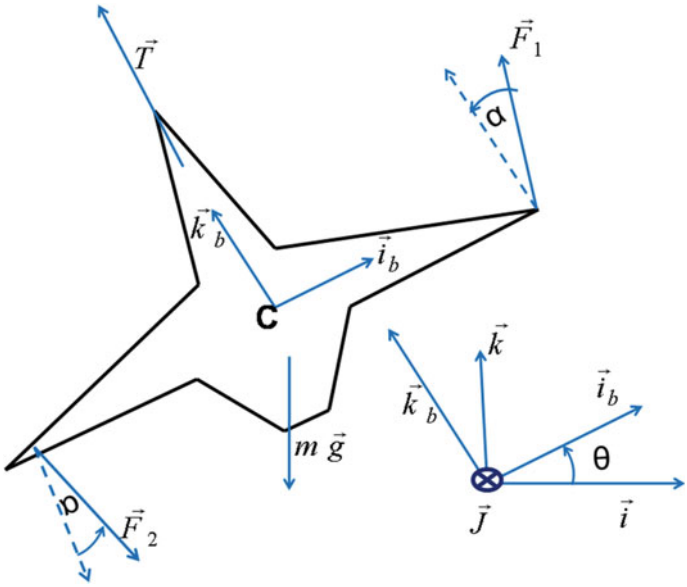

Fig. A.7 VTOL aircraft

$$\vec{T} = T\overrightarrow{k_b} \tag{A.78}$$

$$\overrightarrow{F_1} = \left(\sin\alpha\,\overrightarrow{i_b} + \cos\alpha\overrightarrow{k_b}\right)F \tag{A.79}$$

$$\overrightarrow{F_2} = \left(\sin\alpha\,\overrightarrow{i_b} - \cos\alpha\overrightarrow{k_b}\right)F \tag{A.80}$$

$$m\vec{g} = -mg\vec{k} \tag{A.81}$$

The equations of motion is written in terms of the centre of mass C as

$$m\overrightarrow{a_c} = \vec{T} + \overrightarrow{F_1} + \overrightarrow{F_2} + m\vec{g} \tag{A.82}$$

$$\overrightarrow{\sigma_c} = C\overrightarrow{M_1} \times \overrightarrow{F_1} + C\overrightarrow{M_2} \times \overrightarrow{F_2} \tag{A.83}$$

where $\overrightarrow{\alpha_c}$ is the acceleration of C and $\overrightarrow{\sigma_c}$ is the angular momentum about C. M_1 and M_2 are the points at which the forces F_1 and F_2 are located. Expanding these equations gives

$$m\left(\ddot{x}\vec{i} + \ddot{y}\vec{k}\right) = T\overrightarrow{k_b} + 2F\sin\sin\alpha\,\overrightarrow{i_b} - mg\vec{k} \tag{A.84}$$

$$-J\ddot{\theta}\overrightarrow{j_b} = -2lF\cos\alpha\overrightarrow{j_b} \tag{A.85}$$

where J is the moment of inertia about C, and l is the distance from C to points M_1 and M_2. Now setting

$$u_1 = \frac{T}{m} \tag{A.86}$$

$$u_2 = \frac{2F}{m}\cos\alpha \tag{A.87}$$

$$\varepsilon = \tan\alpha \tag{A.88}$$

$$\lambda = \frac{ml}{J} \tag{A.89}$$

Therefore, projecting into the fixed frame, we finally get the equation of acceleration as follows

$$\ddot{x} = -u_1\sin\theta + \varepsilon u_2\cos\theta \tag{A.90}$$

$$\ddot{z} = u_1\cos\theta + \varepsilon u_2\sin\theta - g \tag{A.91}$$

$$\ddot{\theta} = \lambda u_2 \tag{A.92}$$

Now if we apply the following control inputs u_1 and u_2

$$u_1 = [v_2 \cos x_5 - v_1 \sin x_5 + g \cos x_5] \tag{A.93}$$

$$u_2 = \frac{1}{\varepsilon}[v_1 \cos x_5 + v_2 \sin x_5 + g \sin x_5] \tag{A.94}$$

yield the following state model of VTOL system

$$\begin{aligned}
\dot{x}_1 &= x_2 \\
\dot{x}_2 &= v_1 \\
\dot{x}_3 &= x_4 \\
\dot{x}_4 &= v_2 \\
\dot{x}_5 &= x_6 \\
\dot{x}_6 &= \frac{\lambda}{\varepsilon}[v_1 \cos x_5 + v_2 \sin x_5 + g \sin x_5]
\end{aligned} \tag{A.95}$$

A.8 Mathematical Modeling of Underactuated Surface Vessels

The schematic diagram of the underactuated surface vessel is shown in Fig. A.8. The dynamic equation of the underactuated surface vessel is described in equation (A.96).

$$\begin{aligned}
&m(\ddot{x}\cos\theta + \ddot{y}\sin\theta) + c_x(\dot{x}\cos\theta + \dot{y}\sin\theta) = F \\
&I\ddot{\theta} + c_z\dot{\theta} = T \\
&m(-\ddot{x}\cos\theta + \ddot{y}\sin\theta) + c_y(-\dot{x}\cos\theta + \dot{y}\sin\theta) = 0
\end{aligned} \tag{A.96}$$

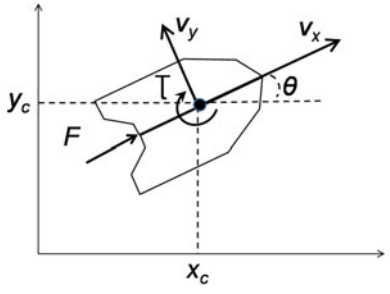

Fig. A.8 Schematic diagram of the underactuated surface vessel

The above dynamic equation can be equivalently expressed as follows

$$\begin{aligned}\ddot{x} &= u_1\\ \ddot{\theta} &= u_2\\ \ddot{y} &= u_1 \tan\theta + \frac{c_y}{m}(\dot{x}\tan\theta - \dot{y})\end{aligned} \tag{A.97}$$

where,

$$u_1 = \frac{1}{m}\left(F\cos\theta - \dot{x}\left(c_y \sin^2\theta + c_x\cos^2\theta\right) + \left(c_y - c_x\right)\dot{y}\sin\theta\cos\theta\right) \tag{A.98}$$

$$u_2 = \frac{1}{I}\left(T - c_z\dot{\theta}\right) \tag{A.99}$$

The above expression of the control inputs yield the following state space structure (where the state variables are chosen as $x_1 = x, x_2 = \theta, x_3 = y, x_4 = v_x$, $x_5 = \omega, x_6 = v_y$)

$$\begin{aligned}\dot{x}_1 &= x_4\\ \dot{x}_2 &= x_5\\ \dot{x}_3 &= x_6\\ \dot{x}_4 &= u_1\\ \dot{x}_5 &= u_2\\ \dot{x}_6 &= u_1\tan x_2 + \frac{c_y}{m}(x_4\tan x_2 - x_6)\end{aligned} \tag{A.100}$$

A.9 Mathematical Modeling of 3-DOF Redundant Manipulator

A planar 3-DOF robot arm is a particular type of robot manipulator with two prismatic and one revolute joint, moving on a horizontal plane. The two prismatic joints are rigid, whereas the revolute joint is coupled to the end effector through an elastic degree of freedom. In addition, all the prismatic joints are actuated. An idealized model of this manipulator is shown in Fig. A.9. The model consists of a

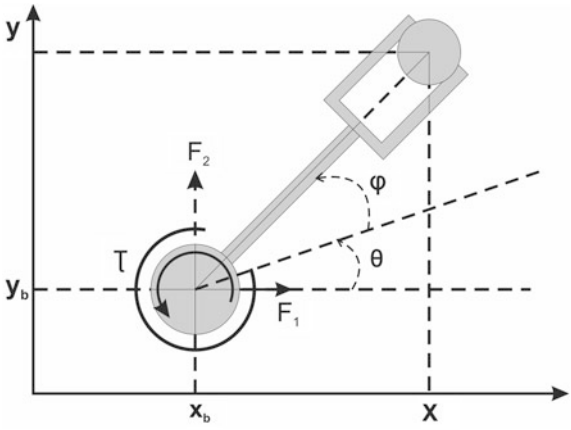

Fig. A.9 Schematic diagram of the three degree of freedom redundant manipulator

base body, which can translate and rotate freely in the plane, and a massless arm at the tip of which the end-effector is attached. The base body is connected to the massless arm by a linear torsional spring whose neutral position is $\varphi = 0$. The Cartesian position of the base body as well as the angle through which the base body is rotated can be controlled. The variable φ measures the deviation of the massless arm from the assigned (φ = 0) value. Whenever the variable is displaced from zero, it induces a restoring torque $-K\varphi$, where K. denotes the torsional spring constant.

We can write the following equation of motions:

$$\begin{aligned}
&(M+m)\ddot{x} + Ml\ddot{\theta}\sin\theta + Ml\dot{\theta}^2\cos\theta = u_x \\
&(M+m)\ddot{y} - Ml\ddot{\theta}\cos\theta + Ml\dot{\theta}^2\sin\theta = u_y \\
&I\ddot{\theta} = u_\theta \\
&\ddot{x}\sin\theta - \ddot{y}\cos\theta = 0
\end{aligned} \tag{A.101}$$

In order to satisfy the above equations it is required that

$$u_\theta = \frac{I}{Ml}(u_x \sin\theta - u_y \cos\theta) \tag{A.102}$$

The above selection yields the following equations of accelerations:

$$\begin{aligned}
&\ddot{x} = u_1 \\
&\ddot{\theta} = u_2 \\
&\ddot{y} = u_1 \tan\theta
\end{aligned} \tag{A.103}$$

where,

$$\begin{aligned} u_1 &= \frac{1}{M+m}\left(u_x \cos\theta + u_y \sin\theta - Ml\dot{\theta}^2\right)\cos\theta \\ u_2 &= \frac{1}{Ml}\left(u_x \sin\theta - u_y \cos\theta\right) \end{aligned} \tag{A.104}$$

The above selection of u_1, and u_2 yield the following state space structure:

$$\begin{aligned} \dot{x}_1 &= x_4 \\ \dot{x}_2 &= x_5 \\ \dot{x}_3 &= x_6 \\ \dot{x}_4 &= u_1 \\ \dot{x}_5 &= u_2 \\ \dot{x}_6 &= u_1 \tan x_2 \end{aligned} \tag{A.105}$$

The state variables are chosen as: $x_1 = x, x_2 = \theta, x_3 = y, x_4 = v_x,\ x_5 = \omega,$ $x_6 = v_y$.